

THE UNIVERSITY OF HULL

**WETTABILITY OF SOLID PARTICLES IN RELATION TO  
PARTICLE-STABILISED FOAMS AND EMULSIONS**

being a Thesis submitted for the Degree of Doctor of Philosophy  
in the University of Hull

by

Karl Matthew Reed  
MPhys (University of Hull)

November 2011

*Dedicated to the memory of my grandmother*

*Margaret Reed*

*Who passed away during the course of this PhD  
We all still miss you a great deal*

## Acknowledgements

Firstly I would like to express my immense gratitude to my supervisor Dr. Tommy Horozov for his patience and help throughout my studies without which I would surely have failed at the first hurdle.

I would like to thank the EPSRC for funding this project. Thanks also go to the Surfactant and Colloid group of Hull University for their continued support, friendship and all the help and advice provided for my projects. Extra appreciation goes to Anaïs Rocher, Benjamin Holt and Michael Thompson for keeping my sanity intact during the most stressful days.

Thanks go to Tony Sinclair for all the SEM images which he has taken and to students, Yanping Xia (Shiny), Yin Wang and Elodie Bénard for experimental data collected in the course of their projects with my help and guidance.

Immense appreciation goes out to all of my friends, near and far, who have offered continued support and brightened my days through the last few years. Especially Abigail Marchant who has helped me out after operations and been a great friend and housemate. Amazing support and patience has also been in plentiful supply from my girlfriend Eileen Kerrone and words cannot describe my love and gratitude for her and her support during this endeavour.

Finally, I wish to express my eternal gratitude and love to all my relatives for all of their support, love and entertainment provided to me over the years. An extra special mention goes my parents Kevin & Susan Reed, my brothers Matthew & Samuel Reed and my grandparents Doreen & Malcolm Attew and Margaret & Maurice Reed. I could not have done this without all of your help so thank you so very much.

## Declaration

Except where explicitly stated, this thesis is the result of my own work. No part of my thesis has already been or is being concurrently submitted for any degree, diploma or qualification at any other university.

The work contained in this thesis has given rise to the following conference presentations:

### Oral presentations:

1. '*Janus particles from Pickering emulsions*', International Workshop on Emulsion Templating for Macroporous Polymers, Imperial College London, London, UK (May 2009).
2. '*Production of Janus particles using particle-stabilised emulsions*', 12<sup>th</sup> European Student Colloid Conference, University of Almeria, Spain (July 2009).
3. '*Contact angles of colloidal particles at air-water and oil-water interfaces*', University of Hull Research Colloquia, Department of Chemistry, University of Hull, UK (July 2010).

### Contributed talks:

4. '*Wettability and Behaviour of Solid Particles in Thin Liquid Films, Foams and Emulsions*' Lecture, UK Colloids 2011, London, UK (July 2011).

### Poster presentations:

5. '*Particle-stabilised emulsions as a tool in the fabrication of Janus particles*', UK Polymer Colloid Forum, University of Hull, UK (September 2009).

Karl M. Reed

26/11/2011

## Abstract

Colloidal particles and surfactants are commonly used, either individually or combined, as stabilisers of emulsions and foams. While the properties of surfactants and particles under a range of conditions and concentrations are relatively well known, there are some areas that require further investigation. The wettability of colloidal particles is one of the main factors that determine how they behave in a given system but determining the wettability is difficult due to the small size of the particles. The Film Calliper Method (FCM) has been proposed as a simple technique for the direct measurement of the contact angles of micrometer and submicrometer particles in their natural environment. One of the main aims of this work was to develop the Film Calliper Method for measuring contact angles at oil - water interfaces. The FCM was therefore used to measure the contact angles at oil - water interfaces for a range of particles, such as latex and silica particles, in different systems. For the first time directly measured contact angles are linked to the types of emulsions stabilised by the particles.

The FCM was also used to directly measure the contact angles of silica particles in cationic surfactant solutions at air and oil interfaces for the first time. The stability of foams and emulsions made with particle - surfactant mixtures were investigated and related to the particle contact angles.

Janus particles are a special category of particles which have different properties on each hemisphere. A method for making Janus particles was developed using template silica particles masked with a polymerised Pickering emulsion. The portion of surface exposed for treating can be tuned by controlling the inherent wettability of the template particles as proven with fluorescence microscopy. Emulsions stabilised by amphiphilic Janus particles made with the method are compared with emulsions stabilised by homogeneous particles with similar wettability.

## List of abbreviations and symbols

The following is a list of abbreviations and symbols used throughout this thesis:

AIBN = Azobisisobutyronitrile

AFM = Atomic force microscope

BMA = Butyl methacrylate

DCDMS = Dichlorodimethylsilane

Decalin = Decahydronaphthalene

DP = Degree of polymerisation

DSA = Drop shape analyser

EHMA = 2-ethylhexylmethacrylate

FCM = Film Calliper Method

GTT = Gel Trapping Technique

$h_e$  = Emulsion height

$h_o$  = Oil height

$h_w$  = Water height

IBMA = Isobutyl methacrylate

mol.% = Molar percentage

o/w = Oil-in-water emulsion

PGMA-PS = poly (glycerol monomethacrylate) - polystyrene

rpm = Revolutions per minute

SAM = Self assembled monolayer

SEM = Scanning electron microscope

SIT = Side Imaging Technique

SMA = Stearyl methacrylate

UV = Ultraviolet

vol.% = Volume percentage

w/o = Water-in-oil emulsion

wt.% = Weight percentage

$\alpha$  = Janus particle angle between the centre of 'apolar' region and Janus boundary

$\Gamma$  = Surfactant coverage per unit area

$\zeta$  = Zeta potential

$\gamma$  = Surface tension

$\lambda$  = Wavelength

$\emptyset$  = Diameter

$\phi_e$  = Volume fraction of emulsion

$\phi_o$  = Volume fraction of oil

$\phi_w$  = Volume fraction of water

$\theta$  = Contact angle

$\theta_a$  = Contact angle of Janus particle 'apolar' region

$\theta_{aw}$  = Contact angle at an air-water interface

$\theta_{ow}$  = Contact angle at an oil-water interface

$\theta_p$  = Contact angle of Janus particle 'polar' region

$\gamma_{SL}$  = Surface free energy at the solid-liquid interface

$\gamma_{SG}$  = Surface free energy at the gas-solid interface

$\gamma_{LG}$  = Surface free energy at the liquid-gas interface

# Contents

|                  |  |           |
|------------------|--|-----------|
| <b>CHAPTER 1</b> | <b>Introduction</b>  | <b>1</b>  |
| <b>1.1</b>       | <b>Wettability of solid particles</b>  | <b>1</b>  |
| 1.1.1            | <i>Contact angle of solid particles at liquid interfaces</i>                       | 1         |
| 1.1.2            | <i>Methods for tuning particle wettability</i>                                     | 3         |
| 1.1.2.1          | <i>Chemical modification of the particle surface</i>                               | 3         |
| 1.1.2.2          | <i>Using surfactants for changing the particle contact angle</i>                   | 5         |
| 1.1.2.1.1        | <i>Surfactant adsorption on fluid-liquid interfaces</i>                            | 6         |
| 1.1.2.1.2        | <i>Surfactant adsorption on solid-liquid interfaces</i>                            | 7         |
| 1.1.3            | <i>Methods for measuring particle contact angles</i>                               | 10        |
| <b>1.2</b>       | <b>Surface - anisotropic (Janus) particles</b>                                     | <b>13</b> |
| 1.2.1            | <i>General characteristics of Janus particles and their potential applications</i> | 13        |
| 1.2.2            | <i>Methods for producing Janus particles</i>                                       | 17        |
| 1.2.2.1          | <i>Synthetic methods for producing Janus particles</i>                             | 17        |
| 1.2.2.2          | <i>Modification of particle monolayers to produce Janus particles</i>              | 18        |
| 1.2.2.3          | <i>Particle stabilised emulsions as a tool for preparation of Janus particles</i>  | 20        |
| 1.2.3            | <i>Properties of Janus particles</i>   | 22        |
| <b>1.3</b>       | <b>Particle-stabilised emulsions</b>   | <b>23</b> |
| 1.3.1            | <i>General emulsion characteristics and stability</i>                              | 23        |
| 1.3.2            | <i>Emulsions stabilised by solid particles alone</i>                               | 26        |
| 1.3.3            | <i>Pickering emulsions from particle-surfactant mixtures</i>                       | 30        |
| <b>1.4</b>       | <b>Particle-stabilised aqueous foams</b>   | <b>31</b> |
| <b>1.5</b>       | <b>Motivation and aims of the thesis</b>   | <b>33</b> |
| <b>1.6</b>       | <b>Outline of thesis</b>   | <b>34</b> |
| <b>1.7</b>       | <b>References</b>  | <b>36</b> |

|                  |  |     |
|------------------|--|-----|
| <b>CHAPTER 2</b> | <b>Experimental</b>  | 40  |
| <b>2.1</b>       | <b>Materials</b>   | 40  |
| 2.1.1            | <i>Solid particles</i>   | 40  |
| 2.1.1.1          | <i>Silica particles</i>  | 40  |
| 2.1.1.2          | <i>Latex particles</i>   | 41  |
| 2.1.2            | <i>Materials used in contact angle measurements, foams and emulsions</i>                     | 43  |
| 2.1.3            | <i>Materials used in the preparation of Janus particles</i>                                  | 44  |
| 2.1.4            | <i>Other chemicals used</i>  | 46  |
| <b>2.2</b>       | <b>Experimental procedures and methods</b>   | 47  |
| 2.2.1            | <i>Hydrophobisation of silica particles</i>  | 47  |
| 2.2.2            | <i>Contact angle measurements on microscope slides</i>                                       | 49  |
| 2.2.3            | <i>Measuring particle contact angles with the Film Calliper Method</i>                       | 50  |
| 2.2.4            | <i>Measuring particle contact angles with the Side Imaging Technique (SIT)</i>               | 55  |
| 2.2.5            | <i>Making emulsions and foams</i>  | 55  |
| 2.2.5.1          | <i>Determining emulsion type</i>   | 57  |
| 2.2.6            | <i>Measuring the absorption of surfactant on silica surfaces</i>                             | 57  |
| 2.2.7            | <i>Producing microscope images of samples</i>  | 58  |
| 2.2.8            | <i>Measuring particle zeta potentials</i>  | 59  |
| 2.2.9            | <i>Measuring the hydrodynamic diameter of emulsion drops and polymers</i>                    | 59  |
| 2.2.10           | <i>Measuring the surface or interfacial tension of TTAB surfactant</i>                       | 59  |
| 2.2.11           | <i>Preparation of Tollen's reagent</i>   | 60  |
| <b>2.3</b>       | <b>References</b>  | 61  |
| <br>             |  |     |
| <b>CHAPTER 3</b> | <b>Direct measurements of colloidal particle contact angles at the oil - water interface</b> | 62  |
| <b>3.1</b>       | <b>Introduction</b>  | 62  |
| <b>3.2</b>       | <b>Experimental</b>  | 63  |
|                  |  | VII |

|   |    |
|---|----|
| <b>3.3 Results and discussion</b>   | 64 |
| 3.3.1 <i>Measuring contact angles of latex particles with the FCM at air-water and oil-water interfaces</i> | 64 |
| 3.3.1.1 <i>Contact angles of carboxylate modified latex particles</i>                                       | 64 |
| 3.3.1.2 <i>Contact angles of polystyrene sulphate latex particles</i>                                       | 67 |
| 3.3.1.3 <i>Contact angles of poly(glycerol monomethacrylate) - Polystyrene latex particles</i>              | 69 |
| 3.3.2 <i>Contact angles of silica particles at air-water and oil-water Interfaces</i>                       | 70 |
| 3.3.2.1 <i>Contact angles of silica particles with chemically modified surfaces (DCDMS)</i>                 | 71 |
| 3.3.2.2 <i>Contact angles of silica particles in the presence of cationic surfactant</i>                    | 77 |
| <b>3.4 Conclusions</b>  | 86 |
| <b>3.5 References</b>   | 88 |

|  |     |
|--|-----|
| <b>CHAPTER 4 Foams and emulsions of silica particle and cationic surfactant mixtures</b>   | 89  |
| <b>4.1 Introduction</b>  | 89  |
| <b>4.2 Experimental</b>  | 91  |
| <b>4.3 Results and discussion</b>  | 92  |
| 4.3.1 <i>Surface and interfacial tensions of surfactant solutions</i>  | 92  |
| 4.3.2 <i>Zeta potential of silica particles in surfactant solutions</i>  | 95  |
| 4.3.3 <i>Adsorption of CPC on the silica particle surface</i>  | 97  |
| 4.3.4 <i>Contact angles of silica particles at the air-water interface in the presence of surfactant</i>                                   | 104 |
| 4.3.5 <i>Differences in foaming between surfactant solutions and surfactant solution/silica particle mixtures</i>                          | 113 |
| 4.3.6 <i>Differences in emulsion type and stability stabilised by surfactant solutions or surfactant solution/silica particle mixtures</i> | 128 |

|                  |   |     |
|------------------|---|-----|
| <b>4.4</b>       | <b>Conclusions</b>  | 137 |
| <b>4.5</b>       | <b>References</b>   | 140 |
|                  |   |     |
| <b>CHAPTER 5</b> | <b>Preparation and properties of Janus particles</b>  | 142 |
| <b>5.1</b>       | <b>Introduction</b>   | 142 |
| <b>5.2</b>       | <b>Experimental</b>   | 145 |
| <b>5.3</b>       | <b>Results and discussion</b>   | 145 |
| 5.3.1            | <i>Janus particle contact angles and wettability</i>  | 145 |
| 5.3.2            | <i>Preparation and polymerisation of Pickering emulsions</i>  | 148 |
| 5.3.3            | <i>Preparation of different Janus particle types by varying the chemical treatment of polymerised Pickering drops</i> | 160 |
| 5.3.3.1          | <i>Metal/ dielectric Janus particles</i>  | 161 |
| 5.3.3.2          | <i>Bifunctional Janus particles</i>   | 162 |
| 5.3.3.3          | <i>Amphiphilic Janus particles and Pickering emulsions stabilised by them</i>   | 171 |
| <b>5.4</b>       | <b>Conclusions</b>  | 184 |
| <b>5.5</b>       | <b>References</b>   | 186 |
|                  |   |     |
| <b>CHAPTER 6</b> | <b>Summary of main findings, conclusions and future work</b>  | 188 |
| <b>6.1</b>       | <b>Main findings and conclusions</b>  | 188 |
| <b>6.2</b>       | <b>Future work</b>  | 191 |

# Chapter 1

## Introduction

The main focus of this thesis is towards the direct measurement of colloidal particle wettability and linking those measurements with the types of emulsions the particles stabilise. This work is extended by investigating the behaviour of particle and surfactant mixtures in relation to changing particle properties and in stabilising foams and emulsions. A method was also developed for making large amounts of particles with dual wettability. This chapter introduces the basic concepts and theory underlying the work detailed in later chapters.

### 1.1 Wettability of solid particles

Solid colloidal particles (1 nm to several tens of micrometres in diameter) are widely used in research and many industries e.g. food, cosmetics, pharmaceuticals, etc.<sup>1</sup>. The particle wettability is amongst the most important characteristics of the solid particles alongside their chemical composition, size, shape and surface charge. It dictates the particle attachment to liquid interfaces and particle behaviour at the surface and in the bulk of liquids. Some basic definitions related to the particle wettability, how it can be controlled and quantified are considered in the next sub-sections.

#### *1.1.1 Contact angle of solid particles at liquid interfaces*

Solid colloidal particles, similar to surfactants, can spontaneously attach to liquid interfaces and stabilise emulsions and foams<sup>2</sup>. Even solid particles with homogeneous surface composition are surface active, because when they migrate

through a water phase and attach to a water-air (or oil) interface, the interfacial areas of both particle-water and water-air (oil) are reduced, thus lowering the free energy of the system. Anisotropic (also called ‘Janus’) particles can be amphiphilic and surface active. Janus particles are considered separately in section 1.2 below. The surface activity of solid particles strongly depends on their wettability which is quantified by the particle contact angle. When a particle sits at a liquid interface (Fig. 1.1), the contact angle is the angle between the tangents to the particle surface and water-air (oil) interface at every point of the three-phase contact line. It is accepted practice to express the particle contact angle as measured through the more polar liquid (usually water). The particle contact angle,  $\theta$ , is related to the interfacial tensions acting between the three phases in contact according to Young’s equation<sup>1</sup>, which in the case of an oil-water interface reads

$$\cos \theta = \frac{\gamma_{so} - \gamma_{sw}}{\gamma_{ow}} \quad (1.1)$$

where  $\gamma_{so}$ ,  $\gamma_{sw}$  and  $\gamma_{ow}$  are the solid-oil, solid-water and oil-water interfacial tensions, respectively.

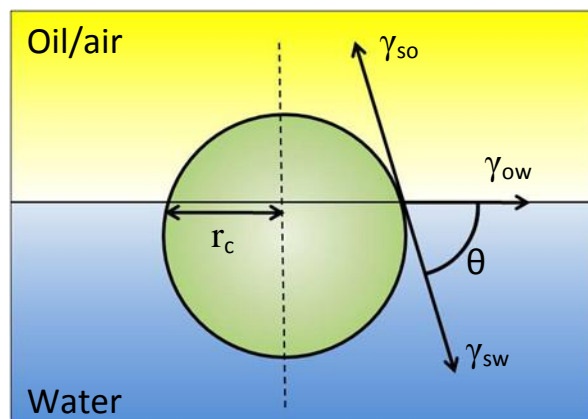


**Figure 1.1.** Diagram showing the contact angle,  $\theta$ , of a spherical particle at an oil-water interface. Also displayed are the interfacial tensions ( $\gamma_{so}$ ,  $\gamma_{sw}$ ,  $\gamma_{wo}$ ) between the solid and liquid phases, and the radius of the three phase contact line,  $r_c$

If the particle is equally wetted by both fluids, its contact angle is  $90^\circ$ . A contact angle of less than  $90^\circ$  corresponds to a hydrophilic particle, where the particle sits mostly within the water phase. The extent of hydrophilicity is shown by the size of the angle, with very small angles corresponding to very hydrophilic particles. Alternatively a contact angle of over  $90^\circ$  corresponds to a hydrophobic particle, with the contact angle increasing towards  $180^\circ$  as the hydrophobicity increases<sup>1,2</sup>.

### *1.1.2 Methods for tuning particle wettability*

Inherent wettability of solid particles is a function of the chemical composition of their surface and is usually predetermined during the particle synthesis. For example, inorganic oxide particles (e.g. alumina, titania, silica) are very well wet by water and their high hydrophilicity is due to the large number of polar hydroxyl groups at the particle surface. Many practical applications require less hydrophilic or even hydrophobic oxide particles to enhance the particle attachment to liquid interfaces or improve particle dispersibility in non-polar organic liquids. Young's equation shown above (eq. 1.1) suggests that the particle contact angle could be changed by altering the respective interfacial tensions. Two of the most common approaches for changing the particle contact angle, thus tuning particle wettability, are considered below.

#### *1.1.2.1 Chemical modification of the particle surface*

Chemical composition of the particle surface can be changed by reacting some of the surface groups with chemical reagents, thus grafting hydrophobic or hydrophilic chains by covalent bonding. The chemically grafted layer is usually referred to as a self-assembled monolayer (SAM) because it is spontaneously formed when the solid surface is put in contact with vapours or solution of the modifying reagent<sup>3</sup>. The SAMs form stable and often highly ordered films on a

variety of solid surfaces<sup>3,4</sup>. Alkylchlorosilanes, alkoxy silanes, or alkylaminosilanes are commonly used to modify hydroxylated surfaces (such as glass or silica), whereas alkanethiols are used for modifying metal surfaces (Fig. 1.2). Silanes react with the silanol groups ( $\equiv\text{SiOH}$ ) from the surface of silica, thus forming Si-O-Si bonds. Di- and trichlorosilanes can self-assemble into very stable polysiloxane coatings and are often preferred for the modification of hydroxylated oxide surfaces<sup>3</sup>. Chemically grafted monolayers on the particle surface alter the solid-fluid interfacial tensions, thus changing the particle contact angle (see eq. 1.1). The degree of surface modification and, therefore the particle contact angle, can be controlled by varying the fraction of reacted surface groups via the reaction time and/or the concentration of silane<sup>5</sup>. Main advantages of this approach for changing particle wettability are in the high stability of modified surfaces and the ability for controlling the chemical composition of the particle surface by grafting different number and/or type of functional groups (e.g. amine, carboxyl, alkyl, etc.).

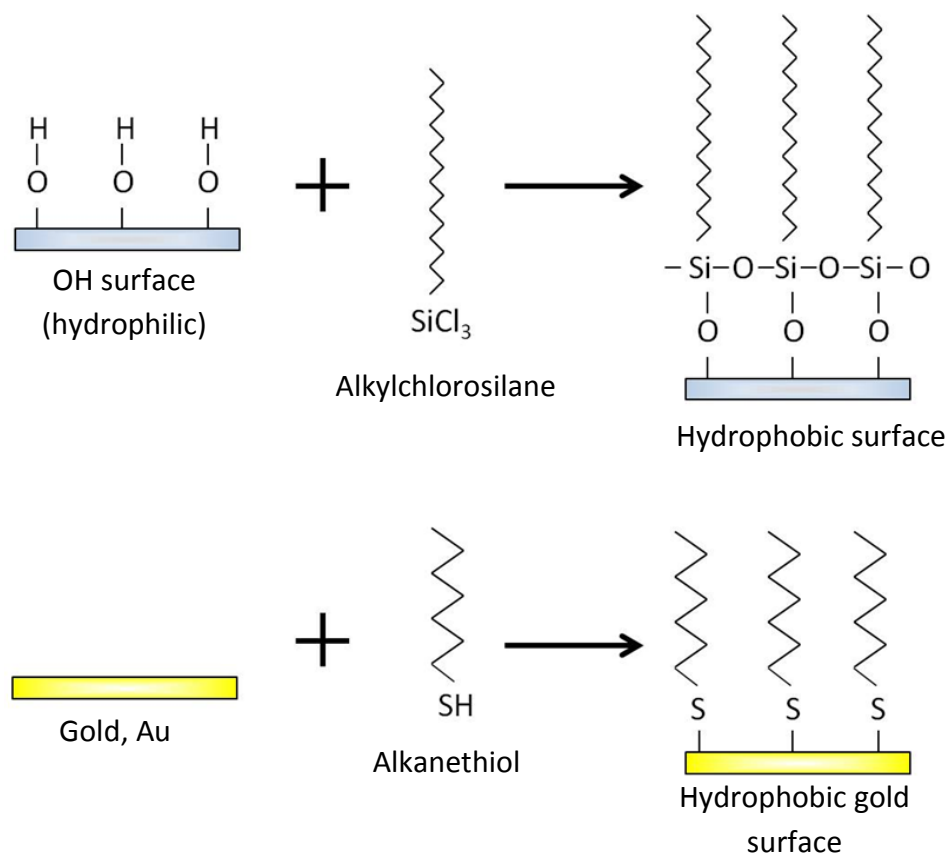


**Figure 1.2.** Schematic showing chemical modification of a hydrophilic surface, rich in hydroxyl groups, by alkytrichlorosilane (top) and a gold surface by alkanethiol (bottom).

#### 1.1.2.2 Using surfactants for changing the particle contact angle

Surfactants (surface active agents) have amphiphilic molecules consisting of two main sections; a hydrophilic (water-liking) ‘head’ and hydrophobic (water-rejecting) ‘tail(s)’ as shown in Fig. 1.3. The tail group consists of one or more hydrocarbon chains and can vary considerably in length. The head-group can vary by chemical structure or composition and may carry electrical charge as a result of dissociation in water. Based on the electrical charge of the dissociated head-group, surfactants are classified into cationic (positive), anionic (negative), non-ionic (no charge), and zwitterionic (neutral net charge but possess both positive and negative charges)<sup>6</sup>. Due to their amphiphilic nature, surfactant molecules spontaneously accumulate (adsorb) at both fluid-liquid and solid-liquid interfaces. Therefore the

change of the particle contact angle in the presence of surfactant comes from changes in all of the interfacial tensions involved in eq. 1.1.

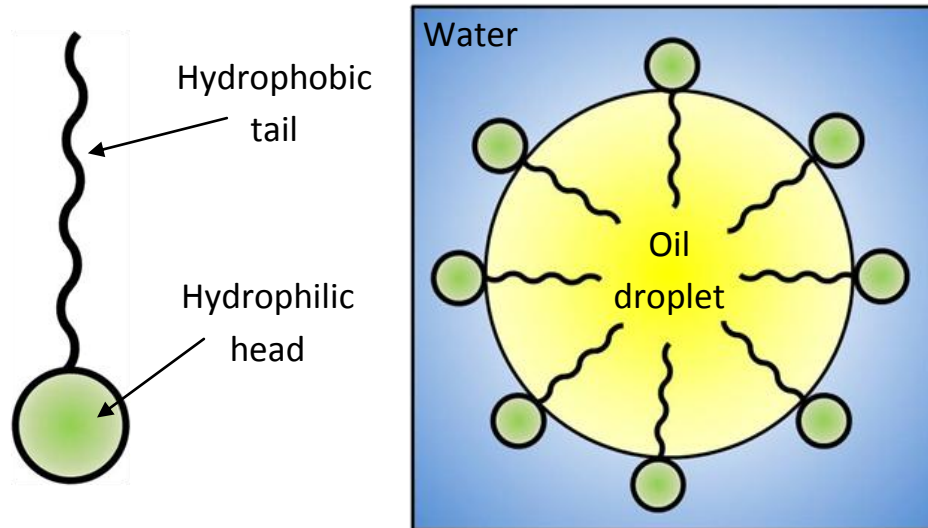


**Figure 1.3.** Schematic representation of a surfactant molecule (left) and an oil droplet in water with surfactant adsorbed at the drop surface (right).

#### *1.1.2.1.1 Surfactant adsorption on fluid-liquid interfaces*

When an air-water or oil-water interface is created in the presence of surfactant, the surfactant molecules spontaneously migrate from the bulk onto the interface and accumulate (adsorb) there. The accumulation of surfactant at the interface continues until an adsorption equilibrium between the interface and the bulk is established. The adsorbed surfactant molecules align at the interface with the hydrophobic tail in the oil (or air) and the hydrophilic head in the water phase (Fig. 1.3), thus reducing the interfacial tension (Fig. 1.4). The adsorption of the surfactant molecules at the interface is driven by hydrophobic interactions in the bulk aqueous phase. The hydrocarbon chains of the surfactant in the aqueous phase are surrounded by a bonded 'cage' of water molecules and the resulting increase in system structure causes a decrease in entropy. The exclusion of hydrocarbon chains from the aqueous phase is therefore an entropically driven

process to decrease the free energy of the system<sup>6,7</sup>. This is also the reason for the formation of surfactant aggregates (micelles) at large concentrations above the critical micelle concentration (cmc).

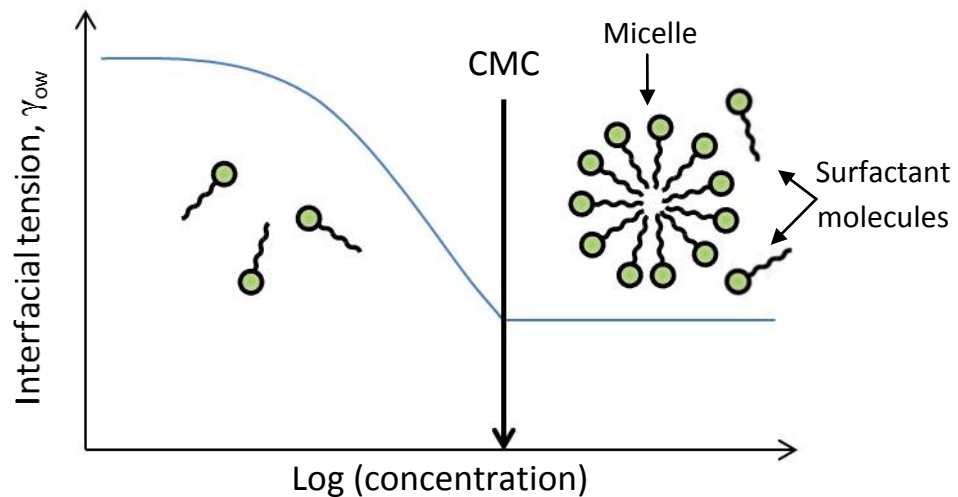


**Figure 1.4.** Variation of oil-water interfacial tension,  $\gamma_{ow}$ , with logarithm of the surfactant concentration in water. Surfactant aggregates (micelles) appear in the solution when the concentration exceeds the critical micelle concentration (cmc). The interfacial tension remains constant above the cmc because aggregated surfactant has no tendency to adsorb to the oil-water interface.

#### 1.1.2.1.2 Surfactant adsorption on solid-liquid interfaces

The amphiphilic nature of surfactant molecules leads to their spontaneous adsorption on solid-liquid interfaces. The surfactant adsorption changes the surface free energy per unit area (interfacial tension) of the solid-liquid interface, thus contributing to the change of the particle contact angle (eq. 1.1). Adsorption of surfactant molecules on solid surfaces is more complex than that at fluid-liquid interfaces. It occurs due to electrostatic and van der Waals interactions, and in some cases hydrogen bonding between the surfactant molecules and the solid surface. The orientation of the adsorbed surfactant molecules depends on the

surfactant type, its concentration and the solid surface properties. It affects the solid wettability and may increase or decrease the particle contact angle depending on the experimental conditions. The surfactant adsorption is significantly enhanced when the charge of the solid surface has the opposite sign to that of the ionic surfactant. For example, cationic surfactants easily adsorb on negatively charged particles such as silica<sup>8-12</sup>. Extensive studies of such systems have shown that there are four distinct adsorption regions over the full range of concentrations up to and above the cmc (Fig. 1.5). At low adsorption densities (region I), the surfactant ions adsorb as individual ions without chain-chain association in a head-on orientation at the particle surface. When the adsorption density reaches a certain level in region II (the "surface concentration" being about that of the cmc), adsorbed ions begin to associate into patches or hemimicelles at the interface through chain-chain interaction of adsorbed surfactant. This is characterized by a marked increase in adsorption and a sharp increase in the contact angle suggesting that the polar heads orient themselves towards the charged surface. In this and the subsequent regions, chain-chain association is the main contributor to the adsorption free energy. In region III, hydrophobic chain interactions are the driving force for adsorption to continue. In addition, electrostatic repulsion causes some of the adsorbed surfactant ions to orient in reverse manner, which results in the contact angle remaining constant or even decreasing as surfactant is added. The onset of Region IV occurs at or near the bulk CMC, when a bilayer or its equivalent is reached. The contact angle decreases further and the surface becomes hydrophilic. Adsorption of cationic surfactant on a negatively charged particle surface also causes sign reversal in the zeta potential of the particles. Trends of the zeta potential and contact angle of quartz as a function of cationic surfactant concentration at neutral pH are illustrated in Fig. 1.6.

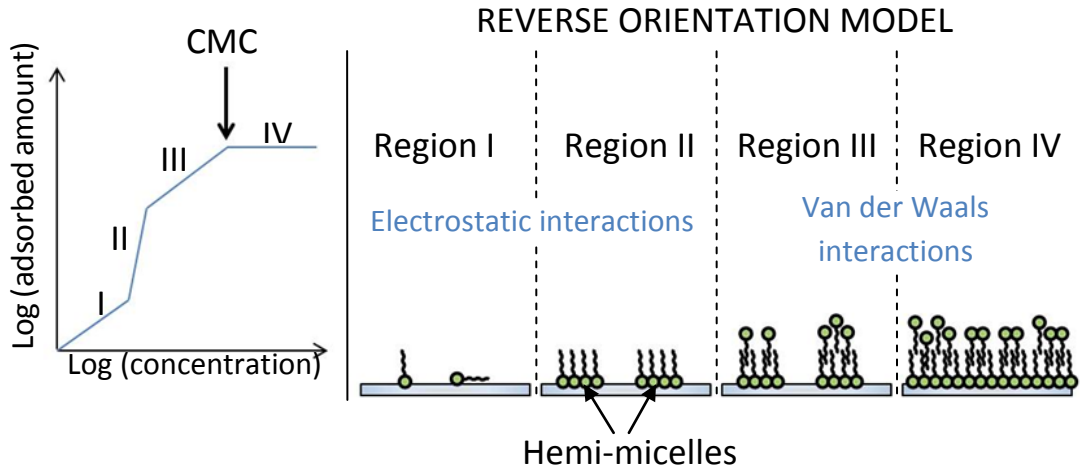


**Figure 1.5.** Adsorption of anionic/cationic surfactants on oppositely charged solid surfaces in water: (left) a typical variation of the adsorbed amount with surfactant concentration; (right) a schematic of the reverse orientation model for adsorption. (Adapted from ref. 9)

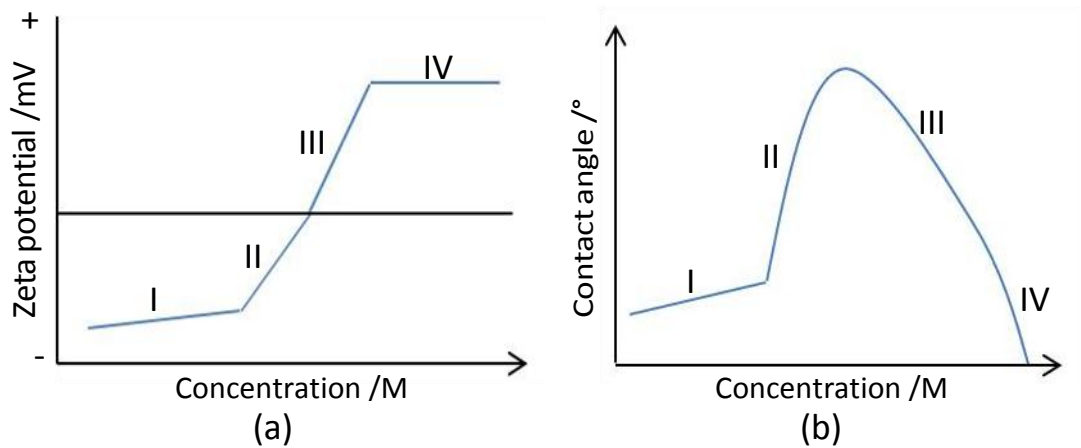


**Figure 1.6.** Trends in zeta potential (a) and contact angle (b) of quartz versus concentration of a cationic surfactant (dodecylpyridium chloride). (Adapted from ref. 10)

### 1.1.3 Methods for measuring particle contact angles

The three phase contact angle of small solid particles adsorbed at the air (oil) - water interface (Fig. 1.7) is directly related to the particle hydrophobicity (wettability) and its knowledge is of great practical importance.

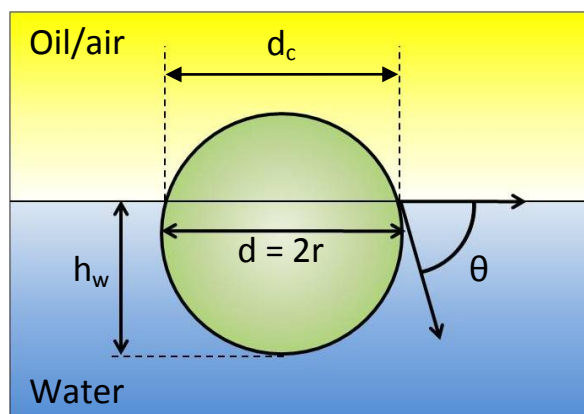


**Figure 1.7.** Side view of a small solid spherical particle with radius  $r$  attached to the oil (or air) - water interface. The depth of immersion in water,  $h_w$ , and the diameter of the three phase contact line,  $d_c$ , depend on particle hydrophobicity measured by the three phase contact angle,  $\theta$ .

There are several experimental methods for measuring the three phase contact angle of small solid particles. The methods can be separated into two categories based on measurements of (i) collective particle properties (i.e. integral methods) and (ii) individual particle properties (i.e. discrete methods).

The first group includes methods in which some properties of a macroscopic amount of solid particles packed together as a porous solid or a particle layer are studied and the contact angle is derived from the results by using appropriate theoretical models. Examples of such methods are the wicking methods<sup>13,14</sup>, immersion calorimetry<sup>15</sup> and inverse gas chromatography<sup>16</sup>. All of them have some drawbacks and limitations related to their applicability to different systems (especially to oil-water interfaces) and some important assumptions for the packing density of particles and in the theoretical models used.

In the discrete methods the contact angle is determined either by measuring the force of detachment of an individual particle from the fluid interface, by side imaging of the particle attached to the fluid interface and measuring its depth of immersion in the fluids directly from the images obtained or by reconstructing the deformed fluid interface around the particle entrapped in a thin liquid film. The force measurement technique employs recent advances in Atomic Force Microscopy (AFM) for measuring very small forces<sup>17</sup>. This sophisticated and expensive technique has many drawbacks, including low productivity and limitations with respect to the particle size which must be greater than  $\sim 2 \mu\text{m}$ . The methods involving side imaging of the particles are less sophisticated and are based on simple relations between the contact angle and the geometrical parameters of the adsorbed spherical particle. When the spherical particle is small and not very dense, the deformation of the fluid interface around it is negligible and the contact angle through the water can be calculated by either of the following equations

$$\sin \theta = \frac{d_c}{d} \quad (1.2)$$

$$\cos \theta = \frac{2h_w}{d} - 1 \quad (1.3)$$

where  $d$  and  $d_c$  are the diameter of the particle and that of the three phase contact line and  $h_w$  is the depth of immersion in water (Fig. 1.7). Since only the ratio between the geometrical parameters is involved their actual values are not important, which is one of the advantages of these methods. For larger particles ( $d \geq \sim 10 \mu\text{m}$ ) optical microscopy has been used for side imaging of the adsorbed particles<sup>18,19</sup>. Although simple, this method is suitable only for relatively large particles. It is also difficult to determine if the particles are adsorbed or just touching the fluid interface. The latter in combination with the curved meniscus at the vessel edge can compromise the measurements.

An interesting extension of the particle side imaging method by means of scanning electron microscopy was introduced recently in the form of the gel trapping technique (GTT)<sup>20,21,22</sup>. In this technique particles of interest are spread at the air (or oil) - water interface at  $\sim 50^{\circ}\text{C}$ . The aqueous phase contains several wt.% of a gelling agent (gelatin). After cooling to room temperature the aqueous phase gels and particles are trapped at the gel - air (oil) interface. The particles are then incorporated in a polymer matrix from the side of the air (oil) by means of a photopolymerisable oil. The adherent gel is removed and images of the particles incorporated in the polymer matrix are taken by a scanning electron microscope. The contact angle is determined by eqs 1.2 or 1.3 with the geometrical parameters measured from the images. The great advantage of this technique is that particles of small size ( $d > \sim 500\text{ nm}$ ) or non-spherical shape can be studied. However, it is an indirect method of measurement where it is not clear if the contact angle measured is affected by the gelling procedure, the significant temperature change, fabrication of the polymer matrix or the gelling agent itself.

The Film Trapping Technique<sup>23-25</sup> allows the contact angle of micrometer size particles at the air-water interface to be determined. In this method the particle is entrapped within a liquid film of equilibrium thickness smaller than the particle diameter. Thus a liquid meniscus (a layer of uneven thickness) is formed around the particle. When observed in reflected monochromatic light, this meniscus appears as an interference pattern of concentric bright and dark fringes. From the radii of the interference fringes, one can restore the meniscus shape by using the solution of the Laplace equation of capillarity. In this way the three-phase contact angle of the particle and the capillary pressure can be determined<sup>23</sup>. The drawbacks of this method are mainly related to the complexity of obtaining and interpreting the experimental data. In addition, the three phase contact angle is determined by extrapolation of the meniscus profile measured at large distances from the particle. Therefore small experimental errors in determining the film thickness can lead to a significant error of the calculated contact angle value. This method is not suitable for particles smaller than  $\sim 1\ \mu\text{m}$  and is rather sophisticated, which could explain why it doesn't appear to be widely used.

Recently, a simple experimental method for determination of the three-phase contact angle of micrometer and submicrometer colloidal particles at liquid interfaces has been developed, the Film Calliper Method (FCM)<sup>26</sup>. Briefly, this method utilizes the behaviour of colloidal particles when they are simultaneously attached to both surfaces of a free-standing thin liquid film, thus forming stable particle bridges. Monochromatic light reflected from the thin film produces an interference pattern of bright and dark fringes which can be observed with a microscope, and used to determine the contact angle. The FCM is explained in more detail in Chapter 2 as it was used for much of the work presented in later chapters.

## **1.2 Surface - anisotropic (Janus) particles**

It is widely believed that novel anisotropic particles will be useful in a variety of roles due to dual particle properties. One example is amphiphilic particles which are theorised to be better stabilisers of foams and emulsions than particles with homogeneous surface wettability. A general overview of such particles is presented below.

### *1.2.1 General characteristics of Janus particles and their potential applications*

Janus particles are named after the two headed Roman god of beginnings and endings called 'Janus'. The idea of the 'Janus particle' was first thought up in the late 1980's<sup>27</sup> and relates to particles which have duality of either a physical or a chemical nature. The Janus particle has two distinct surface segments (Fig. 1.8), each with different properties. For example, each hemisphere of the particle may have a different wettability (contact angle) or surface charge.

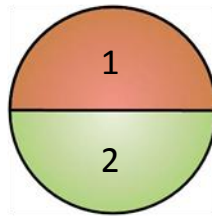


**Figure 1.8.** Janus particles consist of two distinct surface regions, 1 and 2, with different properties e.g. wettability, roughness, surface charge etc. in each region.

This type of particle has received a lot of scientific interest over recent years because the inter-particle interactions are very different to that of homogenous particles and also because external fields can be used to exert control over their movement and orientation. Janus particles are characterised by the so-called ‘Janus balance’<sup>28</sup> and what we shall call ‘Janus contrast’. The ‘Janus balance’, in its simplistic meaning, is the comparative surface area of each segment on the particle. The Janus contrast is the difference in magnitude of each segment property, for example the difference in contact angles between segments 1 and 2.

The Janus particle described above follows a general concept of a spherical particle with a selectively modified surface but other anisotropic particles are also of great interest. There are a number of potential procedures to use when making anisotropic particles allowing for many interesting shapes and properties as an end-product (Fig. 1.9). For instance shape anisotropy could be produced with dumbbell or acorn shaped particles, or any other shapes imaginable. In addition to variations in surface property or particle shape alone, the particles could also be partially raspberry-like.

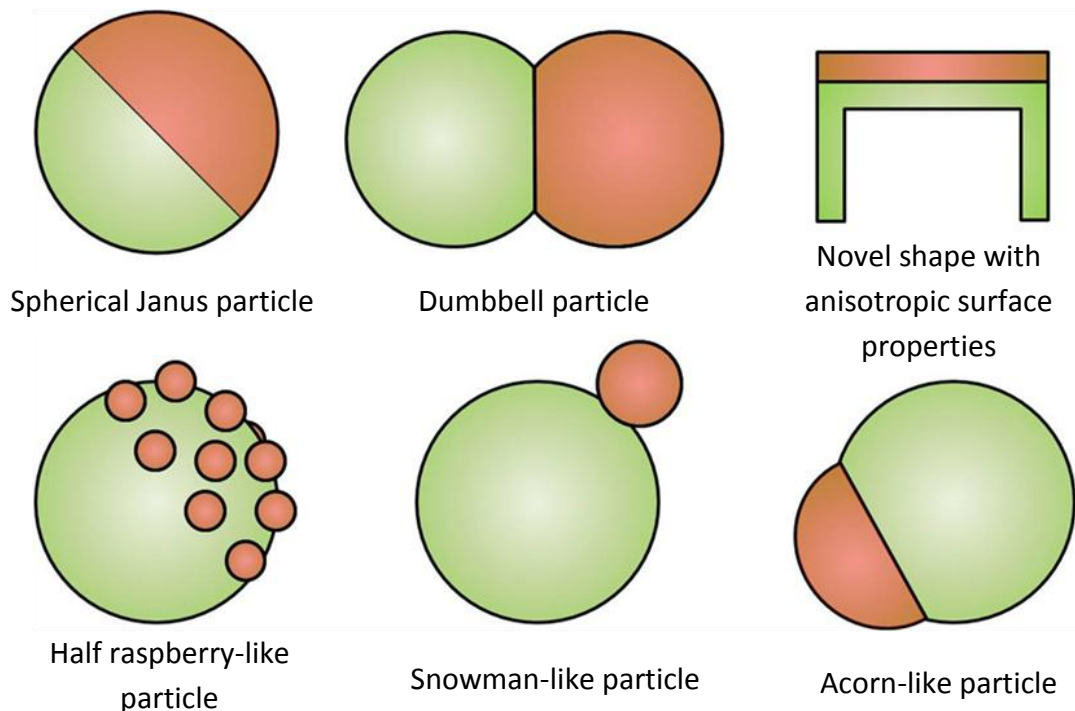


**Figure 1.9.** Examples of different types of anisotropic Janus particle. (Adapted from ref. 38)

There are a number of proposed uses for Janus particles which have been realised for a while but as research and knowledge of Janus particles increases, so more uses for them are predicted.

By making the particles amphiphilic they could act similarly to surfactant molecules and can therefore be used as emulsion stabilisers (Fig. 1.10). This effectively combines the strong interfacial attachment of particles with the interfacial orientation and possible micellisation exhibited by surfactant molecules. It has been shown<sup>29</sup> that the strength of interfacial attachment of amphiphilic Janus particles may be up to 3 times greater than homogeneous particles.

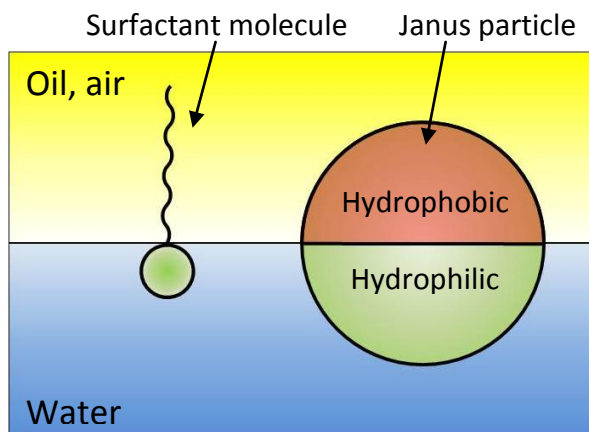


**Figure 1.10.** Diagram showing the oriented attachment of an amphiphilic Janus particle to a water - oil (air) interface, similar to that of a surfactant molecule.

The dual properties of Janus particles allow them to self assemble into structures of various shapes and sizes under the right conditions. The self assembly of the particles could be driven from amphiphilic properties<sup>30</sup>, magnetic dipoles or variations in surface charge<sup>31</sup>. The structures formed are interesting due to differences observed with those formed by amphiphilic surfactant molecules and because they could potentially be used as building blocks for self assembly into novel materials. It has been shown that control of particles in an external field can also force the aggregation of particles into interesting arrangements<sup>32</sup>.

More potential applications have been proposed, especially in the field of biomedicine for drug delivery specifically to target cells and in the production of self-propelled molecules. Most of the published literature generally concentrates on the synthesis and properties of Janus particles produced rather than investigation towards a particular application. One exception to this is work by Anker and Kopelman<sup>33</sup> making magnetically modulated optical nanoprobes (mag-MOONS) which fluoresce on one side only, allowing their orientation to be observed through fluorescence microscopy. These particles can be used to investigate both particle rotation due to Brownian motion and orientation induced by an external magnetic field.

### 1.2.2 Methods for producing Janus particles

In general Janus and shape - anisotropic particles can be made either by direct synthesis or via selective modification of a homogeneous particle surface.

#### 1.2.2.1 Synthetic methods for producing Janus particles

Microfluidic techniques generally involve two immiscible monomers forced into contact through junctions in capillary channels forming a droplet that is a mix of both monomers which, when polymerised produces a solid Janus particle (Fig. 1.11). Due to the immiscibility of the two phases the monomers join up and fuse together but they do not mix so a distinct region of each monomer is produced.

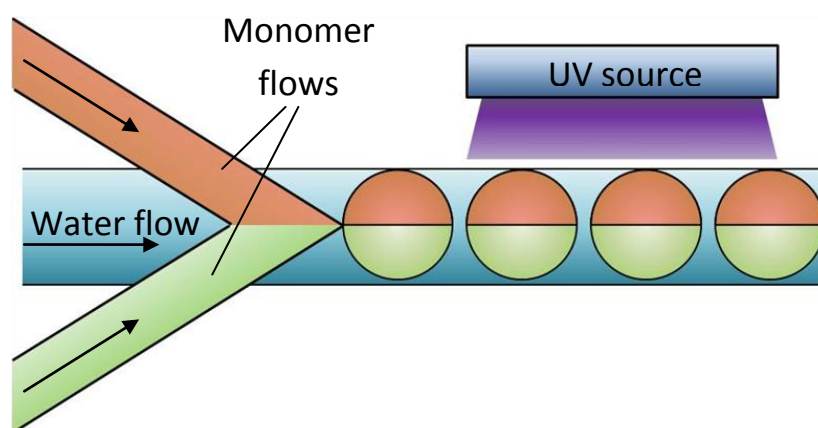


**Figure 1.11.** Diagram showing an example of a basic microfluidic system which could be used to form monomer droplets, with subsequent UV curing to make solid Janus particles.

Perhaps the simplest microfluidic procedures are those that polymerise the Janus droplets within the microfluidic channels with ultraviolet light<sup>34,35</sup> although it has been shown that thermal initiation can also be effective<sup>36</sup>. The diameters of Janus particles produced with the above procedures were between 50 and 120  $\mu\text{m}$ .

Microfluidics provide a reasonably good (if somewhat tricky) level of control over the particle morphologies produced via the control of the various channel flow speeds. The use of microfluidics is generally disadvantaged by low yields (few tenths of a gram) and the need to maintain even laminar flow without cross-mixing of the monomers occurring.

Alternative methods have also been employed such as ‘the dual-supplied spinning disk technique’ described by Perro et al.<sup>37</sup> (but developed by others), where molten polymers were streamed onto the top and bottom surface of a spinning disk which mixed at the edge and jetted off in small Janus droplets, solidifying as they fly through the air. By applying a magnetic field during the drying<sup>38</sup> or polymerisation<sup>39</sup> of droplets containing magnetic particles dipolar Janus particles can be produced. Photoresist layers can also be used to make particles by selective curing of the layer (using a patterned mask) with UV illumination to either create particles or to mask a layer below which is then selectively etched away<sup>40</sup>. Vapour deposition of metals onto similarly etched silicon has been used to make Janus particles<sup>41</sup>.

#### *1.2.2.2 Modification of particle monolayers to produce Janus particles*

The selective modification of the surface of particles in a flat monolayer is perhaps the simplest method available for producing Janus particles and can be performed in a variety of ways as depicted in Fig. 1.12.

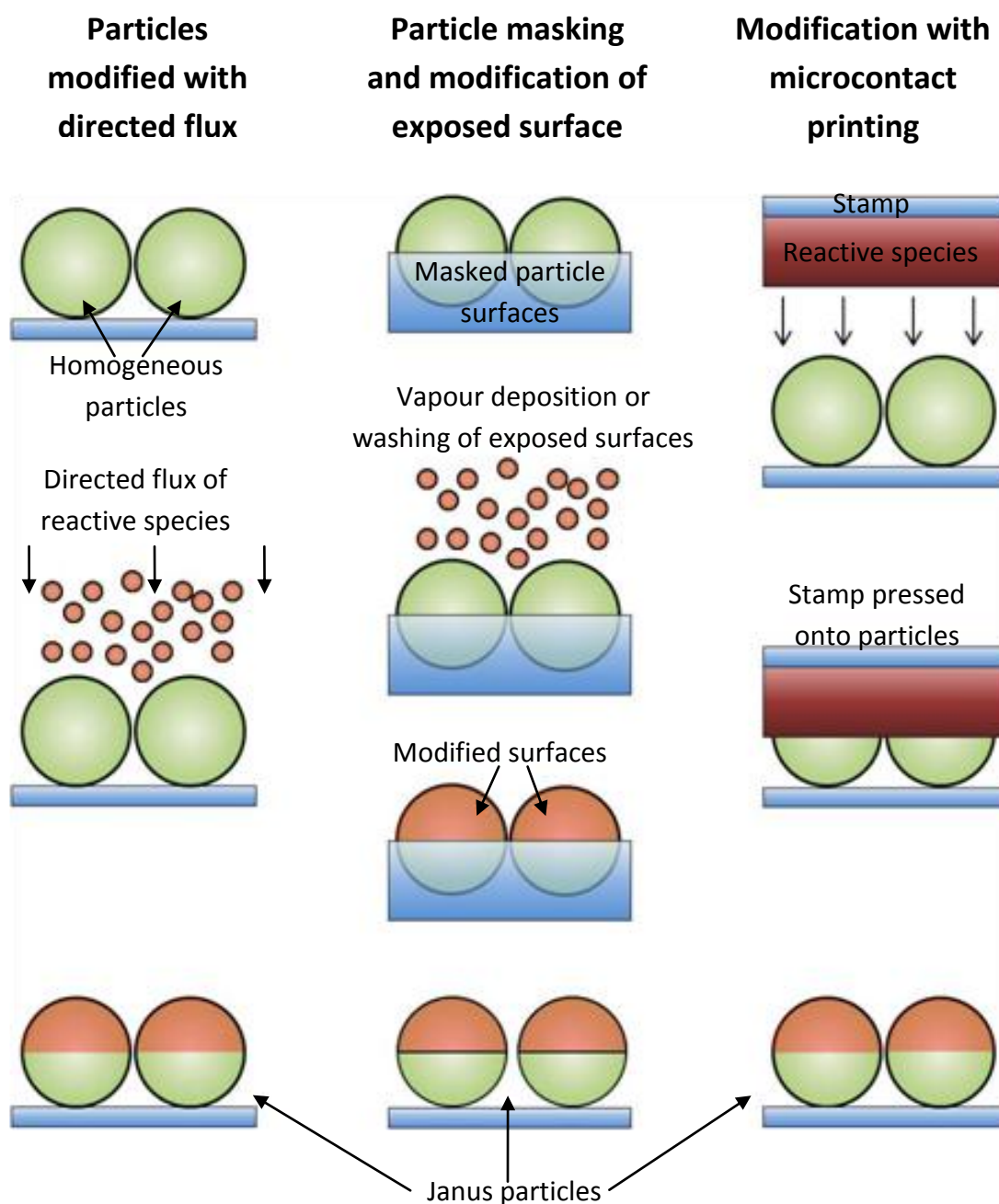


**Figure 1.12.** Schematic representation of procedures used in the modification of monolayers of homogeneous particles.

The deposition of material onto particle surfaces with vapour deposition requires the least amount of preparation, making it an attractive choice of procedure. This technique has been used to deposit thin metal<sup>42</sup> coatings onto fluorescent base particles, acting to partially mask the fluorescence of the particles<sup>43</sup>. Microcontact printing is similar but the deposition of material onto the

particles is made through physical contact with a coating on the surface of a stamp. Paunov et al.<sup>44</sup> investigated the procedure for the attachment of surfactants or colloidal particles onto particle surfaces and succeeded in producing anisotropic particles with raspberry-like regions and also particle doublets.

The best way to control the particle modification is to partially mask the particles making up the monolayer. This masking layer controls the proportion of the particle surface that is exposed for modification and also prevents the particles from moving which could lead to a greater proportion of the surface being modified than desired. The first Janus particles<sup>27</sup> used cellulose varnish as a masking medium for glass particles with diameters of 50 – 90  $\mu\text{m}$ . A photoresist layer can also be cured with a monolayer of particles in place to trap and mask the particle surfaces before the modification step<sup>45,46</sup>. In recent years the ‘gel trapping technique’<sup>47</sup> was developed, initially as a means to determine the contact angle of colloidal particles (see section 1.1.3), but later realised to be useful for producing Janus particles<sup>48</sup>. By choosing base particles of a particular contact angle the penetration depth of the particles and thus the resultant Janus balance can be tuned.

The modification of particle monolayers on a flat surface can be a relatively quick and simple procedure for the production of Janus particles with the opportunity to control the Janus balance of the particles produced. It also allows for the modification of particles of a range of sizes and shapes. However the downside to using particle monolayers is that they have a very low yield of a few milligrams in each batch and this impedes the use of the procedure for industrial purposes.

### *1.2.2.3 Particle stabilised emulsions as a tool for preparation of Janus particles*

Taking the concept of partially masking the particle surface and applying it to particle-stabilised emulsions (see section 1.3 below) enables a much greater number of particles to be masked at any one time compared with the monolayer technique, due to the significant increase in interfacial area. The emulsion drops are

generally solidified (by polymerisation or cooling) to fix the particles in place prior to modification of the exposed particle surfaces. This technique is generally considered to produce the best yield of Janus particles of a range of sizes without diminishing the ability to fine tune the Janus balance or the Janus contrast. With this technique the Janus balance can be varied by adjusting the contact angle of the initial particles to adjust the proportion of the particle surface which is masked (Fig. 1.13).

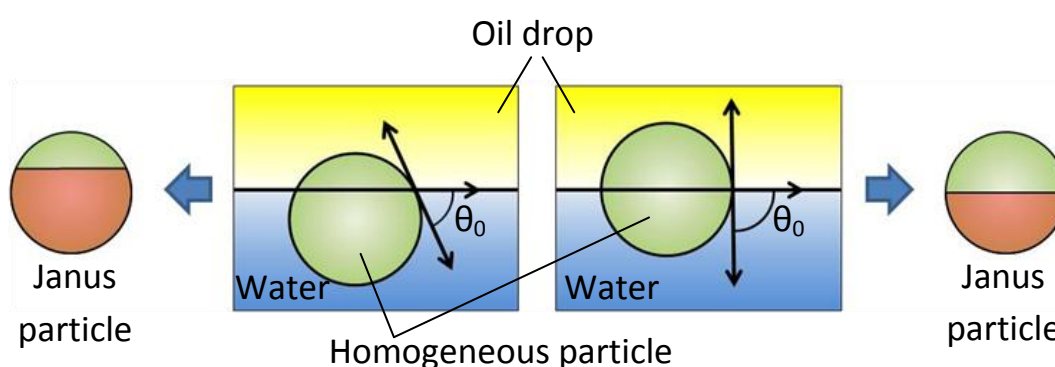


**Figure 1.13.** Diagram displaying how the initial particle contact angle,  $\theta_0$ , can be used to adjust the Janus balance of Janus particles produced using a solidified Pickering emulsion route.

A simple Pickering emulsion route pioneered by Granick et al.<sup>28,49</sup> uses molten paraffin wax as the disperse phase during emulsification which subsequently solidifies on cooling to leave silica particle coated wax beads. After modification of the exposed particle surfaces the wax is dissolved in chloroform to retrieve the Janus particles. Due to its relative simplicity and fine tuning capabilities, this approach has been adopted by other groups<sup>50,51</sup>. Wax emulsions have also been used for subsequent etching of the exposed particle surfaces<sup>52</sup>, producing particles that are anisotropic in both shape and surface chemistry. The disadvantage of using wax is that it is soluble in a range of solvents and has a low melting temperature so options for the treatment and modification of particles may therefore be restricted.

For the Pickering emulsion method polymerisable oils can be used as the disperse phase with styrene generally used in this role<sup>53,54</sup>, however the emulsion route can also be used without solidifying the droplets if the reactive chemical used to modify the particle surfaces is soluble in the continuous phase only<sup>55</sup>.

### *1.2.3 Properties of Janus particles*

Janus particles have been observed to gather at an interface between water and oil whereas bare or fully functionalised homogeneous particles disperse in one phase over the other<sup>28</sup>. Walther et al.<sup>56</sup> show that interfacial tension is significantly reduced in the presence of Janus disks making them ideal as emulsion stabilisers. Nanoscale Janus particles have been used as emulsion stabilisers to produce polystyrene particles<sup>57</sup>, and can be suitable for producing monodisperse polystyrene latex particles<sup>58</sup> where particle concentration can be used to control the size.

Janus particles can be shown to be stimuli-responsive when dispersed in solutions of varying pH as aggregation can occur to create large structures<sup>51</sup> or the particles may aggregate into chains<sup>55</sup> over certain pH ranges. Amphiphilic Janus fibres<sup>59</sup> and curved particles<sup>40</sup> spread at a water surface form apparently random structures where chaining and branching occur while the Janus fibres are also seen to twist around each other. A greater degree of self assembly is sometimes seen with amphiphilic particles with chains of particles formed aligning in the same direction<sup>44</sup> or aggregation into micelles at appropriate concentrations<sup>30,60,61</sup>.

Janus particles with a fluorescent hemisphere can be used as modulated optical nanoproboscopes (MOONs) with which the orientation can be followed based on the intensity of fluorescent light observed. These particles have been used to investigate rotation of particles due to Brownian motion<sup>62</sup> as well as changes in rotation influenced by nearby materials<sup>63</sup> or magnetic fields<sup>64</sup>. Magnetic fields have been shown to align disperse particles into chains<sup>65</sup> and near complete control of a

Janus particle can be achieved with three magnetic fields and optical trapping so that both the position and rotation of the particle can be controlled to a high degree<sup>46</sup>. Similar control of particle orientation using electrical switching can be used to make an optical display with coloured Janus particles<sup>36</sup>.

Finally, Bucaro et al.<sup>41</sup> used amphiphilic Janus disks coated with gold on one face which were suspended at the interface of an oil drop floating on water with the hydrophobic gold faces oriented upwards into the oil phase. This arrangement of closely packed gold disk faces acted as a mirror. The focal length of the mirror could be controlled by varying the contact angle formed by the oil droplet in the water, achieved with an applied voltage.

### **1.3 Particle-stabilised emulsions**

#### *1.3.1 General emulsion characteristics and stability*

When two immiscible liquids (e.g. water and oil) are mixed an emulsion is formed with droplets of one liquid (the disperse phase) within the other liquid (the continuous phase). Emulsion research has drawn a lot of attention as emulsions appear in many forms from food or cleaning products to cosmetics and industrial processes. Without some form of emulsifier present the droplets are expected to be unstable and swiftly combine until the individual bulk phases are separated. Emulsifiers, or surface active agents, can be in the form of molecules such as amphiphilic surfactants or colloidal particles. With emulsifiers present either a macro- or micro- emulsion can form. If the interfacial energy is high macro-emulsions tend to form which are thermodynamically unstable whereas micro-emulsions are thermodynamically stable emulsions and form spontaneously<sup>66</sup>. Micro-emulsions are not considered further in this thesis and so the term 'emulsions' will be used to mean macro-emulsions. Emulsions generally exist as either oil-in-water (o/w) or water-in-oil (w/o) emulsions, where the continuous

phase is water and oil respectively. The type of emulsion produced depends on the volume fraction of each phase and the emulsifier(s) used.

The emulsions are stabilised kinetically and are considered stable as long as the number, size and distribution of the droplets remains constant over the experimental timescale. Flocculation, creaming/sedimentation, coalescence and Ostwald ripening are the four main instabilities (Fig. 1.14) which lead to breakdown of an emulsion and may occur consecutively or simultaneously.

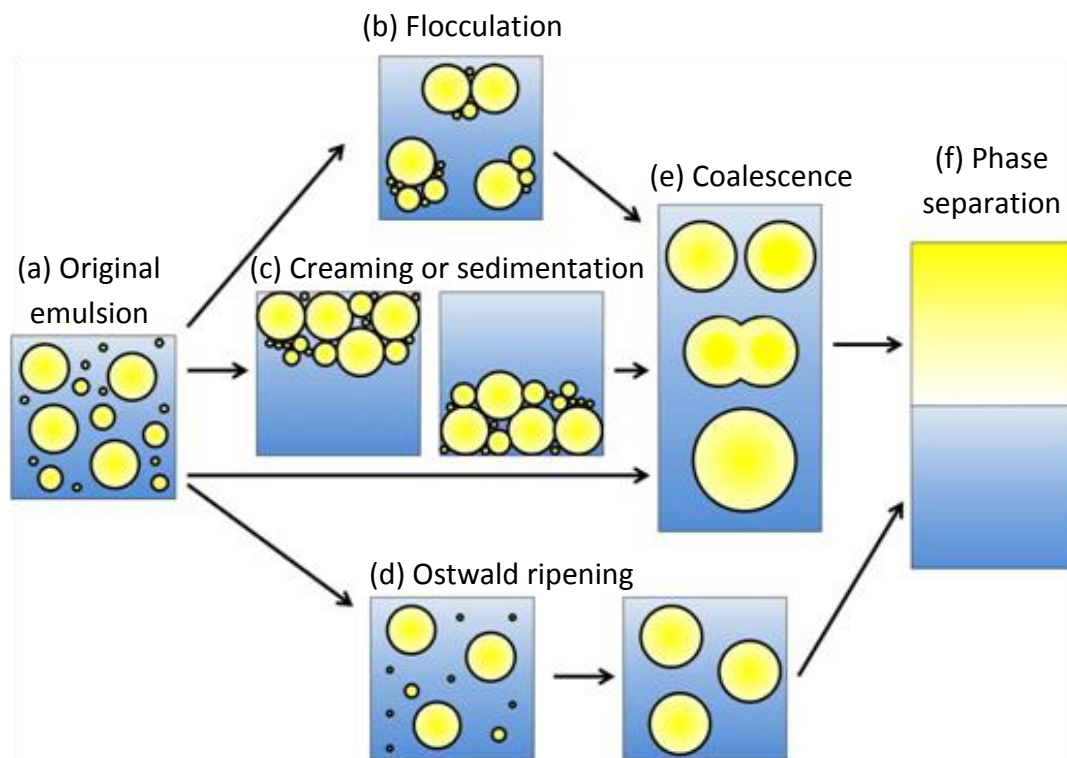


**Figure 1.14.** The different processes involved in the breakdown of an unstable emulsion. (Adapted from ref. 67)

With flocculation the droplets gather together in aggregates that are distributed throughout the emulsion volume, with the number of droplets remaining the same. Droplets coming into near contact act under DLVO theory and as such, if a negative potential energy exists the droplets will stick together. This process is reversible in that the flocculated droplets can be separated by gentle

agitation if the inter-drop forces are weak but will require more energy to break up the aggregates if the interactive forces are strong. Polydisperse samples where differently sized droplets cream (or sediment) at different rates have a greater chance of flocculation occurring because the droplets come into close proximity with greater frequency<sup>66</sup>. Excess surfactants can increase the rate of flocculation due to depletion attraction of droplets<sup>66</sup>. It occurs when droplets come close enough that surfactant micelles are excluded from the intervening film of continuous phase and an imbalance in concentration arises. This causes the intervening fluid to move into the bulk continuous phase to restore equilibrium concentration and draws the droplets together. Polymeric stabilisers can help to reduce flocculation if the chains protruding from the droplet surfaces prevent the droplets from approaching too near.

In an o/w emulsion creaming is the migration of the oil drops to the upper surface of the emulsion phase while sedimentation is present in w/o systems as the droplets migrate to the bottom of the emulsion phase. Creaming and sedimentation are gravity driven effects caused by differences in density between the continuous and the disperse phase, and will therefore be much more rapid with a larger density difference between phases. The creaming process can be slowed by reducing the density difference, increasing the viscosity of the continuous phase, or by creating smaller droplets which decreases the speed of creaming<sup>66</sup>. The rate of creaming can be increased by flocculation as the effective radius of the aggregated droplets is greater than that of the individual droplets. Creaming is also a reversible process.

Coalescence is an irreversible process in which two or more droplets combine together to produce a single larger droplet, which can lead to complete phase separation if the process repeats throughout the emulsion. Coalescence occurs when the droplets approach until the film of continuous phase separating them is thin enough to rupture. A number of factors can affect the rate of coalescence such as droplet interfacial tension, stabilising barriers around the droplets (such as surfactants or particles) and the viscosity of the continuous phase. The close

packing of flocculated and creamed emulsion drops can also increase the rate of coalescence. It has been suggested that coalescence occurs when molecular and thermal waves in the thin film separating the close droplets cause localised film thinning which leads to rupture<sup>66</sup>.

Ostwald ripening is another irreversible process, and arises due to differences in the aqueous phase solubility of oil in emulsion drops of varying size. More precisely, the oil in smaller drops are more soluble in the continuous phase than oil in the larger droplets<sup>66</sup>. This leads to the oil dissolving from the smallest droplets and diffusing through the continuous phase to then condense onto the larger droplets. The process causes the growth of larger droplets at the expense of smaller droplets and therefore an increase in average drop size and a decrease in drop count. Theoretically this would occur until just one drop remains but in practice as the average drop size increases, the rate of Ostwald ripening decreases. Stability against Ostwald ripening can be increased with suitable additives or by using a disperse phase which is less soluble in the continuous phase.

### *1.3.2 Emulsions stabilised by solid particles alone*

The surface activity and strong energy of attachment of particles make them ideal for use as emulsion stabilisers. Particle-stabilised emulsions, also known as Pickering emulsions<sup>1</sup> could be extremely stable (for years!). The great stability of these emulsions can be attributed to the strong energy of particle attachment to the oil-water interface. The particle wettability has a pronounced effect on the energy required to detach a particle from a liquid interface,  $\Delta G_d$ , which, for a spherical particle with radius  $r$ , is given by the equation<sup>1</sup>

$$\Delta G_d = \pi \gamma_{ow} r^2 (1 - |\cos\theta|)^2 \quad (1.4)$$

$\Delta G_d$  is greatest when the particles have medium wettability<sup>68</sup> (contact angles close to 90°) at which point the energy required to detach a particle from the

interface into either phase is several thousand times the thermal energy ( $kT$ ), even for very small particles with diameters  $\sim 10$  nm. Close to either extreme of wettability ( $0^\circ$  or  $180^\circ$ ) when the particle sits mostly in its preferred phase it can be detached from the interface with relative ease.

The particle wettability is also very important for the type of Pickering emulsion they can stabilise<sup>2</sup>. If the volumes of oil and aqueous phase are equal, hydrophilic particles (contact angle  $< 90^\circ$ ) will stabilise oil-in-water emulsions while hydrophobic particles (contact angle  $> 90^\circ$ ) will preferentially stabilise water-in-oil emulsions (Fig. 1.15). It is therefore expected that a phase inversion in the emulsion would occur if the particle wettability changed from hydrophilic to hydrophobic or vice versa (the so-called transitional phase inversion). For systems of unequal phase volumes a balance is achieved between emulsion type driven by the phase volumes and that of the particle wettability. Therefore, for example, hydrophobic particles may stabilise oil-in-water emulsions when the volume of water is greater than oil<sup>2</sup>. If a stable emulsion is formed and the system properties are subsequently changed by altering the liquid volume fractions a transition from one emulsion type to the other can occur which is called 'catastrophic inversion'<sup>2</sup>. The phase volume fractions at which the inversion occurs depends on the wettability of the stabilising particles and the nature of the oil<sup>2</sup>.

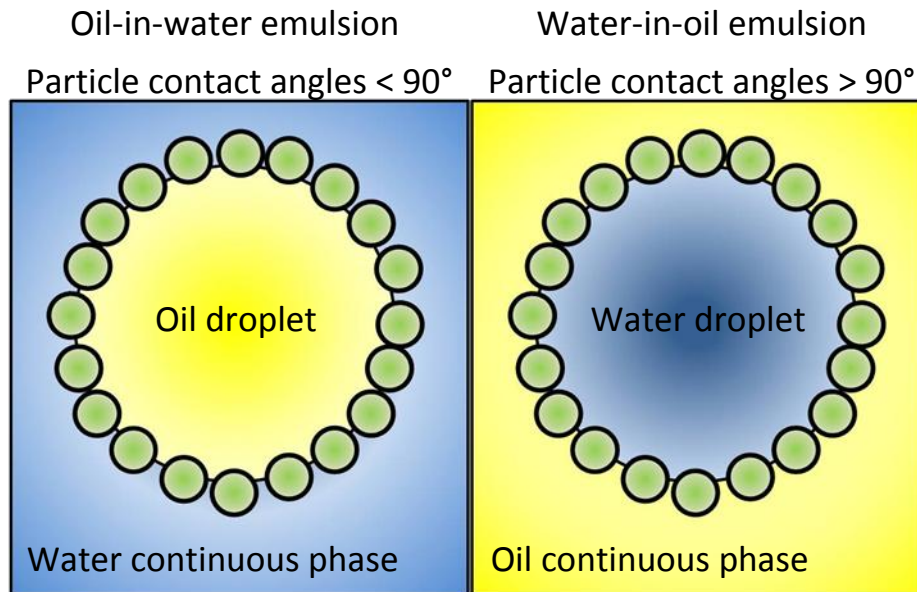
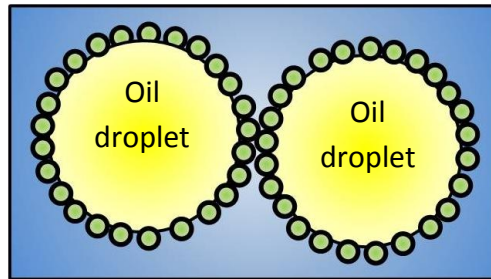


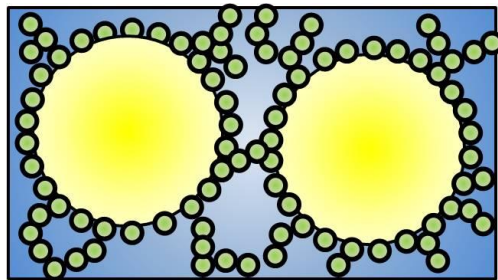
**Figure 1.15.** Diagram of Pickering emulsion drops stabilised with (left) hydrophilic particles and (right) hydrophobic particles.

Particles can act to stabilise emulsion drops in a variety of ways depending on the particle concentration in the emulsion. When the concentration of particles is high, and assuming particles with large free energy of attachment to the interface, it is expected that the droplet surfaces will be completely covered with a layer of particles (Fig. 1.16a). For droplet coalescence to occur the particles must be removed from the interface since the close packed layer on each droplet will form a physical barrier and lateral movement of the particles over the droplet surface is restricted<sup>67</sup>. The stability of the thin film separating droplets is also greater as film drainage is slowed and the capillary pressure needed to break the film is increased. If the particle concentration is sufficiently high it is also possible that a network of particles in the continuous phase between droplets can occur (Fig. 1.16b), preventing drops from coming into contact and slowing creaming of the emulsion.

(a) Bilayers of particles and thin liquid films separating droplets



(b) Networks of particles separating droplets



(c) Layer of bridging particles

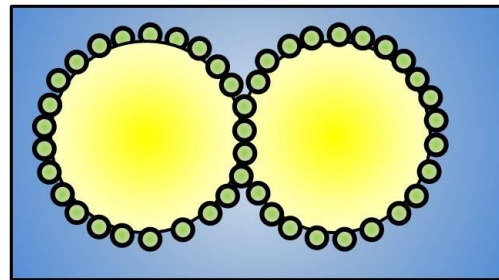


**Figure 1.16.** Diagram showing the possible mechanisms of emulsion stabilisation with colloidal particles. (Adapted from ref. 67)

When the particle coverage on emulsion drops is lower, stability may arise from particles forming smaller ‘islands’ or networks of particles around the droplets to act as barriers to coalescence. Particles of certain wettability may also bridge the film separating two emulsion drops (Fig. 1.16c). The bridging particles are simultaneously adsorbed at the interface of both droplets and can prevent the droplets from coming into contact, thus stabilising against coalescence. This is only beneficial when the particles preferentially sit more in the continuous phase. Bridging particles that sit more in the disperse phase or with contact angle of  $\sim 90^\circ$  bring the interface of both droplets into contact and will therefore encourage coalescence<sup>67</sup>.

### *1.3.3 Pickering emulsions from particle-surfactant mixtures*

When surfactants are used to make emulsions, increased stability may arise from a reduction in the interfacial tension<sup>69</sup> and Gibbs-Marangoni elasticity effects<sup>70,71</sup>. The concentration of surfactant is a key factor in determining the extent of these processes. Mixtures of particles and surfactant can offer great advantages in terms of stability under the right conditions. As described in section 1.1.2.1.2 surfactant adsorbs onto the particle surfaces with increasing surfactant concentration, first increasing, then decreasing the particle contact angle.

The behaviour of emulsions stabilised by a mixture of particles and surfactant is influenced by a balance of the interfacial tension, the particle contact angle and the particle surface charge, all of which vary with the surfactant concentration. The ability of particle-surfactant mixtures to stabilise emulsions is generally greater than that of the individual components over a range of surfactant concentrations, with the greatest stability observed when the particle contact angle is  $\sim 60 - 80^\circ$ <sup>12,72</sup>. At such surfactant concentrations where these particle contact angles are produced the energy of particle detachment from the interface is often high and particle flocculation in the continuous phase adds to stability against droplet coalescence. With increasing surfactant concentration a double phase inversion from o/w to w/o and back to o/w may occur due to changes in the particle wettability and surface charge caused by adsorption of the surfactant molecules<sup>12,73</sup>. The first inversion occurs when a monolayer of surfactant adsorbs onto the particles making them hydrophobic and relatively uncharged. Flocculation of particle dispersions is observed to be greatest at such surfactant concentrations where particles are most hydrophobic with very little surface charge. The second emulsion phase inversion relates to a bilayer of surfactant forming on particle surfaces with the head groups exposed, making the surfaces hydrophilic and highly charged. At surfactant concentrations above cmc the surfactant competes for the oil - water interface, greatly reducing the stabilising role of the particles<sup>74</sup>. The nature of the mechanisms involved in stability of emulsions by particle-surfactant mixtures are not yet fully understood, especially as the contact angles of particles within the surfactant

solutions has not presently been measured. Indeed indirectly measured contact angles have sometimes been at odds with that expected for the emulsion type and dispersion activity observed<sup>73</sup>.

#### **1.4 Particle-stabilised aqueous foams**

Aqueous foams are similar to emulsions in that they are made from immiscible phases mixed together, in this case a gas (usually air) is the non-aqueous phase and air bubbles are produced instead of droplets. Foams are also unstable without an added stabiliser. Foams with a gas volume fraction lower than 0.74 will mostly consist of spherical bubbles while foams with a volume fraction of gas greater than 0.74 will have bubbles which are polyhedral in shape with just a thin liquid film separating them.

The destabilising processes that occur in foams are similar to those which occur in emulsions. Much like 'creaming' the bubbles will rise to the liquid surface, often becoming closely packed, the film separating bubbles can rupture leading to bubble 'coalescence' and similarly to 'Ostwald ripening' the gas molecules may diffuse through the disjoining liquid films in a process termed 'disproportionation'<sup>72</sup>. In foams the migration of bubbles to the liquid surface is followed by the drainage of liquid from the volume of foam due to gravitational forces. This drainage causes tighter packing of the bubbles as the films separating the bubbles become thinner. After the films thin to micrometer thickness the rate of drainage due to gravity reduces greatly and becomes the less predominant factor<sup>70</sup>. For thinner liquid films the predominant factor for drainage is ejection of liquid to plateau borders between bubbles. This is because the pressure in the planar region of bubble contact is uniform but not in the plateau borders where the interface is curved, creating a capillary pressure which acts to thin the films. The liquid may also evaporate from the upper portion of the foam which further thins the stabilising films.

Particle stabilised foams can offer some advantages over foams stabilised by surfactants, especially with regards to foam lifetime<sup>75</sup>. The rigid shell of stabilising particles surrounding the bubbles takes a lot of energy to displace, aiding stability against coalescence and diffusion of gas across the thin film<sup>76</sup>. As the bubbles shrink in size due to disproportionation the particles at the interface become tightly packed, preventing lateral movement of the particles (improving stability to coalescence) and eventually reaches a point where further shrinking would require expulsion of particles from the interface. At this point the bubble can become misshaped as the surface is stressed<sup>77</sup> and leads to a reduction in Laplace pressure which can halt diffusion of gas from the bubble. With higher concentrations of particles extra stability is also achieved by particles forming networks between foam bubbles affecting film drainage and thinning<sup>76</sup>.

The ability of particles to stabilise foams varies with contact angle and has been shown<sup>78</sup> to be optimal at intermediate hydrophobicities and poor for very hydrophilic or hydrophobic particles. At and above 90° the maximum capillary pressure needed to rupture films stabilised by bridging particles drops to zero so the films would be unstable<sup>79</sup>. However at lower contact angles where the maximum capillary pressure to rupture films is higher, the energy of particle attachment to the interface is low. The optimum stability of the foam occurs when the contact angle is balanced between these opposing effects. The maximum capillary pressure required for film rupture is higher for bilayers of particles, for which the pressure drops to zero at 129° rather than 90°<sup>79</sup>. This means that slightly hydrophobic particles can stabilise foams but will benefit from a higher particle concentration to encourage bilayers over bridging monolayers between bubbles. Similarly, smaller particles should stabilise the films better with higher maximum capillary pressure for rupture<sup>79</sup>, however this is counterbalanced by the lower energy of attachment to the interface<sup>80</sup>. Therefore the optimum particle size for stabilising foams is also a balance between the opposing effects.

## 1.5 Motivation and aims of the thesis

The contact angle of solid particles at the liquid-fluid interface is a key parameter in particle-stabilised foams and emulsions. It determines the foaming or antifoam action of solid particles<sup>1,76,78</sup>, the emulsion type<sup>1,2,67,80</sup>, and affects the mechanism of stabilisation in particle-stabilised emulsions<sup>67,79</sup>. Despite the great importance of the particle contact angle its direct measurement is difficult because of the small particle size. In the existing literature, important conclusions for the effect of particle contact angle on the particle behaviour in solid-stabilised foams and emulsions have been made using indirect information about the particle wettability. For example, the widely accepted rule that hydrophilic particles stabilise oil-in-water (o/w) emulsions, while hydrophobic particles give water-in-oil (w/o) emulsions<sup>1,2</sup> has been deduced from indirect measurements of the particle contact angle values on a macroscopic piece of material with similar surface chemistry<sup>12,73</sup> or deduced from the chemical composition of the particle surface<sup>2</sup>. Therefore, one of our aims in the present study is to develop the Film Calliper Method (FCM) for measuring particle contact angles at oil - water interfaces; to investigate the type of particle-stabilised emulsions and link it to the contact angle values measured directly on the particle surface by the FCM.

Most of the particle-stabilised foam and emulsion systems used in practice contain surfactants. The roles of surfactant and particle combinations when stabilising emulsions and foams is not yet fully understood. Therefore a significant part of the present work aims to reveal the link between the wettability of the particles, their stabilising ability and mechanisms of stabilisation in foams and emulsions from particle-surfactant mixtures. This is achieved by investigating foams and emulsions of silica particle and cationic surfactant mixtures and measuring the particle contact angles directly on the particle surface using the FCM.

Janus particles with dual wettability have received a lot of scientific interest over recent years<sup>33,37,47,49</sup>. It is widely believed that such particles will provide, among other things, advantages to particle-stabilised foams and emulsions<sup>29,56-58</sup>. It has

been shown theoretically that amphiphilic Janus particles should be superior to homogeneous particles in stabilising emulsions<sup>29</sup>. Nevertheless, the ability of Janus particles to stabilise emulsions has not been systematically investigated. To develop a method for making significant amounts of amphiphilic Janus particles with controlled structure and investigate their ability to stabilise emulsions are also amongst the main objectives of this thesis.

## **1.6 Outline of thesis**

The rest of this Thesis is structured as follows:

Chapter 2 summarises the materials and procedures used for the work presented. Chapter 3 details the work performed to further develop the Film Calliper Method for use with a range of particles at water and air or oil interfaces. Measurements at water-air and water-oil interfaces were carried out using latex particles with varying size and surface structure, silica particles which had been pre-treated to alter the wettability and silica particles in surfactant solution. The systems measured were used to produce emulsions and relationships are drawn between the emulsion types and contact angles measured.

The work on combinations of silica particles and surfactant is further extended in chapter 4. Two separate cationic surfactants were used to investigate changing system characteristics with varying surfactant concentration, such as the solution surface tension or particle contact angle. These are linked to surfactant adsorption on the particle surface for one of the surfactants used. Foams and emulsions were made which displayed synergistic behaviour between the particles and surfactant, greatly enhancing the stabilising properties. The changes observed between samples with and without particles are then linked to the measured particle properties.

Chapter 5 details the development of a method for producing large quantities of particles with dual wettability and work performed in refining the method. Examples of Janus particles produced are presented to show the control and flexibilities of the method. The chapter is finished off with an investigation into amphiphilic particles and their use as emulsion stabilisers.

The final chapter of the thesis summarises the conclusions made and presents ideas for future work. The references used throughout the thesis are listed at the end of the chapter they were respectively used in.

## 1.7 References

1. B. P. Binks and T. S. Horozov, *Colloidal Particles at Liquid Interfaces*, Cambridge University Press (Cambridge), 2006, p. 1-74.
2. R. Aveyard, B.P. Binks and J.H. Clint, *Adv. Colloid Interfac.*, 2003, **100-102**, 503.
3. A. Ulman, *Chem. Rev.*, 1996, **96**, 1533.
4. S. Onclin, B. J. Ravoo and D. N. Reinhoudt, *Angew. Chem. Int. Edit.*, 2005, **44**, 6282.
5. T. S. Horozov, R. Aveyard, J. H. Clint, and B. P. Binks, *Langmuir*, 2003, **19**, 2822.
6. J. Eastoe in, *Colloid Science: Principles, Methods and Applications*, T. Cosgrove, ed., Blackwell Publishing (Oxford), 2005, p.50 - 56.
7. P. W. Atkins, *Physical Chemistry: sixth edition*, Oxford University Press (Oxford), 2000, p. 704.
8. L.K. Koopal, T. Goloub, A. de Keizer and M.P. Sidorova, *Colloid. Surface. A*, 1999, **151**, 15.
9. R. Atkin, V.S.J. Craig, E.J. Wanless and S. Biggs, *Adv. Colloid Interfac.*, 2003, **103**, 219.
10. D.W. Fuerstenau and R. Jia, *Colloid. Surface. A*, 2004, **250**, 223.
11. B.P. Binks, J.A. Rodrigues and W.J. Frith, *Langmuir*, 2007, **23**, 3626.
12. Z.-G. Cui, L.-L. Yang, Y.-Z. Cui and B.P. Binks, *Langmuir*, 2010, **26 (7)**, 4717.
13. E. W. Washburn, *Phys. Rev.* 1921, **17**, 374.
14. C. J. van Oss, R. F. Giese, Z. Li, K. Murphy, J. Norris, M. K. Chaudhury and R. J. Good, *J. Adhes. Sci. Technol.*, 1992, **6 (4)**, 413.
15. N. Yan, Y. Maham, J. H. Masliyah, M. R. Gray and A. E. Mather, *J. Colloid Interf. Sci.*, 2000, **228**, 1.
16. D. R. Lloyd, T. C. Ward and H. P. Schrieber, *Inverse Gas Chromatography: Characterisation of Polymers and Other Materials*, American Chemical Society (Washington), 1989.
17. G. Gillies, K. Büscher, M. Preuss, M. Kappl, H.-J. Butt and K. Graf, *J. Phys.-Condens. Mat.*, 2005, **17**, S445.
18. Z. Horvolgyi, S. Nemeth and J. H. Fendler, *Colloid. Surface. A*, 1993, **71**, 327.
19. R. Aveyard, J. H. Clint, D. Nees and V. N. Paunov, *Langmuir*, 2000, **16**, 1969.

20. V. N. Paunov, *Langmuir*, 2003, **19**, 7970.
21. O. J. Cayre and V. N. Paunov, *Langmuir*, 2004, **20**, 9594.
22. L.N. Arnaudov, O.J. Cayre, M.A. Cohen Stuart, S.D. Stoyanov and V.N. Paunov, *Phys. Chem. Chem. Phys.*, 2010, **12**, 328.
23. A. Hadjiiski, R. Dimova, N. D. Denkov, I. B. Ivanov and R. Borwankar, *Langmuir*, 1996, **12**, 6665.
24. I. B. Ivanov, A. Hadjiiski, N. D. Denkov, T. D. Gurkov, P. A. Kralchevsky and S. Koyasu, *Biophys. J.*, 1998, **75**, 545.
25. A. Hadjiiski, S. Tcholakova, I. B. Ivanov, T. D. Gurkov and E. F. Leonard, *Langmuir*, 2002, **18**, 127.
26. T. S. Horozov, D. A. Braz, P. D. I. Fletcher, B. P. Binks and J. H. Clint, *Langmuir* 2008, **24**, 1678.
27. C. Casagrande, P. Fabre, E. Raphael and M. Veyssie, *Europhys. Lett.*, 1989, **9**, 251.
28. S. Jiang and S. Granick, *Langmuir*, 2008, **24**, 2438.
29. B. P. Binks and P. D. I. Fletcher, *Langmuir*, 2001, **17**, 4708.
30. R. Erhardt, M. Zhang, A. Boker, H. Zetti, C. Abetz, P. Frederik, G. Krausch, V. Abetz and A. H. E. Muller, *J. Am. Chem. Soc.*, 2003, **125**, 3260.
31. L. Hong, A. Cacciuto, E. Luijten and S. Granick, *Nano Lett.*, 2006, **6**, 2510.
32. A. K. F. Dyab and V. N. Paunov, *Mater. Res. Soc. Symp. P.*, 2009, 1135.
33. J. N. Anker and R. Kopelman, *Appl. Phys. Lett.*, 2003, **82**, 1102.
34. C. Chen, R. K. Shah, A. R. Abate and D. A. Weitz, *Langmuir*, 2009, **25**, 4320.
35. Z. Nie, W. Lei, M. Seo, S. Xu and E. Kumacheva, *J. Am. Chem. Soc.*, 2009, **128**, 9408.
36. T. Nisisako, T. Torii, T. Takahashi and Y. Takizawa, *Adv. Mater.*, 2006, **18**, 1152.
37. A. Perro, S. Reculosa, S. Revaine, E. Bourgeat-Lami and E. Duguet, *J. Mater. Chem.*, 2005, **15**, 3745.
38. O. D. Velev, A. M. Lenhoff and E. W. Kaler, *Science*, 2000, **287**, 2240.
39. A. K. F. Dyab, M. Ozmen, M. Ersoz and V. N. Paunov, *J. Mater. Chem.*, 2009, **19**, 3475.
40. A. B. D. Brown, C. G. Smith and A. R. Rennie, *Phys. Rev. E*, 2000, **62**, 951.

41. M. A. Bucaro, P. R. Kolodner, J. A. Taylor, A. Sidorenko, J. Aizenberg and T. N. Krupenkin, *Langmuir*, 2009, **25**, 3876.
42. S. Gangwal, O. J. Cayre and O. D. Velev, *Langmuir*, 2008, **24**, 13312.
43. C. J. Behrend, J. N. Anker and R. Kopelman, *Appl. Phys. Lett.*, 2004, **84**, 154.
44. O. Cayre, V. Paunov and O. D. Velev, *J. Mater. Chem.*, 2003, **13**, 2445.
45. Z. Bao, L. Chen, M. Weldon, E. Chandross, O. Cherniavskaya, Y. Dai and J. B.–H. Tok, *Chem. Mater.*, 2002, **14**, 24.
46. R. M. Erb, N. J. Jenness, R. L. Clark and B. B. Yellen, *Adv. Mater.*, 2009, **21**, 1.
47. V. N. Paunov and O. J. Cayre, *Adv. Mater.*, 2004, **16**, 788.
48. V. N. Paunov and O. J. Cayre in, *Nanostructured and Advanced Materials*, A. Vaseashta, D. Dimova-Malinovska and J. M. Marshall, eds., Springer (Dordrecht), 2005, p. 365.
49. L. Hong, S. Jiang and S. Granick, *Langmuir*, 2006, **22**, 9495.
50. A. Perro, F. Meunier, V. Schmitt and S. Ravaine, *Colloid Surface A*, 2009, **332**, 57.
51. S. Berger, A. Synytska, L. Ionov, K.-J. Eichhorn and M. Stamm, *Macromolecules*, 2008, **41**, 9669.
52. B. Liu, C. Zhang, J. Liu, X. Qu and Z. Yang, *Chem. Commun.*, 2009, **26**, 3871.
53. Y. He and K. Li, *J. Colloid Interf. Sci.*, 2007, **306**, 296.
54. J. Zhang, X. Wang, D. Wu, L. Liu and H. Zhao, *Chem. Mater.*, 2009, **21**, 4012.
55. D. Suzuki, S. Tsuji and H. Kawaguchi, *J. Am. Chem. Soc.*, 2007, **129**, 8088.
56. A. Walther, X. Andre, M. Drechsler, V. Abetz and A. H. E. Muller, *J. Am. Chem. Soc.*, 2007, **129**, 6187.
57. Y. K. Takahara, S. Ikeda, S. Ishino, K. Tachi, K. Ikeue, T. Sakata, T. Hasegawa, H. Mori, M. Matsumura and B. Ohtani, *J. Am. Chem. Soc.*, 2005, **127**, 6271.
58. A. Walther, M. Hoffman and A. H. E. Muller, *Angew. Chem. Int. Edit.*, 2008, **47**, 711.
59. A. Walther, M. Drechsler, S. Rosenfeldt, L. Harnau, M. Ballauf, V. Abetz and A. H. E. Muller, *J. Am. Chem. Soc.*, 2009, **131**, 4720.
60. D. Lanson, M. Schappacher, R. Borsali and A. Deffieux, *Macromolecules*, 2007, **40**, 5559.
61. K. Ishizu, J. Satoh, K. Toyoda and A. Sogabe, *J. Mater. Sci.*, 2004, **39**, 4295.

62. C. Behrend, J. N. Anker, B. H. McNaughton, M. Brasuel, M. A. Philbert and R. Kopelman, *J. Phys. Chem. B.*, 2004, **108**, 10408.
63. J. Choi, Y. Zhao, D. Zhang, S. Chien and Y.H. Lo, *Nano Lett.*, 2003, **3**, 995.
64. C. J. Behrend, J. N. Anker, B. H. McNaughton and R. Kopelman, *J. Magn. Magn. Mater.*, 2005, **293**, 663.
65. N. Zhao and M. Gao, *Adv. Mater*, 2009, **21**, 184.
66. B. P. Binks, *Modern Aspects of Emulsion Science*, Royal Society of Chemistry (Cambridge), 1998, p. 1-33.
67. R. J.G. Lopetinsky, J. H. Masliyah and Z. Xu "Solids - Stabilized Emulsions: A Review" in, *Colloidal Particles at Liquid Interfaces*, B. P. Binks and T. S. Horozov, eds., Cambridge University Press (Cambridge), 2006, p. 186-224.
68. T.S. Horozov, B.P. Binks, R. Aveyard and J.H. Clint, *Colloid. Surface. A*, 2006, **282-283**, 377.
69. D. Weaire and S. Hutzler, *The Physics of Foams*, Clarendon Press (Oxford), 1999
70. D. J. Shaw, *Introduction to Colloid and Surface Chemistry: 4<sup>th</sup> Edition*, Butterworth-Heinemann (Oxford), 2000, p. 272.
71. L. L. Schramm, *Emulsions, Foams and Suspensions*, Wiley VCH (Weinheim), 2005, p. 89.
72. T. N. Hunter, R. J. Pugh, G. V. Franks and G. J. Jameson, *Adv. Colloid Interfac.*, 2008, **137**, 57.
73. B. P. Binks and J. A. Rodrigues, *Angew. Chem. Int. Edit.*, 2007, **119**, 5485.
74. B. P. Binks, M. Kirkland and J. A. Rodrigues, *Soft Matter*, 2008, **4**, 2373.
75. Z. Du, M. P. Bilbao-Montoya, B. P. Binks, E. Dickinson, R. Ettelaie and B. S. Murray, *Langmuir*, 2003, **19**, 3106.
76. T. S. Horozov, *Curr. Opin. Colloid In.*, 2008, **13**, 134.
77. A. B. Subramaniam, C. Mejean, M. Abkarian and H. A. Stone, *Langmuir*, 2006, **22**, 5986.
78. B. P. Binks and T. S. Horozov, *Angew. Chem. Int. Edit.*, 2005, **117 (24)**, 3788.
79. G. Kaptay, *Colloid Surface. A*, 2006, **282-283**, 387.
80. B. P. Binks, *Curr. Opin. Colloid In.*, 2002, **7**, 21.

## Chapter 2

### Experimental

#### 2.1 Materials

##### *2.1.1 Solid particles*

##### *2.1.1.1 Silica particles*

Precipitated silica particles were obtained from two sources in the form of dry powders with a range of sizes and narrow size distributions. Silica particles with diameters 0.5, 0.7 and 1.0  $\mu\text{m}$  were purchased from Fiber Optic Center Inc., USA - via Blue Helix, UK. The manufacturer quotes particle density of 1.8  $\text{g}/\text{cm}^3$ , purity of > 99.9 % and standard deviation of the particle size smaller than 10 %. Scanning electron microscope (SEM) images of these particles are shown in Fig. 2.1. To clean these particles they were dispersed in 25 ml ethanol (analytical grade, Fisher Scientific) and put in an ultrasonic bath (Grant Ultrasonic bath MXB6) for ten minutes. After sedimenting the dispersion with a bench centrifuge (Baird + Tatlock Auto bench centrifuge, Mark IV) the ethanol was removed and replaced with milli-Q water (25 ml). The process was repeated until the particles had been washed with three lots of fresh milli-Q water after which the water was removed and the particles were dried in an oven overnight.

Monodisperse silica particles with diameters  $2.76 \pm 0.15 \mu\text{m}$ ,  $5.84 \pm 0.26 \mu\text{m}$  and  $7.75 \pm 0.29 \mu\text{m}$  were purchased from microParticles GmbH and used as received (Fig. 2.1).

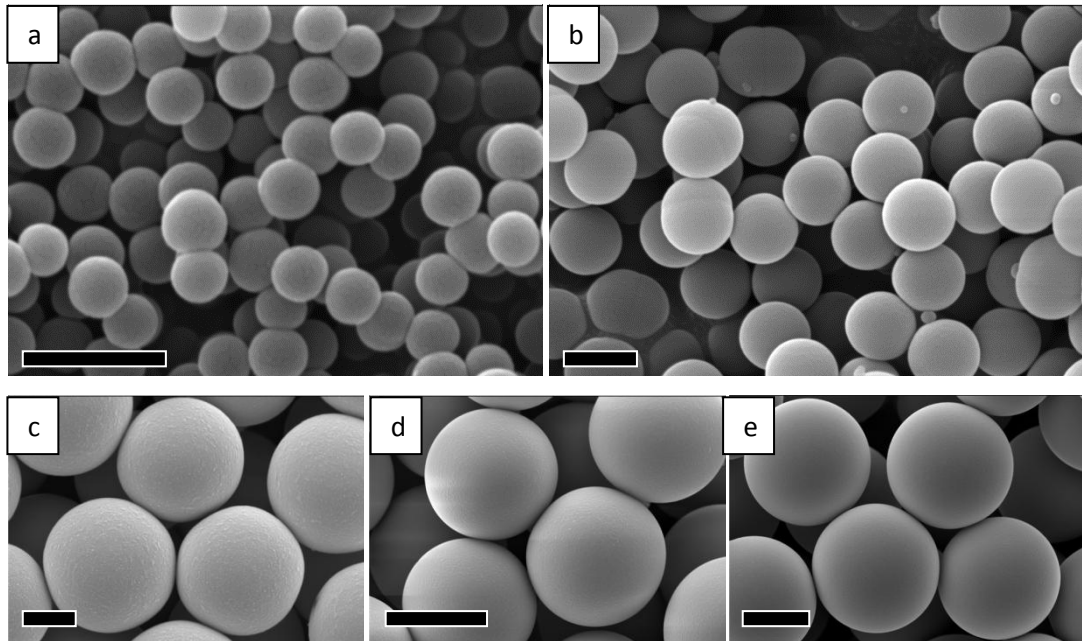


**Figure 2.1.** SEM images of silica particles used in this thesis, shown as received. Particles from Blue helix in sizes of 0.5  $\mu\text{m}$  (a) and 1  $\mu\text{m}$  (b) are shown with the 2.76  $\mu\text{m}$  (c), 5.84  $\mu\text{m}$  (d) and 7.75  $\mu\text{m}$  (e) particles from microparticles GmbH. Scale bars are 1  $\mu\text{m}$  in images a-c and 4  $\mu\text{m}$  in images d and e.

#### *2.1.1.2 Latex particles*

Two series of monodisperse latex particles with different functionality and diameters in the range 0.9 - 6.0  $\mu\text{m}$  were used as received from Invitrogen Molecular Probes (Table 2.1). Carboxylate modified polystyrene latex (CML) particles have surface carboxyl groups and according to the supplier are hydrophilic and negatively charged in water. Polystyrene sulphate latex (SL) particles are also negatively charged and classified as hydrophobic latex by the supplier. Both types of latex particle were supplied as aqueous dispersions in purified surfactant-free water.

**Table 2.1.** Properties of carboxylate modified latex (CML) and sulphate latex (SL) particles from Invitrogen Molecular Probes (data supplied by the manufacturer). The surface groups per particle refer to carboxyl groups (-COOH) on the CML particles and sulphate groups (SO<sub>4</sub><sup>-</sup>) on the SL particles.

| Latex type | Diameter / $\mu\text{m}$ | Number of surface groups per particle | Area per surface group / $\text{nm}^2$ |
|------------|--------------------------|---------------------------------------|--|
| CML        | $0.90 \pm 0.02$          | $5.5 \times 10^6$                     | 0.46                                   |
| CML        | $1.20 \pm 0.02$          | $3.5 \times 10^7$                     | 0.13                                   |
| CML        | $2.00 \pm 0.04$          | $4.1 \times 10^8$                     | 0.03                                   |
| CML        | $3.00 \pm 0.09$          | $3.0 \times 10^8$                     | 0.09                                   |
| CML        | $6.00 \pm 0.51$          | $2.3 \times 10^9$                     | 0.05                                   |
| SL         | $0.89 \pm 0.03$          | $9.9 \times 10^5$                     | 2.51                                   |
| SL         | $1.80 \pm 0.04$          | $4.3 \times 10^6$                     | 2.37                                   |
| SL         | $2.90 \pm 0.12$          | $1.0 \times 10^7$                     | 2.64                                   |
| SL         | $5.60 \pm 0.39$          | $4.0 \times 10^7$                     | 2.46                                   |

Poly(glycerol monomethacrylate)-Polystyrene (PGMA-PS) latex particles with different sizes and degree of polymerisation (DP) of PGMA were synthesised<sup>1</sup> and supplied by Professor Steve Armes' research group at Sheffield University (Table 2.2). To synthesize these particles PGMA macromonomer was first dissolved in a mixture of methanol and water and heated. Azobisisobutyronitrile (AIBN) initiator dissolved in styrene was added to the reaction vessel and then the solution was stirred for 24 h at 70 °C. The resulting latex was purified by three centrifugation /redispersion cycles into methanol followed by three cycles replacing each decanted supernatant with deionised water.

**Table 2.2.** Summary of PGMA-PS latexes prepared by alcoholic dispersion polymerisation using azobisisobutyronitrile (AIBN) initiator at 70 °C. The AIBN wt.% values are relative to the amount of styrene used. Particle diameters are measured by Disk Centrifuge Photosedimentometry (DCP).

| Sample code | Stabiliser type    | MeOH :H <sub>2</sub> O mixture | AIBN /wt.% | Stabiliser /wt.% | Monomer conversion /% | Solids content after purification /% | DCP diameter /nm |
|-------------|--------------------|--------------------------------|------------|------------------|-----------------------|--------------------------------------|------------------|
| AW54        | PGMA <sub>70</sub> | 90:10                          | 1          | 2.5              | 61                    | 4.28                                 | 796 ± 167        |
| KLT208      | PGMA <sub>50</sub> | 90:10                          | 1          | 10               | 100                   | 9.60                                 | 834 ± 65         |
| AW52        | PGMA <sub>30</sub> | 98:2                           | 1          | 10               | 60                    | 4.87                                 | 820 ± 90         |

### 2.1.2 Materials used in contact angle measurements, foams and emulsions

Oils used in contact angle measurements and emulsions are summarised in Table 2.3. Before use they were passed 3 times through basic alumina (99 %, Acros Organics) to remove polar impurities.

**Table 2.3.** Summary of oils used for contact angle measurements and emulsions. Oil properties are from the suppliers with densities specified for 25 °C.

| Oil                           | Supplier            | Purity /% | Density /g cm <sup>-3</sup> | Refractive index |
|-------------------------------|---------------------|-----------|-----------------------------|------------------|
| Decahydronaphthalin (decalin) | Sigma-Aldrich       | 98        | 0.896                       | 1.474            |
| Dodecane                      | Lancaster synthesis | 99+       | 0.749                       | 1.422            |

The cationic surfactants tetradecyltrimethylammonium bromide (TTAB, 99 %, Sigma, Fig. 2.2) and cetylpyridinium chloride (CPC, Sigma, Fig. 2.3) were used in contact angle measurements, foams and emulsions. TTAB with a critical micelle concentration of 3.5 mM at room temperature<sup>2-5</sup>, was used at various concentrations between  $5 \times 10^{-4}$  and 30 mM.

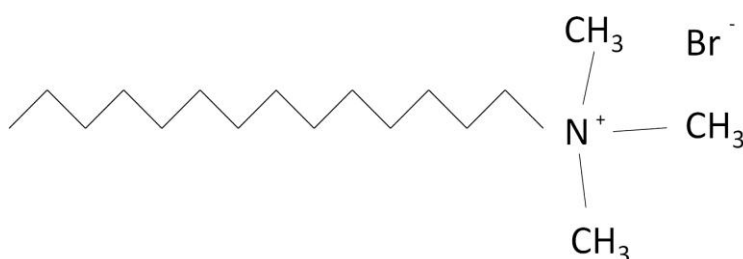


**Figure 2.2.** Molecular structure of tetradecyltrimethylammonium bromide (TTAB)

Cetylpyridinium chloride (CPC) with critical micelle concentration of 0.9 mM<sup>6-8</sup> was used at concentrations between 0.01 and 5 mM.

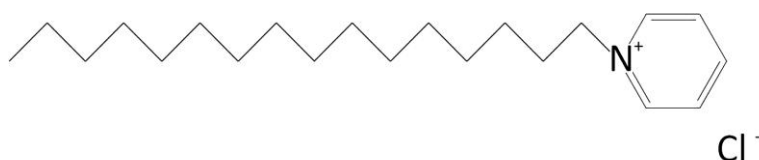


**Figure 2.3.** Molecular structure of cetylpyridinium chloride (CPC)

### *2.1.3 Materials used in the preparation of Janus particles*

Polymerisable oils (monomers) such as styrene and methacrylates (see table 2.4) were used in polymerisable Pickering emulsions with silica particles and azobisisobutyronitrile (AIBN, 98 %, Acros Organics) as thermo-initiator. Before use,

the monomers were passed through basic alumina to remove polymerisation inhibitors and impurities.

**Table 2.4.** Summary of polymerisable oils used to make Pickering emulsions for the preparation of Janus particles. Included are the densities of the monomers (at 25 °C), provided by the supplier and the glass transition temperatures ( $T_g$ ) of the homopolymers<sup>9</sup>. ( $T_g$  for stearyl methacrylate from ref. 10)

| Monomer                   | Supplier       | Purity /%       | Density /g cm <sup>-3</sup> | Polymer $T_g$ /°C |
|---------------------------|----------------|-----------------|-----------------------------|-------------------|
| Butyl methacrylate        | Acros Organics | 99              | 0.894                       | 20                |
| Isobutyl methacrylate     | Aldrich        | 97              | 0.886                       | 53                |
| 2-ethylhexyl methacrylate | Acros Organics | 99              | 0.884                       | -10               |
| Stearyl methacrylate      | Aldrich        | Technical grade | 0.864                       | 38                |
| Styrene                   | Sigma-Aldrich  | ≥ 99            | 0.906                       | 100               |

Tollen's reagent (made using the procedure detailed in section 2.2.11) was used to make Janus particles with a silver hemisphere. The materials used in the preparation of this were silver nitrate (≥ 99 %, Alfa Aesar), potassium hydroxide (laboratory grade, Fisher Scientific), d-glucose (anhydrous, analytical grade, Fisher Scientific) and ammonia solution (33 w/w, Prime Chemicals) were used. Silica particles were also treated with 3-Aminopropyltriethoxysilane (APTES, Fluorochem) and then Rhodamine B isothiocyanate (mixed isomers, > 70 %, Aldrich) to make fluorescent Janus particles. Chloroform (laboratory grade, Fisher Scientific) was used to dissolve the polymers and retrieve the Janus particles.

#### *2.1.4 Other chemicals used*

A solution of dichlorodimethylsilane (DCDMS, 99.5 %, Fluka) in anhydrous toluene (99.8 %, Sigma-Aldrich) was used to hydrophobise silica particles and slides. Nitric acid (70 %, laboratory grade, Fisher Scientific) was used to hydrophilise silica particles and slides and was also used to clean glassware for the Tollen's reagent. Sodium hydroxide (analytical grade, Fisher Scientific) and hydrochloric acid (HCl, 36 %, analytical grade, Fisher Scientific) were used to change the pH of particle dispersions for the measurement of zeta potential without added background electrolyte.

Fluorescent dyes were used with select TTAB emulsions to determine the emulsion type. Fluorescein 5(6)-isothio-cyanate (90 %, Sigma-Aldrich) in water was used to dye the aqueous phase and Nile red dye (technical grade, Sigma) dissolved in acetone (99.98 %, Fisher Scientific) was used to dye the oil phase.

Methanol (analytical grade, Fisher Scientific) was used to aid the spreading of particles at aqueous surfaces for contact angle measurements. Ethanol (analytical grade, Fisher Scientific) and isopropanol (analytical grade, Fisher Scientific) were used to clean equipment and silica particles or glass slides. Sulfochromic acid was made using sulphuric acid (> 95 %, analytical grade, Fisher Scientific) and potassium dichromate (> 99 %, Sigma-Aldrich) and was used to clean glassware in preparation for contact angle measurements with the Film Calliper Method (FCM).

Experiments were performed using deionised water with resistivity of ~18 M $\Omega$  cm obtained by treating water through an Elgastat Prima reverse osmosis unit and then a Millipore Milli-Q reagent water system. Aqueous phase in some experiments contained sodium chloride (NaCl, 99.5 %, BDH) as background electrolyte.

## 2.2 Experimental procedures and methods

### 2.2.1 Hydrophobisation of silica particles

Particles of varying hydrophobicity were desired for making emulsions and as templates for Janus particles. These particles were produced by hydrophobising the surface of silica particles with a silanising agent. Solutions of dichlorodimethylsilane (DCDMS) in toluene were used for this procedure. Different extents of hydrophobicity were achieved by changing the concentration of DCDMS. For more information on DCDMS concentrations used (up to 0.2M) and the resultant contact angles measured see section 3.3.2.1.

To get an approximate measure of the degree of hydrophobicity of the silica particles after the procedure, glass microscope slides were treated simultaneously in the same solutions for the duration of the procedure. As the materials are similar an idea of the surface contact angle can be determined with sessile water drops on the large flat surface of the slides. The microscope slides were initially cut in half long ways (in order to fit into the procedure vessels) and then cleaned by sonication in isopropanol and then de-ionised water before drying in an oven.

The DCDMS in anhydrous toluene solutions were first prepared in volumetric flasks to varying concentrations with approximately 36 ml of the solutions to be used in each sample vessel. Clean volumetric flasks were pre-treated to hydrophobise the inner surface by sealing the flasks overnight with 0.5 ml DCDMS inside. The flasks were cleaned after this to remove excess DCDMS using chloroform and ethanol and were then left to dry naturally before the DCDMS/toluene solutions were put in them. The pre-treatment of the flasks helped to keep them moisture free and meant that on addition of the DCDMS solution no hydrophobisation of the flasks would take place which could have altered the solution concentration.

The vessels used for the silanisation reaction and subsequent cleaning were Oak Ridge Teflon® centrifuge tubes supplied by Nalgene. These vessels are resistant to many chemicals while also able to withstand temperatures up to 200 °C and high centrifugation speeds. Each sample was set up in a centrifuge tube as shown below in Fig. 2.4 which is presented to aid the description of the method.

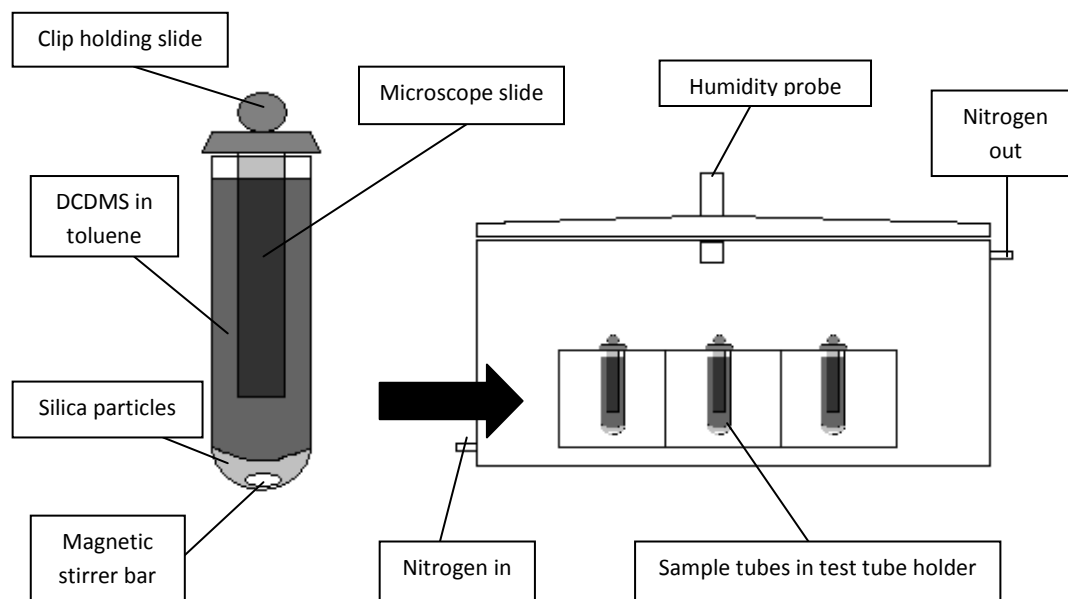


**Figure 2.4.** Schematic of the experimental setup used for the hydrophobisation of silica particles. On the left is the centrifuge tube which contains the particles and the silanising fluid. Up to six of these vessels could be fit into the main box (shown on the right) while still achieving optimal stirring of each sample.

Each sample vessel contained 1.5 g of pre-cleaned and oven-dried (Advantage –Lab oven) silica particles to be treated. A magnetic stirrer bar was used to keep the particles dispersed during the procedure and the microscope slide was suspended with a clip over the top of the vessel to keep it from interfering with the stirring. Once the vessel was topped up with DCDMS solution and the microscope slides were in position the vessels were placed in a test tube rack inside an airtight plastic container. The container was modified to allow a through-flow of nitrogen and the lid was modified to fit a humidity probe. A humidity probe (meter DT-615 from

CEM) was fixed into the lid and then the box was sealed and positioned on a multiplace stirrer (Komet Variomag Poly 15 from Thermo Electron Corporation) so that the samples were each over a stirring position. The box was purged with dry nitrogen until the humidity dropped to the limit of the meter (at ~0.1 % relative humidity). The system was left stirring for an hour with regular checks on the humidity level and on the samples to ensure they remained dispersed. If the relative humidity rose above 1 % the box was again purged with nitrogen.

After one hour 0.5 ml of ethanol was added to each vessel to react with the remaining DCDMS. The slides were removed, rinsed in chloroform and then sonicated in a fresh volume of chloroform. The chloroform was washed off by sonicating in ethanol and then the slides were dried in the oven. The particle dispersion was centrifuged at 4000 rpm for 15-20 minutes and then the toluene removed. After this they were sonicated in chloroform for 5 minutes and then centrifuged once more. This was repeated again with chloroform and then with ethanol before drying in the oven.

### *2.2.2 Contact angle measurements on microscope slides*

Glass microscope slides which were hydrophobised simultaneously with silica particles could be used to measure the contact angle. The slides were initially etched (with a glass etching pen) to mark out small square segments approximately 10 mm long and wide, a suitable size both for measurements and to fit in a 20 x 20 mm cuvette. The slides could then be split into the separate segments when required. Prior to measurements the slides were sonicated in ethanol for 5 minutes to remove contaminants and then dried with nitrogen.

The contact angle was measured with a Krüss Drop Shape Analyser (DSA) 10. This instrument was used to observe the side-on profile of sessile liquid drops on a glass microscope slide and from the profile of the drop the three-phase contact angle was determined.

With the hydrophobised slides the advancing and receding contact angles were measured for a droplet changing in volume by  $6 \mu\text{l min}^{-1}$ . The rate of volume change was controlled using a syringe pump (New era systems, Inc., model NE-1000) and measurements were taken in two second intervals. For measurements under oil the slides were placed in a 20 x 20mm glass cuvette which had been cleaned in ethanol the same way as the slides. Oil was added to the cuvette until the slide was fully immersed and then left for 15 minutes to equilibrate. The advancing and receding contact angle measurements were then made as before.

### *2.2.3 Measuring particle contact angles with the Film Calliper Method*

This section describes the Film Calliper Method (FCM)<sup>11</sup> which was used for measuring the contact angles of colloidal particles bridging a vertical thin liquid film. The experimental setup for the FCM is shown in Fig. 2.5. Particles bridging the thin liquid film were observed with a horizontal microscope using reflected monochromatic light which formed an interference pattern. The vertical liquid film was supported in a glass ring which was in turn attached via a needle to a 1ml glass syringe. The syringe allowed control of the volume of liquid within the ring and was used to withdraw some of the liquid to thin the film. It is during this film thinning that particles may bridge both film surfaces.

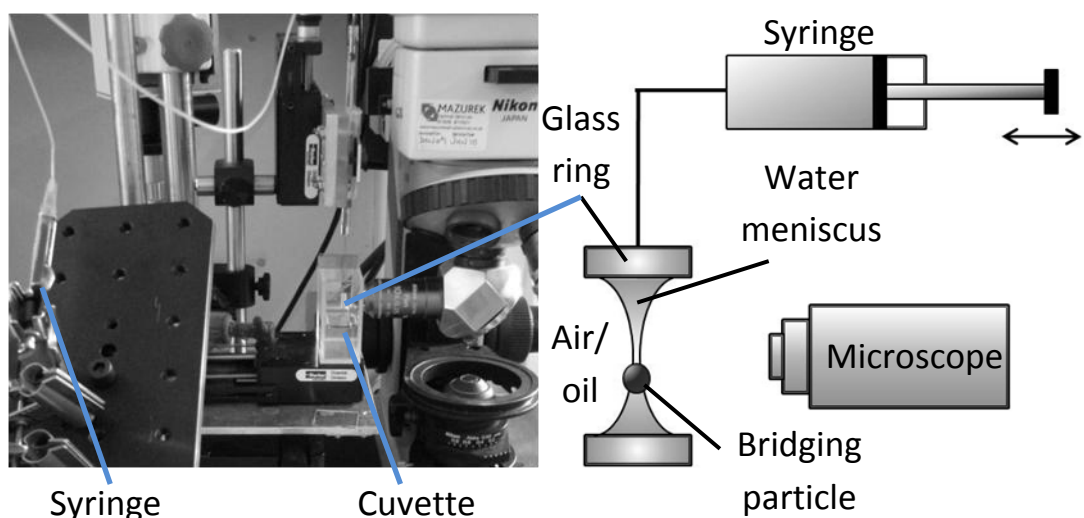


**Figure 2.5.** Photograph of the experimental setup for the FCM (left), and a schematic of the main components (right). To collect the water in the ring it was pulled through the bulk aqueous liquid in the cuvette, which had particles spread at its surface.

The glass ring was suspended from a manually adjustable mount so that the ring could be moved swiftly through the bulk liquid surface and the surface layer of particles in the cuvette, acting to trap them within the ring. The cuvette and the holder for the ring were positioned on a moveable stage to allow for adjusting the focus. The monochromatic light source was a mercury lamp housed in the microscope ( $\lambda = 546 \text{ nm}$ ) and a fibre optic light source was used to backlight the film if greater contrast between the interference pattern and the bridging particles was required. Observations of the thin films were made with a Nikon Optiphot-2 microscope fitted with a QICAM Fast 1394 camera from QImaging. An attachment was used enabling side-on images to be taken with 10, 20 and 40 x long distance objectives. Image-Pro Plus software (version 6.0.0.260, Media Cybernetics Inc.) was used to save the microscope images.

Prior to setup all glassware was soaked in sulfochromic acid to clean off organic impurities and rinsed, first with tap water and then washed thoroughly with milli-Q water. Needle tips and syringe plungers were cleaned with tissue soaked in

ethanol to remove any dust and grime and then left to air dry. The ring used to support the thin film during measurements was first sonicated in ethanol, then chloroform, ethanol again and then finally with milli-Q water.

Initially, the cuvette was filled with the aqueous solution to be measured. A pipette attached to a tap-mounted vacuum was used to clean the surface of the solution by slowly removing liquid from the surface until the cuvette was just under half filled. A 6  $\mu\text{l}$  spreading suspension of particles was then carefully syringed at the liquid surface to encourage the particles to attach to the air/water interface. The spreading suspension consisted of approximately 2 wt.% particles in a mixture of the aqueous phase and methanol in equal volumes. After the particles were spread at the aqueous surface the cuvette was covered for half an hour, preventing dust from settling onto the liquid while allowing the particles to equilibrate and the methanol to evaporate off.

The cuvette was put in position and the ring clamped to hang inside the cuvette, at rest above the liquid surface and face-on with the microscope. The cuvette opening was covered with microscope slides to give the thin films extra stability by minimising air disturbances and evaporation. To collect liquid and particles in the ring it was moved vertically to fully immerse in the liquid and then swiftly moved back into the resting position. A thin film with particles bridging it could be formed when the volume in the ring was reduced using the syringe. Increasing the volume of liquid in the ring caused the thin film area to shrink and the particles were observed to move also, remaining at the same film thickness. Further increasing the volume could be used to close the thin film and reform the bulk phase in the ring. For each image a film with at least 9 bridging particles was desired and several images were taken for each sample. Between images the ring was re-immersed to refresh the liquid and particles.

Monochromatic light reflected off the thin liquid film produced an interference pattern of concentric bright and dark fringes as shown in Fig. 2.6. The light intensity profile from the centre of the film to the point at which the bridging

particles were positioned could be measured from the microscope images and used to determine the thickness of the film for each dark fringe using the equation<sup>11</sup>,

$$h = m\lambda / 2n_f \quad (2.1)$$

where  $m$  is the order of interference,  $\lambda$  is the wavelength of the monochromatic light source and  $n_f$  is the refractive index of the liquid film. The order of interference of the first dark fringe in Fig. 2.6 is  $m = 1$ <sup>11</sup>. Using the light intensity profile the film thickness in a line extending radially from the centre can be calculated and is also shown in Fig. 2.6.

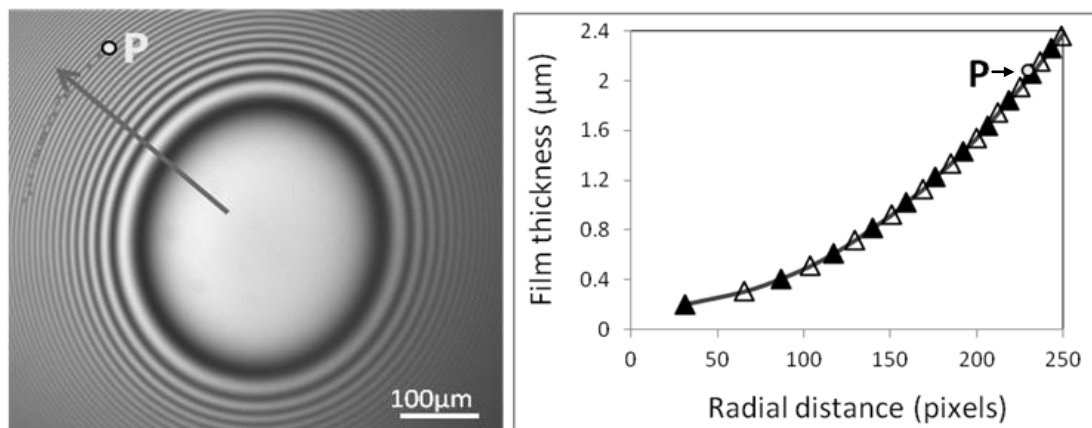


**Figure 2.6.** Interference pattern produced by monochromatic light ( $\lambda = 546 \text{ nm}$ ) reflected off a thin liquid film (left). Bridging particles are visible (P) and their position is marked on the plot of film thickness (right), calculated for the bright and dark fringes (white and black triangles respectively).

By using the interference pattern to calculate the film thickness,  $h_e$ , at the equilibrium position of the particles and knowing the particle diameter,  $d$ , the particle contact angle,  $\theta$ , can be determined using the equation:

$$\cos \theta = h_e / d \quad (2.2)$$

The particle is in equilibrium with the film when deformation of the film surface is a minimum and the film thickness correlates with the particle contact angle (Fig. 2.7 top). Movement of the particle into thinner or thicker regions of the film will cause surface deformations, increasing the interfacial area and therefore the surface free energy,  $\Delta E$ , will increase. The particles are therefore expected to move into a position where the film thickness  $h = h_e$ , surface deformations are minimal and the surface free energy is a minimum. This is, assuming that the film thickness across the particle surface remains equal to  $h_e$ , which directly relates to the particle contact angle as shown by eq. 2.2. If the film thickness across the particle surface does not remain equal to  $h_e$  the particle will also not be in the minimum energy position and will again move to a position where this is achieved.

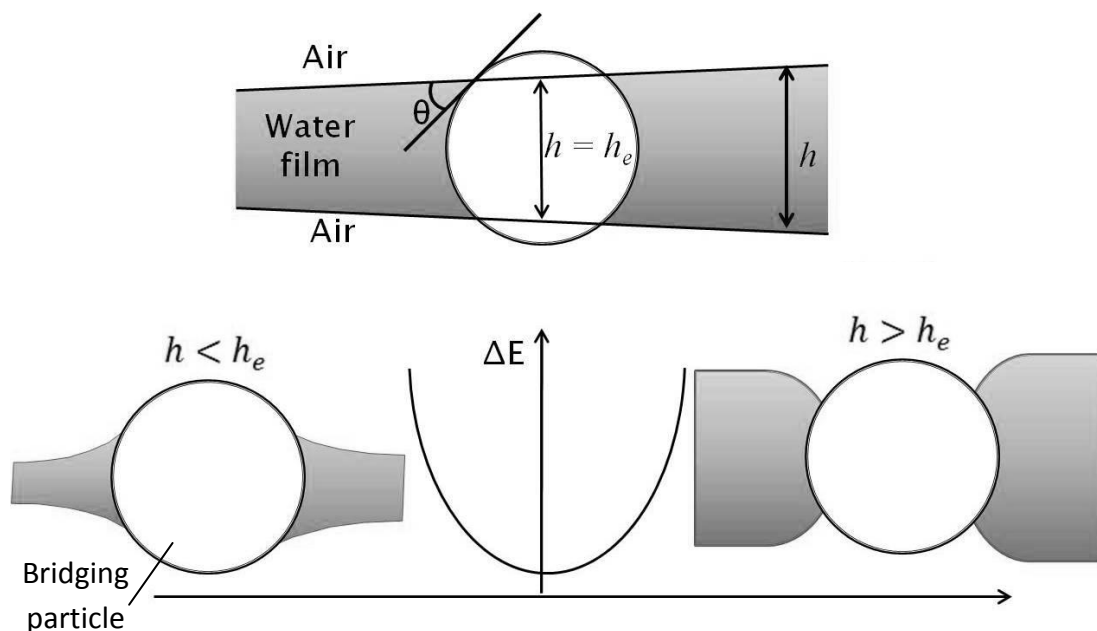


**Figure 2.7.** Sketch of a particle bridging a film of varying thickness and the expected increase of surface free energy due to surface deformations caused if the particle moves into film regions that are thinner (left) or thicker (right) than the equilibrium film thickness which directly relates to the particle wettability (top) via eq. 2.2.

For measurements at the oil-water interface the oil was pipetted into the cuvette atop the aqueous phase after air-water measurements were completed.

Before the oil was added the ring was filled with aqueous phase to prevent displacement by the oil and interference with aqueous thin film formation. For these measurements the ring remained in the oil phase while images were taken.

#### *2.2.4 Measuring particle contact angles with the Side imaging Technique (SIT)*

The contact angles of 7.75  $\mu\text{m}$  silica particles were measured by observing their depth of immersion at the aqueous-air or aqueous-oil interface. As previously detailed<sup>11</sup> the contact angle,  $\theta$ , was calculated with the equation  $\cos \theta = (2h_w/d) - 1$ , where  $d$  is the particle diameter and  $h_w$  is the depth of particle immersion in the water. The particles were spread at the planar aqueous surface in a cuvette using isopropanol as a spreading solvent. Side-on images of the particles were taken with a horizontal microscope (Optiphot 2, Nikon) using long working distance objectives in transmitted light.

#### *2.2.5 Making emulsions and foams*

To compare the measured particle contact angles with the behaviour of the particles in experimental conditions emulsions were made with equal volumes of aqueous and oil phase. Details of the emulsion systems studied are given in Table 2.5. All emulsions were made with decalin oil, except when using PGMA-PS particles where dodecane was used to fit in with collaborative work with other research groups. The concentration of particles and total emulsion volume varied between different systems as a result of particle availability and cost.

Hand-shaken emulsions were produced vigorously over 10 seconds with all samples from each emulsion series shaken simultaneously. The emulsions with surfactant solutions as the aqueous phase were produced over 30 seconds using an Ultra-Turrax homogeniser (IKA Labortechnik T25 Basic) fitted with a 10 mm head. TTAB ( $5 \times 10^{-4}$  – 10 mM) emulsions with 1  $\mu\text{m}$  silica particles were homogenised at

8000 rpm while those with 2.76  $\mu\text{m}$  silica particles and CPC (0.01 - 1.0 mM) emulsions were made at 9500 rpm. Foams were also made with 5 ml surfactant solutions in sealed vessels by hand shaking 30 times over 30 seconds. In foams stabilised with a mixture of particles and surfactant, 1  $\mu\text{m}$  silica particles were added at 4 wt.%.

**Table 2.5.** List of emulsion systems used, with main constituents and emulsification methods detailed. Further details are provided in the main text.

| Particle material         | Particle size / $\mu\text{m}$ | Particle conc. /wt.% | Aqueous phase             | Oil phase | Total emulsion volume /ml | Method of emulsification |
|---------------------------|-------------------------------|----------------------|---------------------------|-----------|---------------------------|--------------------------|
| CML latex                 | 0.9 -6.0                      | 2                    | NaCl solution (1mM)       | Decalin   | 1.2                       | Hand-shaking 10 secs     |
| PGMA-PS latex             | 0.8                           | 3                    | NaCl solution (0.1mM)     | Dodecane  | 2.0                       | Hand-shaking 10 secs     |
| Silica treated with DCDMS | 0.5, 0.7, 1.0                 | 2                    | Milli-Q water             | Decalin   | 2.0                       | Hand-shaking 10 secs     |
| Janus particles           | 0.5, 1.0                      | 2                    | Milli-Q water             | Decalin   | 2.0                       | Hand-shaking 10 secs     |
| Silica                    | 1.0                           | 4                    | CPC + TTAB surf. solution | Decalin   | 10.0                      | Ultraturrax 30 secs      |
| Silica                    | 2.76                          | 3, 9                 | TTAB surf. solution       | Decalin   | 10.0                      | Ultraturrax 30 secs      |

In all experiments where silica particles were to be used with surfactant solutions they were first allowed to fully equilibrate with the surfactant over time. Particle suspensions of 4 wt.% were made in surfactant solutions of the appropriate concentration. These suspensions were sonicated in an ultrasonic bath (Grant, MXB6) for ten minutes to break up aggregates and then stirred for at least a day in a sealed vessel. Immediately before use they were again sonicated for 5 minutes to disperse the particles and break up aggregates.

Photographic images of the emulsions and foams were taken with a Fujifilm FinePix F480 8.2 mega pixel camera and edited using Adobe Photoshop CS3 version 10.0 (2007) by Adobe Systems Inc. and Microsoft Office Picture Manager version 12.0 (2006) by Microsoft Corporation.

### *2.2.5.1 Determining emulsion type*

To determine the emulsion types produced the drop test was used. The emulsion was pipetted into a vessel of water and a vessel of oil while watching to see which liquid the emulsion droplets dispersed into. When pipetted into a fluid which matched the continuous phase the emulsion droplets dispersed into the bulk fluid. When pipetted into a fluid matching the disperse phase, the emulsion volume was contained and did not disperse. For the TTAB and 2.76  $\mu\text{m}$  silica particle stabilised emulsions fluorescent dyes were introduced to the emulsion on a microscope slide to aid in determining the emulsion type. Fluorescein dye ( $10^{-5}$  M in milli-Q water) was used to determine the aqueous phase and Nile red dye dissolved in acetone ( $10^{-4}$  M) was used to highlight the oil phase.

### *2.2.6 Measuring the absorption of surfactant on silica surfaces*

Cetylpyridinium chloride (CPC) solutions have an ultraviolet (UV) absorbance profile which varies with the concentration of the solution. This provides the opportunity to determine the adsorption of CPC surfactant on silica particles by measuring the change in UV adsorption between fresh solutions and those that were used as particle dispersions.

Silica particle (1  $\mu\text{m}$ ) suspensions of 4 wt.% were prepared in solutions of a range of CPC concentrations. These suspensions were stirred over 24 hours in a sealed vessel to equilibrate. They were then centrifuged to sediment the particles so that the supernatant could be removed before being transferred to a UV quartz cuvette for UV absorption measurements.

UV Absorption measurements were performed with a UV/VIS spectrometer (Lambda 40) by Perkin Elmer. To contain the solutions two UV quartz cuvettes were used with 10mm path lengths. The absorbance spectrum of each was compared to

ensure that differences between their absorbance profiles were negligible. One cuvette was used for milli-Q water alone and the other for CPC solutions.

The UV absorbance profiles were measured for a wavelength range of 200 to 300 nm for each sample but before each measurement a baseline reference had to be measured with milli-Q water. After use the cuvettes were washed with deionised water and then cleaned in alcoholic potassium hydroxide solution.

### *2.2.7 Producing microscope images of samples*

Optical microscope observations of thin films for measuring the contact angles of particles with the Film Calliper Method were taken with a Nikon Optiphot-2 microscope. The microscope was fitted with an attachment enabling horizontal observation with 10, 20 and 40 x objectives. Microscope images of emulsions and polymer surfaces were taken with a Nikon Labophot microscope, with 4, 10, 20 and 40 x objectives. Both microscopes were fitted with a QICAM Fast 1394 camera from QImaging. Image-Pro Plus software (version 6.0.0.260, Media Cybernetics Inc.) was used to edit and save the microscope images.

Images of fluorescent emissions were taken with an Olympus BX 51 microscope fitted with an Olympus DP70 camera using 2, 10, 20 and 50 x objectives assorted filters and a mercury lamp. Image-Pro Plus software (version 6.0.0.260, Media Cybernetics Inc.) was used to edit and save the microscope images.

Scanning electron microscope (SEM) images of silica particles and polymer surfaces were taken using a Zeiss EVO 60 SEM instrument with a voltage of 22 kV, a maximum resolution of 3 nm and a probe current of 20 pA. To improve electron reflectance of the samples they were coated with a carbon film.

### *2.2.8 Measuring particle zeta potentials*

The zeta potential of particles was measured with a Malvern Zetasizer 3000 instrument which uses a laser with a wavelength of 633 nm at 10 mW. A flow-cell was used for the measurements. Zetasizer 3000 Advanced software (PCS version 1.41, Malvern Instruments Ltd.) was used with the instrument. All measurements were performed at 25 °C. Zeta potentials of silica particles in surfactant solutions were performed at the natural solution pH. Other measurements on silica particles with no surfactant involved were over a range of pH from 1 to 10. The pH for each suspension was set by drop-wise addition of either hydrochloric acid or sodium hydroxide solution and measured with a glass electrode fitted to a Fisherbrand Hydrus 400 pH unit at 25 °C. Background electrolyte was not used.

### *2.2.9 Measuring the hydrodynamic diameter of emulsion drops and polymers*

The hydrodynamic diameters of emulsion droplets or polymer beads were measured by light diffraction with a Malvern Mastersizer 2000 instrument using a Malvern Hydro 2000SM cell and a Hydro 2000SM water pump which was controlled with a Malvern QS Dispersion Unit Controller. The software used with the instrument was Mastersizer 2000 version 5.00.

### *2.2.10 Measuring the surface or interfacial tension of TTAB surfactant and decalin oil*

Surface and interfacial tensions of TTAB surfactant solutions and decalin oil were measured with a Krüss K12 tensiometer using a Du Nouy ring (platinum/iridium alloy). The tensiometer was connected to a thermostated water bath to maintain a constant stage temperature of 25 °C. Prior to measurements the glassware was thoroughly cleaned in alcoholic potassium hydroxide and the ring was cleaned in water, ethanol and then dried over a Bunsen flame before use. After

attaching the ring to the tensiometer balance the weight was zeroed while in the light phase of the system to be measured (air for surface tension, decalin for interfacial tension). The ring was then lowered until fully immersed in the heavy phase and the oil was added if interfacial tension measurements were to be made. The ring was pulled upwards to form a meniscus until the maximum pressure on the ring was measured from which the tension was determined. Without fully lowering the meniscus repeat measurements were made over time until surface equilibrium was assumed to be reached, as shown by a plateau in the readings which otherwise decreased over time.

#### *2.2.11 Preparation of Tollen's reagent*

Tollen's reagent was used to deposit a layer of silver onto silica particles attached to the surface of polymer. To prepare Tollens reagent ammonia was added dropwise to 30 ml silver nitrate solution (0.1 M) until brown precipitate had formed and subsequently dissolved. To this 15 ml potassium hydroxide solution (0.8 M) was added and then further ammonia until the solution again turned clear. This solution was transferred to the vessel to be used for the silvering procedure along with the particle sample and then 5 ml glucose solution (0.3 M) was added. To carry out the silvering procedure the vessel was sealed and shaken for 5 minutes before a thorough washing with deionised water. Prior to making the solutions the glassware was cleaned with concentrated nitric acid.

### 2.3 References

1. K. L. Thompson, S. P. Armes, D. W. York and J. A. Burdis, *Macromolecules*, 2010, **43**, 2169.
2. J. Stiernstedt, J. C. Fröberg, F. Tiberg and M. W. Rutland, *Langmuir*, 2005, **21**, 1875.
3. C. Ström, P. Hansson, B. Jönsson and O. Söderman, *Langmuir*, 2000, **16**, 2469.
4. M.-F. Ficheux, L. Bonakdar, F. Leal-Calderon and J. Bibette, *Langmuir*, 1998, **14**, 2702.
5. L. Sepúlveda and J. Cortés, *J. Phys. Chem.-US.*, 1985, **89**, 5322.
6. E. W. Anacker, *J. Phys. Chem.-US*, 1958, **62 (1)**, 41.
7. E. E. Makhaeva, H. Tenhu and A. R. Khokhlov, *Polymer*, 2000, **41**, 9139.
8. T. P. Goloub, L. K. Koopal, B. H. Bijsterbosch and M. P. Sidorova, *Langmuir*, 1996, **12**, 3188.
9. Sigma-Aldrich Co. LLC. (2011) 'Thermal transitions of homopolymers', Available online: [www.sigmaaldrich.com/materials-science/polymer-science.html](http://www.sigmaaldrich.com/materials-science/polymer-science.html), (Accessed 23/09/2011).
10. Polysciences, Inc. (2011), 'Stearyl methacrylate' product page, Available online: [www.polysciences.com](http://www.polysciences.com), (Accessed 20/10/2011).
11. T. S. Horozov, D. A. Braz, P. D. I. Fletcher, B. P. Binks and J. H. Clint, *Langmuir*, 2008, **24**, 1678.

## Chapter 3

### Direct measurements of colloidal particle contact angles at the oil - water interface

#### 3.1 Introduction

Solid colloidal particles can strongly attach to liquid interfaces and stabilise foams and emulsions<sup>1-4</sup>. The contact angle of solid particles at the liquid-fluid interface is a key parameter in these systems. It determines the foaming or antifoam action of solid particles<sup>5-10</sup>, the emulsion type<sup>1-4</sup>, and affects the mechanism of stabilisation in particle-stabilised emulsions<sup>11,12</sup>. It is accepted that hydrophilic particles with contact angles  $\theta_{ow} < 90^\circ$  stabilise oil-in-water (o/w) emulsions, while hydrophobic particles ( $\theta_{ow} > 90^\circ$ ) give water-in-oil (w/o) emulsions<sup>3,4,12</sup>. However, these important conclusions for the effect of particle contact angle on the emulsion type are based on indirect information about the particle wettability obtained by measuring the contact angle on a macroscopic piece of material with similar surface chemistry<sup>3,12,13</sup> or deduced from the chemical composition of the particle surface<sup>3,6</sup>. The direct measurement of the contact angle of solid particles used as emulsion stabilisers is difficult because of the small particle size. Only a few of the methods discussed in Chapter 1 are capable of measuring the contact angle of individual colloidal particles at oil-water interfaces. The Film Calliper Method<sup>13</sup> (FCM) described in Chapter 2 has significant advantages over the other techniques. It has been demonstrated that the FCM works well at the air-water interface, but it has never been used for measuring particle contact angles at oil-water interfaces.

The main objectives of the present study are:

- (i) to further develop the FCM for measuring particle contact angles at oil-water interfaces,

(ii) to investigate the type of particle-stabilised emulsions and link it to the contact angle values measured directly on the particle surface by the FCM.

The systems studied are briefly described in the next sub-section. It is followed by results and discussion where FCM contact angle measurements at oil-water interfaces are presented for latex particles (charge and sterically stabilised) and silica particles which have been modified chemically or with cationic surfactant. The contact angles are linked to the emulsion types stabilised with the particles. The chapter is finished with a summary of conclusions and a list of the references used.

### **3.2 Experimental**

We investigate several systems of practical importance. These are: (i) latex particles with surface chemistry predetermined by their synthesis, (ii) silica particles with chemically modified surfaces and (iii) mixtures of silica particles and a cationic surfactant. Particle contact angles at the air-water interface have also been measured and are shown for comparison.

Initial tests involved an investigation of contact angles on particles of varying size for which latex particles were used because their surface composition is relatively well quantified. Two different types of charge stabilised latex were used for this, sulphate particles which were described as hydrophobic by the producer and carboxylate modified latex (CML) particles which were described as being hydrophilic and highly charged (see Table 2.1). Contact angles were then measured for sterically stabilised latex particles with varying degrees of polymerisation (Table 2.2). Silica particles of variable wettability were also used with the wettability controlled either through chemical modification of the particle surface or by the presence of surfactant solutions. Silica particles with diameters of 700 nm and 1  $\mu\text{m}$  were hydrophobised with different concentrations of dichlorodimethylsilane

(DCDMS) (Chapter 2.1.4). Details of the silica particles are presented in Chapter 2.1.1.1 while the hydrophobising procedure using DCDMS is detailed in Chapter 2.2.1. Silica particles with 2.76  $\mu\text{m}$  diameters were dispersed in aqueous solutions of tetradecyltrimethylammonium bromide (TTAB) cationic surfactant at concentrations of  $5 \times 10^{-4}$  to 3 mM (Chapter 2.1.2). Oils used in the experiments were decalin and dodecane (see Table 2.3). They were purified as described in Chapter 2.1.2. The experimental setup and procedure for using the FCM are detailed in Chapter 2.2.3.

### **3.3 Results and discussion**

#### *3.3.1 Measuring contact angles of latex particles with the FCM at air-water and oil-water interfaces*

##### *3.3.1.1 Contact angles of carboxylate modified latex particles*

Contact angles of carboxylate modified latex (CML) particles with diameters in the range 0.9 – 6.0  $\mu\text{m}$  are shown in Fig. 3.1.

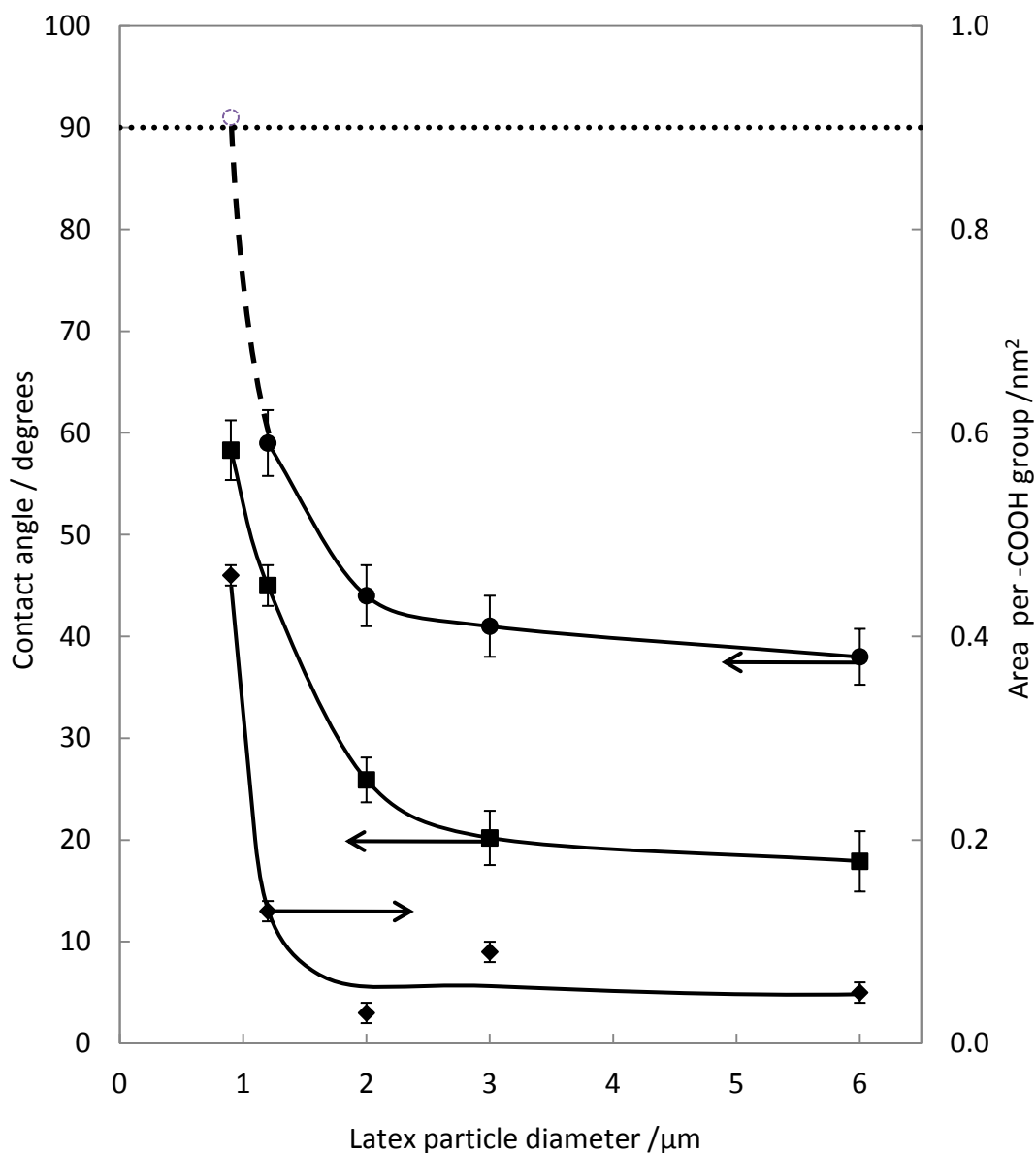


**Figure 3.1.** Contact angles and area per -COOH group (diamonds) for CML latex particles of varying diameter. Contact angles were measured at the air-water interface (squares) and decalin-water interface (circles) using the Film Calliper Method. Information for the area per -COOH group was supplied by the manufacturer. Measurements were performed at room temperature within milli-Q water at neutral pH. The dashed line at 90 degrees is included as a visual aid.

The CML particles were measured to be hydrophilic at the air-water interface ( $\theta_{ow} < 90^\circ$ ) with contact angles increasing as the particle diameter decreased. Contact angles of  $\sim 20^\circ$  were measured for the larger particles with a sharp increase in contact angle observed for the  $0.9 \mu\text{m}$  particles to  $58^\circ$ . The change in the contact angle with particle diameter is shown to correspond with data for the area per carboxyl group on the particles. With a greater area per carboxyl group the number density of groups on the surface is lower, such as for the  $0.9 \mu\text{m}$  particles, and the hydrophobicity is therefore significantly higher.

The contact angles at the decalin interface were greater than those at the air interface but followed a similar trend. The contact angle of the  $0.9 \mu\text{m}$  CML particles at the decalin interface could not be measured as the film ruptured when the particles attached to the film, suggesting that the particle contact angle was greater than  $90^\circ$ . Hence, these particles should stabilise w/o emulsions in contrast to the bigger particles with contact angles  $< 90^\circ$ . Images of emulsions made from equal volumes of decalin and aqueous suspensions of 2 wt.% CML particles are shown in Fig. 3.2. The CML particles with contact angles smaller than  $90^\circ$  gave o/w emulsions evident from the creaming observed. The opposite emulsion type (w/o) was obtained in the presence of the smallest particles since their contact angle was bigger than  $90^\circ$ . The emulsion type deduced from the creaming/sedimentation behaviour was also confirmed by drop tests. These results demonstrate that the data for the particle contact angles measured by the FCM at the oil-water interface can be used to predict the type of particle-stabilised emulsions. The results also show that the wettability of similar latex particles could be very different due to variations in the surface composition introduced at their synthesis.

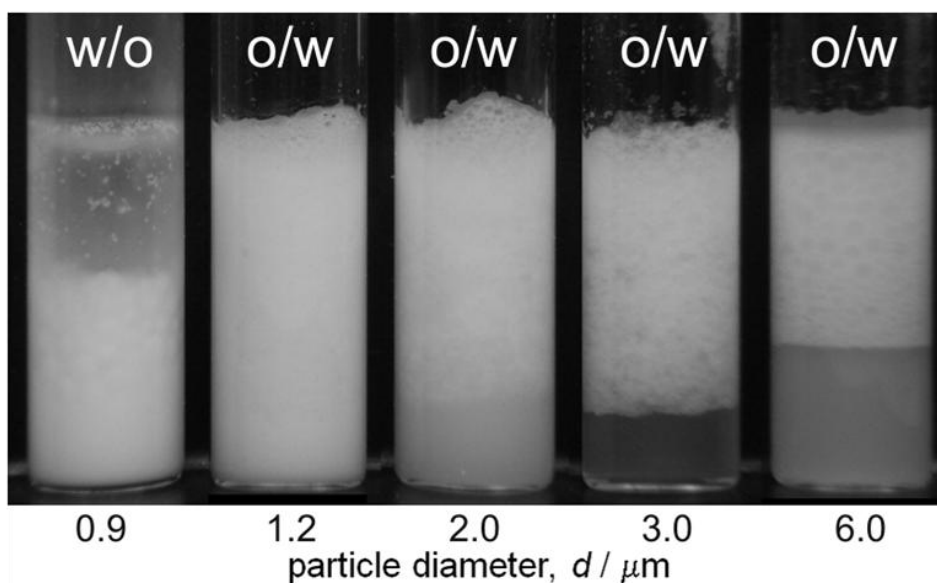


**Figure 3.2.** Images of hand shaken emulsions made from equal volumes of decalin and aqueous suspensions of 2wt.% CML particles with different diameters (shown) at 1 mM NaCl background electrolyte.

### 3.3.1.2 Contact angles of polystyrene sulphate latex particles

Contact angles of sulphate latex particles at the air-water interface measured by the FCM are shown in Fig. 3.3. The contact angle increases from  $\sim 41^\circ$  to  $\sim 55^\circ$  with decreasing particle size from 5.6 to 0.9  $\mu\text{m}$ . The observed variation of the contact angle with particle size is smaller than that for CML particles. The area per sulphate group at the particle surface is almost the same irrespective of the particle size (Fig. 3.3). Hence the variation in the sulphate latex particle contact angle with particle size cannot be explained by changes in the surface composition as in the case of CML particles. Other factors, such as differences in the particle surface roughness, could be responsible for the observed changes in the contact angle of sulphate latex particles. These need further investigation.

The sulphate latex particles caused rupturing of the water film in decalin, thus suggesting that their contact angles at the decalin-water interface were greater than  $90^\circ$ . This finding is consistent with the manufacturer information that the sulphate latex particles are hydrophobic.

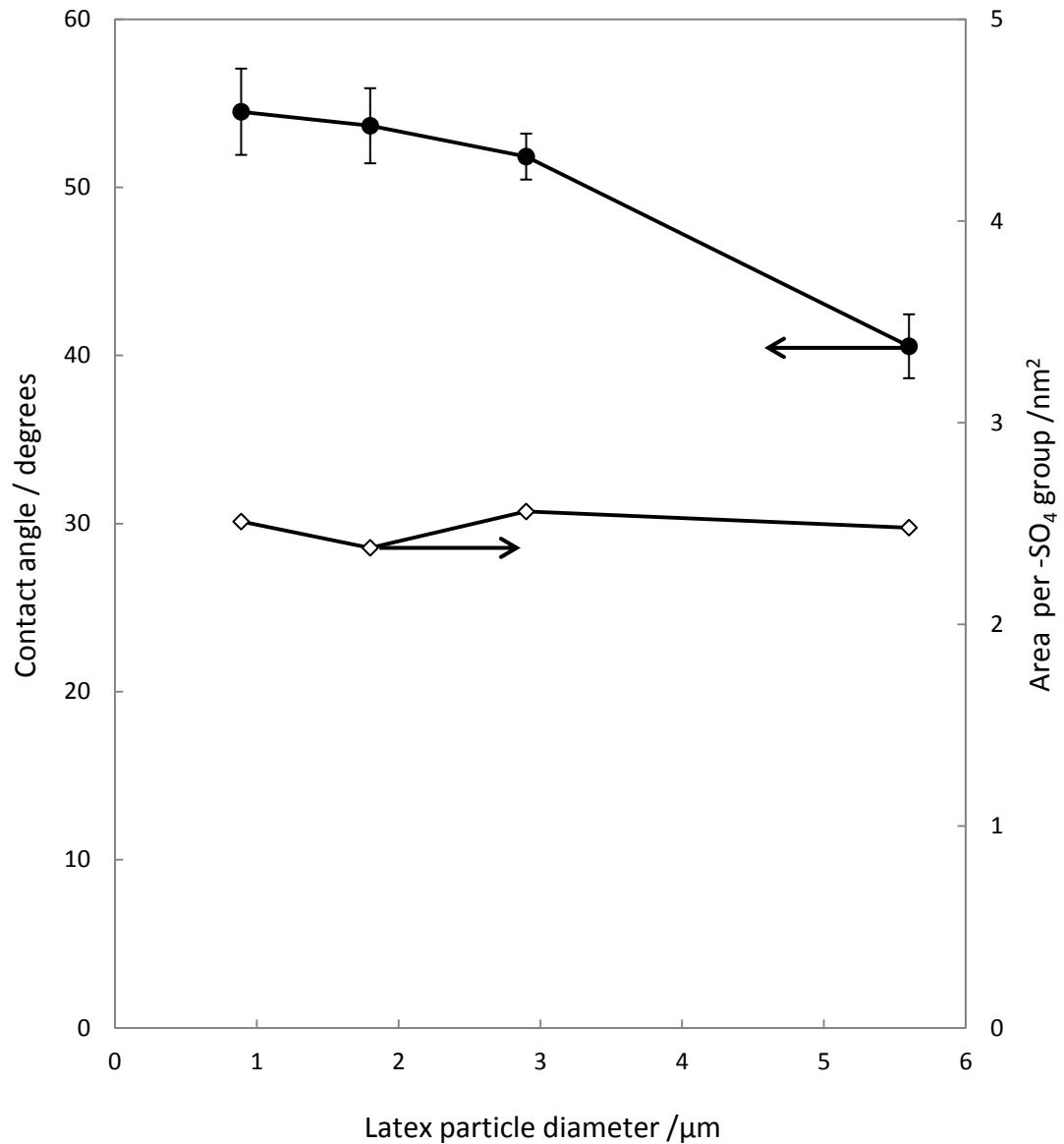


**Figure 3.3.** Contact angles of sulphate latex particles at the air-water interface (filled circles) and area per  $-\text{SO}_4$  group (open diamonds) versus particle diameter. Contact angles were measured using the Film Calliper Method. Information for the area per  $-\text{SO}_4$  group ( $\pm 0.01 \text{ nm}^2$ ) was supplied by the manufacturer. Measurements were performed at room temperature within milli-Q water at neutral pH.

### 3.3.1.3 Contact angles of poly(glycerol monomethacrylate)-Polystyrene latex particles

Poly (glycerol monomethacrylate) - Polystyrene (PGMA-PS) latex particles sterically stabilised by PGMA chains of varying degree of polymerisation (DP) of 30, 50 and 70 attached to the surface but very similar in size have been studied. Contact angles at the air-water and dodecane-water interface have been measured in order to investigate the effect of DP of PGMA on the particle wettability. The results are summarised in Table 3.1.

**Table 3.1.** Contact angles of PGMA-PS latex particles with different degree of polymerisation (DP) of PGMA chains at the air-water and dodecane-water interfaces measured with the FCM in the presence of 0.1 mM NaCl in the aqueous phase at pH  $7.0 \pm 0.1$ .

| Sample code | Particle diameter /nm | DP of PGMA | Contact angle /degrees |                |
|-------------|-----------------------|------------|------------------------|----------------|
|             |                       |            | Air-water              | Dodecane-water |
| AW52        | $820 \pm 90$          | 30         | $49 \pm 3$             | $68 \pm 6$     |
| KLT208      | $834 \pm 65$          | 50         | $46 \pm 2$             | $76 \pm 6$     |
| AW54        | $796 \pm 167$         | 70         | $46 \pm 2$             | $59 \pm 7$     |

It is seen that the air-water contact angle decreases slightly from  $49^\circ$  at DP = 30 to  $46^\circ$  at DP = 50 and levels off at a higher DP, although the observed tendency is rather weak bearing in mind the experimental error. The contact angles at the dodecane-water interface are bigger than those at the air-water surface. Significant aggregation of the particles at the dodecane-water interface has made the determination of the contact angles more difficult and contributed to the bigger uncertainties in comparison to those at the air-water interface. The dodecane-water contact angles for all the particles were similar within the experimental error

irrespective of the DP of PGMA. One can conclude that the increase of the DP of PGMA from 30 to 70 (hence, the length of the PGMA chains grafted at the particle surface) does not significantly affect the contact angle of the PGMA-PS latex particles. A similar 'saturation' of the contact angle at hydrophobic alkylamine films on macroscopic flat surfaces has been observed<sup>14</sup> with the increase of the alkyl chain length from C<sub>4</sub> to C<sub>18</sub>.

The average particle contact angle at the dodecane-water interface is  $69 \pm 7^\circ$ . Hence all studied particles are hydrophilic and should stabilise o/w emulsions. This hypothesis has been tested by preparing emulsions from equal volumes of dodecane and 3 wt.% particle suspensions in water containing  $10^{-4}$  M NaCl by hand-shaking. The emulsions were unstable to creaming but stable to coalescence for at least a week. Their type in each case was confirmed to be oil in water by drop test. This confirms the hydrophilic nature of the PGMA-PS particles and demonstrates that the FCM can be used for measuring the contact angles of sterically stabilised sub-micron particles at oil-water interfaces.

### *3.3.2 Contact angles of silica particles at air-water and oil-water interfaces*

The wettability of silica particles is often controlled to enhance the particle attachment to liquid interfaces or to improve particle dispersibility in non-polar organic liquids. Two of the most common approaches for changing the particle wettability are with surfactants or chemical modification of the particle surface (see section 1.1.2). Quantifying the change in particle wettability, or contact angle, has so far been achieved only through indirect means. Here the contact angles of particles, which have been modified by chemically altering the particle surface or by dispersion in surfactant solution, are measured directly using the FCM.

### *3.3.2.1 Contact angles of silica particles with chemically modified surfaces (DCDMS)*

The surfaces of silica particles were hydrophobised to different extents using solutions of dichlorodimethylsilane (DCDMS) in toluene as described in section 2.2.1. Contact angles of 1  $\mu\text{m}$  silanised silica particles were measured at the air-water and decalin-water interfaces using the FCM. The obtained results are plotted versus concentration of DCDMS solution used for particle silanisation in Fig. 3.4.

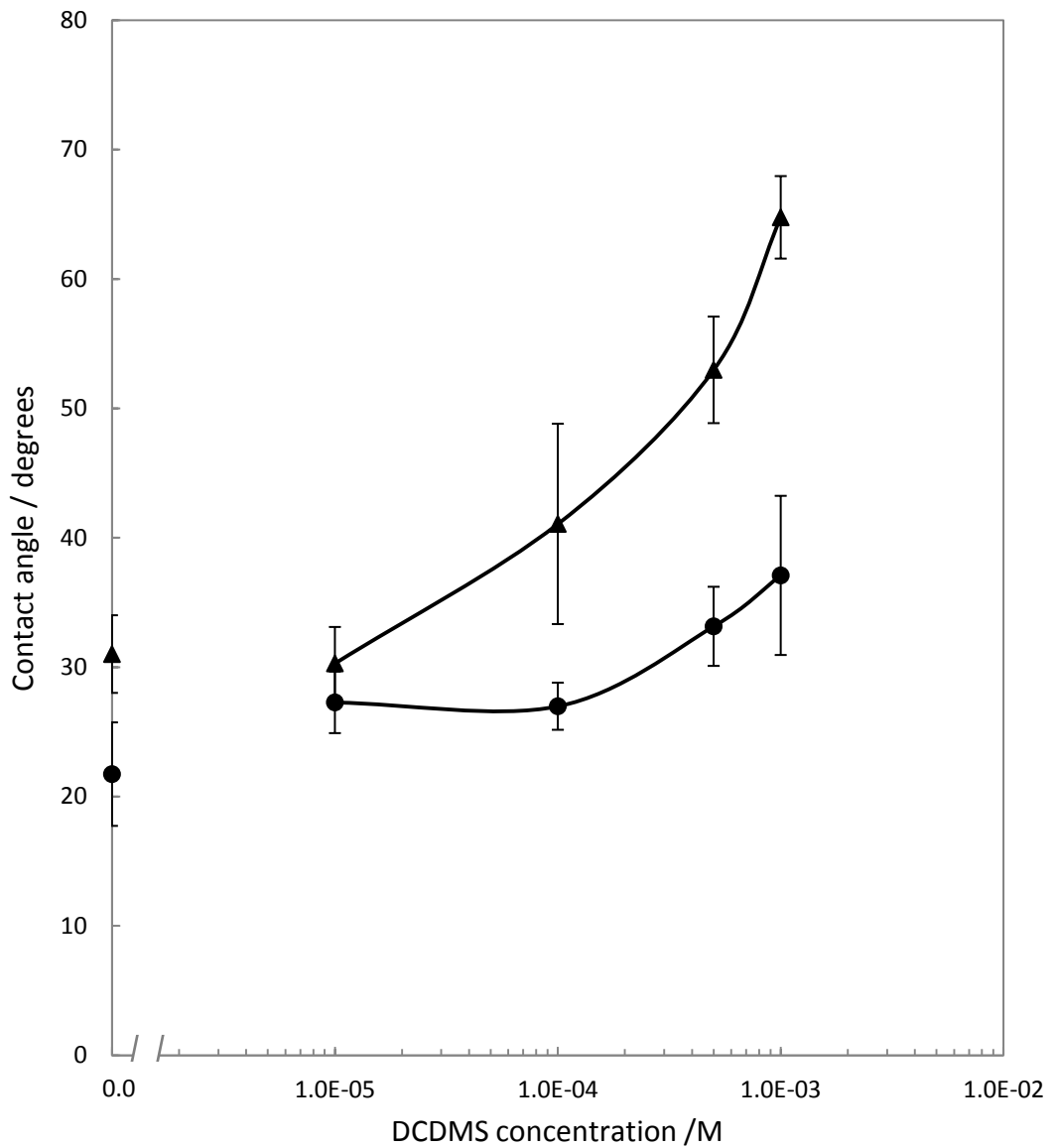


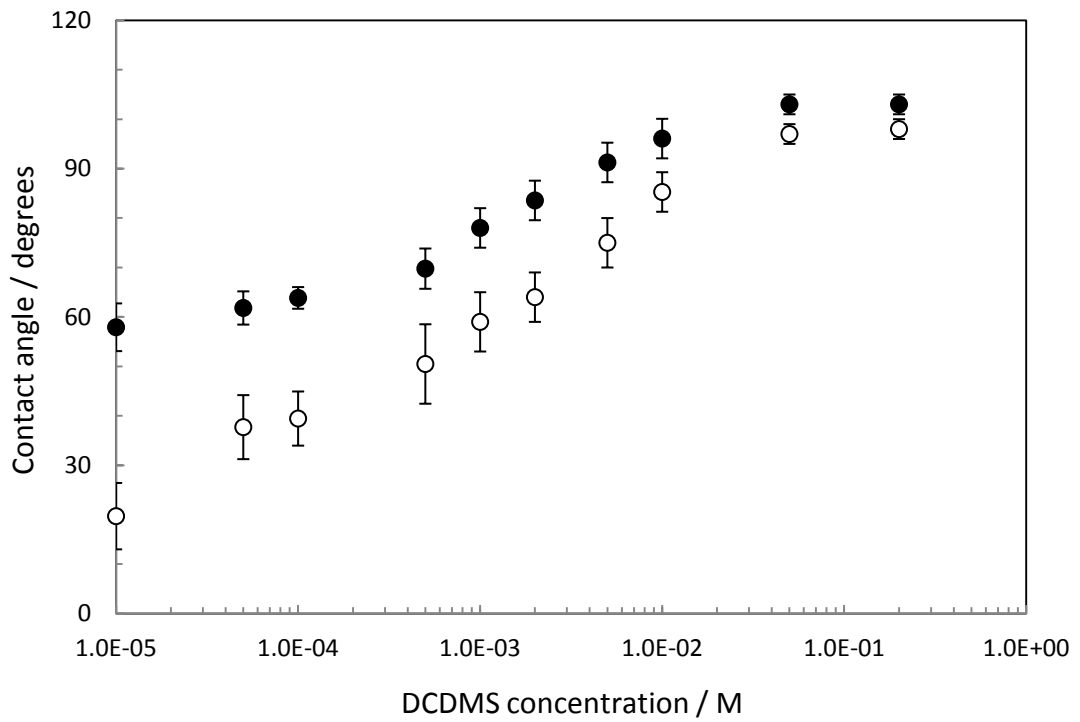
**Figure 3.4.** Contact angles of 1  $\mu\text{m}$  silica particles measured with the FCM at the air-water (circles) and decalin-water (triangles) interface versus concentration of DCDMS solutions used for particle hydrophobisation. Lines are drawn to guide the eye.

The particle contact angles at both air-water and oil-water interfaces increase with the concentration of DCDMS solutions used for their hydrophobisation. The decalin-water contact angles are bigger than those at the air-water interface. Similar trends are observed for contact angles of smaller silica particles with a diameter of 700 nm (Table 3.2). The contact angles of hydrophobised 700 nm particles are slightly bigger than those of 1  $\mu\text{m}$  particles hydrophobised by DCDMS at the same concentration, although the contact angles of the original particles are practically the same. The observed difference could be due to differences in the density and/or chemical reactivity of the surface silanol groups involved in the hydrophobisation with DCDMS. This needs further investigation.

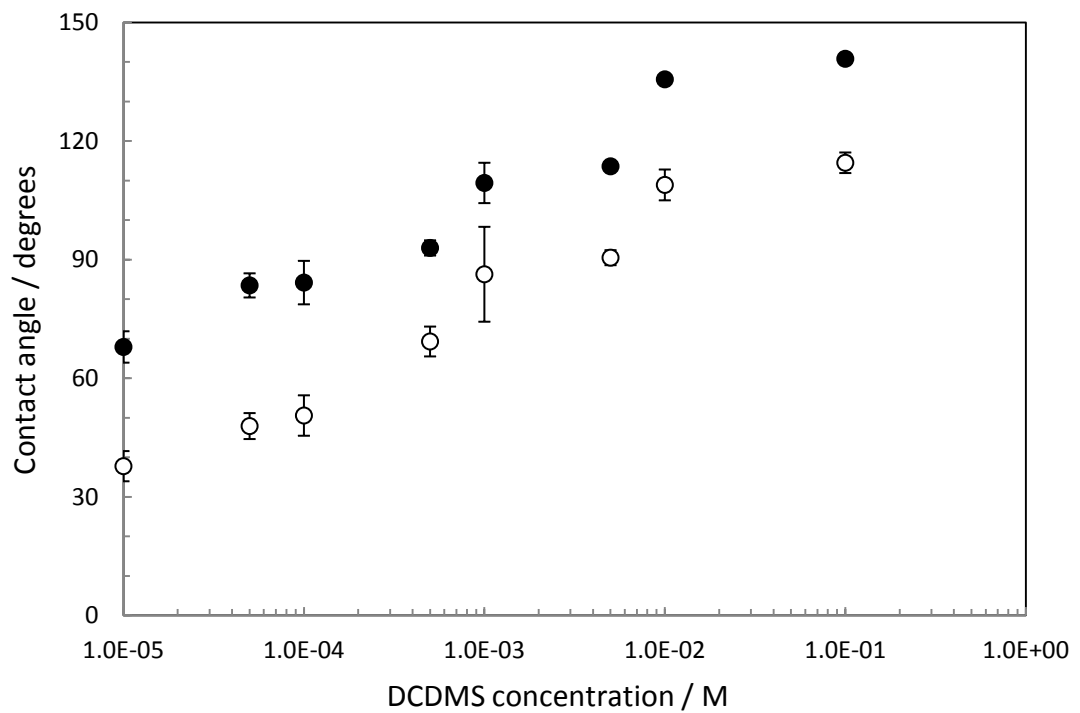
**Table 3.2.** Contact angles of hydrophobised silica particles with diameters of 700 nm and 1  $\mu\text{m}$  measured by the FCM at the air-water,  $\theta_{aw}$ , and decalin-water,  $\theta_{ow}$ , interfaces.

| [DCDMS] used to hydrophobise particles /M | $\theta_{aw}$ / degrees |                     | $\theta_{ow}$ / degrees |                     |
|---|-------------------------|---------------------|-------------------------|---------------------|
|   | d = 700 nm              | d = 1 $\mu\text{m}$ | d = 700 nm              | d = 1 $\mu\text{m}$ |
| 0   | 25 $\pm$ 3              | 22 $\pm$ 4          | 28 $\pm$ 9              | 30 $\pm$ 3          |
| 1.0 $\times 10^{-5}$                      | 36 $\pm$ 3              | 27 $\pm$ 2          | 46 $\pm$ 16             | 30 $\pm$ 3          |
| 5.0 $\times 10^{-4}$                      | 44 $\pm$ 2              | 33 $\pm$ 3          | 65 $\pm$ 4              | 53 $\pm$ 4          |

The contact angles of water drops on macroscopic glass slides hydrophobised by DCDMS were measured using the sessile drop method (see section 2.2.2 of Chapter 2). The obtained results for the advancing and receding contact angles at the air-water and decalin-water interface are plotted against DCDMS concentration in Fig. 3.5. The advancing angles are bigger than the receding ones due to the contact angle hysteresis. The contact angles at both air-water and decalin-water interfaces increase with the DCDMS concentration. Similar trends are observed for the contact angles of DCDMS treated silica particles measured by the FCM (Fig. 3.4).



(a)



(b)

**Figure 3.5.** Advancing (filled circles) and receding (open circles) contact angles of water drops on glass slides hydrophobised at different DCDMS concentrations measured in: (a) air and (b) decalin by the DSA 10 instrument.

Contact angles of 1  $\mu\text{m}$  silica particles measured by the FCM are compared to those measured on glass slides hydrophobised simultaneously with the particles in Table 3.3.

**Table 3.3.** Contact angles of 1 $\mu\text{m}$  hydrophobised silica particles at the air-water,  $\theta_{aw}$ , and decalin-water,  $\theta_{ow}$ , interfaces measured by the FCM, and the type of emulsions made from equal volumes of decalin and water in the presence of 2 wt.% silica particles in water. The values in brackets are average contact angles of water drops on glass plates hydrophobised simultaneously with the particles by DCDMS solutions.

| [DCDMS] /M         | $\theta_{aw}$ / degrees |                 | $\theta_{ow}$ / degrees |                  | Emulsion type |
|--------------------|-------------------------|-----------------|-------------------------|------------------|---------------|
| $1 \times 10^{-5}$ | $27 \pm 2$              | ( $39 \pm 19$ ) | $30 \pm 3$              | ( $53 \pm 15$ )  | o/w           |
| $1 \times 10^{-4}$ | $27 \pm 2$              | ( $52 \pm 12$ ) | $41 \pm 8$              | ( $67 \pm 17$ )  | o/w           |
| $5 \times 10^{-4}$ | $33 \pm 3$              | ( $60 \pm 10$ ) | $53 \pm 4$              | ( $81 \pm 12$ )  | o/w           |
| $1 \times 10^{-3}$ | $37 \pm 6$              | ( $69 \pm 10$ ) | $65 \pm 3$              | ( $98 \pm 12$ )  | o/w           |
| $5 \times 10^{-2}$ | > 90                    | ( $100 \pm 3$ ) | > 90                    | ( $125 \pm 10$ ) | w/o           |

It is seen that the contact angles of both silica particles and glass slides increase with increasing concentration of DCDMS as expected. It was found that the silica particles treated with the most concentrated DCDMS solution ( $5 \times 10^{-2}$  M) broke the water films after bridging in the FCM experiments. This suggests that the contact angle of these particles is bigger than  $90^\circ$ , although its actual value could not be determined. The contact angles measured on glass slides are systematically bigger than those on silica particles. Similar discrepancy between the air-water contact angles on hydrophobised glass slides and 3  $\mu\text{m}$  silica particles has been reported previously<sup>13</sup> and attributed to the differences in the surface chemical compositions and surface roughness. In addition, the contact angle hysteresis could

also contribute to the observed discrepancy. In the FCM measurements, the particles are initially attached to one of the film surfaces. Immediately after they become attached to the opposite film surface, the particles are in a thicker film region. They then spontaneously move into a thinner film region to reduce deformation and minimize the surface free energy (see Fig. 2.7). As a result, the three-phase contact line recedes across the particle surface. It is therefore expected that a receding contact angle could be determined. For particles with a smooth and chemically homogeneous surface the contact angles should practically coincide with the equilibrium contact angle. However, particles with a rough or inhomogeneous surface may encounter pinning of the three-phase contact line. This could result in hysteresis and measurement of a contact angle lower than the equilibrium contact angle. The differences in contact angles measured with the FCM on silica particles and with the sessile drop method on glass slides are likely due to a combination of hysteresis effects and differences in the surface composition.

The measured particle contact angles (Table 3.3) suggest that particles silanised at DCDMS concentrations up to  $1 \times 10^{-3}$  M are hydrophilic and should stabilise o/w emulsions, while those silanised at  $5 \times 10^{-2}$  M DCDMS are hydrophobic ( $\theta > 90^\circ$ ) and should stabilise w/o emulsions from equal volumes of oil and water. To test this hypothesis, emulsions were made from equal volumes of decalin and water in the presence of 2 wt.% silica particles. Hydrophilic particles were dispersed in water, whereas the hydrophobic ones were dispersed in decalin. The emulsion type was determined by drop test (see section 2.2.5.1) and the results are shown in Table 3.3 above. It is seen that the emulsions made with DCDMS treated particles are o/w type when the particle contact angle is less than  $90^\circ$ . The opposite type of emulsion (w/o) was obtained in the presence of hydrophobic particles with contact angle  $> 90^\circ$ . These results show that the FCM can be used for measuring the contact angle of micron and submicron particles with chemically modified surfaces at both air-water and oil-water interfaces. They confirm that a change in the Pickering emulsion type from o/w to w/o does occur when the contact angle measured directly on the particle surface exceeds  $90^\circ$ .

### *3.3.2.2 Contact angles of silica particles in the presence of cationic surfactant*

Cationic surfactants strongly adsorb at negatively charged silica surfaces and have a pronounced effect on the particle contact angle at the air-water and oil-water interfaces (see section 1.1.2.1.2). This can be used to tune the particle wettability by varying the concentration of the surfactant in the particle-surfactant mixtures. Nevertheless, reliable methods for measuring the contact angle of colloidal particles in the presence of surfactants do not exist. The Gel trapping technique, for instance, cannot be used for measuring particle contact angles at fluid-water interfaces in the presence of cationic surfactants due to strong interactions of such surfactants with the negatively charged molecules of the gelling agent (gelan)<sup>15</sup>.

Here we apply the FCM for measuring the contact angle of 2.76  $\mu\text{m}$  silica particles at the air-water and decalin-water interfaces in the presence of tetradecyltrimethylammonium bromide (TTAB) at concentrations up to the cmc (3.5 mM<sup>16-19</sup>) in the aqueous phase.

Contact angles of silica particles at the air-water and decalin-water interfaces in the presence of TTAB in the aqueous phase determined by the FCM are shown in Fig. 3.6 and Table 3.4. At the air-water interface the particle contact angles increased with increasing surfactant concentration, reaching a maximum in the range 0.5 – 1.0 mM, and then decreased at concentrations approaching cmc. The particles were found to be hydrophilic ( $\theta < 90^\circ$ ) for the complete range of surfactant concentrations with maximum contact angle of  $\sim 50^\circ$ .

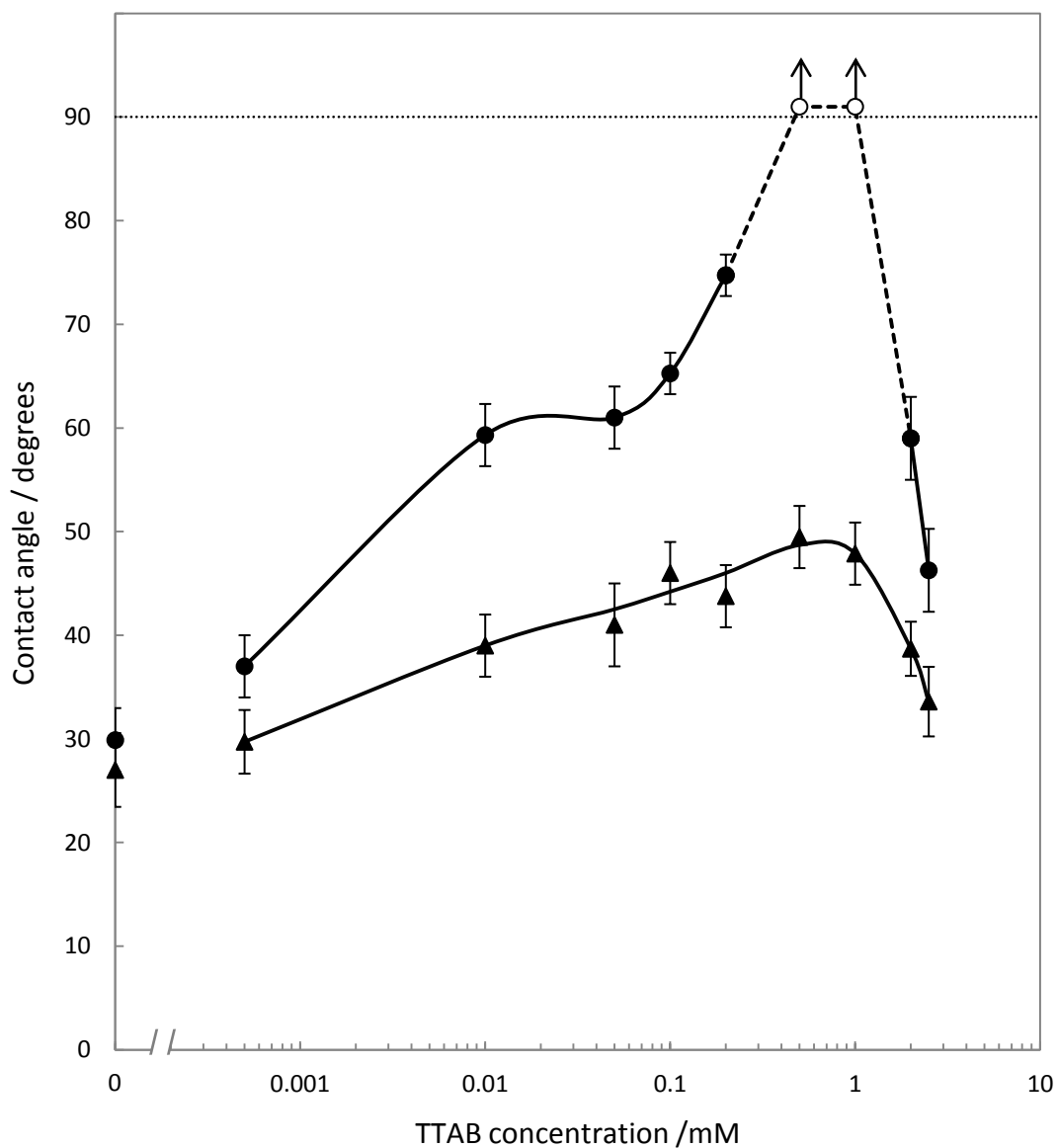


**Figure 3.6.** Contact angles of silica particles with a diameter of 2.76  $\mu\text{m}$  at the air-water (triangles) and decalin-water (circles) interface versus TTAB concentration in the aqueous phase with no extra electrolyte added. The pH is not adjusted and decreases with the TTAB concentration in the range 6.8 - 5.0  $\pm$  0.2. Empty circles correspond to contact angles > 90 degrees. Lines are drawn to guide the eye.

**Table 3.4.** Contact angles of silica particles with a diameter of 2.76  $\mu\text{m}$  at the air-water,  $\theta_{\text{aw}}$ , and decalin-water,  $\theta_{\text{ow}}$ , interfaces measured by the FCM in the presence of TTAB in the aqueous phase, and the type of emulsions made from equal volumes of decalin and water in the presence of 3 wt.% silica particles in the TTAB solution.

| [TTAB] /mM           | $\theta_{\text{aw}}$ / degrees | $\theta_{\text{ow}}$ / degrees | Emulsion type |
|----------------------|--------------------------------|--------------------------------|---------------|
| 0                    | $27 \pm 4$                     | $30 \pm 3$                     | o/w           |
| $5.0 \times 10^{-4}$ | $30 \pm 3$                     | $37 \pm 3$                     | o/w           |
| $1.0 \times 10^{-2}$ | $39 \pm 3$                     | $59 \pm 3$                     | o/w           |
| $5.0 \times 10^{-2}$ | $41 \pm 4$                     | $61 \pm 3$                     | o/w           |
| 0.1                  | $46 \pm 3$                     | $65 \pm 2$                     | o/w           |
| 0.2                  | $44 \pm 3$                     | $75 \pm 2$                     | o/w           |
| 0.5                  | $49 \pm 3$                     | > 90                           | w/o           |
| 1.0                  | $48 \pm 3$                     | > 90                           | w/o           |
| 2.0                  | $39 \pm 3$                     | $59 \pm 4$                     | o/w           |
| 2.5                  | $34 \pm 3$                     | $46 \pm 4$                     | o/w           |

The trend of contact angle with increasing surfactant concentration is as expected<sup>20</sup> (see section 1.1.2.1.2). At lower concentrations surfactant molecules adsorb to the silica surface with tail groups extended outwards, increasing the hydrophobicity of the particle and the particle contact angle increases. At high surfactant concentrations approaching the cmc the surfactant molecules adsorb to the surface with the head groups outwards, thus making the particles less hydrophobic and the contact angle decreases. Therefore the particle contact angle shows a maximum at a certain intermediate surfactant concentration. At surfactant concentrations above the cmc a complete bilayer of surfactant is expected on the particle surface making the particle very hydrophilic (see Fig. 1.5).

The silica particle contact angle at the decalin-water interface follows a similar trend to that obtained for the contact angle at the air-water surface with the

increase of TTAB concentration. Initial increase of the contact angle is again observed, followed by a decrease in contact angle at TTAB concentrations near to cmc. At the concentrations relating to maximum contact angle in air, the film in decalin was ruptured by particles and therefore particle contact angles at these concentrations (0.5 and 1.0 mM TTAB) are expected to be greater than  $90^\circ$ . In order to verify the contact angle values obtained by the FCM we have measured the contact angle of larger silica particles with diameter  $7.75\ \mu\text{m}$  at selected concentrations of TTAB using the Side Imaging Technique (SIT). Particle suspensions in TTAB solutions were spread at the air-water or decalin-water interface and side images of the particles attached to the liquid interface were taken by a horizontal microscope as described in section 2.2.4. Typical images are shown in Fig. 3.7. The particle and its reflection are clearly seen, thus making it possible to locate the liquid interface (dashed lines). Drawing a circle around the particle image allowed us to measure the particle diameter,  $d$ , its depth of immersion into the aqueous phase,  $h_w$ , and to calculate the contact angle by the formula,  $\cos \theta = 2h_w/d - 1$  (see eq. 1.3). The obtained results are summarised in Table 3.5 and compared to the particle contact angles measured by the FCM.

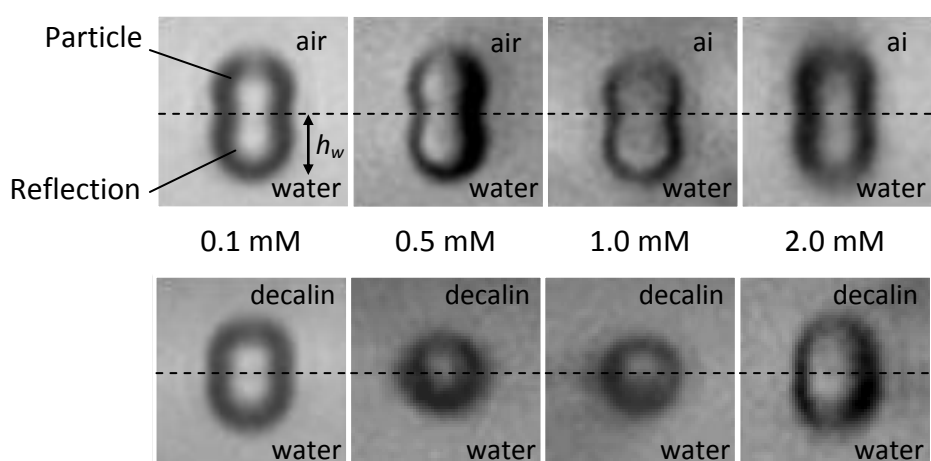


**Figure 3.7.** Side images of silica particles with diameter  $7.75\ \mu\text{m}$  attached to the interface of aqueous TTAB solutions at concentrations shown, in contact with air (top) and decalin (bottom), used to determine the particle contact angles by the Side Imaging Technique.

**Table 3.5.** Contact angles of silica particles in aqueous TTAB solutions at air-water and decalin-water interfaces measured by the Side Imaging Technique (SIT) and the Film Calliper Method (FCM). The particle diameters in SIT and FCM measurements are 7.75  $\mu\text{m}$  and 2.76  $\mu\text{m}$ , respectively.

| [TTAB]<br>/mM | SIT contact angle / degrees |               | FCM contact angle / degrees |               |
|---------------|-----------------------------|---------------|-----------------------------|---------------|
|               | air-water                   | decalin-water | air-water                   | decalin-water |
| 0.1           | 48 $\pm$ 3                  | 64 $\pm$ 4    | 46 $\pm$ 3                  | 65 $\pm$ 2    |
| 0.5           | 48 $\pm$ 4                  | 95 $\pm$ 3    | 49 $\pm$ 3                  | > 90          |
| 1.0           | 46 $\pm$ 4                  | 94 $\pm$ 3    | 48 $\pm$ 3                  | > 90          |
| 2.0           | 40 $\pm$ 3                  | 72 $\pm$ 4    | 39 $\pm$ 3                  | 59 $\pm$ 4    |

The contact angles measured by both methods are in very good agreement. The values obtained at the air-water interface by the SIT are almost an exact match with those determined by the FCM and coincide within the experimental error. The same is true for the contact angle values at the decalin-water interface measured by both methods at 0.1 mM TTAB. The oil-water contact angle measured by the SIT at 2.0 mM TTAB is slightly higher but close to that determined by the FCM. More importantly, the contact angles at 0.5 and 1 mM TTAB obtained by the SIT are close to but greater than 90° as deduced from the FCM measurements.

The images in Fig. 3.8 show emulsions made from equal volumes of decalin and aqueous suspensions of 2.76  $\mu\text{m}$  silica particles in TTAB solution of varying concentration. Oil-in-water emulsions were produced with all surfactant concentrations except 0.5 and 1.0 mM where a change to w/o emulsions occurred. The surfactant concentrations at which emulsion inversion occurred coincided with those at which the measured contact angles exceeded 90° (hydrophobic particles). The inversion of emulsion type was confirmed by adding fluorescent dyes to the continuous phase of the emulsions. Water-soluble fluorescein isothiocyanate dye stained the continuous phase of o/w emulsions and oil-soluble Nile red dye stained the continuous phase of w/o emulsions as shown in Fig. 3.9. When added to the

opposite emulsion type the dyes preferentially dissolved into the emulsion drops rather than the continuous phase.

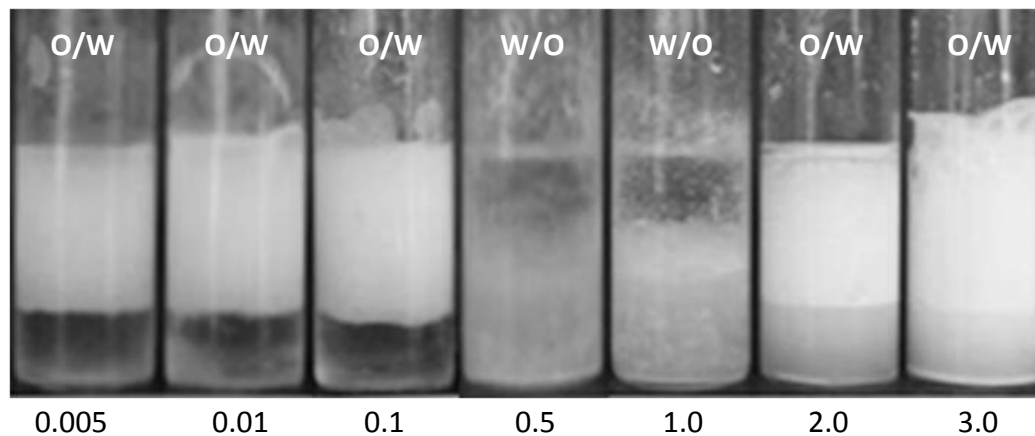


**Figure 3.8.** Images of emulsions taken 2 hours after preparation from equal volumes of decalin and TTAB solutions at concentrations shown (in mM) in the presence of 3 wt.% silica particles with a diameter of 2.76  $\mu\text{m}$ . The emulsions were homogenised with an Ultra-Turrax homogeniser (head 10 mm, IKA) at 9500 rpm for 30 secs. The emulsion type shown is determined by drop tests.

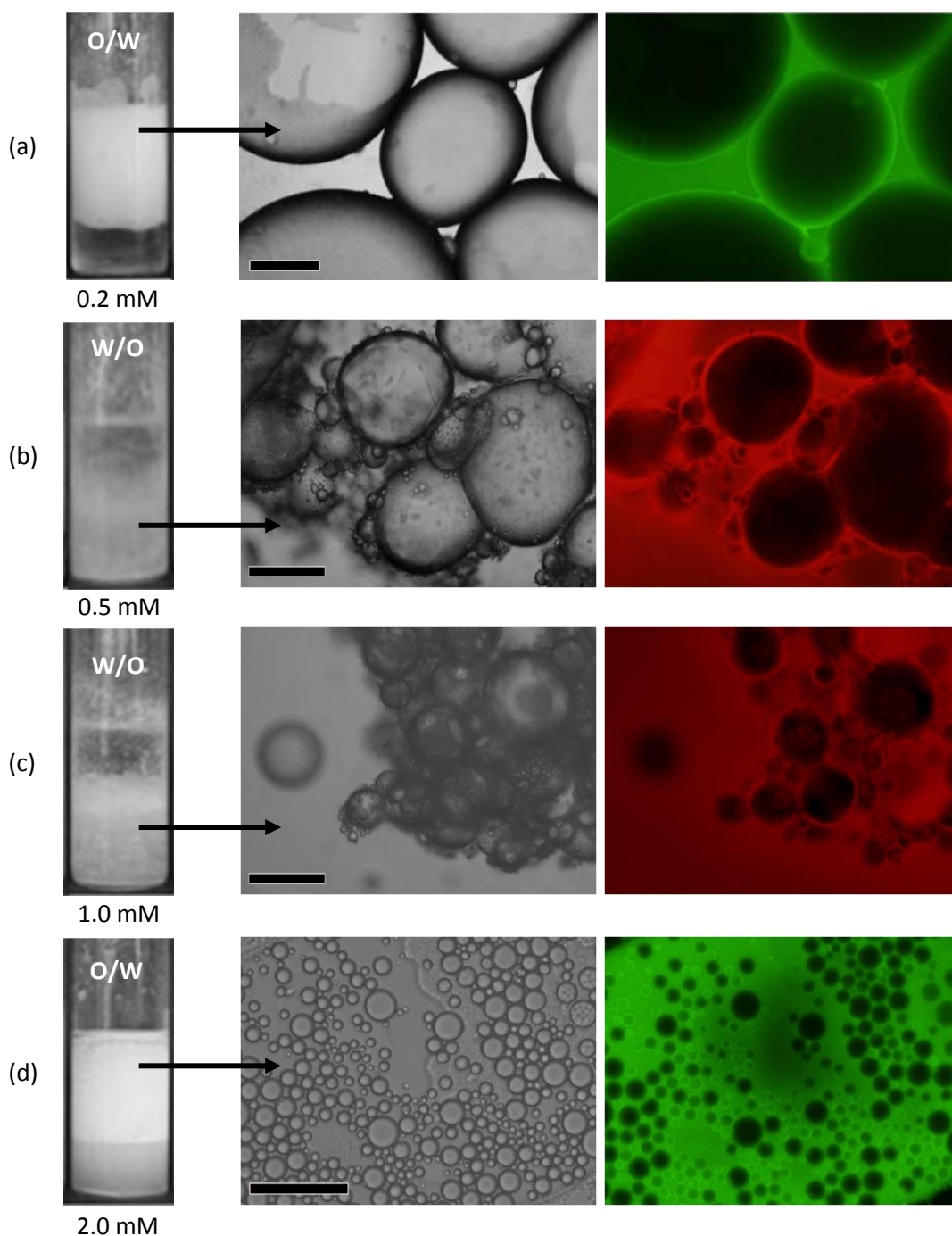


**Figure 3.9.** Images of emulsions taken at lower (left) and higher magnification 2 h after preparation from equal volumes of decalin and TTAB solutions at concentrations shown in the presence of 3 wt.% silica particles with a diameter of 2.76 μm. The emulsion type determined by drop tests (shown) is confirmed by the fluorescent microscopy images (right) obtained after staining the continuous phase with: (a, d) water-soluble fluorescein isothiocyanate (FITC) and (b, c) oil-soluble Nile Red fluorescent dyes. The scale bars are: (a) 200 μm, (b, c) 100 μm and (d) 50 μm

Such a double phase inversion in Pickering emulsions from silica particles and single chain cationic surfactant has not been reported before. Binks et al.<sup>21</sup> did not observe phase inversion in emulsions from water, dodecane and silica nanoparticles (Ludox) in the presence of cetyltrimethylammonium bromide (CTAB) in a broad range of CTAB concentrations (from zero up to 100 times cmc). All emulsions studied were o/w type. An important difference between their and our experiments is that we used much bigger silica microparticles. Although the wt.% concentrations in both studies are similar, their systems contained a much bigger number of particles that could result in a significant excess of particles in the continuous phase unattached to emulsion droplet surfaces. This suggests that the mechanism of stabilisation in their experiments could be different to that in ours. To test this hypothesis additional emulsions were made at a much higher concentration of 2.76  $\mu\text{m}$  particles (9 wt.%).

With greater particle concentration (9 wt.%) the emulsion type was o/w at 0.5 mM so the higher particle concentration prevented the emulsion inversion seen with the 3 wt.% emulsion. At 1.0 mM TTAB an o/w/o was formed with the higher particle concentration. It is therefore concluded that the particle concentration is an important factor in determining whether emulsion inversion will occur with particle-surfactant mixtures. There are two factors hypothesised to explain this behaviour. Firstly, that the surfactant molecules absorb to the interface quicker than the much larger particles, initially forming oil droplets in an aqueous continuous phase, as observed for surfactant systems in the absence of particles. Secondly, that aggregation of particles prior to attaching to the droplets prevents the particles from absorbing to the interface in a manner typical of hydrophobic particles. The particle aggregates may attach to droplet surfaces with the bulk of the aggregate in the continuous phase, as the adsorbed particles are unable to cross the interface. The curvature of the interface, with the adsorbed aggregates, would then favour that of o/w emulsions. In sedimentation tests it was observed that the particles aggregated and sedimented quickly at 0.5 and 1.0 mM which supports the ideas above.

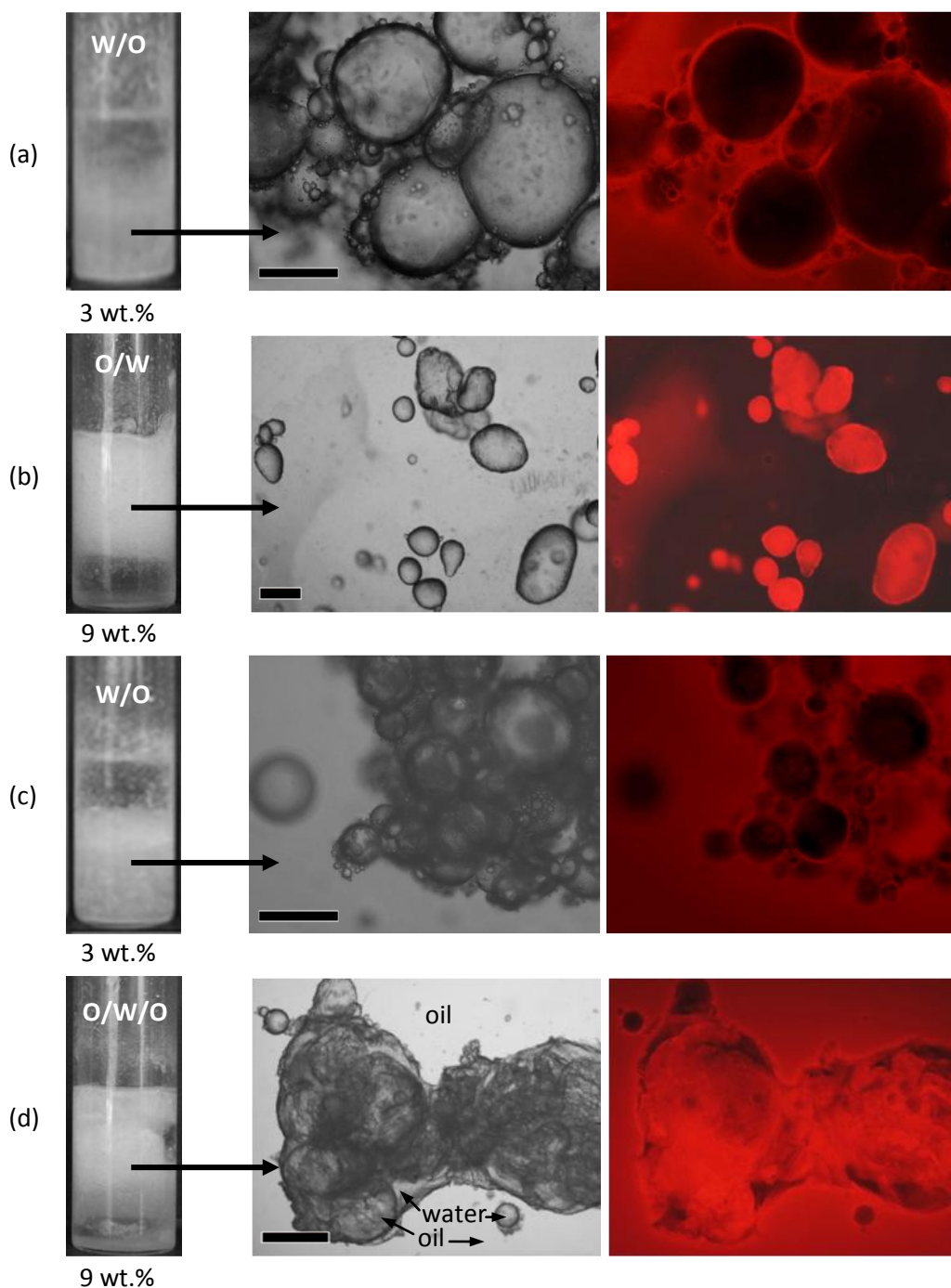


**Figure 3.10.** Images of emulsions taken at lower (left) and higher magnification after preparation from equal volumes of decalin and TTAB solutions at concentrations (a, b) 0.5 mM and (c, d) 1.0 mM in the presence of silica particles with a diameter of 2.76  $\mu\text{m}$  at concentrations in the aqueous phase equal to (a, c) 3 wt.% and (b, d) 9 wt.%. The emulsion type determined by drop tests (shown) is confirmed by the fluorescent microscopy images (right) obtained after staining the continuous phase with oil-soluble Nile Red fluorescent dye. The scale bars are: (a, c) 100  $\mu\text{m}$ , (b, d) 400  $\mu\text{m}$ .

### 3.4 Conclusions

The Film Calliper Method was further developed from measuring contact angles at air-water interfaces to successfully measure the contact angles of colloidal particles directly at oil-water interfaces also. The technique was shown to be compatible with a variety of particle types, aqueous solutions and oils. The directly measured contact angles were compared with emulsions stabilised and it was shown that particles determined to be hydrophilic ( $\theta < 90^\circ$ ) stabilised oil-in-water emulsions while hydrophobic particles ( $\theta > 90^\circ$ ) stabilised water-in-oil emulsions. This relationship between the particle contact angle and the emulsion type was demonstrated for particles of different chemical nature and also for particle-surfactant mixtures.

The contact angles of charge stabilised latex particles were shown to depend strongly on the density of surface groups. Emulsions stabilised by CML particles were oil-in-water with particles measured to be hydrophilic (with high density of surface groups) and water-in-oil for particles measured to be hydrophobic (low density of surface groups). With sulphate latex particles a decrease in contact angle was measured with increasing size despite relatively consistent density of surface groups and is assumed to be due to differences in surface roughness. At the oil-water interface the sulphate particles were observed to rupture the FCM film suggesting contact angles  $> 90^\circ$ , consistent with the manufacturer's description of the particles being hydrophobic. The contact angles of sterically stabilised latex particles were also measured, showing that changing the length of the steric groups did not significantly affect the contact angle. It is hypothesised that the steric chain lengths used were large enough to have 'saturated' the contact angle, as observed previously<sup>14</sup>. The particles were measured to be hydrophilic and they all stabilised oil-in-water emulsions.

Contact angles of particles hydrophobised with DCDMS solutions increased with increasing DCDMS concentration. Particles with contact angles  $< 90^\circ$  stabilised o/w emulsions while particles with contact angles  $> 90^\circ$  stabilised w/o emulsions.

Contact angles of particles measured with the FCM were systematically lower than average contact angles measured with the sessile drop method on glass slides. These differences are attributed to differences in surface chemical composition and surface roughness. Contact angles of 700 nm particles were greater than those of 1  $\mu\text{m}$  particles when the particles were hydrophobised but not for untreated particles. This suggests differences in the density and/or reactivity of the surface silanol groups but requires further investigation.

The contact angles of particles in TTAB surfactant solutions, measured directly with the FCM, initially increased up to a maximum before decreasing at concentrations approaching cmc. At the air-water interface the particles were all hydrophilic but at the oil-water interface the contact angles were higher, causing the film to rupture at the concentration range relating to maximum contact angles (0.5 – 1.0 mM). Measurements by FCM were compared with measurements of the contact angles of 7.75  $\mu\text{m}$  particles using the Side Imaging Technique. The contact angles measured with both methods were a close match and with concentrations at which particles broke the FCM film, suggesting contact angles  $> 90^\circ$ , the SIT measurements were also greater than  $90^\circ$ . Oil-in-water emulsions were produced with the hydrophilic particles and inversion to water-in-oil emulsions occurred when contact angles exceeded  $90^\circ$ . It was shown that this inversion to water-in-oil emulsion type could be prevented by increasing the particle concentration.

### 3.5 References

1. W. Ramsden, *P. R. Soc. London*, 1903, **72**, 156.
2. S.U. Pickering, *J. Chem. Soc. Trans.*, 1907, **91**, 2001.
3. R. Aveyard, B. P. Binks and J. H. Clint, *Adv. Colloid Interfac.*, 2003, **100–102**, 503.
4. F. Leal-Calderon and V. Schmitt, *Curr. Opin. Colloid In.*, 2008, **13**, 217.
5. B. S. Murray and R. Ettelaie, *Curr. Opin. Colloid In.*, 2004, **9**, 314.
6. B. P. Binks and T. S. Horozov, *Angew. Chem. Int. Edit.*, 2005, **44**, 3722.
7. U. T. Gonzenbach, A. R. Studart, E. Tervoort & L. J. Gauckler, *Angew. Chem. Int. Edit.*, 2006, **45**, 3526.
8. T. S. Horozov, *Curr. Opin. Colloid In.*, 2008, **13**, 134.
9. E. Dickinson, *Curr. Opin. Colloid In.*, 2010, **15**, 40.
10. A. Stocco, F. Garcia-Moreno, I. Manke, J. Banhart and D. Langevin, *Soft Matter*, 2011, **7**, 631.
11. V. O. Ikem, A. Menner, T. S. Horozov and A. Bismarck, *Adv. Mater.*, 2010, **22**, 3588.
12. T. S. Horozov and B. P. Binks, *Angew. Chem. Int. Edit.*, 2006, **45**, 773.
13. T. S. Horozov, D. A. Braz, P. D. I. Fletcher, B. P. Binks and J. H. Clint, *Langmuir*, 2008, **24 (5)**, 1678.
14. W. A. Zisman, *in Contact angle, wettability, and adhesion*, Adv. Chem. Series, vol. 43, R. F. Gould, ed., American Chemical Society, Washington, 1964, p.10.
15. V. N. Paunov, *Langmuir*, 2003, **19**, 7970.
16. J. Stiernstedt, J. C. Fröberg, F. Tiberg and M. W. Rutland, *Langmuir*, 2005, **21**, 1875.
17. C. Ström, P. Hansson, B. Jönsson and O. Söderman, *Langmuir*, 2000, **16**, 2469.
18. M.-F. Ficheux, L. Bonakdar, F. Leal-Calderon and J. Bibette, *Langmuir*, 1998, **14**, 2702.
19. L. Sepúlveda and J. Cortés, *J. Phys. Chem.-US.*, 1985, **89**, 5322.
20. D.W. Fuerstenau and R. Jia, *Colloid Surface. A*, 2004, **250**, 223.
21. B. P. Binks, J. A. Rodrigues and W. J. Frith, *Langmuir*, 2007, **23**, 3626.

## Chapter 4

### Foams and emulsions of silica particle and cationic surfactant mixtures

#### 4.1 Introduction

Foams and emulsions can be stabilised by surfactants or solid particles alone, but in many systems and processes of practical interest (food and cosmetic products, flotation of minerals, etc.) mixtures of particles and surfactants are involved<sup>1</sup>. When surfactants are used to stabilise foams or emulsions the stability arises mostly from lowering the surface/interfacial tension<sup>2</sup> and Gibbs-Marangoni elasticity effects<sup>3</sup>. The concentration of surfactant is a key factor in determining the manner in which surfactant acts in regards to these processes. In particle-stabilised systems stability arises from the physical barriers to coalescence created by particles at bubble/droplet surfaces or networks of flocculated particles in the continuous phase preventing bubble/droplet contact (see Fig. 1.16). The effectiveness of particles in this role depends on particle size and contact angle which have been related to stability via the energy of detachment<sup>4</sup> and the maximum capillary pressure for breaking the liquid films separating the bubbles/drops covered with particles<sup>5,6</sup>. The concentration of particles is an important factor in determining the stabilising mechanism of foam or emulsion systems; at low concentrations stability will be produced by bridging particles or small islands of particles which move to points of droplet contact whereas monolayers of particles coating the droplets will occur at high concentrations. If the particles are able to move laterally along the drop/bubble surface, away from the point of contact, instability can occur despite other factors.

When both types of stabilisers (surfactant and particles) are present, the stability of a foam/emulsion system results from the complex interplay and mutual influence of the particles and surfactant. Adsorption of the surfactant on the

particle surface changes the particle wettability, but also reduces the concentration of free surfactant in the solution. These effects are very significant in mixtures where the particles and surfactant molecules bear opposite electric charges. Such mixed systems of silica particles and cationic surfactants are investigated here. When dispersed in water the dissociated charges on silica particles are negative while those of a cationic surfactant head group are positive so charge attraction will exist. It is generally thought<sup>7</sup> that there is a 4 stage process to surfactant adsorption on silica based on the overall surfactant concentration. At low concentrations individual surfactant molecules adsorb to the surface by the head group with the tail either protruding outwards or parallel to the surface. As the concentration increases more molecules adsorb, forming hemi-micelles with the tail groups extending into the aqueous phase, thus increasing particle hydrophobicity and decreasing the net charge. This state is often referred to as the charge compensation point (ccp) at which the surface charge is neutralised, the particle hydrophobicity (and hence contact angle) is approximately maximum and aggregation of particles is expected to occur<sup>8</sup>. As the concentration is increased further, tail association occurs and additional surfactant will adsorb onto the first layer with head groups outwards, acting to lower the hydrophobicity and increase the net positive charge. The final stage occurs close to the critical micelle concentration (cmc) when a complete bilayer of surfactant is formed rendering the particles hydrophilic and positively charged. It has also been suggested<sup>9</sup> that surfactant may adsorb onto the silica surface in spherical surfactant aggregates, and that such aggregates may be present when the surface coverage is low<sup>10</sup>.

The stability of foams or emulsions by a mixture of particles and surfactant is influenced greatly by a balance of the surface/interfacial tension and the particle contact angle, both of which are affected by the surfactant concentration. It is generally found that an intermediate concentration of surfactant produces the greatest stability for foams and emulsions when the particle contact angle is ~60 - 80 degrees<sup>11,12</sup>. At these concentrations the energy of particle detachment from the interface is generally high (see eq. 1.4) and particle flocculation in the continuous phase adds to the stability against coalescence. If the contact angles exceed 90°

particles could destabilise the system or cause inversion from o/w to w/o emulsions<sup>12</sup>. At high surfactant concentrations (close to cmc) the surfactant competes for the liquid - air (or oil) interface, greatly reducing the stabilising role of the particles<sup>13</sup>.

Despite previous research<sup>8,13,14</sup>, the combined action of surfactant and particles in stabilising emulsions and foams is not yet fully understood. The lack of reliable methods for direct measurements of particle contact angles in surfactant systems is amongst the reasons holding back the progress in this field. Previous studies on the role of particles in foam/emulsion systems containing surfactants relied on indirect information about the particle wettability obtained by measuring the contact angle on a macroscopic piece of material with similar surface chemistry<sup>12-15</sup>.

In the previous chapter (Chapter 3) it was demonstrated that the FCM can be used for direct measurements of colloidal particle contact angles at air - water and oil - water interfaces even in the presence of surfactant. Here, the aim is to investigate foams and emulsions of silica particle and cationic surfactant mixtures and measure the particle contact angles using the FCM in order to reveal the link between the wettability of the particles, their stabilising ability and mechanisms of stabilisation in the studied systems. Adsorption of surfactant on the particle surface and its effect on the particle charge (zeta potential) as a function of the surfactant concentration are also investigated and correlated to the particle contact angles obtained for these systems.

## **4.2 Experimental**

Investigations were performed into the changes in system properties and stabilisation of foams and emulsions with mixtures of silica particles and cationic surfactants. Two cationic surfactants were used; tetradecyltrimethylammonium bromide (TTAB) and cetylpyridinium chloride (CPC), with critical micelle

concentrations of 3.5 mM<sup>16-19</sup> and 0.9 mM<sup>20-22</sup>, respectively, at 25 °C (section 2.1.2). Silica particles 1 µm in diameter were investigated for adsorption of CPC surfactant on the silica surface, changes in contact angle and particle charge, and for stabilising foams and emulsions. Silica particles with diameter of 2.76 µm have been used for measuring changes in contact angle and for making emulsions. Both sets of particles are described in section 2.1.1.1. The oil used was decalin which was passed three times through basic alumina before use (section 2.1.2).

### 4.3 Results and discussion

#### *4.3.1 Surface and interfacial tensions of surfactant solutions*

The surface and interfacial tensions measured for TTAB surfactant are shown in Table 4.1 and Fig. 4.1. The surface tension decreases with increasing surfactant concentration until a concentration of 3 mM, above which the surface tension plateaus at ~36 mN m<sup>-1</sup> and suggests that the cmc is close to 3 mM. A similar trend has been observed previously<sup>23</sup> and the surface tension values obtained were a close fit to those in the literature<sup>24,25</sup>. The interfacial tension with decalin as the light phase was measured and shows the same trend to that of the surface tension. The interfacial tension of pure water and decalin was 42.4 mN m<sup>-1</sup>. This decreased with increasing concentration to ~6 mN m<sup>-1</sup> at 3 mM and remained constant at higher concentrations as with the surface tension. The data for surface and interfacial tension both show that the TTAB cmc is close to 3 mM, close to the 3.5 mM reported in the literature<sup>16-19</sup>. The surface tension of CPC solutions<sup>23,26,27</sup> is seen to follow the same trend as that of TTAB with surface tension decreasing as surfactant concentration increases (Fig. 4.1).

**Table 4.1.** Surface and interfacial tension of aqueous TTAB solutions measured by the Du Nouy ring method at 25 °C. Interfacial tension was measured with a decalin light phase. Uncertainty in the measurements is  $\pm 0.2$ .

| [TTAB] /mM | Surface tension<br>/mN m <sup>-1</sup> | Interfacial tension<br>/mN m <sup>-1</sup> |
|------------|--|--|
| 0          | 72.5                                   | 42.4                                       |
| 0.01       | 71.4                                   | 39.3                                       |
| 0.1        | 67.0                                   | 32.2                                       |
| 0.5        | 60.9                                   | 25.0                                       |
| 1.0        | 54.9                                   | 22.0                                       |
| 2.0        | 44.9                                   | 10.6                                       |
| 3.0        | 36.2                                   | 5.6  |
| 10.0       | 36.1                                   | 5.6  |
| 30.0       | 36.1                                   | 5.3  |

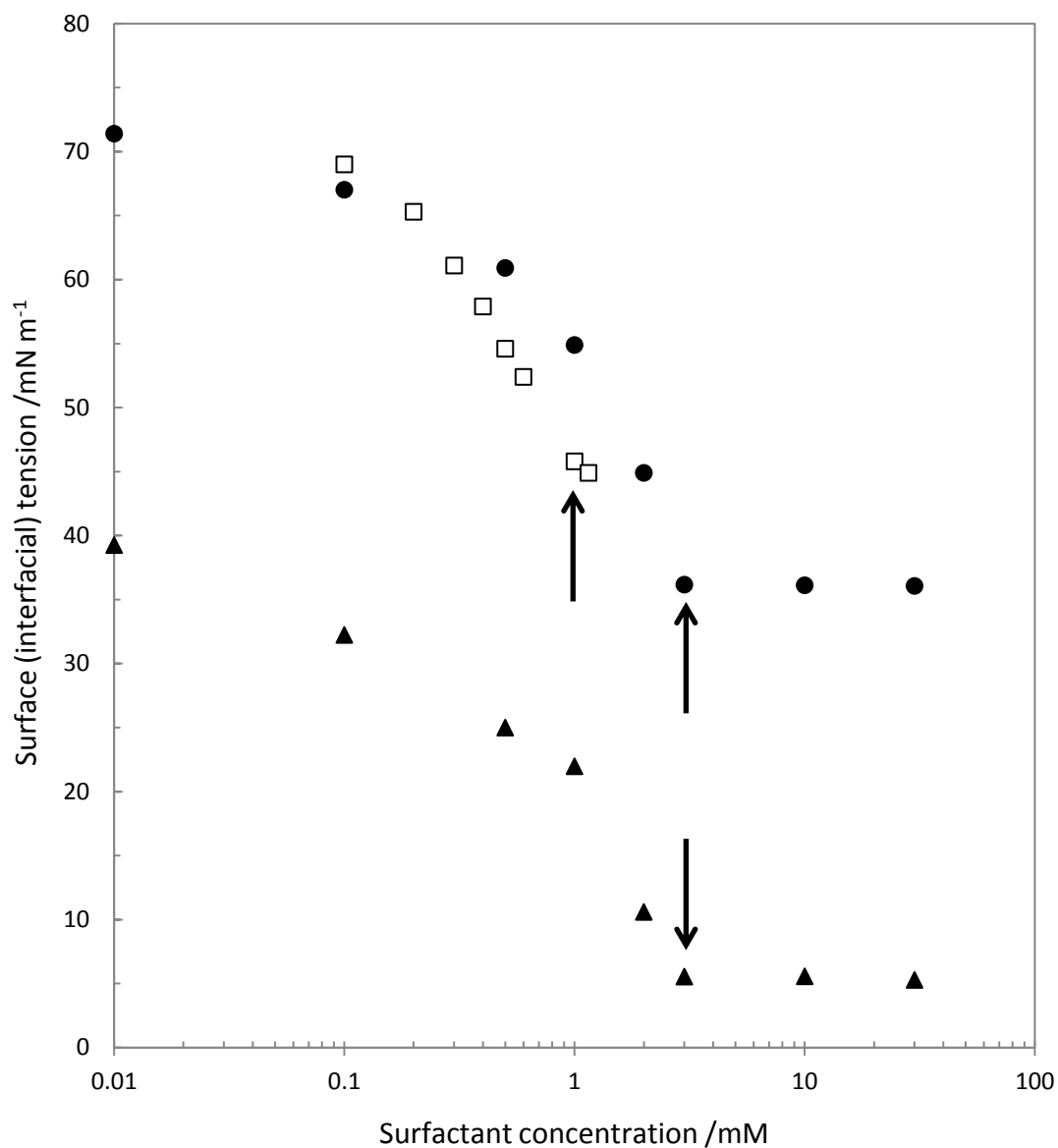
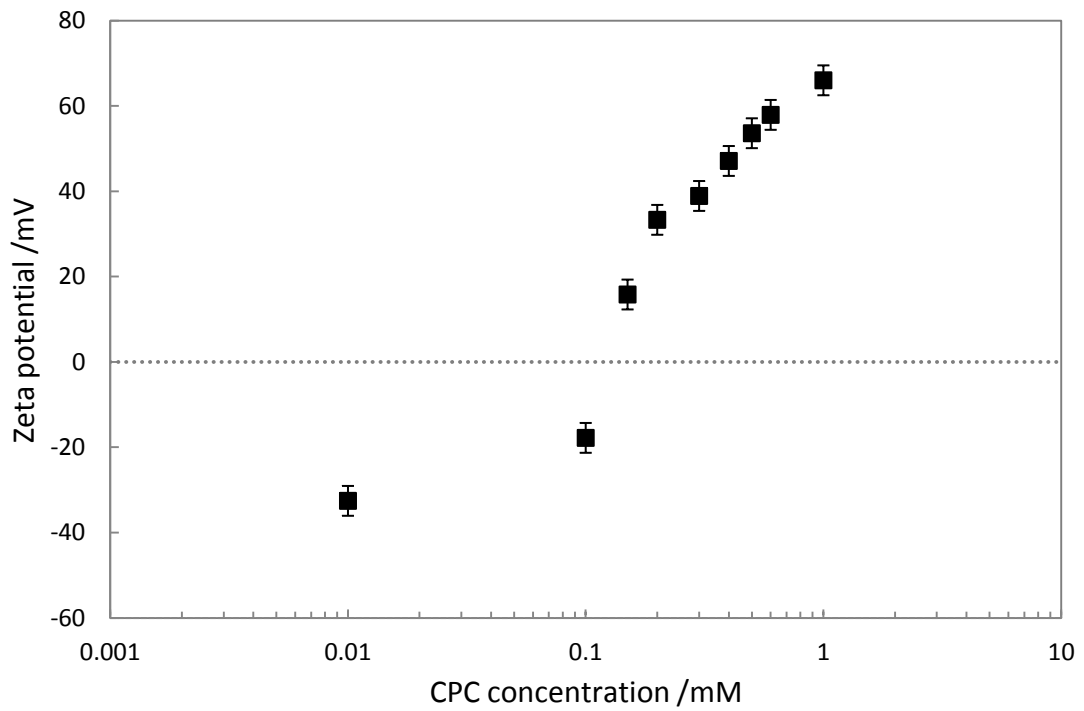


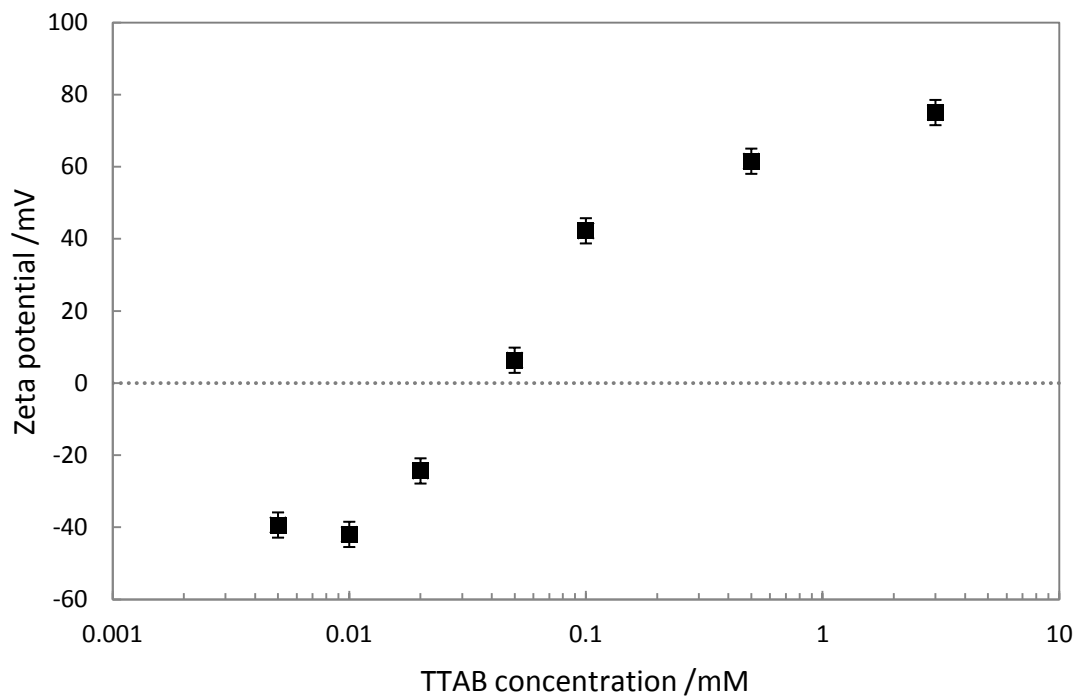
**Figure 4.1.** Surface tension (circles) and decalin-water interfacial tension (triangles) of TTAB solutions measured by the Du Nouy ring method at 25 °C. The uncertainty in these measurements is  $\pm 0.2 \text{ mN m}^{-1}$ . Open squares show the surface tension of CPC solutions<sup>26</sup>. The respective critical micelle concentrations are shown with arrows.

#### *4.3.2 Zeta potential of silica particles in surfactant solutions*

The zeta potentials of 1  $\mu\text{m}$  silica particles in CPC solutions are shown in Fig. 4.2a. At low surfactant concentrations the particles are negatively charged (-33 mV). With increasing surfactant concentration the particle charge gradually increases up to 0.1 mM at which a large change in charge occurs for a small increase in surfactant concentration and particle charge shifts from negative to positive. At concentrations above this the positive charge increases to 66 mV at 1 mM (near cmc). The same trend is observed with 1  $\mu\text{m}$  particles in TTAB (Fig. 4.2b) with particle charge -40 mV at low concentrations, a large change in surface charge and sign close to 0.05 mM, before levelling off and reaching a charge of +75 mV at 3 mM (near cmc). The trends determined are the same as those shown in Fig. 1.6, and match with previous observations of cationic surfactant molecules absorbing on negatively charged particles<sup>9,14,28</sup>.



(a)



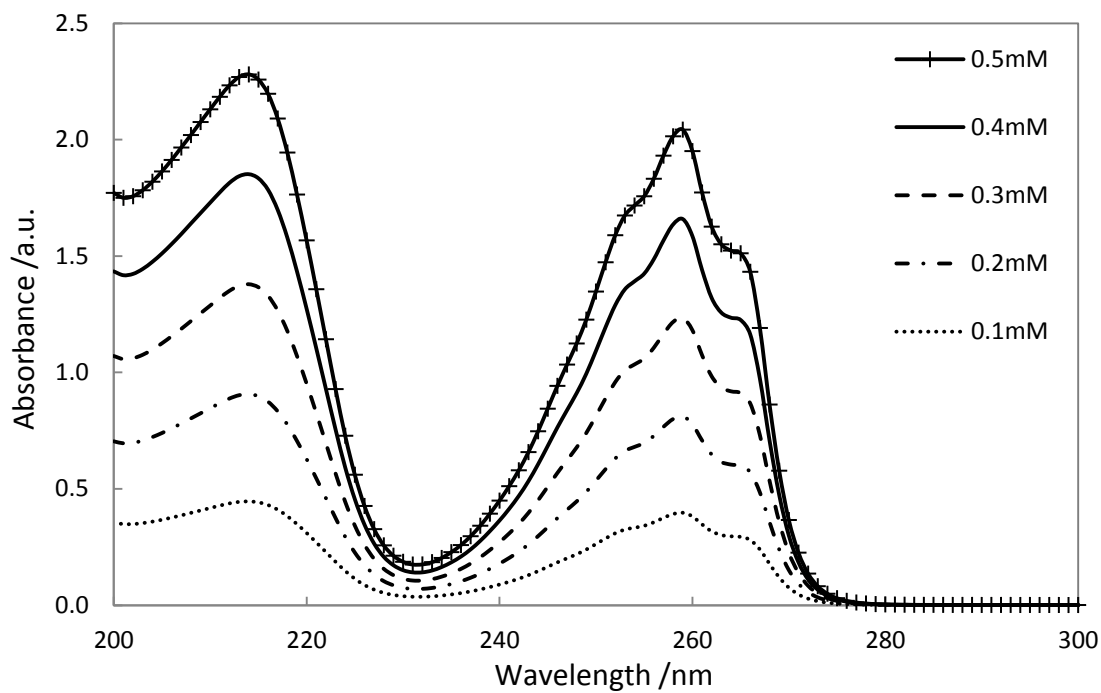
(b)

**Figure 4.2.** Zeta potential of silica particles with diameter 1  $\mu\text{m}$  in aqueous surfactant solutions versus total concentration of (a) CPC and (b) TTAB at natural pH and ionic strength.

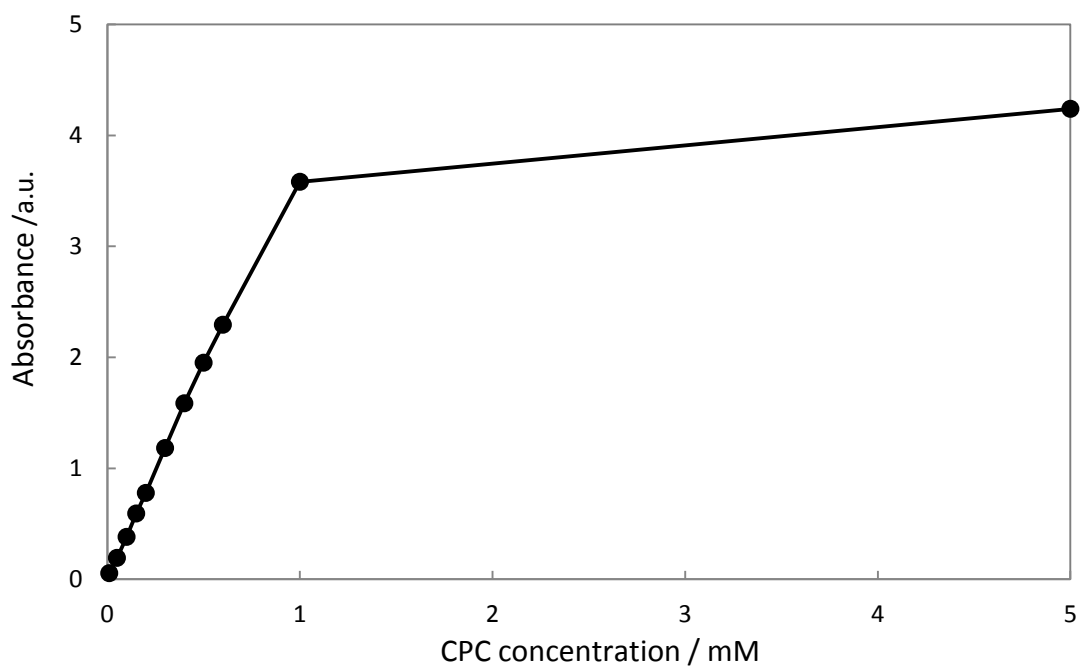
#### *4.3.3 Adsorption of CPC on the silica particle surface*

Aqueous solutions of CPC show strong UV light absorbance at a wavelength of 260 nm (Fig. 4.3). The absorbance at this wavelength depends on the CPC concentration. This can be used for determining the CPC concentration in a solution by measuring its absorbance, if the absorbance versus concentration dependence is known. The adsorption of CPC on the surface of silica particles reduces its concentration in the solution, hence the adsorbed amount can be calculated from the decrease of the CPC concentration in the clear solution obtained after centrifugation of an equilibrated particle suspension.

The UV absorbance of CPC solutions with varying concentration was measured in order to create a calibration curve. Three measurements were performed with each pure solution to determine the average and standard deviation. These measurements were performed against a 'background' sample of milli-Q water (i.e. zero concentration solution of CPC) which acted as the baseline. Fig. 4.1a shows the UV absorbance curves measured for various concentrations over the wavelength range 200 – 300 nm. The values at 260 nm were taken for the calibration curve, as has been used previously<sup>29</sup>. A plot of changing absorbance with surfactant concentration is shown in Fig. 4.1b. In the low concentration range the increase of absorbance was linear, however at the cmc of the surfactant (~1 mM) the gradient of the line changed dramatically. Therefore, measurements at lower concentrations alone were used for producing the calibration. The calibration line for determining the surfactant concentration from a set measurement of UV absorbance was obtained from the best linear fit to the concentration versus absorbance data (Fig. 4.4).



(a)



(b)

**Figure 4.3.** (a) UV absorbance ( $\pm 0.001$  a.u.) of CPC surfactant solutions and (b) UV absorbance ( $\pm 0.001$  a.u.) at a wavelength of 260 nm for a range of surfactant concentrations.

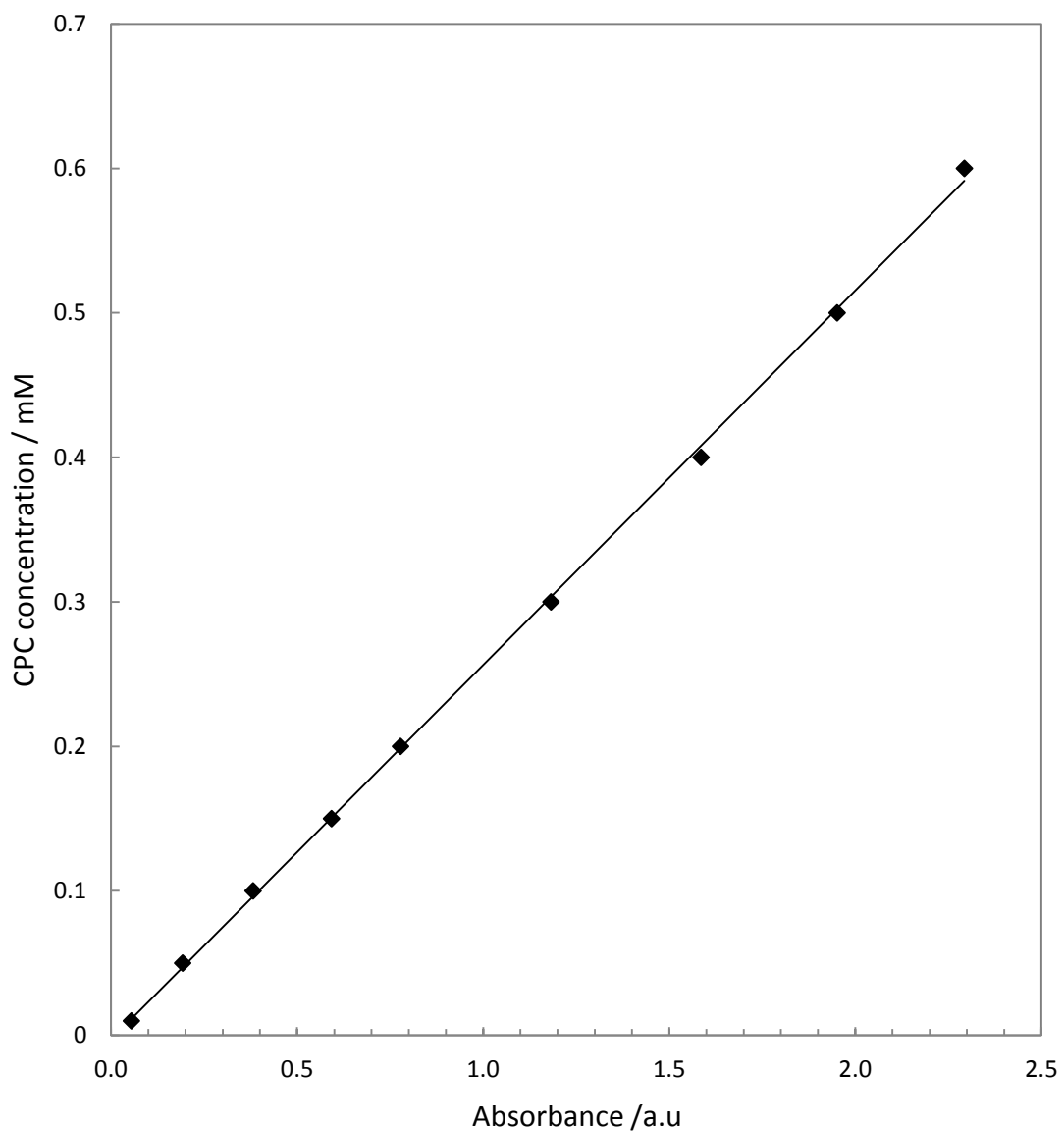


**Figure 4.4.** Calibration line of CPC concentration versus UV absorbance measured at 260 nm. The fit of this calibration line gives equation 4.1.

A linear relationship between the CPC concentration,  $C$ , and the absorbance at 260 nm,  $A$ , was found for  $A \leq 2.3$  a.u. and the calibration equation (4.1) was obtained.

$$C = (0.259 \pm 0.002)A - (0.003 \pm 0.003) \quad (4.1)$$

This equation holds true for absorbance measurements up to 2.3 a.u. (0.6 mM) although above this, up to 3.6 a.u. (1 mM), there is still a relatively close match between the actual and calculated solution concentrations. If a solution of a higher concentration needed to be measured it was diluted by a set volume, measured and then the original concentration calculated.

To determine the CPC adsorption on the particle surface, suspensions of silica particles in CPC solutions of varying surfactant concentration were prepared and left to equilibrate for 24 hours. The supernatant was subsequently removed after sedimenting the particles and UV absorbance measurements were acquired. Using equation 4.1 and the measurements of supernatant UV absorbance the concentration of each supernatant was determined and the drop in concentration which had occurred was calculated. From the drop in concentration and total particle surface area, the adsorption of the surfactant onto the silica surface ( $\Gamma$ ) was calculated for a range of initial surfactant concentrations (Fig. 4.5).  $\Gamma$  increases with surfactant concentration, but reaches a plateau near the cmc (0.9mM<sup>21,22</sup>). Similar trend of  $\Gamma$  with CPC concentration has been reported for the adsorption on the surface of fumed silica particles<sup>8,29</sup>.

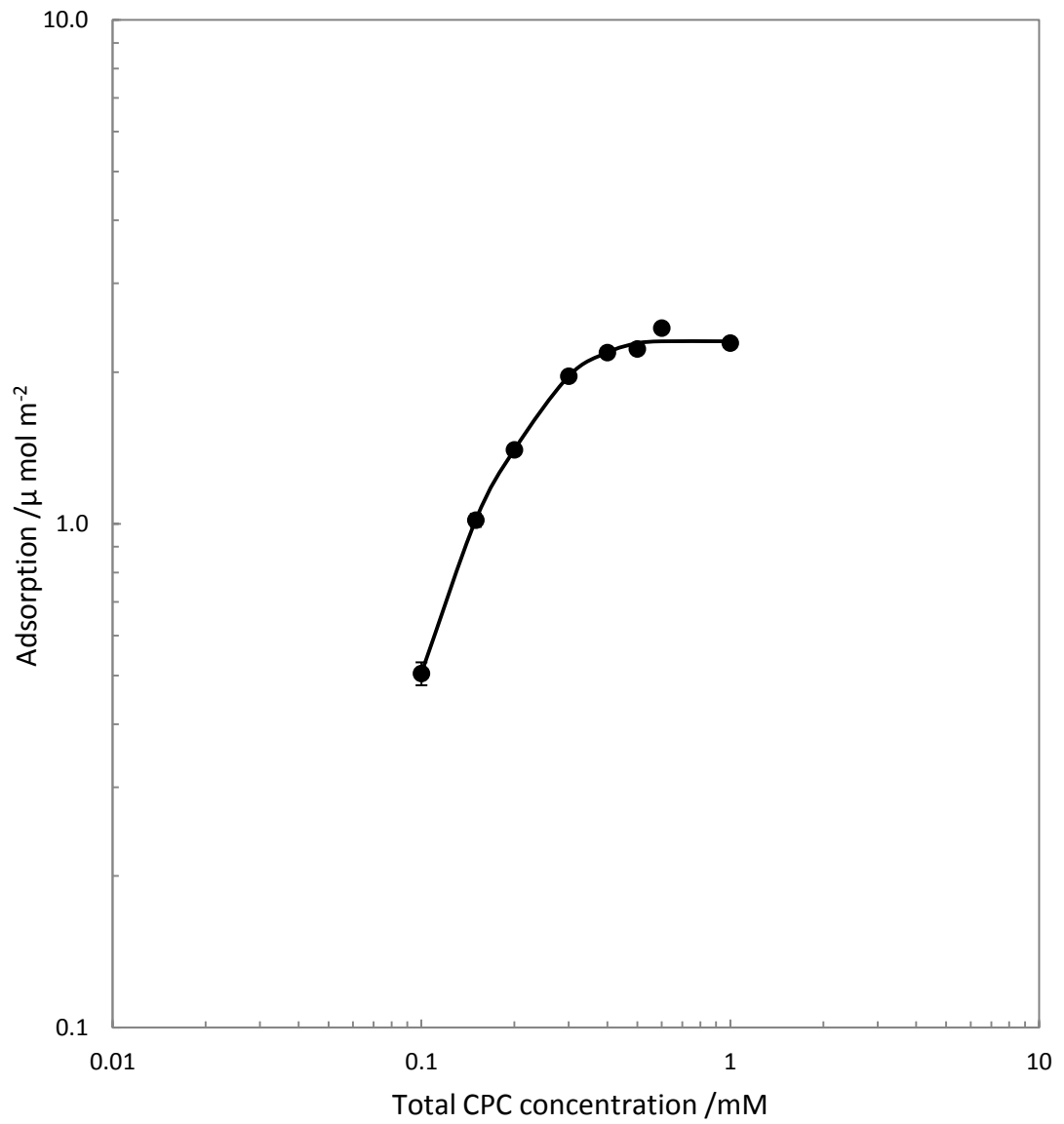


**Figure 4.5.** CPC adsorption ( $\pm 0.04 \mu\text{mol m}^{-2}$ ) onto  $1 \mu\text{m}$  silica particles versus total CPC concentration in 4 wt.% aqueous suspensions at room temperature with no added electrolyte.

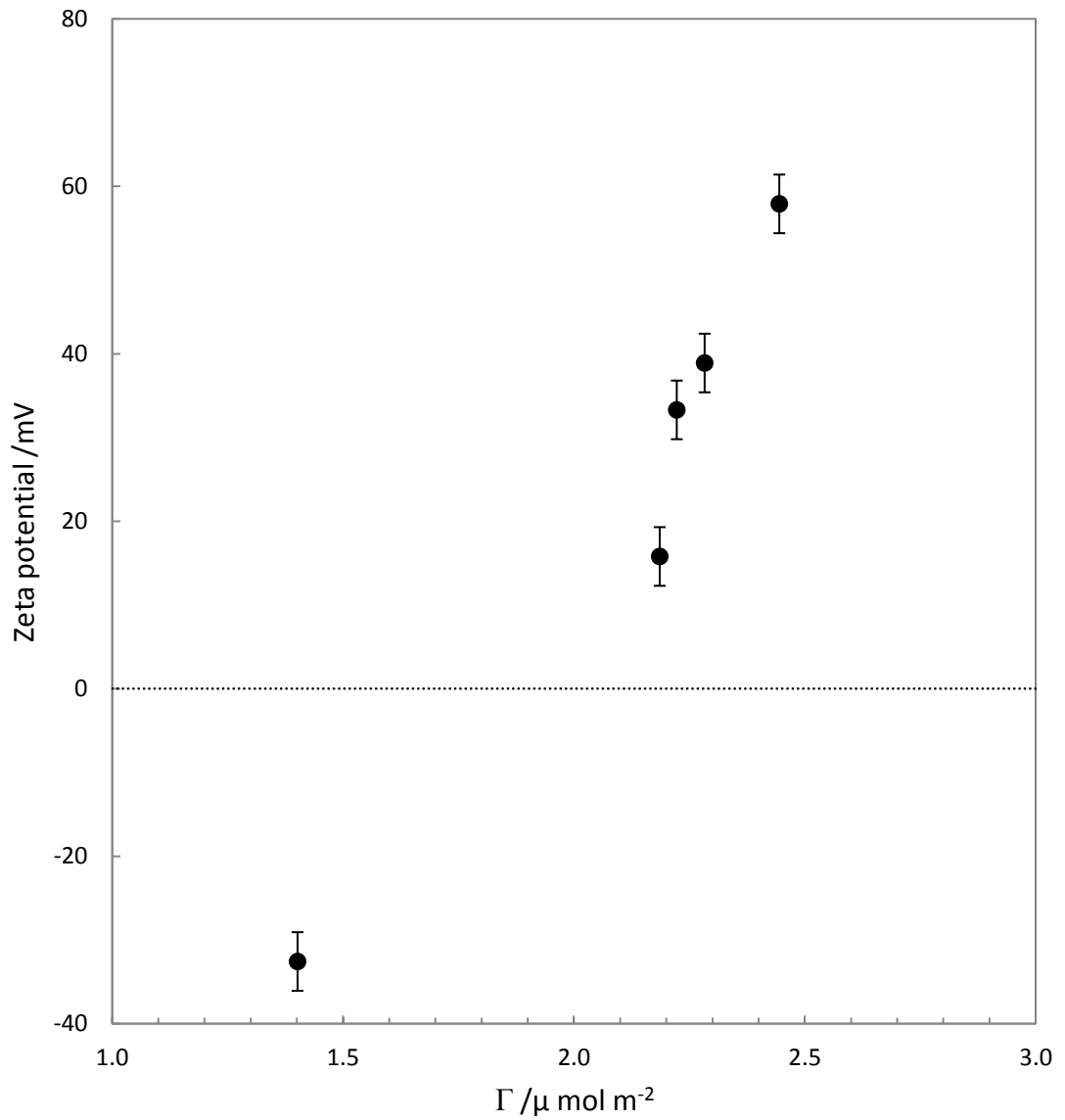


**Figure 4.6.** Zeta potentials measured on 1  $\mu\text{m}$  silica particles in CPC solutions versus the surfactant adsorption. Measurements were performed at room temperature with no added electrolyte.

The change of zeta potential with surfactant adsorption is shown in Fig. 4.6. The particle charge is shown to change proportionally with increasing surfactant adsorption. This to be expected as the positive charge of the surfactant headgroups counterbalances the negative surface charge. The pH of CPC solutions both with and without particles, are shown in table 4.2. With surfactant solution the pH is constant across the concentration range but the pH of particle suspensions decreases with increasing surfactant concentration. This occurs because the adsorption of cationic surfactant encourages dissociation of hydroxyl groups on the silica surface, releasing hydrogen ions into solution, and thus decreasing the pH.

**Table 4.2.** Measurements of the pH of CPC solutions and suspensions of 1  $\mu\text{m}$  silica particles at 25 °C.

| [CPC] /mM | pH $\pm$ 0.2 |                  |
|-----------|--------------|------------------|
|           | no particles | 4 wt.% particles |
| 0         | 7.4          | 6.8              |
| 0.1       | 7.2          | 6.5              |
| 0.15      | 6.9          | 6.9              |
| 0.2       | 7.0          | 6.8              |
| 0.3       | 7.0          | 5.0              |
| 0.4       | 7.0          | 4.5              |
| 0.5       | 6.9          | 4.4              |
| 0.6       | 7.0          | 4.3              |
| 1.0       | 6.8          | 4.3              |
| 5.0       | 6.8          | 4.0              |

The concentration of TTAB surfactant solutions cannot be determined with photometric methods in the same way as CPC, however changes in zeta potential (Fig. 4.2b) and pH of TTAB solutions and suspensions (Table. 4.3) show the same trends as those with CPC surfactant.

**Table 4.3.** Measurements of the pH of TTAB solutions and suspensions of 1  $\mu\text{m}$  silica particles at 25  $^{\circ}\text{C}$ .

| [TTAB] /mM         | pH $\pm$ 0.2 |                  |
|--------------------|--------------|------------------|
|                    | No particles | 4 wt.% particles |
| 0.0                | 7.4          | 6.8              |
| $5 \times 10^{-4}$ | 6.7          | 6.6              |
| $5 \times 10^{-3}$ | 6.8          | 6.6              |
| 0.01               | 6.8          | 6.5              |
| 0.02               | 6.9          | 6.5              |
| 0.05               | 6.6          | 6.2              |
| 0.1                | 7.0          | 6.2              |
| 0.5                | 7.0          | 6.1              |
| 1.0                | 6.9          | 5.4              |
| 2.0                | 7.0          | 5.3              |
| 3.0                | 7.0          | 5.0              |
| 10.0               | 6.7          | 4.8              |

#### *4.3.4 Contact angles of silica particles at the air-water interface in the presence of surfactant*

In order to relate the surfactant adsorption to the silica particle wettability, measurements of the particle contact angle at varying concentrations of CPC were made using the Film Calliper Method (FCM). These results are shown in Fig. 4.7 for contact angles at an air - aqueous solution interface. The contact angle increases with increasing surfactant concentration until an adsorption of  $\Gamma \approx 2 \mu\text{mol m}^{-2}$  is reached, but rapidly decreases at higher concentrations and  $\Gamma$ . The trend in the particle contact angle with CPC concentration can be understood using the reverse orientation model for the adsorption of surfactant molecules discussed in chapter 1 (Fig. 1.5). At low CPC concentrations, the CPC molecules adsorb on silica in head-on orientation exposing the hydrophobic tails towards the water, hence the silica particle surface becomes more hydrophobic and the contact angle increases. At higher concentrations surfactant molecules aggregated against the extended hydrophobic tails, thus exposing the hydrophilic heads towards water and the

particle contact angle decreases. Therefore the contact angle of silica particles passes through a maximum at some intermediate concentration of CPC, while the adsorption monotonically increases. Above the cmc, a complete bilayer of surfactant molecules surrounding the particles can be formed and the particle contact angle could drop to zero degrees, but  $\Gamma$  reaches a plateau.

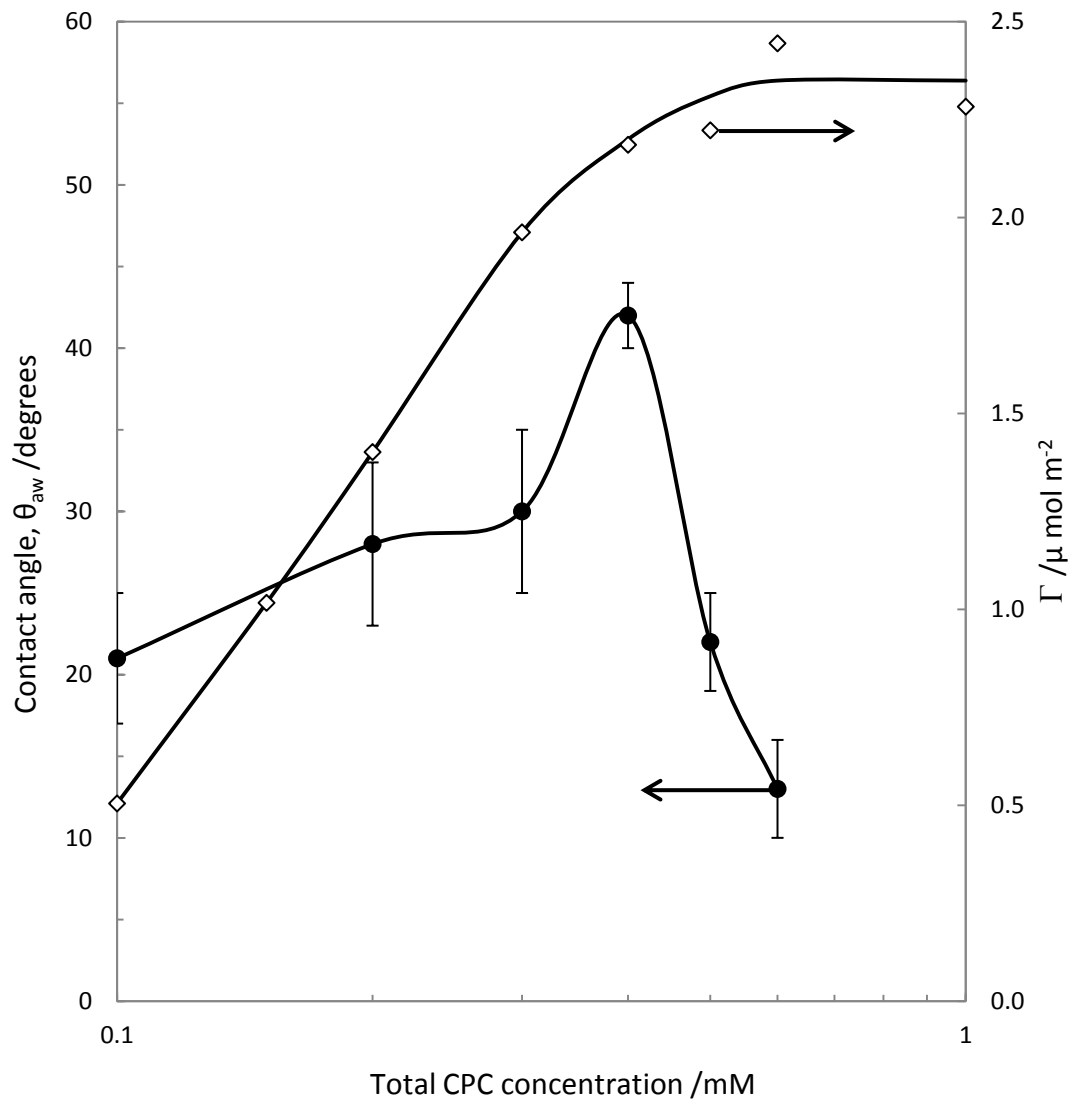


**Figure 4.7.** Surfactant adsorption ( $\pm 0.04 \mu\text{mol m}^{-2}$ ) and particle contact angle both plotted as a function of total surfactant concentration in 4 wt.% aqueous suspensions of silica particles with  $1 \mu\text{m}$  diameter.

The relationship between the CPC adsorption and silica particle contact angle is illustrated in Fig. 4.8, where the contact angle at the air-aqueous CPC solution interface is plotted against the adsorption,  $\Gamma$ . The contact angle of bare silica ( $22 \pm 3^\circ$ ) gradually increases with  $\Gamma$  until it reaches its maximum value of  $42 \pm 2^\circ$  at  $\Gamma = 2.17 \mu\text{mol m}^{-2}$ . After the maximum,  $\theta_{\text{aw}}$  rapidly drops to very small values ( $\sim 10^\circ$ ) due to a small change in the CPC adsorption.

Particle sedimentation in CPC solutions was observed over time and the fastest sedimentation related to a concentration of 0.4 mM, where the particles were measured to be the most hydrophobic (see figure 4.9 a and b). The rapid sedimentation at this CPC concentration suggests that the electrostatic repulsion between the silica particles is largely reduced due to the adsorption of surfactant, hence the net particle charge should be close to zero. This apparently contradicts to the zeta potential versus CPC concentration dependence shown in Fig. 4.2. To resolve this apparent discrepancy one should take into account that the particle concentration in the zeta potential measurements (less than 0.04 wt.%) is much smaller than that in the adsorption and contact angle experiments (4 wt.%). Hence the adsorbed amount of CPC on the particle surface in the zeta potential experiments is negligible and the equilibrium concentration of CPC in the solvent is practically equal to the total CPC concentration in the suspension. In concentrated suspensions, the equilibrium and total CPC concentrations could be very different and this should be taken into account when comparing the results for zeta potential with those for the adsorption and contact angle.

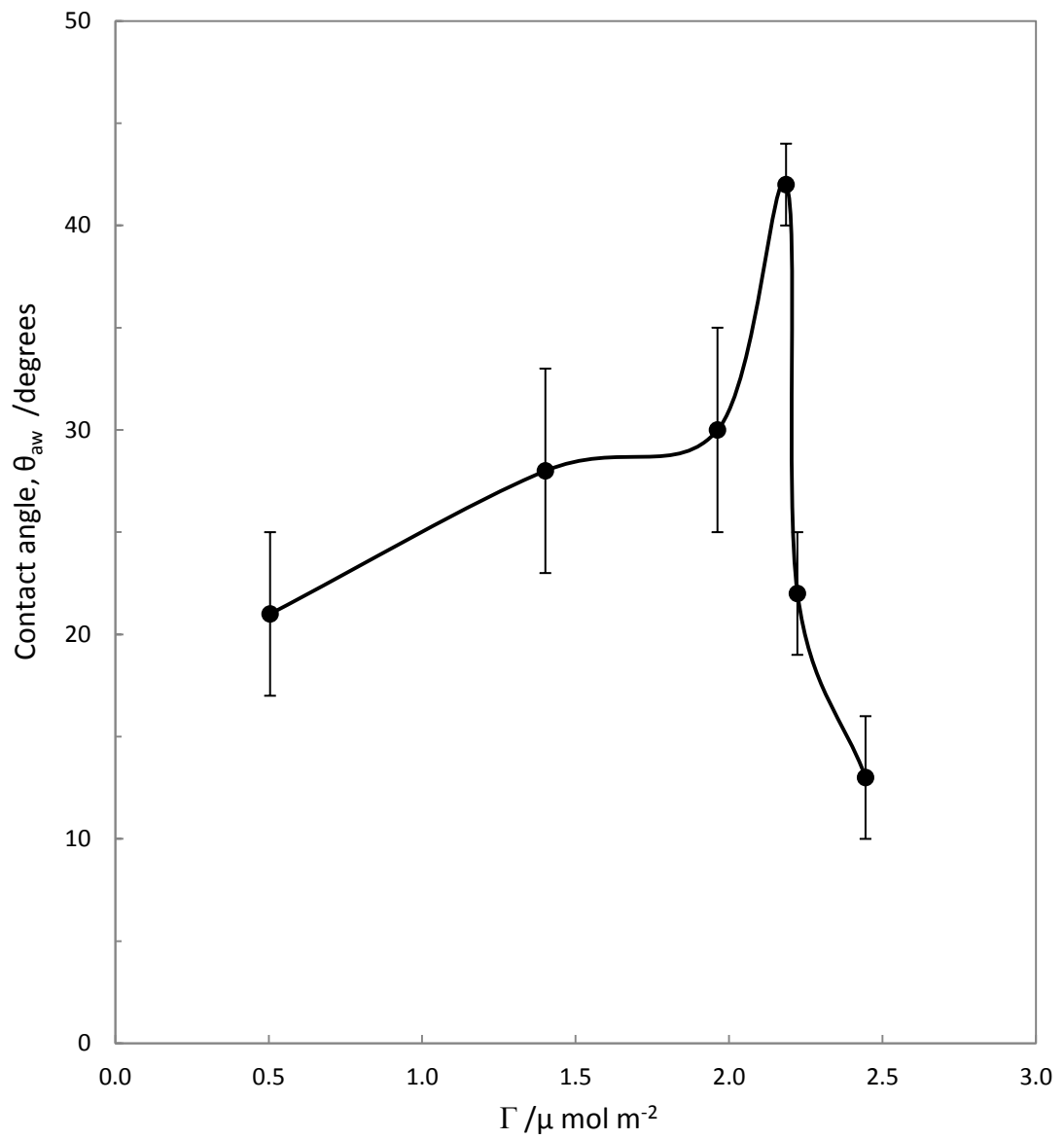
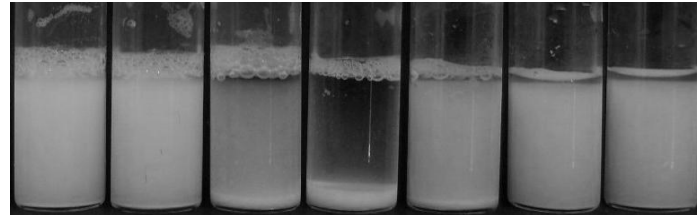


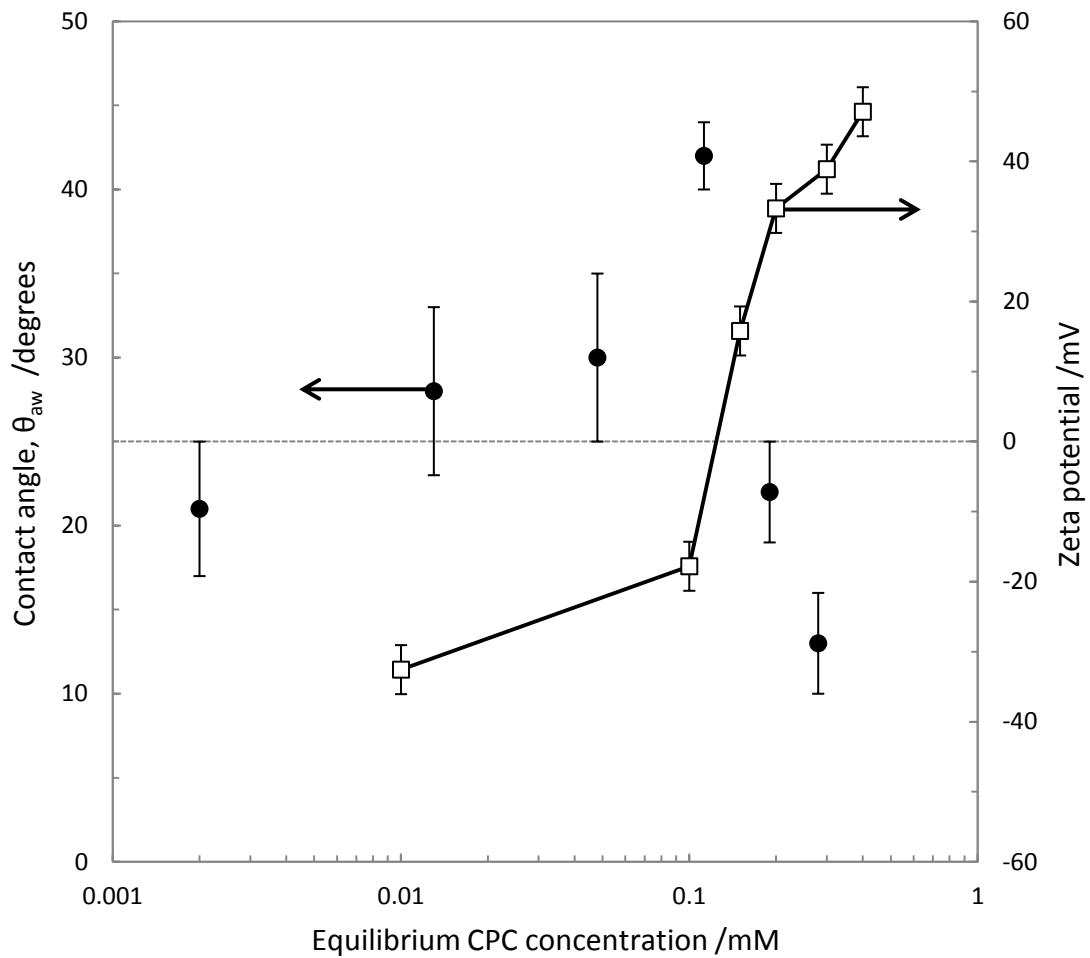
**Figure 4.8.** Contact angles of 1  $\mu\text{m}$  silica particles versus the surfactant adsorption at the silica surface.

Particle contact angles at the air - aqueous CPC solution interface and zeta potential of 1  $\mu\text{m}$  silica particles are plotted against equilibrium CPC concentration in Fig. 4.9 for comparison. It is seen that the equilibrium concentration relating to maximum hydrophobicity and zero net particle charge is  $\sim 0.1$  mM. At the same equilibrium concentration (0.11 mM) the greatest aggregation and sedimentation of particles is also observed and resolves the discrepancy described above.



[CPC]<sub>equilibrium</sub>: 0.002 0.013 0.048 0.11 0.19 0.28 0.67  
 [CPC]<sub>total</sub>: (0.1) (0.2) (0.3) (0.4) (0.5) (0.6) (1.0)

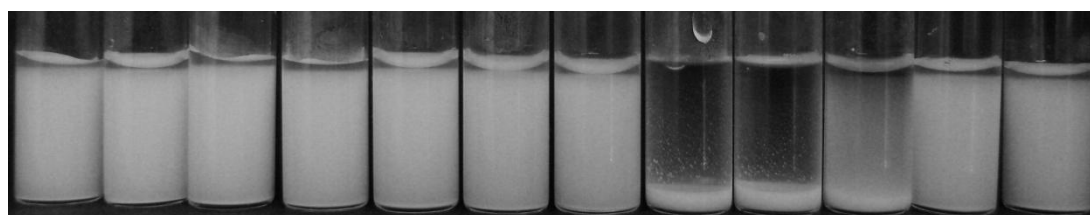
(a)



(b)

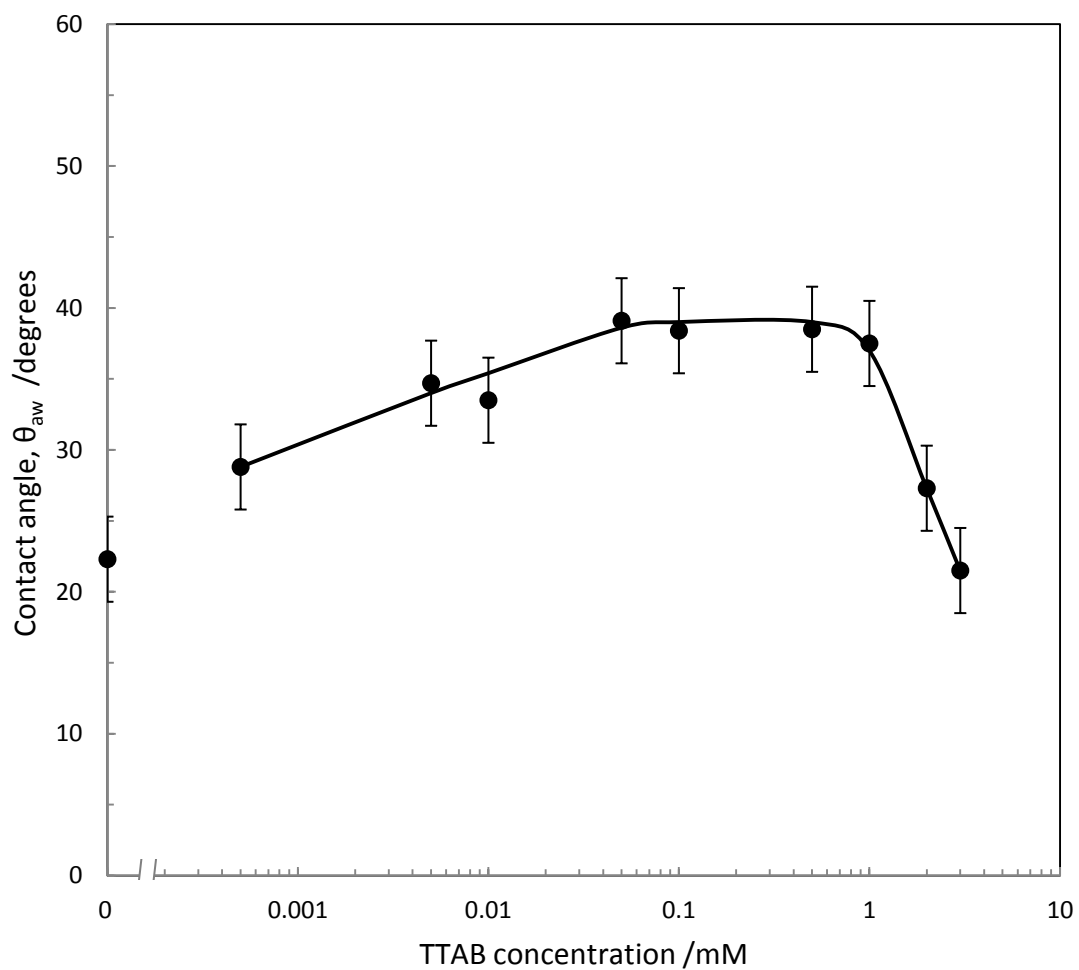
**Figure 4.9.** (a) Images of 4 wt.% silica particle suspensions in CPC solutions with varying concentrations (shown) taken 1 hour after homogenisation. (b) Contact angles (filled circles) at the air - aqueous CPC solution interface and zeta potential (boxes) of 1  $\mu$ m silica particles versus equilibrium CPC concentration. For details see the text.

The contact angles of 1  $\mu\text{m}$  silica particles at the air - aqueous TTAB solution interface were measured and are compared with the stability of suspensions in Fig. 4.10. The contact angles of silica particles at the air surface increase gradually with TTAB concentration to 0.05 mM where it plateaus at  $39^\circ$ , before rapidly decreasing at concentrations greater than 1 mM, to  $22^\circ$  approaching cmc. A similar trend was observed for the contact angle of larger silica particles in TTAB solutions (Chapter 3, Fig. 3.6), although the contact angle values were 10 – 30 % larger than those for 1  $\mu\text{m}$  silica particles. The discrepancy could be due to differences in the number density of silanol groups at the surface of these silica particles obtained from different suppliers. The particle contact angle versus TTAB concentration dependence is similar to that obtained with CPC, but there is a broad region of TTAB concentrations where the contact angle does not change appreciably and stays close to its maximum value ( $\sim 39^\circ$ ).



0.0 0.0005 0.005 0.01 0.02 0.05 0.1 0.5 1.0 2.0 3.0 10.0

(a)



(b)

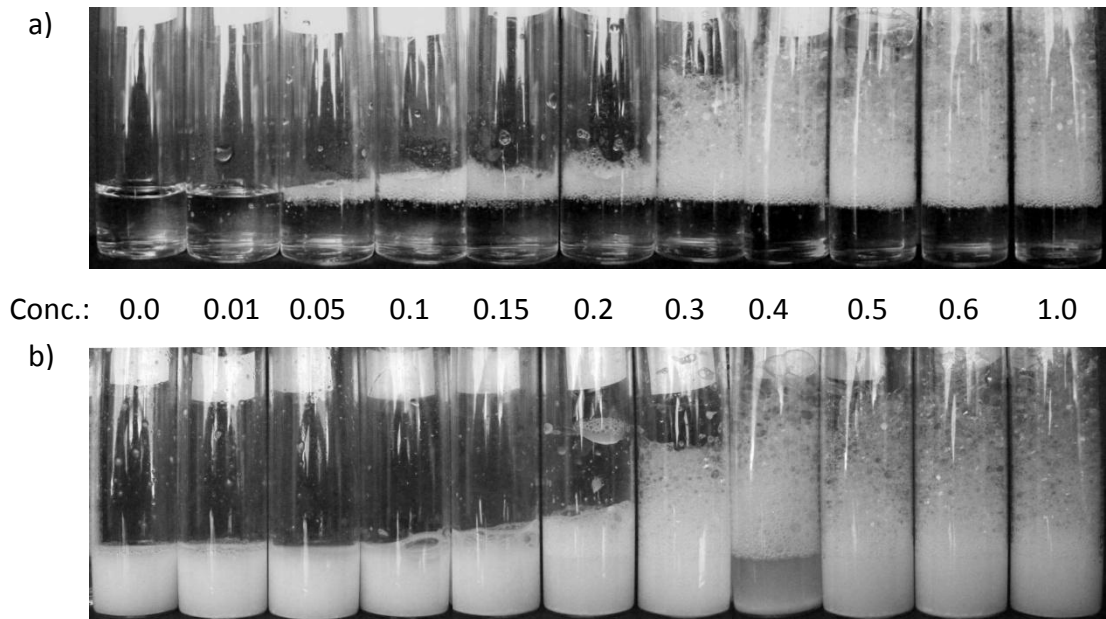
**Figure 4.10.** (a) Suspensions of silica particles with a diameter of 1  $\mu\text{m}$  in TTAB solutions with varying concentrations (shown in mM) after standing for 1 hour and (b) contact angle of the same particles measured by the FCM as a function of TTAB concentration.

#### *4.3.5 Differences in foaming between surfactant solutions and surfactant solution/silica particle mixtures*

Suspensions of 4 wt.% silica particles in both CPC and TTAB solutions of varying concentrations were used to produce foams. The foamability of the suspensions and stability of the foams were determined and compared to those of surfactant solutions in the absence of particles. Images taken shortly after the foam was produced (~5 minutes) by hand-shaking and at a later time are shown in Figs. 4.11 and 4.12 for both CPC and TTAB, respectively. It is seen that the amount of foam varies with the surfactant concentration and foam ageing time. These dependencies are even clearer in Figs. 4.13 - 4.16 where the foam heights measured at different times are plotted against the total surfactant concentration for CPC and TTAB, respectively.

At low surfactant concentrations the initial amount of foam produced is very low for both CPC and TTAB, both with and without particles present. The initial foam height increases significantly at intermediate concentrations, then plateaus approaching cmc with foam height > 45 mm in all samples. CPC solutions without particles could not stabilise the foam for up to 24 hours (Fig. 4.13) at any surfactant concentration, however with particles present the foam was much more stable at intermediate surfactant concentrations for up to a month (Fig. 4.14), with half of the foam remaining at a surfactant concentration of 0.4 mM. At high CPC concentrations breakdown of the foam occurred within 24 hours even with particles present. Foams made from TTAB solutions alone (Fig. 4.15) were present for up to a week at 3 mM (cmc) with ~13 mm foam remaining but complete or near complete foam breakdown was observed at all other concentrations. With a mixture of 4 wt.% particles and TTAB solutions (Fig. 4.16) the foams were more stable at intermediate concentrations (0.05 - 0.5 mM) for over a week, similarly to CPC, with almost all of the initial foam remaining. At high TTAB concentrations the foam stability with particles present was nearly identical to that of surfactant alone, with ~13 mm foam remaining at cmc after a week.

Time = 5 minutes



Time = 24 hours

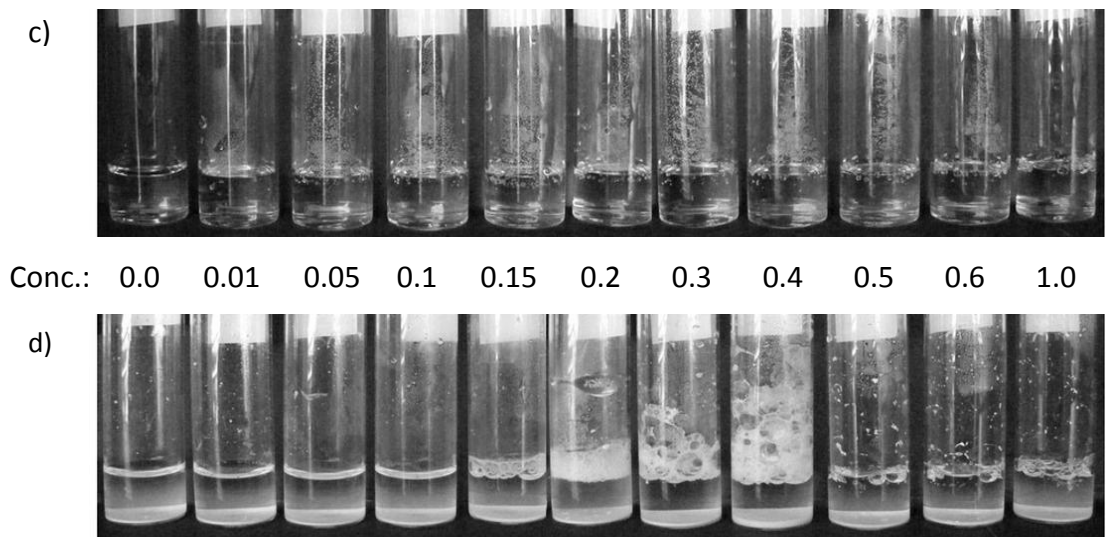
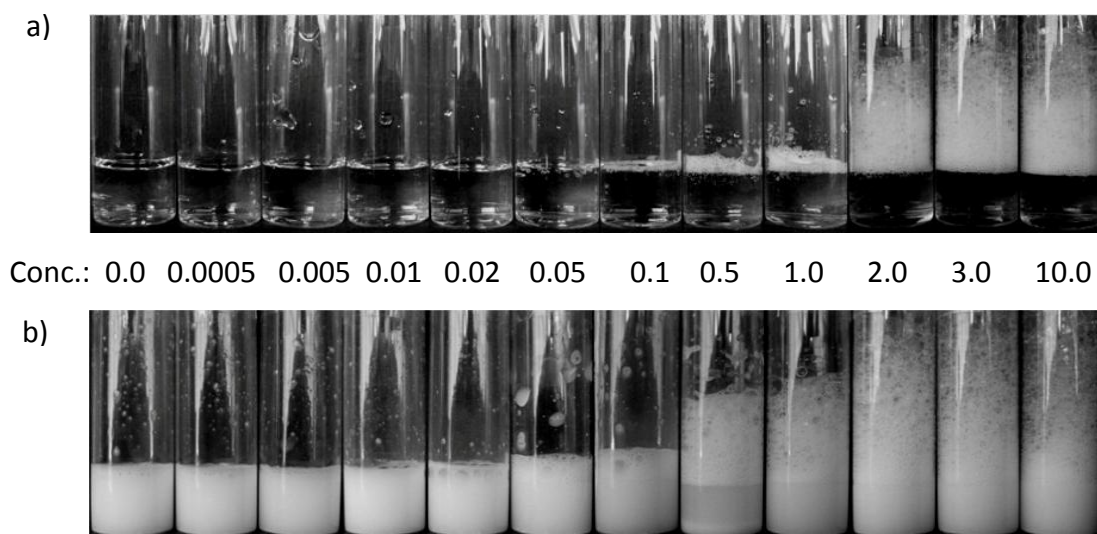


Figure 4.11. Images of foams produced from CPC solutions of varying concentrations (listed in mM) in the absence (a, c) and presence of 4 wt.% silica particles with diameter of 1  $\mu\text{m}$  (b, d) taken 5 min (a, b) and 24 h (c, d) after foaming.

Time = 5 minutes



Time = 1 week

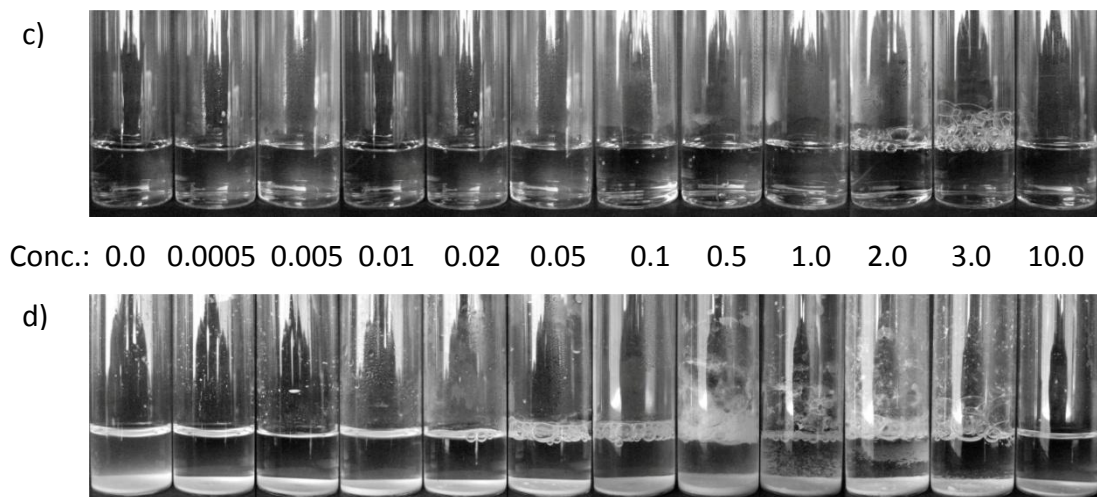
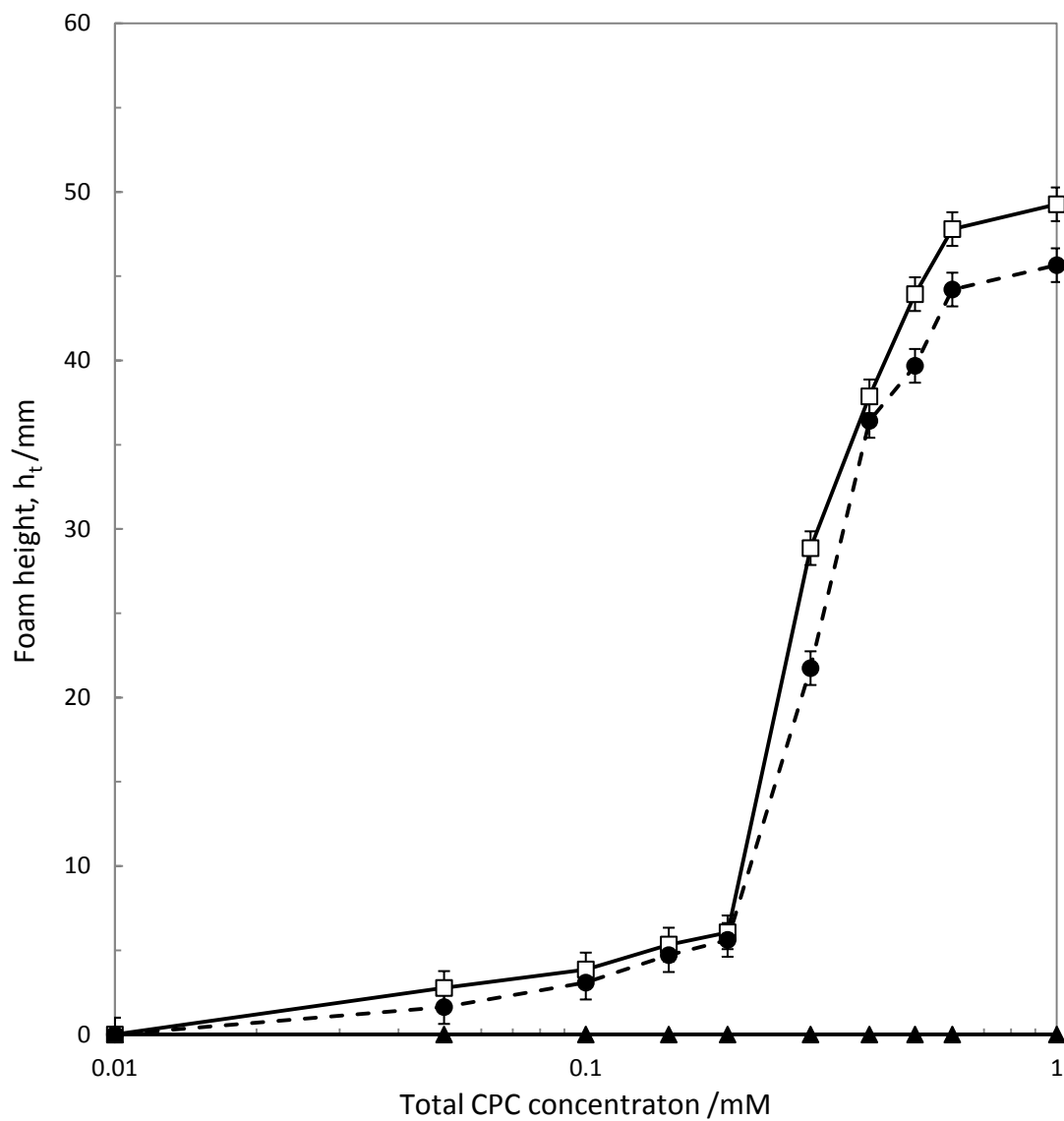
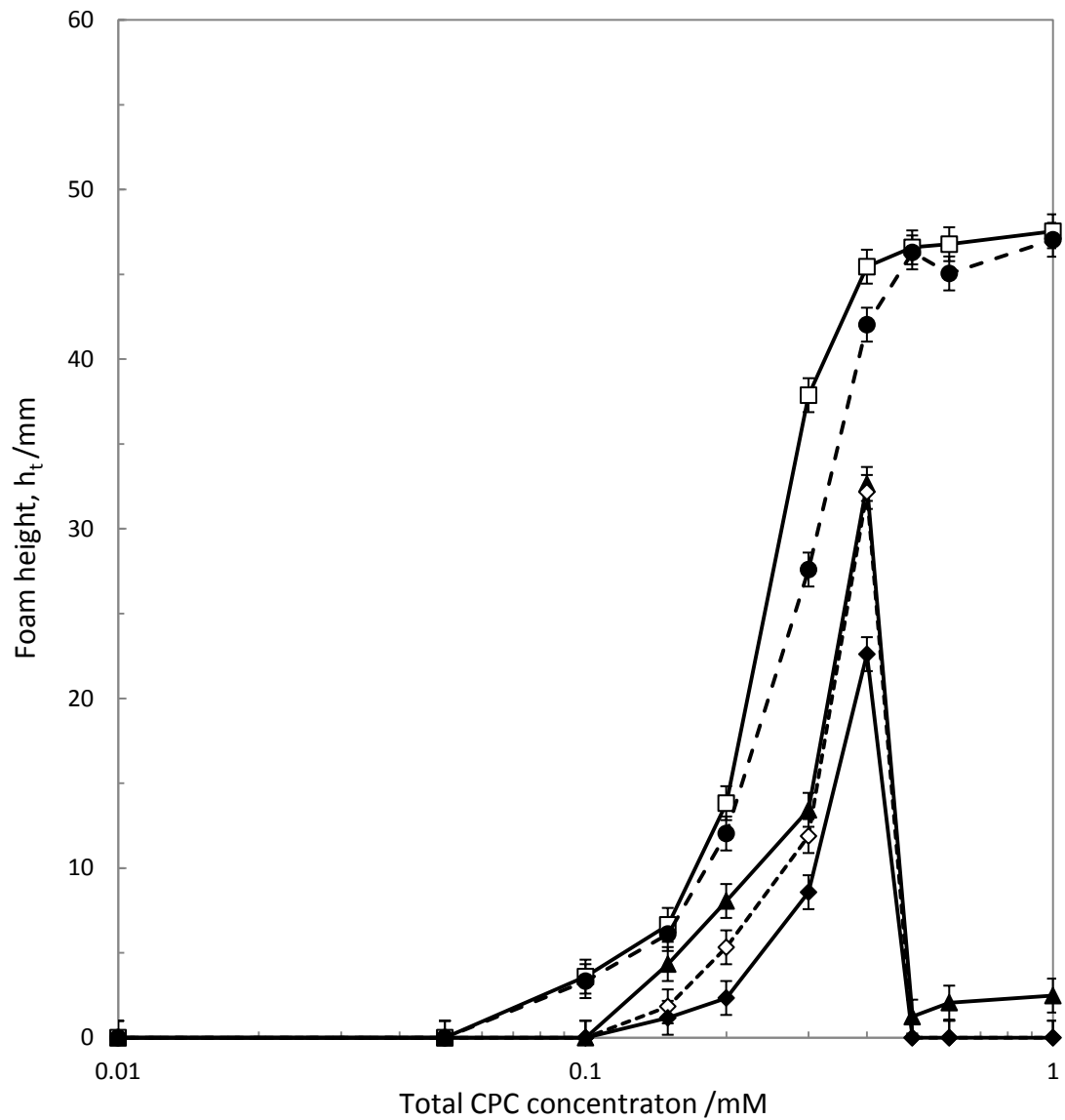


Figure 4.12. Images of foams produced from TTAB solutions of varying concentrations (listed in mM) in the absence (a, c) and presence of 4 wt.% silica particles with diameter of 1  $\mu\text{m}$  (b, d) taken 5 min (a, b) and 1 week (c, d) after foaming.



**Figure 4.13.** Foam height versus CPC concentration measured 5 min (open squares), 1 h (circles) and 24 h (triangles) after foaming by hand shaking of 5 ml aqueous solutions without added particles.



**Figure 4.14.** Foam height versus CPC concentration measured 5 min (boxes), 1 h (circles), 24 h (triangles), 1 week (open diamonds) and 1 month (full diamonds) after foaming by hand shaking of 5 ml aqueous suspensions containing 4 wt.% silica particles with diameters of 1  $\mu\text{m}$ .

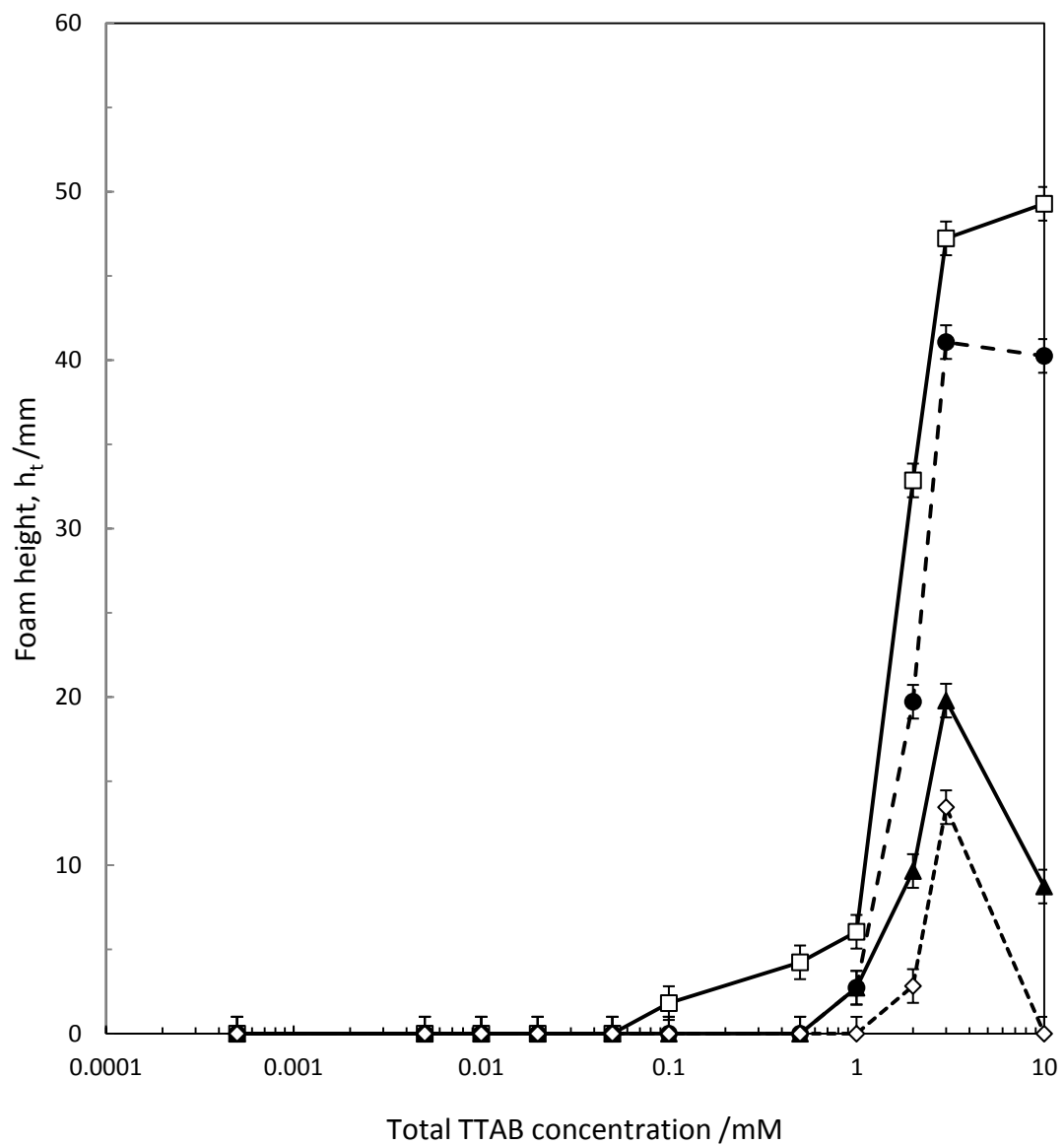


**Figure 4.15.** Foam height versus TTAB concentration measured 5 min (boxes), 1 h (circles), 24 h (triangles) and 1 week (open diamonds) after foaming by hand shaking of 5 ml aqueous solutions without added particles.

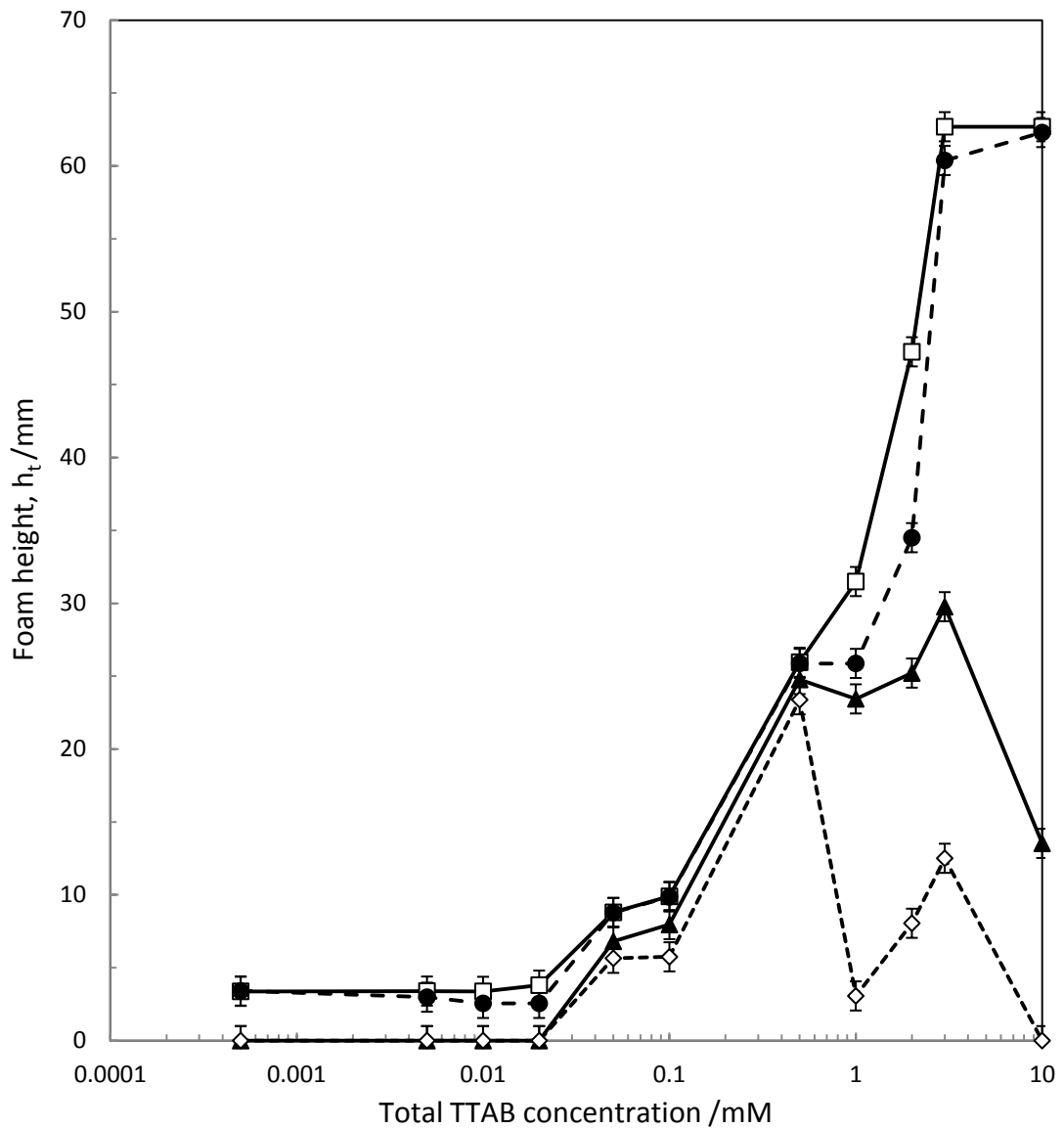
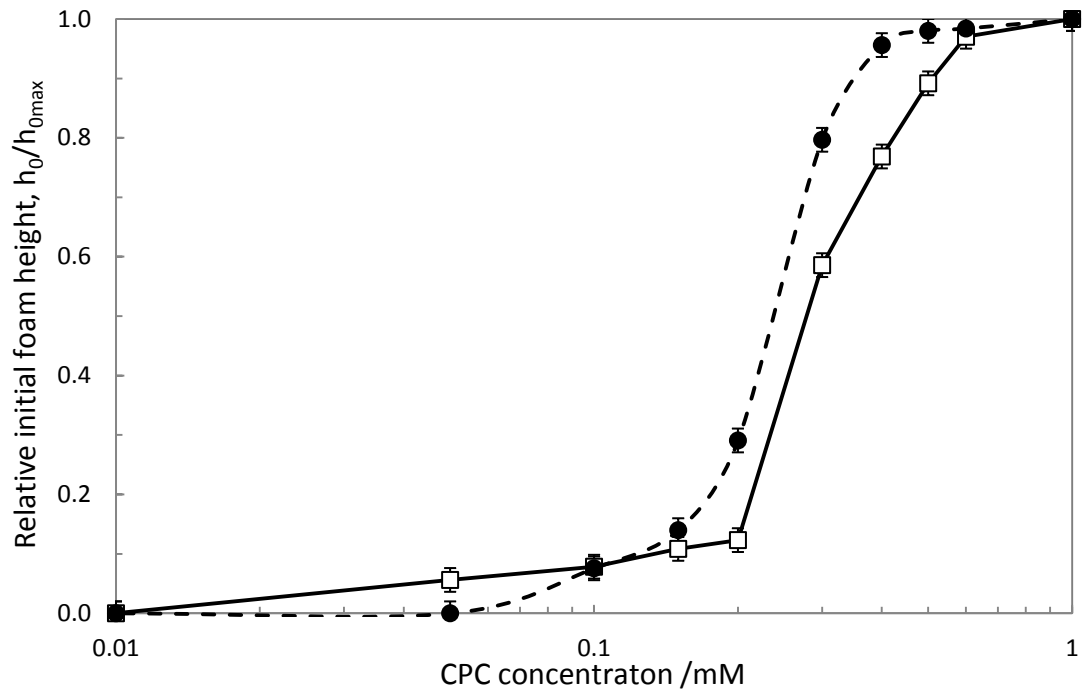
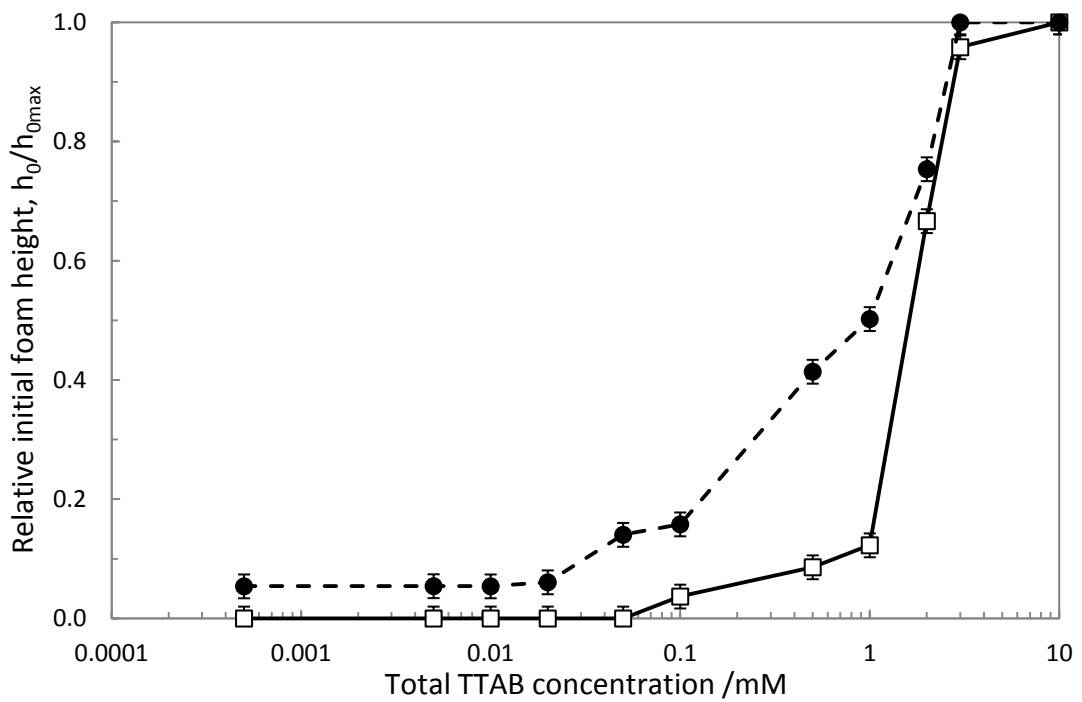


**Figure 4.16.** Foam height versus TTAB concentration measured 5 min (boxes), 1 h (circles), 24 h (triangles) and 1 week (empty diamonds) after foaming by hand shaking of 5 ml aqueous suspensions containing 4 wt.% silica particles with diameters of 1  $\mu\text{m}$ .

The amount of foam obtained shortly after foaming is a measure of the foamability. The initial foam height scaled with the maximum initial height,  $h_0/h_{0max}$  is plotted versus total surfactant concentration in Fig. 4.17.



(a)



(b)

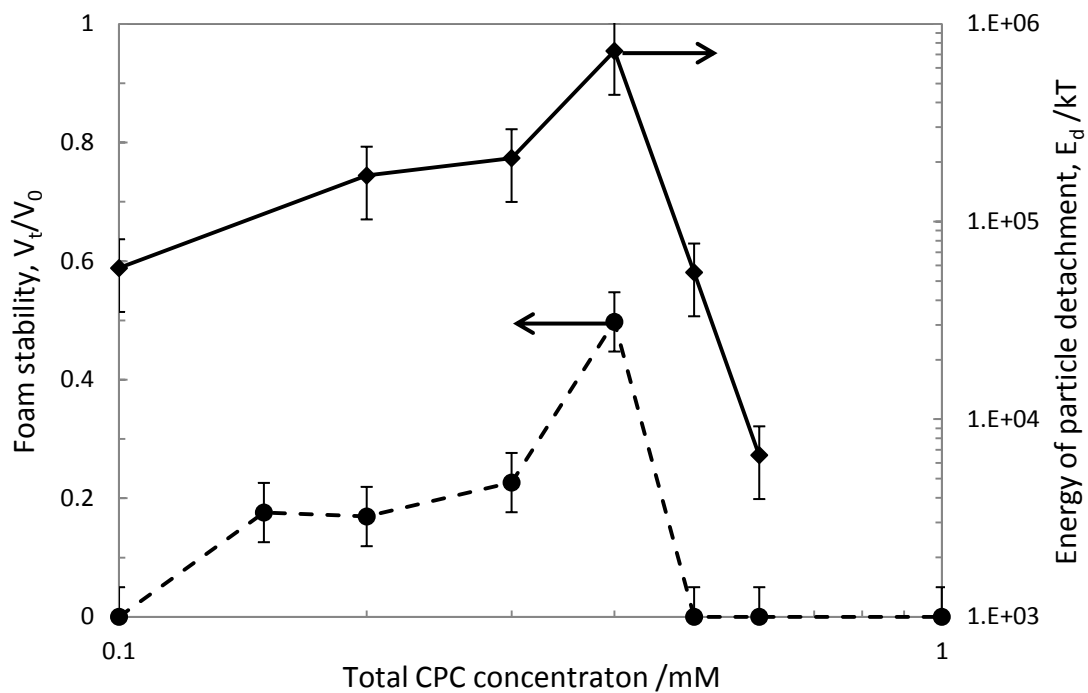
**Figure 4.17.** Relative initial foam height obtained after hand shaking of 5 ml solutions of (a) CPC and (b) TTAB in the absence (boxes) or presence (circles) of 4 wt.% silica particles with diameter of 1  $\mu$ m versus total surfactant concentration.

The foamability ( $h_0/h_{0max}$ ) of both CPC and TTAB solutions rapidly increases as the surfactant concentration approaches the cmc. The addition of 4 wt.% particles improves the foamability of the surfactant solutions at those concentrations where the particle contact angle is close to its maximum value. This effect is more pronounced for TTAB where a plateau of the particle contact angle values was observed in a broad range of surfactant concentrations. At surfactant concentrations close to and above the cmc the particles do not affect the foamability of solutions, probably because their attachment to the bubbles is hindered by the surfactant adsorbed at the bubble surface<sup>13</sup>.

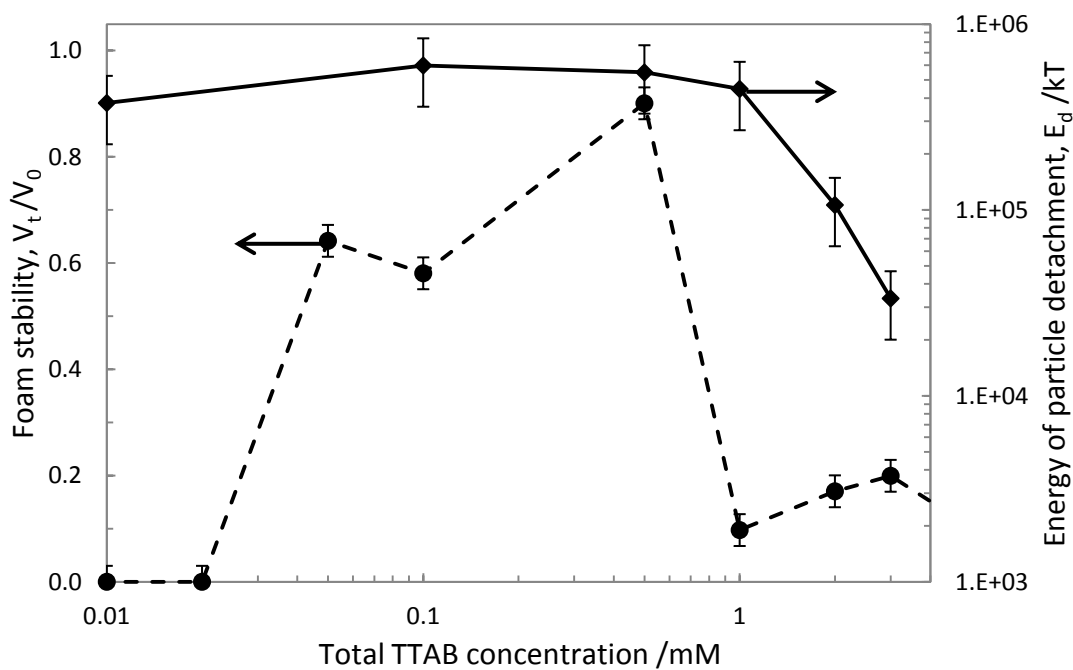
The stability of the foams with added particles in a certain range of CPC and TTAB concentrations is significantly different to that without particles (Figs. 4.13 – 4.16). The foams with no added particles are (almost) completely destroyed 24 h after preparation, while some of the foams with particles survive for at least 1 week. The change of the foam volume with time can be used to characterise the foam stability:

$$\text{Foam stability} = \frac{V_t}{V_0} \quad (4.2)$$

where  $V_0$  is the initial foam volume and  $V_t$  is the foam volume measured at time  $t$ . According to eq. 4.2, the foam stability at a certain time can vary between zero (completely unstable foams) and 1 (completely stable foams). The long term stability of foams from CPC and TTAB solutions in the presence of 4 wt.% silica particles is shown in Fig. 4.18. The maximum stability is observed at the surfactant concentration where the particle contact angle is largest.



(a)



(b)

**Figure 4.18.** Stability of foams (circles) obtained from surfactant solutions of (a) CPC, after 1 month and (b) TTAB, after 1 week, in the presence of 4 wt.% silica particles with diameter of 1  $\mu\text{m}$ . The energy of particle detachment from the air-solution interface into solution (diamonds) is calculated using eq. 1.4 and the surface tension data from Fig. 4.1.

Using the surface tension and contact angle data the detachment energy of the particles from air - aqueous solution interfaces into the solution,  $E_d$ , was calculated using eq. 1.4 (Fig. 4.18). The detachment energy alone cannot explain the lack of foam at lower surfactant concentrations and the sharp decrease in the foam stability at higher concentrations.  $E_d$  is much larger than the thermal energy by several orders of magnitude in the whole concentration range studied. Therefore, if the particles can enter the air - water interface, they will become irreversibly attached to the bubble surface and should stabilise the foam. Hence, the key question is whether the particles are able to enter the air - water interface at the studied conditions. The stability of the asymmetric liquid film formed between the particle and the bubble surface (the wetting film) should significantly affect the ability of the particle to attach to the interface. At low surfactant concentrations smaller than  $\sim 0.02$  mM, the wetting film should not be very stable<sup>30</sup> and particles should easily attach to the bubbles during the foam generation. However, the foamability of dilute surfactant solutions is low<sup>31</sup> due to the high surface tension ( $> 65$  mN m<sup>-1</sup>) and foam stability at such surfactant concentrations is also low. In order to remain stable, any bubbles formed should be covered with dense particle monolayers to prevent coalescence<sup>6</sup>. The lack of foam at low surfactant concentrations suggests that the amount of particles attached to the surface of bubbles during the foaming process by hand shaking for a very limited time  $\sim 30$  s is insufficient to prevent them from coalescing. Increasing the foaming time and particle concentration is expected to produce more foam, however this requires further investigation.

The stability of wetting film between the particle and bubble surface is expected to increase with the surfactant concentration due to the increasing number of surfactant molecules adsorbed at the interface and stronger electrostatic repulsions that result<sup>30</sup>. The particles may not be able to enter the air-water interface at greater surfactant concentrations, near the cmc. This would prevent the particles from contributing to the foam stability. Our observations on the particle behaviour in vertical aqueous films during FCM measurements give strong evidence in support of this hypothesis. We have found that when silica

particles are attached only to one of the film surfaces, they move downwards due to gravity, thus entering thinner parts of the film meniscus (Fig. 4.19). In some cases, depending on the surfactant concentration, the wetting film between the particle and the opposite film surface becomes unstable and breaks (Fig. 4.19 c1-c2); the particle bridges both film surfaces and very rapidly moves into a thinner part of the film to diminish the deformations of the film surfaces and minimise the surface free energy (Fig. 4.19 c2-c3). This process is very fast ( $< 100$  ms) and the particles appear to “jump” from thicker to thinner film regions during microscope observations (Fig. 4.19 a,b). We call this gravity driven process spontaneous bridging. Such spontaneous bridging was not observed at all TTAB concentrations studied (Table 4.4). We have calculated the critical thickness,  $h_{cr}$ , for rupture of the wetting film (see Fig. 4.20) when spontaneous bridging occurred. The values of  $h_{cr}$  are summarised in Table 4.4 together with the foam stability at various surfactant concentrations. In the absence of surfactant, spontaneous bridging was not observed. In this case the wetting film is stable because it is formed between a negatively charged silica particle (zeta potential  $-30$  mV) and negatively charged air - water interface<sup>30</sup>. In the presence of TTAB the wetting film becomes unstable and breaks at a certain critical thickness due to reduced electrostatic repulsions. The critical thickness,  $h_{cr}$ , decreases from  $\sim 410$  nm at  $5 \times 10^{-4}$  mM to  $\sim 130$  nm at  $0.5$  mM TTAB, hence the wetting film stability increases with the surfactant concentration. The lack of spontaneous bridging at concentrations above  $0.5$  mM TTAB suggests that the wetting films are stable at surfactant concentrations approaching the cmc. This should hinder the attachment of particles to bubbles during foam generation and the particles would play a marginal role (if any) in the foam stabilisation. This is supported by our findings that the foam stability at such TTAB concentrations is low and unaffected by the presence of  $4$  wt.% particles. Similar observations were made for the CPC systems, but further experiments are needed to quantify the observed effects. Our results suggest that the stability of wetting films (i.e. kinetic factors) could be more important than the free energy of particle attachment/detachment (thermodynamic factors) in determining if the presence of particles in surfactant solutions will provide benefits to foam production and stability.

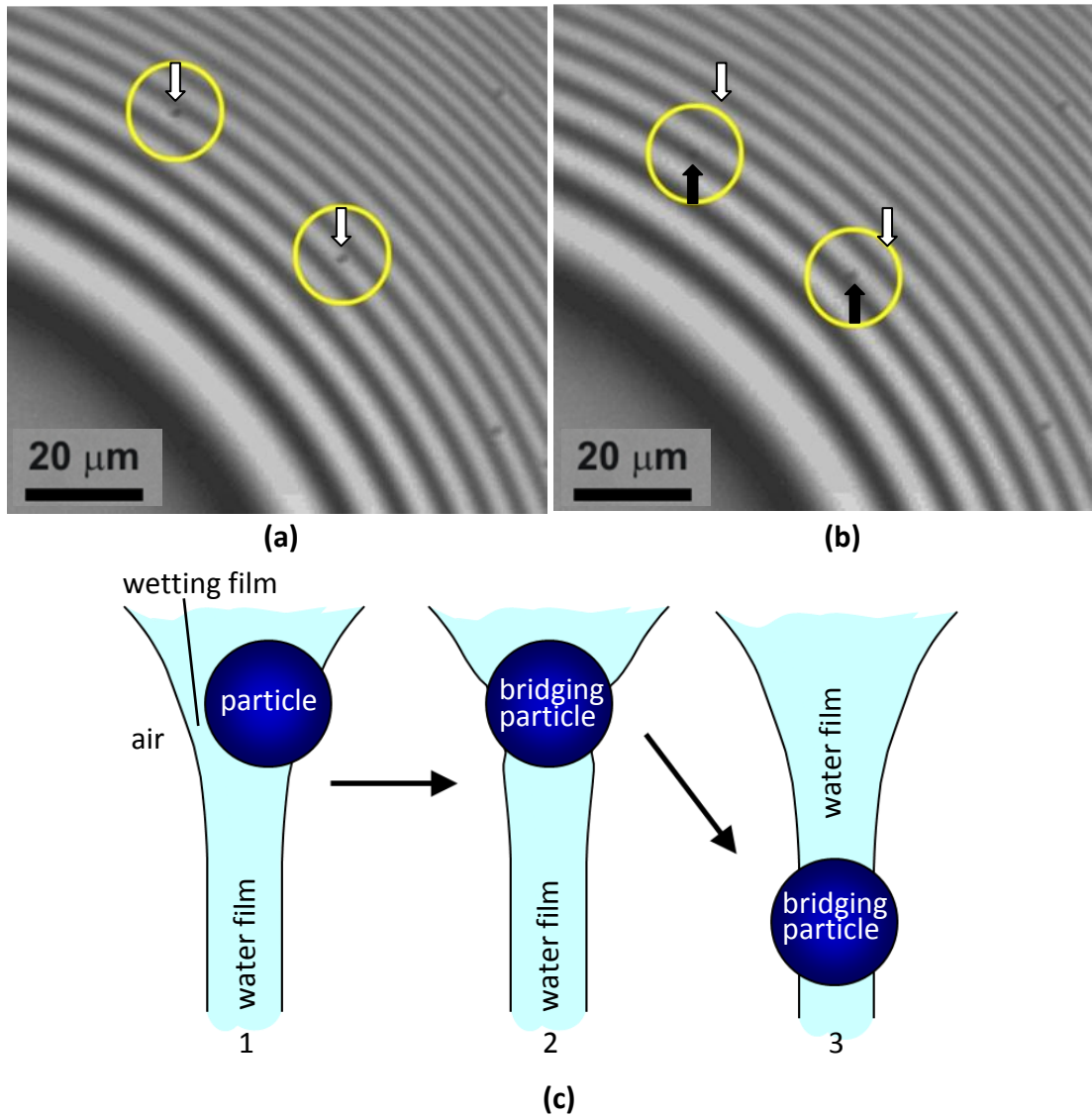


**Figure 4.19.** (a, b) Consecutive images at 100 ms intervals of a vertical film of 0.1 mM TTAB solution in air taken in monochromatic reflected light. (c) Schematics of spontaneous particle bridging: 1 – just before bridging, 2 – just after bridging, 3 – the bridging particle attains its equilibrium position. Particles of interest in (a) and (b) are encircled. White arrows in (a) point to particles just before bridging (c-1); black arrows in (b) point to the same particles after bridging (c-3); white arrows in (b) show the location of particles before bridging.

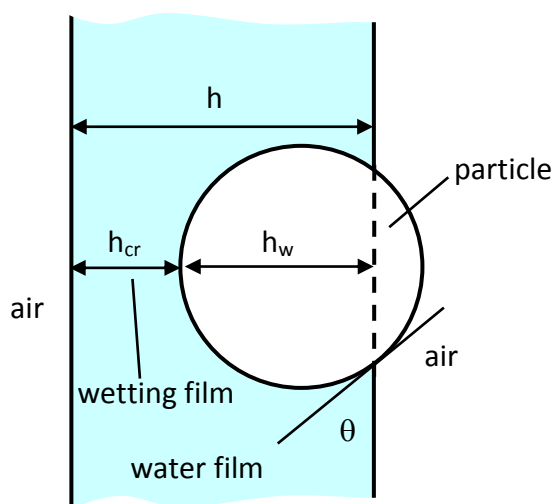


**Figure 4.20.** Schematic of a particle with diameter  $d$  just before bridging the surfaces of a water film in air at a film thickness  $h$ . The thickness of the wetting film,  $h_{cr}$ , is calculated by the formula  $h_{cr} = h - h_w$ , where  $h_w = (1 + \cos\theta)d/2$ .

**Table 4.4.** Spontaneous bridging of aqueous films in air by 1  $\mu\text{m}$  silica particles and the critical thickness of the wetting film,  $h_{cr}$ , between the particle and the film surface just before bridging at various TTAB concentrations in the film.

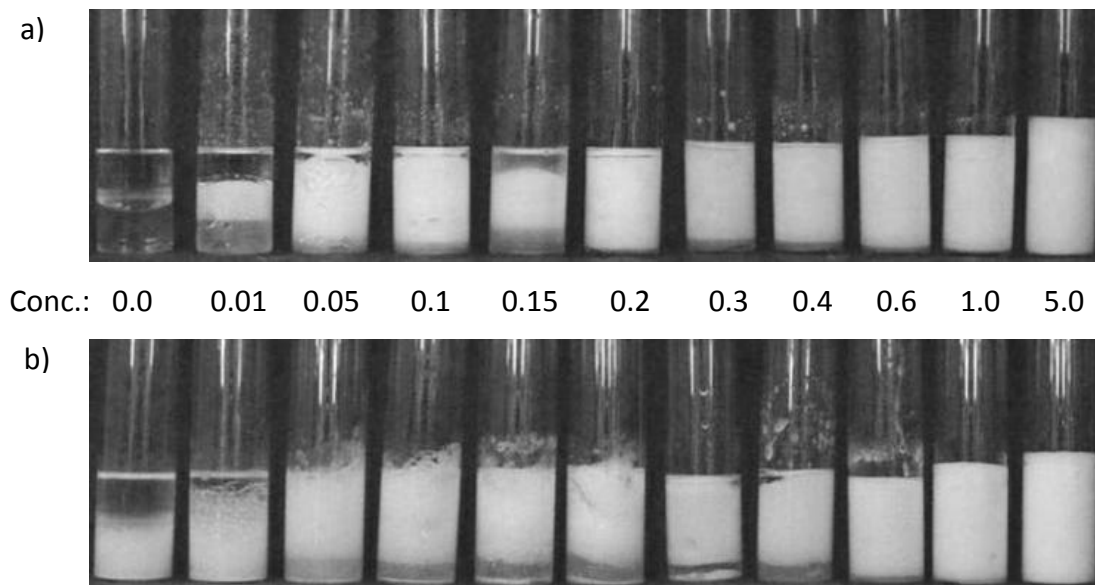
| [TTAB] /mM | Spontaneous bridging | $h_{cr} / \mu\text{m}$ | Foam stability<br>$V(1 \text{ week})/V(\text{initial})$ |
|------------|----------------------|------------------------|---|
| 0          | No                   | N/A                    | 0.00  |
| 0.0005     | Yes                  | $0.41 \pm 0.03$        | 0.00  |
| 0.01       | Yes                  | $0.29 \pm 0.04$        | 0.00  |
| 0.05       | Yes                  | $0.26 \pm 0.02$        | 0.64  |
| 0.1        | Yes                  | $0.24 \pm 0.02$        | 0.58  |
| 0.5        | Yes                  | $0.13 \pm 0.02$        | 0.90  |
| 1.0        | No                   | N/A                    | 0.10  |
| 2.0        | No                   | N/A                    | 0.17  |

#### *4.3.6 Differences in emulsion type and stability stabilised by surfactant solutions or surfactant solution/silica particle mixtures*

Emulsions from equal volumes of decalin and aqueous solutions of CPC and TTAB in the absence and presence of 1 $\mu$ m silica particles were investigated in order to determine the effect of particles on their type and stability. Images of the emulsions approximately 5 minutes and 1 week after emulsification with an Ultra-Turrax homogeniser for 30 seconds are shown in Figs. 4.21 and 4.22. The type of all emulsions was oil-in-water as determined by drop tests (see Chapter 2).

All emulsions produced were unstable to creaming but generally had a longer lifetime than the foams. Indeed once initial coalescence and creaming within the first hour has ceased most of the samples, especially when stabilised with particles, change imperceptibly over the following 1 week period.

Time = 5 minutes



Time = 1 week

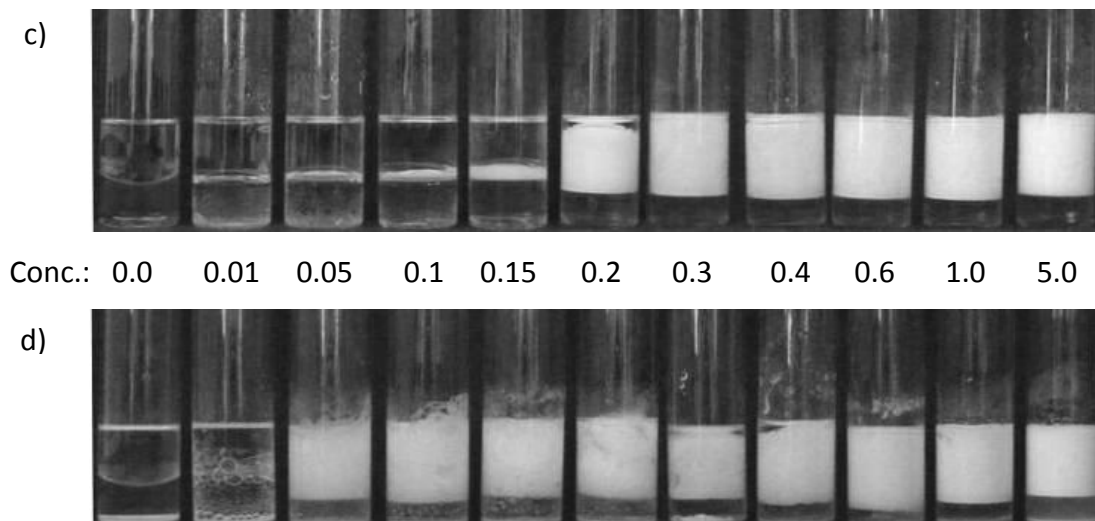
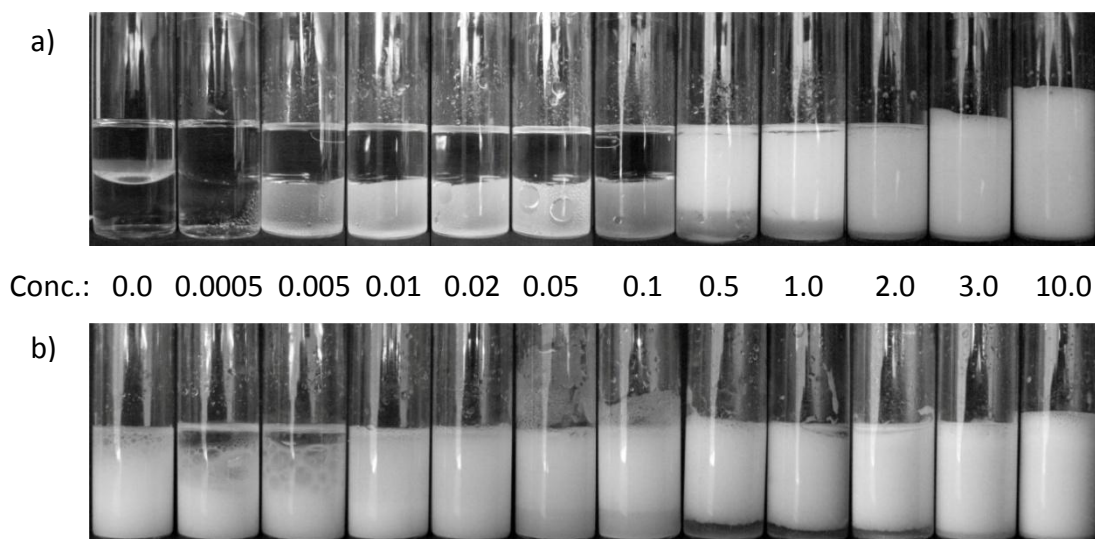


**Figure 4.21.** Images of emulsions produced from equal volumes of decalin and aqueous CPC solutions of varying concentrations (listed in mM) in the absence (a, c) and presence of 4 wt.% silica particles with diameter of 1  $\mu\text{m}$  (b, d), taken 5 min (a, b) and 1 week (c, d) after emulsification with an Ultra-Turrax homogeniser at 9500 rpm for 30 seconds.

Time = 5 minutes



Time = 1 week

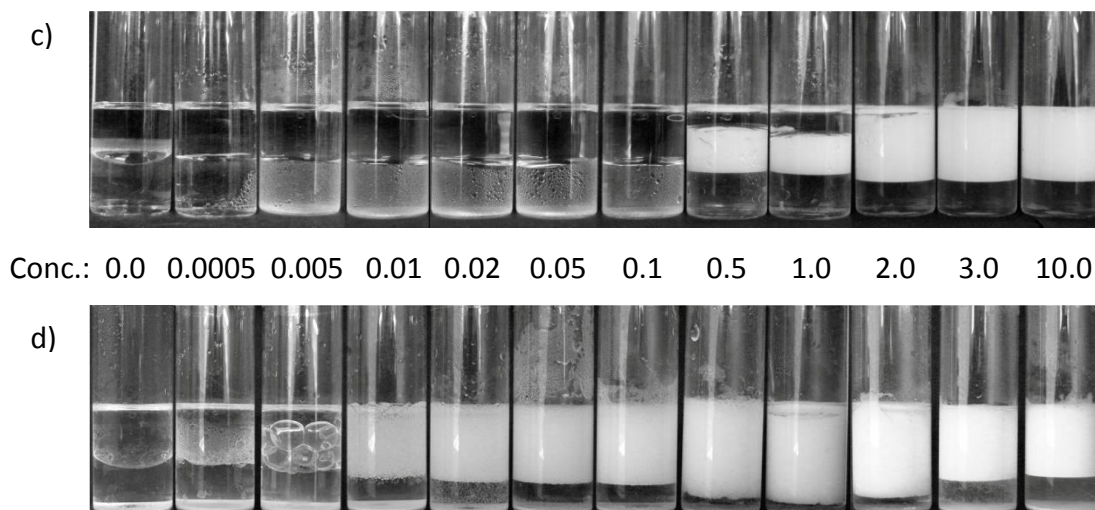


**Figure 4.22.** Images of emulsions produced from equal volumes of decalin and aqueous TTAB solutions of varying concentrations (listed in mM) in the absence (a, c) and presence of 4 wt.% silica particles with diameter of 1  $\mu\text{m}$  (b, d), taken 5 min (a, b) and 1 week (c, d) after emulsification with an Ultra-Turrax homogeniser at 8000 rpm for 30 seconds.

The emulsion stability can be quantified by monitoring the volume fractions of oil,  $\phi_O$ , water,  $\phi_W$ , and emulsion,  $\phi_E$ , with time. The volume fractions are calculated by the following equations

$$\phi_O = \frac{V_{OR}(t)}{V_O} \quad (4.3)$$

$$\phi_W = \frac{V_{WR}(t)}{V_W} \quad (4.4)$$

$$\phi_E = \frac{V_{ER}(t)}{V_O + V_W} \quad (4.5)$$

where  $V_O$  and  $V_W$  are the volumes of oil and water used for making the emulsion,  $V_{OR}(t)$ ,  $V_{WR}(t)$  and  $V_{ER}(t)$  are the volumes of oil, water and emulsion (cream or sediment, depending on the emulsion type) resolved at time  $t$  after emulsification. In the case of o/w emulsions investigated here,  $\phi_W$  shows the stability against creaming,  $\phi_O$  - that against coalescence and  $\phi_E$  is the outcome of both destructive processes.

Volume fractions of oil, water and emulsion (cream) are shown for the CPC system in Fig. 4.23. At concentrations less than 0.2 mM the fraction of oil resolved is high without particles present and correlates with a low fraction of emulsion resolved ( $< 0.2$ ) showing that the emulsions were not stable against coalescence. At concentrations  $\geq 0.2$  mM the opposite is apparent with a high fraction of emulsion resolved ( $> 0.6$ ) and low fraction of oil resolved showing that the stability against coalescence was much greater at these concentrations. With 4 wt.% particles present the fraction of oil resolved is low at all concentrations greater than 0.01 mM and for these the fraction of emulsion resolved was high showing strong stability against coalescence. The addition of particles therefore increases stability against coalescence at lower concentrations of 0.05 – 0.2 mM but has little influence at other concentrations. The fraction of water resolved is similar for all

the emulsions but lower for a mixture of particles and CPC solution, except for concentrations of cmc and above where the fraction of water is the same. With particles present a minimum in the fraction of water resolved occurred at 0.6 mM, just below cmc, and correlates with the greatest stability against coalescence. The addition of particles therefore produced a slight increase in stability against creaming at concentrations lower than cmc.

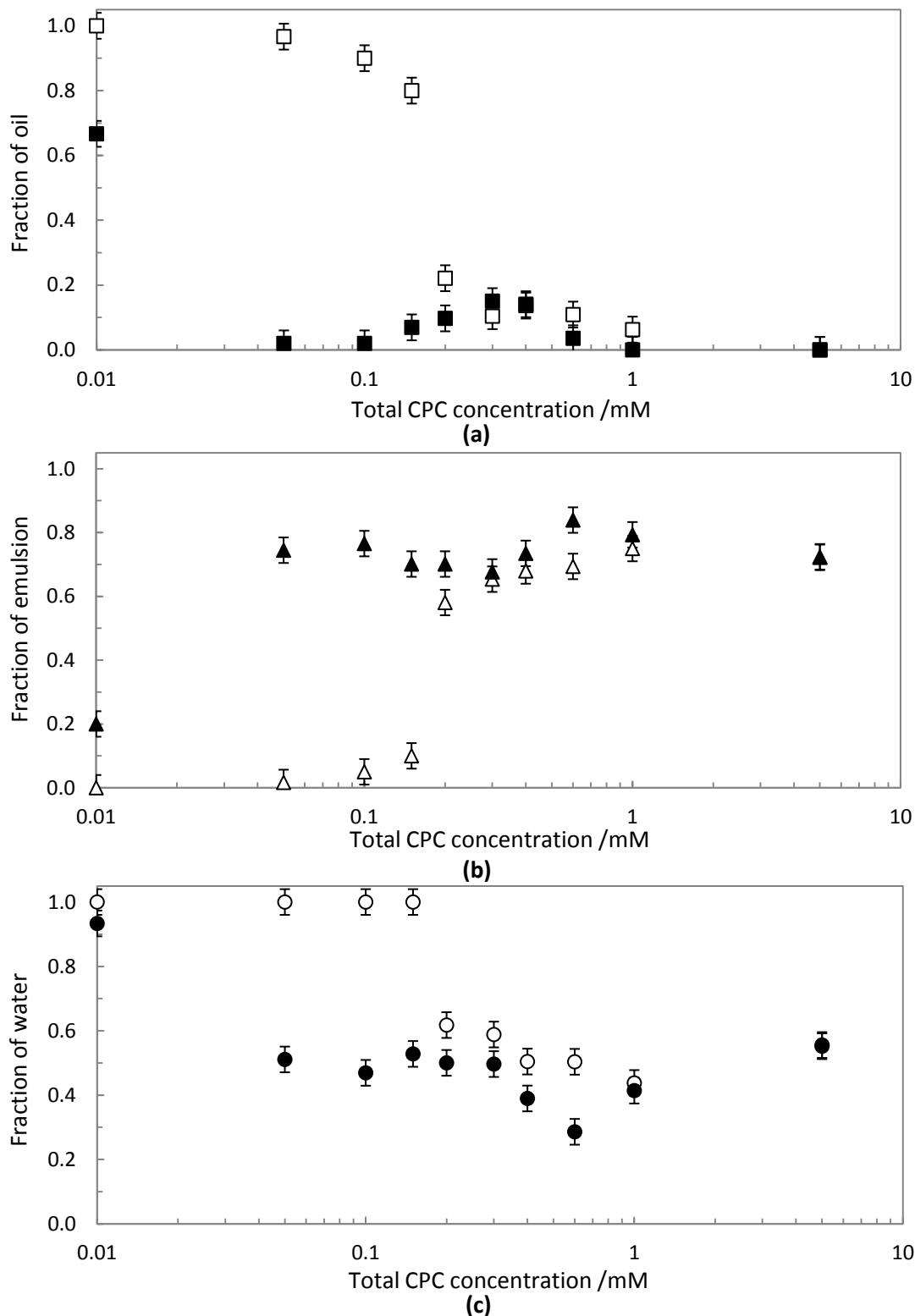


**Figure 4.23.** Fractions of oil (a), cream (b) and water (c) resolved from decalin-in-water emulsions ( $V_O = V_W = 5$  mL) one week after emulsification with an Ultra-Turrax homogeniser at 9500 rpm for 30 seconds without (open symbols) and with 4 wt.% silica particles with a diameter of 1  $\mu$ m in aqueous CPC solutions (solid symbols) versus total CPC concentration.

The volume fractions of oil, water and emulsion (cream) are shown for the TTAB system in Fig. 4.24. At concentrations less than 0.5 mM the fraction of oil resolved is high without particles present and correlates with a low fraction of emulsion resolved showing that the emulsions were not stable against coalescence. At concentrations  $\geq 0.5$  mM the fraction of emulsion resolved is higher and the fraction of oil is lower (less than 0.4) showing that there was increased stability against coalescence at these concentrations. With particles present the fraction of oil resolved is low at all concentrations  $\geq 0.01$  mM and at these surfactant concentrations the fraction of emulsion resolved was high ( $> 0.6$ ) showing strong stability against coalescence. The addition of particles therefore greatly increased stability against coalescence at these surfactant concentrations (0.01 - 2 mM) but had little influence at higher concentrations (cmc and above) which displayed similar stability against coalescence to emulsions stabilised only with surfactant. At cmc and above the fraction of water resolved is identical for emulsions with and without particles but at lower concentrations (0.5 – 2 mM) the fraction of water resolved is lower for emulsions with particles present ( $\leq 0.3$ ) compared to that without particles ( $\sim 0.6 - 0.8$ ). With particles present a minimum in the fraction of water resolved occurred at 1mM, just below cmc, and correlates with the greatest stability against coalescence, as with CPC. The addition of particles therefore increased the stability against creaming for concentrations below cmc.

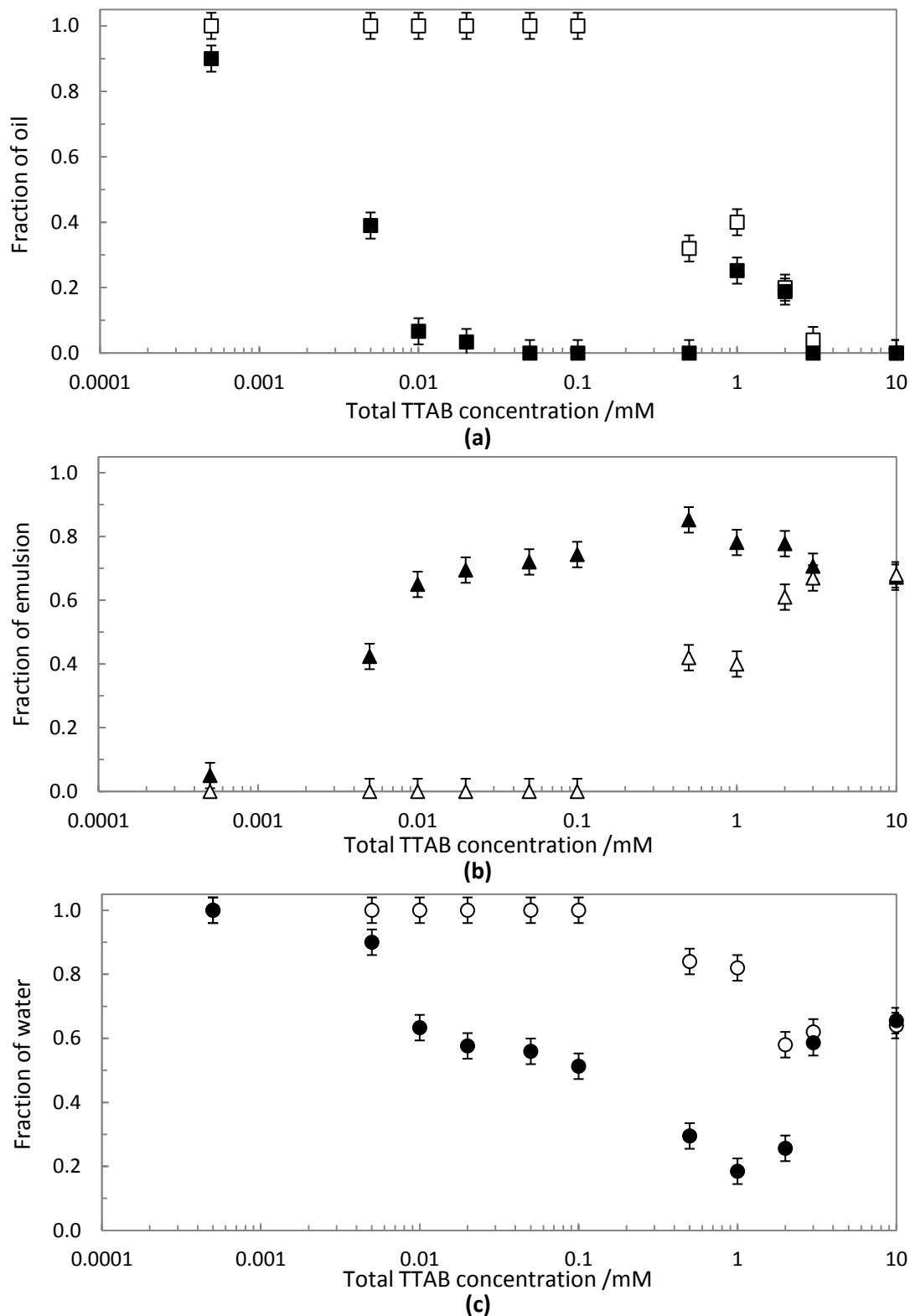


**Figure 4.24.** Fractions of oil (a), cream (b) and water (c) resolved from decalin-in-water emulsions ( $V_O = V_W = 5$  mL) one week after emulsification with an Ultra-Turrax homogeniser at 8000 rpm for 30 seconds without (open symbols) and with 4 wt.% silica particles with a diameter of 1  $\mu$ m in aqueous TTAB solutions (solid symbols) versus total TTAB concentration.

The emulsion stability of surfactant solutions without particles increases with increasing concentration towards cmc. The emulsion stability with TTAB increases with decreasing interfacial tension and although such measurements between decalin and CPC solutions are not available it is assumed that a similar trend would also be observed. With the addition of particles the emulsion stability at lower surfactant concentrations is increased significantly. At and above cmc emulsion stability matches that of surfactant only samples. In the absence of particles the emulsions remained after a week but the TTAB samples with the greatest volumes of emulsion were at concentrations where the interfacial tension was lowest (close to and above cmc).

In emulsions stabilised with 2.76  $\mu\text{m}$  silica particles and TTAB surfactant (Chapter 3, Fig. 3.8) the emulsion type inverted to w/o at higher contact angles  $> 90^\circ$  (TTAB concentration 0.5 and 1.0 mM). This was observed to be prevented by increasing the particle concentration so that the total particle surface area was closer to that of the 1  $\mu\text{m}$  systems. Therefore when the number of particles is greater the oil droplets must be stabilised by particles networking in the aqueous phase, preventing the creation of water droplets within an oil continuous phase. At TTAB concentrations of 0.02 - 1 mM the emulsions were observed to become viscous and flocculated, whereas at other surfactant concentrations the emulsion droplets flowed freely. The concentration range 0.02 - 1 mM correlates with low particle charge and high contact angles so stability against particle aggregation and networking is expected to be lower. As with the air - water interface, spontaneous bridging was observed with surfactant films in oil at surfactant concentrations below 0.5 mM. The critical film thickness for rupture decreases with increasing surfactant concentration as with the air-water interface, showing that the wetting film becomes more stable. Approaching cmc the wetting film is stable and restricts the attachment of particles to the interface. This was supported by microscope images of emulsion droplets (Fig. 4.25). At surfactant concentrations  $\leq 1$  mM full or close to full coverage of droplet surfaces by stabilising particles was observed. At concentrations approaching cmc (2 - 3 mM) the number of particles stabilising the droplets was much lower while above cmc no particles were observed on the

surface of any emulsion drops. In correlation with the stability of the wetting film above cmc the emulsions were seen to be predominantly (or completely) stabilised by surfactant and the average drop size was very small as a result (tens of  $\mu\text{m}$ ).

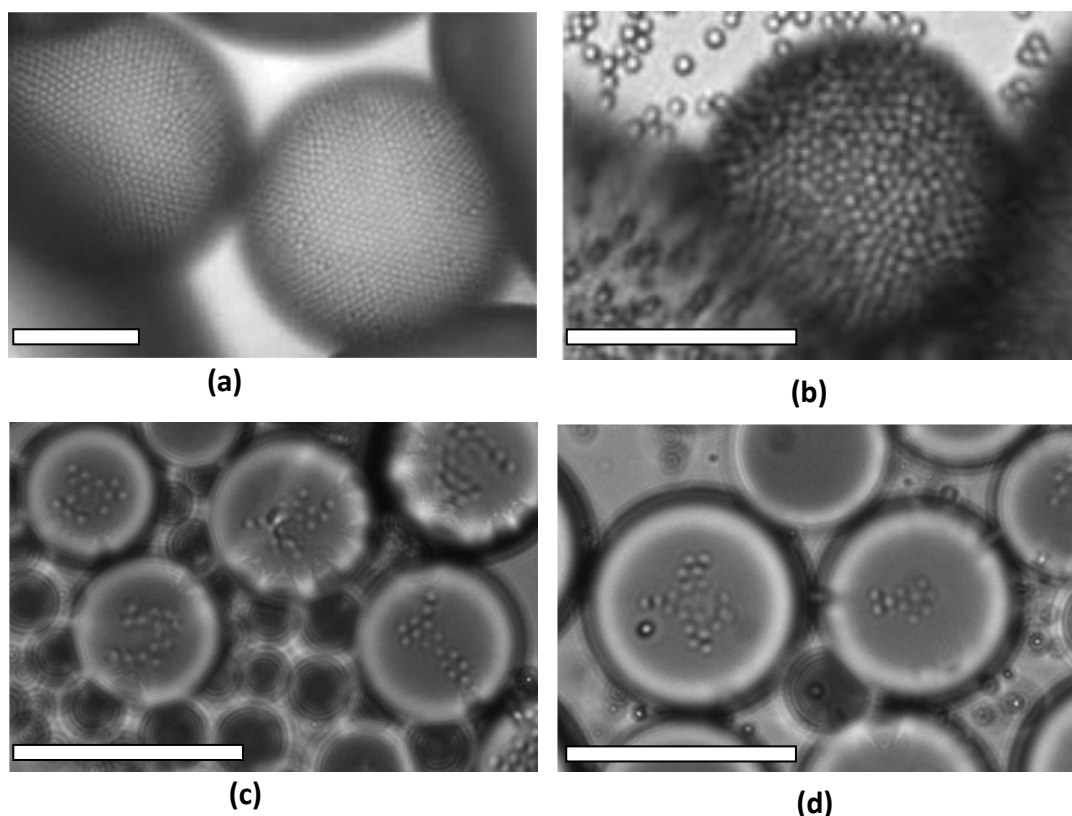


**Figure 4.25.** Microscope images of decalin-in-aqueous TTAB solution emulsion drops in the presence of  $2.76\ \mu\text{m}$  silica particles at a concentration of 3 wt.% in the aqueous phase. The surfactant concentrations are (a) 0.0005, (b) 0.1, (c) 2.0 and (d) 3.0 mM TTAB. Scale bars are equal to  $50\ \mu\text{m}$ .

#### 4.4 Conclusions

The properties of surfactant-particle mixtures have been shown to result from the complex interplay and mutual influence of the particles and surfactant. The adsorption of surfactant at air-water and oil-water interfaces causes a reduction in the surface and interfacial tensions with increasing surfactant concentration, reaching a minimum and plateau at cmc where the interface is saturated with

surfactant molecules. The adsorption of cationic surfactant (CPC) on silica surfaces was shown to increase with increasing concentration, also reaching a plateau at cmc. Increasing adsorption causes a change in the particle surface charge from negative to positive and a decrease in suspension pH occurs as dissociation of hydroxyl surface groups increases. Particle hydrophobicity increases gradually with increasing surfactant concentration (and adsorption), reaches a maximum and then decreases rapidly approaching cmc. This fits with the reverse orientation model described in Chapter 1 (Figs. 1.5 and 1.6). Similar changes in silica particle properties were also shown with TTAB surfactant. An increase in the rate of particle aggregation and sedimentation was observed at an equilibrium suspension concentration (after surfactant adsorption on particles) which matched that of the maximum particle hydrophobicity and neutral particle charge.

Foamability of CPC and TTAB solutions/suspensions increased with surfactant concentration, with a rapid increase approaching cmc. The addition of particles improved the foamability when contact angles were near maximum but made no difference to the foamability close to, or above cmc. The stability of foams without particles was low and they broke down within 24 hours. With particles present foam remained after a week, however increased stability only occurred at concentrations where particle contact angles were near the maximum.

The energy of particle detachment from the air - water interface into solution was much greater than  $kT$  across the range of surfactant concentrations used and therefore particles should have provided strong foam stability. At low surfactant concentration the surface tension was higher and bubbles were larger. It is proposed that the particle coverage achieved on the large bubbles was insufficient for prevention of coalescence. At low surfactant concentrations ( $\leq 0.5$  mM) spontaneous bridging of a liquid film by particles occurred when the wetting film between particle and bubble surface became unstable. The separation distance for spontaneous bridging to occur decreased with increasing surfactant concentration, suggesting that the wetting films become more stable with increasing concentration. This was proven close to cmc where the wetting film was very

stable, spontaneous bridging did not occur and it became increasingly difficult to attach particles to the interface. Our results suggest that the stability of wetting films (i.e. kinetic factors) could be more important than the free energy of particle attachment/detachment (thermodynamic factors) for the stabilisation of foams from mixtures of surfactants and solid microparticles.

All emulsions produced with 1  $\mu\text{m}$  particles (4 wt.%) and surfactant were oil-in-water emulsions and had greater lifetimes than the foams but were unstable to creaming both with and without particles. Emulsion stability increased with increasing surfactant concentration, with addition of particles making no difference to the volume of emulsion produced at high concentrations close to cmc. This is again due to strong wetting films preventing particle attachment at the interface. At intermediate concentrations the stability of emulsions against coalescence was much greater with particles present and increased stability against creaming also occurred.

Emulsion inversion was observed when using 2.76  $\mu\text{m}$  silica particles in TTAB (3 wt.%) at concentrations where the contact angle was maximum and  $> 90^\circ$ . This is different to the emulsion series made with 1  $\mu\text{m}$  particles where no inversion was observed and is due to the lower number of particles present in the suspension. This was proven by making emulsions with the larger particles at a higher concentration (9 wt.%) with total surface area closer to that of the 1  $\mu\text{m}$  particles and was observed to prevent inversion to w/o emulsions. The stability against emulsion inversion is attributed to particle networks in the aqueous phase which prevent the formation of water droplets with an oil continuous phase.

Microscope images of emulsion drops showed that at lower concentrations a monolayer of particles stabilised droplets. Approaching cmc the number of particles stabilising droplets reduced significantly while above cmc no particles were seen attached to droplet surfaces. This correlates with observations of spontaneous bridging which showed that the wetting films at the oil-water interface became more stable with increasing surfactant concentration.

## 4.5 References

1. B. P. Binks and T. S. Horozov, *Colloidal Particles at Liquid Interfaces*, Cambridge University Press (Cambridge), 2006.
2. D. Weaire and S. Hutzler, *The Physics of Foams*, Clarendon Press (Oxford), 1999.
3. L. L. Scramm, *Emulsions, Foams and Suspensions*, Wiley VCH (Weinheim), 2005, P. 89.
4. R. J.G. Lopetinsky, J. H. Masliyah and Z. Xu "Solids - Stabilized Emulsions: A Review" in, *Colloidal Particles at Liquid Interfaces*, B. P. Binks and T. S. Horozov, eds., Cambridge University Press (Cambridge), 2006, p. 186-224.
5. G. Kaptay, *Colloid Surface. A*, 2006, **282-283**, 387.
6. T. S. Horozov, *Curr. Opin. Colloid In.*, 2008, **13**, 134.
7. P. Wängnerud, D. Berling and G. Olofsson, *J. Colloid Interf. Sci.*, 1995, **169**, 365.
8. L. K. Koopal, T. Goloub, A. de Keizer and M. P. Sidorova, *Colloid Surface. A*, 1999, **151**, 15.
9. J. J. Adler, P. K. Singh, A. Patist, Y. I. Rabinovich, D. O. Shah and B. M. Moudgil, *Langmuir*, 2000, **16**, 7255.
10. J. H. Harwell, J. C. Hoskins, R. S. Schechter and w. H. Wade, *Langmuir*, 1985, **1**, 251.
11. T. N. Hunter, R. J. Pugh, G. V. Franks and G. J. Jameson, *Adv. Colloid Interfac.*, 2008, **137**, 57.
12. Z.-G. Cui, L.-L. Yang and B. P. Binks, *Langmuir*, 2010, **26 (7)**, 4717.
13. B. P. Binks, M. Kirkland and J. A. Rodrigues, *Soft Matter*, 2008, **4**, 2373.
14. B. P. Binks, J. A. Rodrigues and W. J. Frith, *Langmuir*, 2007, **23**, 3626.
15. R. Aveyard, B.P. Binks and J.H. Clint, *Adv. Colloid Interfac.*, 2003, **100–102**, 503.
16. J. Stiernstedt, J. C. Fröberg, F. Tiberg and M. W. Rutland, *Langmuir*, 2005, **21**, 1875.
17. C. Ström, P. Hansson, B. Jönsson and O. Söderman, *Langmuir*, 2000, **16**, 2469.
18. M.-F. Ficheux, L. Bonakdar, F. Leal-Calderon and J. Bibette, *Langmuir*, 1998, **14**, 2702.
19. L. Sepúlveda and J. Cortés, *J. Phys. Chem-US.*, 1985, **89**, 5322.

20. T. P. Goloub, L. K. Koopal, B. H. Bijsterbosch and M. P. Sidorova, *Langmuir*, 1996, **12**, 3188.
21. E. W. Anacker, *J. Phys. Chem.*, 1958, **62 (1)**, 41.
22. E. E. Makhaeva, H. Tenhu and A. R. Khokhlov, *Polymer*, 2000, **41**, 9139.
23. S. P. Moulik, M. E. Haque, P. K. Jana and A. R. Das, *J. Phys. Chem.*, 1996, **100**, 701.
24. K. Mędrzycka and W. Zwierzykowski, *J. Colloid Interf. Sci.*, 2000, **230**, 67.
25. E. A. Sinister, R. K. Thomas, J. Penfold, R. Aveyard, B. P. Binks, P. Cooper, P. D. I. Fletcher, J. R. Lu and A. Sokolowski, *J. Phys. Chem.-US*, 1992, **96**, 1383.
26. U. R. Dharmawardana, S. D. Christian, E. E. Tucker, R. W. Taylor and J. F. Scamehorn, *Langmuir*, 1993, **9**, 2258.
27. E. A. Hauser and G. E. Niles, *J. Phys. Chem.-US*, 1941, **45 (6)**, 954.
28. D.W. Fuerstenau and R. Jia, *Colloid Surface. A*, 2004, **250**, 223.
29. T. P. Goloub and L. K. Koopal, *Langmuir*, 1997, **13**, 673.
30. D. Exerowa, N.V. Churaev, T. Kolarov, N.E. Esipova, N.Panchev and Z.M.Zorin, *Adv. Colloid Interfac.*, 2003, **104**, 1.
31. R. J. Pugh, *Adv. Colloid Interfac.*, 1996, **54**, 67.

## Chapter 5

### Preparation and properties of Janus Particles

#### 5.1 Introduction

As previously mentioned Janus particles are particles with a surface which is split into two regions of different chemical composition. These particles are of great interest as building blocks for either self-<sup>1,2</sup> or directed-<sup>3</sup> assembly into various shapes or structures, for the observation of particle orientation<sup>4,5</sup> or directed orientation<sup>6,7</sup> driven by the dipolar nature of the particles, and for potential benefits as amphiphilic stabilisers<sup>8</sup>. Over the past decade research in the area has stepped up greatly with many methods for producing these particles now identified varying greatly in regards to the yield, particle diameter and control of the Janus balance (see section 1.2). Investigations into the behaviour of these particles under a range of conditions and for a variety of uses are presently in the infant stage, especially so when concerning spherical Janus particles.

The most significant research group in this field over previous years has been Granick et al.<sup>9</sup> who have developed a patented method of preparing relatively large yields of Janus particles in a controllable fashion. This method uses solidified Pickering emulsions to partially mask particles ready for treatment<sup>9</sup>. The work presented in this chapter also uses particle-stabilised emulsions for the benefits of larger yield and control of the Janus balance but has distinct differences to their procedure. Polymerisable oil is used instead of wax which can, in solid form, offer much greater temperature resistance than wax, greater rigidity of the solid globules and possibly better chemical resistance, allowing for more freedom in the treatment of particle surfaces. In addition, the wettability of the template particles used in our procedure is permanently altered by treatment of bare silica particles with silane solutions of varying concentration. The procedure does not therefore

use surfactants and the wettability of the template particles is retained in the masked region, even after retrieval and washing of the Janus particles.

To date most of the investigation work using amphiphilic Janus-like particles has been aimed at proving their Janus nature rather than investigating their abilities as stabilisers of emulsions or foams. Proving the Janus nature is generally performed in a 2-phase system of oil and water by measuring the contact angle of the particles at the interface<sup>10,11</sup> or by observing which phase the particles preferentially disperse into, whereby the amphiphilic particles are commonly seen to sit at the interface between phases<sup>8, 12</sup>.

Investigations into amphiphilic particles as emulsion stabilisers generally use particles different to the traditionally imagined spherical Janus particle (hundreds of nanometers to micrometers in diameter). These works use for example, dimer<sup>13, 14</sup> or mushroom<sup>15</sup> shaped particles or very small particles<sup>16</sup> (~20 nm diameter). Granick et al. showed amphiphilic Janus particles to stabilise emulsions over extended periods of time<sup>17</sup>, however those emulsions were only compared with those made by untreated hydrophilic silica particles, not homogeneous particles of intermediate contact angles.

The aim of this chapter is to develop a method for making particles with dual wettability (Janus particles), and to then use those particles as emulsion stabilisers. The general outline of the procedure for making the particles, based on a particle stabilised emulsion route is shown in Fig. 5.1. First the template silica particles with controlled wettability are used to stabilise o/w emulsions of water and polymerisable oil, which contains a thermally-activated initiator. The particle-stabilised emulsions are heated to polymerise the droplets and then, once cooled, the solid globules (polymer beads) are separated from the continuous phase and excess dispersed particles by filtration. The solid polymer partially masks the surface of the silica particles trapped at the polymer bead surface, allowing just the exposed portions to be chemically modified. The polymer is finally dissolved with an appropriate solvent (e.g. chloroform) to release the Janus particles.

Different types of Janus particles were made to show that dual properties were achieved. Particles with dual wettability made using the method detailed were used to stabilise emulsions, which were compared to those stabilised by particles with homogeneous properties.

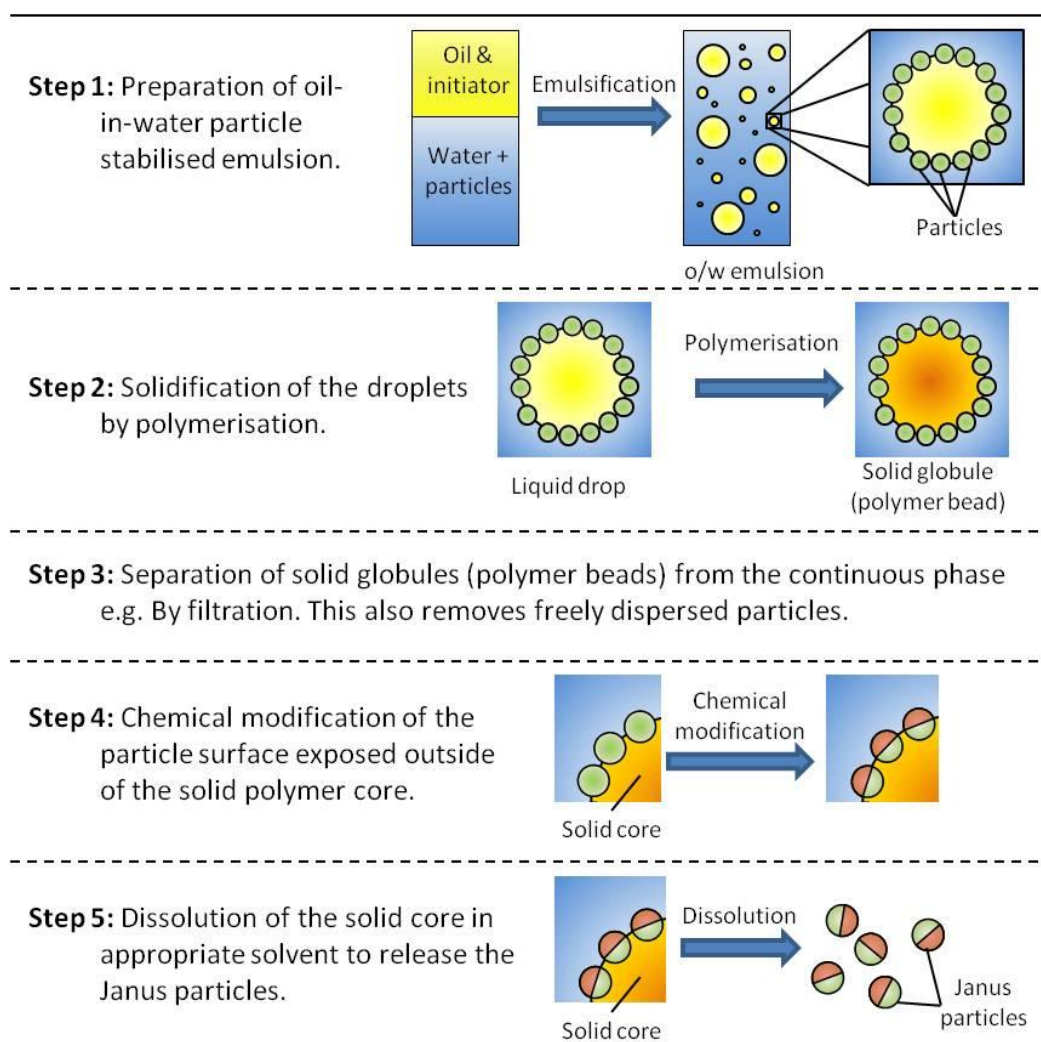


**Figure 5.1.** Procedure for the preparation of Janus particles using particle-stabilised emulsions

## 5.2 Experimental

In this chapter silica particles with a narrow size distribution were used with diameters of 0.5, 1.0, 2.76, 5.84 and 7.75  $\mu\text{m}$  (see section 2.1.1.1). The wettability of these particles was adjusted using solutions of dichlorodimethylsilane (DCDMS) in toluene as described in section 2.2.1. The oils used were butyl methacrylate (BMA), 2-ethylhexyl methacrylate (EHMA), isobutyl methacrylate (IBMA), stearyl methacrylate and styrene (Table 2.4). Impurities and polymerisation inhibitors were removed by passing the oils through basic alumina, with polymerisation initiated thermally using the initiator azobisisobutyronitrile (AIBN), both of which are described in section 2.1.3. The materials used to modify the template particles are also described in the same section.

## 5.3 Results and discussion

### 5.3.1 Janus particle contact angles and wettability

There are important differences in the structure and wetting behaviour of Janus and homogeneous particles. Wetting properties of colloidal particles with chemically homogeneous surfaces are well characterised by the particle contact angle,  $\theta$ . Hydrophilic homogeneous particles ( $\theta < 90^\circ$ ) have lower surface energy when dispersed in water rather than in oil. The opposite is true for hydrophobic particles ( $\theta > 90^\circ$ ). The contact angle of the particle dictates its position at the oil-water or air-water interface. For example, the depth of immersion into water,  $h_w$ , of a spherical particle with radius  $r$ , is  $h_w = r(1 + \cos \theta)$ . Janus particles have two distinct surface regions with different contact angles (Fig. 5.2). Following the early work of Casagrande and Veyssie<sup>10,11,18</sup> we label these as a “polar” region with contact angle  $\theta_p$  and an “apolar” region with contact angle  $\theta_a$ . The “polar” region has higher affinity to water and lower contact angle than the “apolar” region, i.e.  $\theta_p < \theta_a$ . There is no need to assume that the “polar” region is hydrophilic, nor that the “apolar” one is hydrophobic<sup>11</sup> and the contact angles of both regions could be

simultaneously lower or higher than  $90^\circ$ . The wetting properties of a Janus particle also depend on the relative areas of both regions<sup>10, 11</sup> with area fractions  $\phi_a$  and  $\phi_p = 1 - \phi_a$ . It is convenient to express these using the central angle  $\alpha$  measured from the middle of the “apolar” region to the boundary between the regions (Fig. 5.2). The relationship between  $\alpha$  and  $\phi_a$  is

$$\phi_a = (1 - \cos \alpha) / 2 \quad (5.1)$$

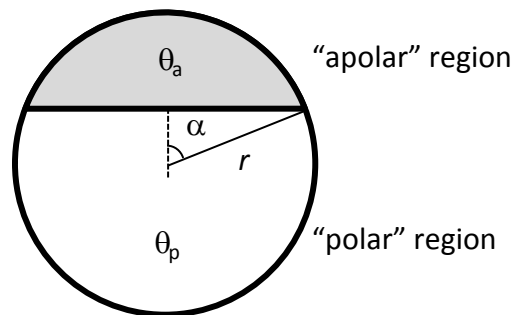


**Figure 5.2.** Schematic of a spherical Janus particle with radius  $r$ . The “polar” region has higher affinity to water and lower contact angle than the “apolar” region, i.e.  $\theta_p < \theta_a$ .

Hence the wetting properties of a Janus particle can be fully characterised by the three angles,  $\theta_p$ ,  $\theta_a$  and  $\alpha$ . Assuming that the Janus particle is oriented with its “polar” region towards the water (Fig. 5.3), it has been shown that for a given set of angles there is a unique attachment with lowest free energy<sup>10,11</sup> and equilibrium contact angle  $\theta$ . Three distinct modes of attachment can be distinguished, depending of the relative magnitude of the angles  $\theta_p$ ,  $\theta_a$  and  $\alpha$ <sup>11</sup>. When  $\theta_p \leq \alpha \leq \theta_a$  the three phase contact line is pinned at the boundary between the regions, hence  $\theta = \alpha$ . This mode of attachment is unique for the Janus particles and can be named ‘J-mode’<sup>10,11</sup>. The other two modes, named here as ‘H1’ and ‘H2’, are similar to the

attachment of a homogeneous particle and the equilibrium contact angle equals that of the “polar” or “apolar” region, respectively (Table 5.1 and Fig. 5.3).

**Table 5.1.** Modes of attachment to a fluid-liquid interface for a Janus particle with  $\theta_p < \theta_a$ , the condition for  $\alpha$  that must be fulfilled and the respective equilibrium contact angle.

| Mode of attachment | Condition for $\alpha$               | Equilibrium contact angle, $\theta$ |
|--------------------|--------------------------------------|-------------------------------------|
| H1                 | $\alpha < \theta_p$                  | $\theta = \theta_p$                 |
| J                  | $\theta_p \leq \alpha \leq \theta_a$ | $\theta = \alpha$                   |
| H2                 | $\alpha > \theta_a$                  | $\theta = \theta_a$                 |

Note that we do not impose the conditions  $\theta_p < 90^\circ$ ,  $\theta_a > 90^\circ$  as assumed previously<sup>10,11,18-20</sup>. Our approach is more general so all three modes of Janus particle attachment could be realised for any value of the equilibrium contact angle either smaller or bigger than  $90^\circ$ . Examples of Janus particles when both regions are simultaneously hydrophilic or hydrophobic will be shown later in this chapter. One should expect that the equilibrium contact angle of Janus particles will determine their interfacial behaviour and the type of emulsions they could stabilise. Similar to homogeneous particles, Janus particles with  $\theta < 90^\circ$  could be labelled as hydrophilic and would stabilise o/w emulsions, while those with  $\theta > 90^\circ$  could be considered as hydrophobic and would preferably stabilise w/o emulsions. These hypotheses have been tested by experiments and the obtained results will be discussed later in this chapter.

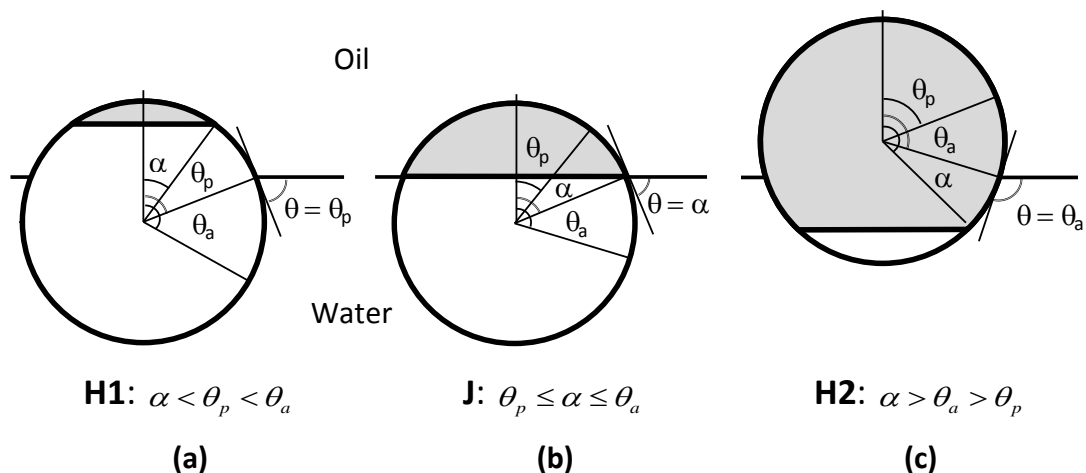


**Figure 5.3.** Janus particle modes of attachment to a fluid-liquid interface, (a) H1-mode: the three-phase contact line (t.c.l.) is located within the region with the lower contact angle  $\theta_p$ . (b) J-mode: the t.c.l. is located at the boundary between the regions with different wettabilities. (c) H2-mode: the t.c.l. is located within the region with the higher contact angle  $\theta_a$ . H1 and H2 modes are similar to the attachment of a homogeneous particle, while the J-mode is unique for amphiphilic Janus particles.

### 5.3.2 Preparation and polymerisation of Pickering emulsions

Pickering emulsions were chosen as the best method for producing Janus particles since the yield is expected to be greater compared to other methods (see section 1.2.2). Following our research strategy described above we use methacrylic and styrene monomers as an oil phase because they can be polymerised in the presence of appropriate initiators at elevated temperature and the resulting polymers can be easily dissolved in various solvents (e.g. chloroform), which is an important requirement for the last step of Janus particle preparation (see Fig. 5.1). It is known that the particles must be partially hydrophobic in order to stabilise Pickering emulsions<sup>21</sup>. The initially trialled approach was to use a cationic surfactant solution as the aqueous phase to hydrophobise silica particles so that they could stabilise oil-in-water emulsions of polymerisable monomer. This approach has the advantage that the ratio between the masked and unmasked portions of the

particles attached to the emulsion droplets could be varied by altering the concentration of the surfactant used, thus tuning the angle  $\alpha$  of the Janus particles produced as described previously<sup>22</sup>. Using aqueous suspensions of 3 wt.% silica particles with a diameter of 1  $\mu\text{m}$  in dilute TTAB solutions and 30 vol.% 2-ethylhexyl methacrylate (EHMA) as an oil phase, we were able to make stable o/w Pickering emulsions. However it was found that the emulsions droplets were not covered by a monolayer of discrete silica particles but by a layer of particle aggregates with uneven thickness. As a result, the depth of immersion of the particles into the oil droplet varied greatly. This suggested that it would be impossible to control and tune the angle  $\alpha$  of the Janus particles which could be produced from these emulsions after polymerisation. In addition, we observed a strong interference between the surfactant and water soluble thermo initiators which inhibited the polymerisation process. To overcome the above issues the particles were pre-treated to varying degrees with a silane in order to hydrophobise the surface without the use of surfactant. The oil-soluble thermo initiator azobisisobutyronitrile (AIBN) was used in systems containing such particles and no problems were encountered with emulsifying or polymerising the systems for 2 hours at 70 °C. Optical and electron microscopy of the polymerised Pickering drops revealed that they were predominantly covered by a monolayer of particles (Fig. 5.5). The angle  $\alpha$  can be estimated from the SEM images by measuring the height of the particle exposed in air (initially in water),  $h_w$  and its diameter,  $d$  (see Fig. 5.4) using the equation:

$$\cos \alpha = \frac{2 h_w}{d} - 1 \quad (5.2)$$

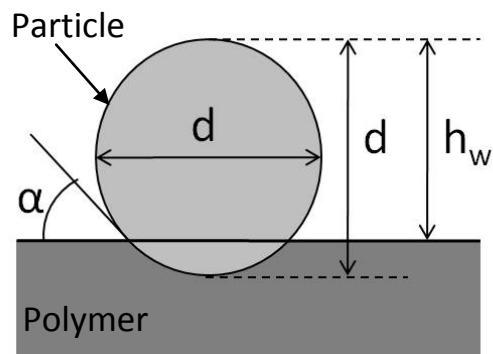


**Figure 5.4.** The contact angle,  $\alpha$ , of a particle at the polymer surface can be estimated using eq. 5.2 by measuring the diameter,  $d$  and height of particle exposed,  $h_w$ .

Measuring the contact angle  $\alpha$  of 50 particles at a poly-EHMA surface for the system shown in Fig. 5.5 SEM images and eq. 5.2 yielded an average value of  $69 \pm 4^\circ$ . This value is not very different from the average contact angle of water drops on similarly treated glass slides in EHMA monomer ( $78 \pm 8^\circ$ ) measured before polymerisation at room temperature. These results suggest that the area fractions of the two regions at the Janus particle surface (see eq. 5.1) can be varied by changing the hydrophobicity of the silica particles used in the polymerised Pickering emulsions.

The method for emulsification was investigated with hand-shaking, stirring, ultrasonication and homogenisation with an Ultra-Turrax homogeniser. Both ultrasonication and stirring alone failed to produce sufficient emulsification. Emulsion droplets made with an Ultra-Turrax at 8000 rpm were sometimes more polydisperse in size than the hand-shaken emulsion but the hand-shaken drops were generally larger and had non-spherical shapes (see Fig. 5.6). The Ultra-Turrax homogenisation was selected for use to enhance the reproducibility of the experimental conditions. Different homogenisation speeds were investigated but little change was observed in the polymerised products, likely caused by emulsion instabilities prior to full polymerisation. Although the Pickering emulsions were stable against coalescence at room temperature for days, we observed that without

stirring, the emulsion droplets would regularly fuse together during polymerisation at 70 °C. Further emulsions were therefore diluted and stirred during polymerisation to reduce aggregation and coalescence. The polymerised Pickering emulsion drops are herein termed 'polymer beads' in order to avoid confusion. These so-called beads consist of a polymer core with a layer of particles attached to the surface.

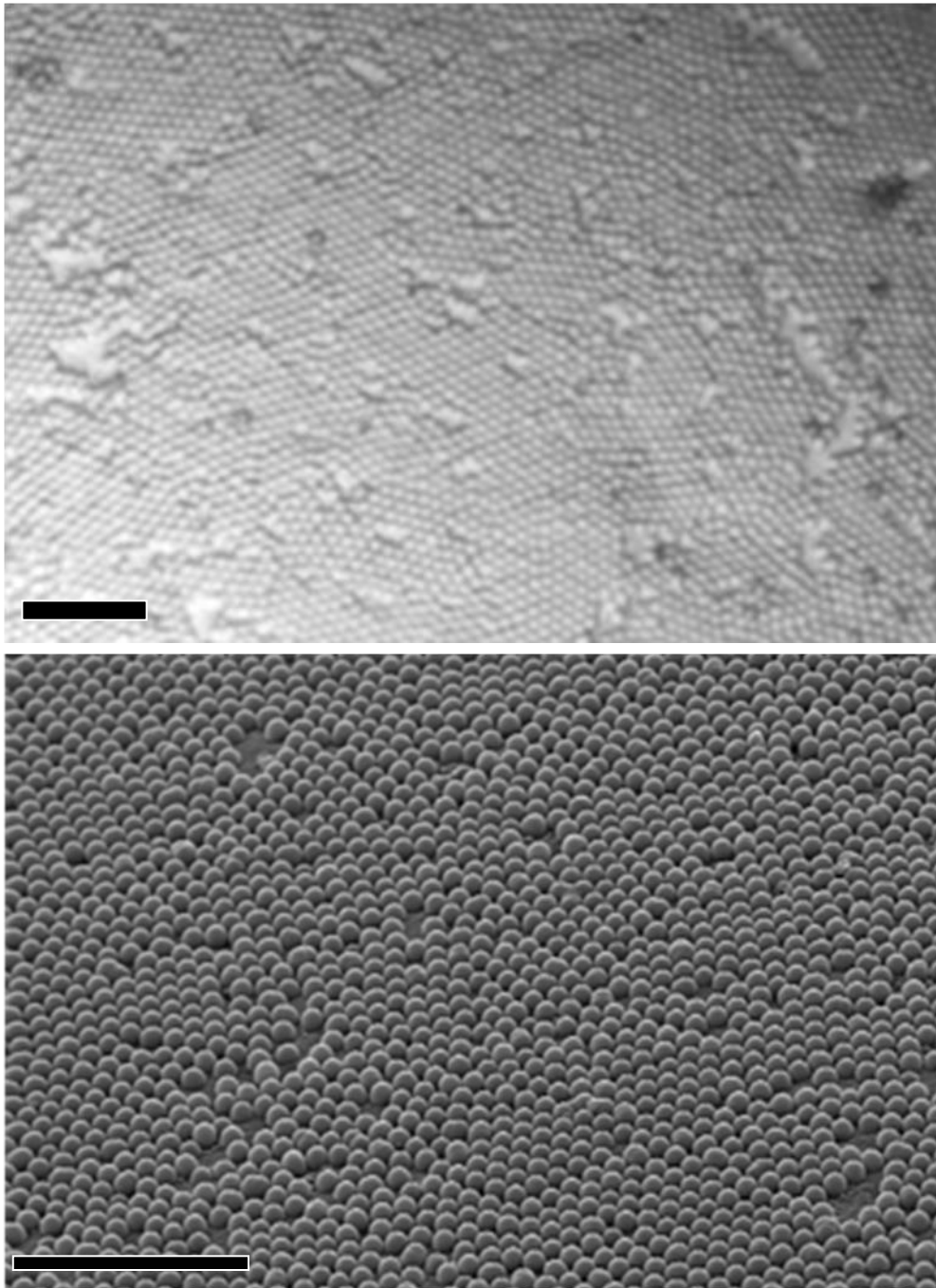


**Figure 5.5.** Silica particles on the surface of an EHMA polymer bead imaged with optical microscopy (top) and scanning electron microscopy (bottom). Particles can be seen covering the polymer surface as a monolayer with some defects of bare polymer. The emulsion (prior to polymerisation) was made via Ultra-Turrax homogenisation over 5 minutes using 3 wt.% of 1  $\mu\text{m}$  silica particles, pre-treated with  $5 \times 10^{-4}$  M DCDMS, in water and 30 vol.% of EHMA as an oil phase. The scale bars are 10  $\mu\text{m}$ .

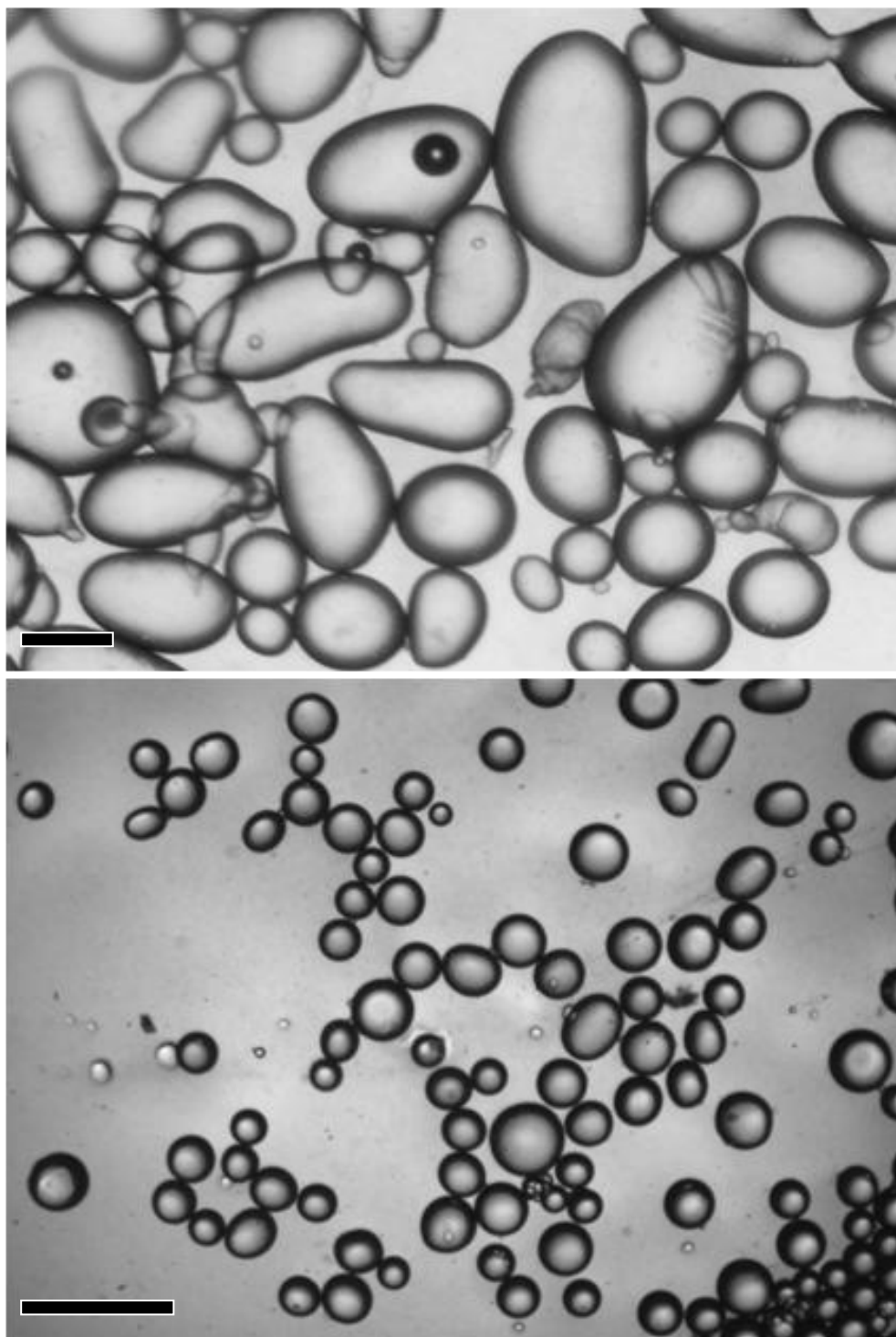


**Figure 5.6.** Oil-in-water Pickering emulsions formed by hand-shaking (top) over 30 seconds with 30 shakes and with the Ultra-Turrax (bottom) homogeniser at 8000 rpm over 5 minutes with 2 minutes total mixing time. Emulsions were made using 1  $\mu\text{m}$  silica particles in water (3 wt.%) with a 30 vol.% oil phase of EHMA (1 mol.% AIBN). The scale bars are 400  $\mu\text{m}$ .

The initial experiments were carried out with EHMA monomer as the oil phase. The main problem with the polymer formed with EHMA was that it had a low glass transition temperature ( $-10\text{ }^{\circ}\text{C}^{23}$ ), which means that at room temperature the polymer was relatively soft and the polymerised drops tended to stick together or onto any surface they touched if left dry. The polymer therefore had to be kept in water at all times to prevent deformation of either the polymer or the coating layer of particles and could have created problems further on so an alternative monomer was sought.

The monomers tested were butyl methacrylate (BMA), 2-ethylhexyl methacrylate (EHMA), isobutyl methacrylate (IBMA), stearyl methacrylate and styrene. Series of samples were prepared for each oil to investigate polymerisation at different temperatures (0, 40, 70, 75 and 80 °C), concentrations of initiator (0.5, 1.0 and 2.0 mol.% AIBN) and a range of polymerisation timescales (1 - 4 and 20 hours). Some of these systems did not polymerise. The polymers were qualitatively investigated for flexibility, stickiness, air bubbles in the polymer, polymerisation time, and the appearance of the water phase after polymerisation. Isobutylmethacrylate with 1 mol.% AIBN polymerised at 75 °C for 2 hours was found to be the best system from those tested.

As a final comparison between the more promising monomers they were used to make emulsions and then turned into polymer beads. It was found that the emulsion droplets made with each oil were effectively the same, all relatively polydisperse in microscope observations and with similar drop sizes between oils, as measured with a Malvern Mastersizer 2000 instrument. Typical emulsion drop size profiles are shown in Fig. 5.7 for the different monomer oils.

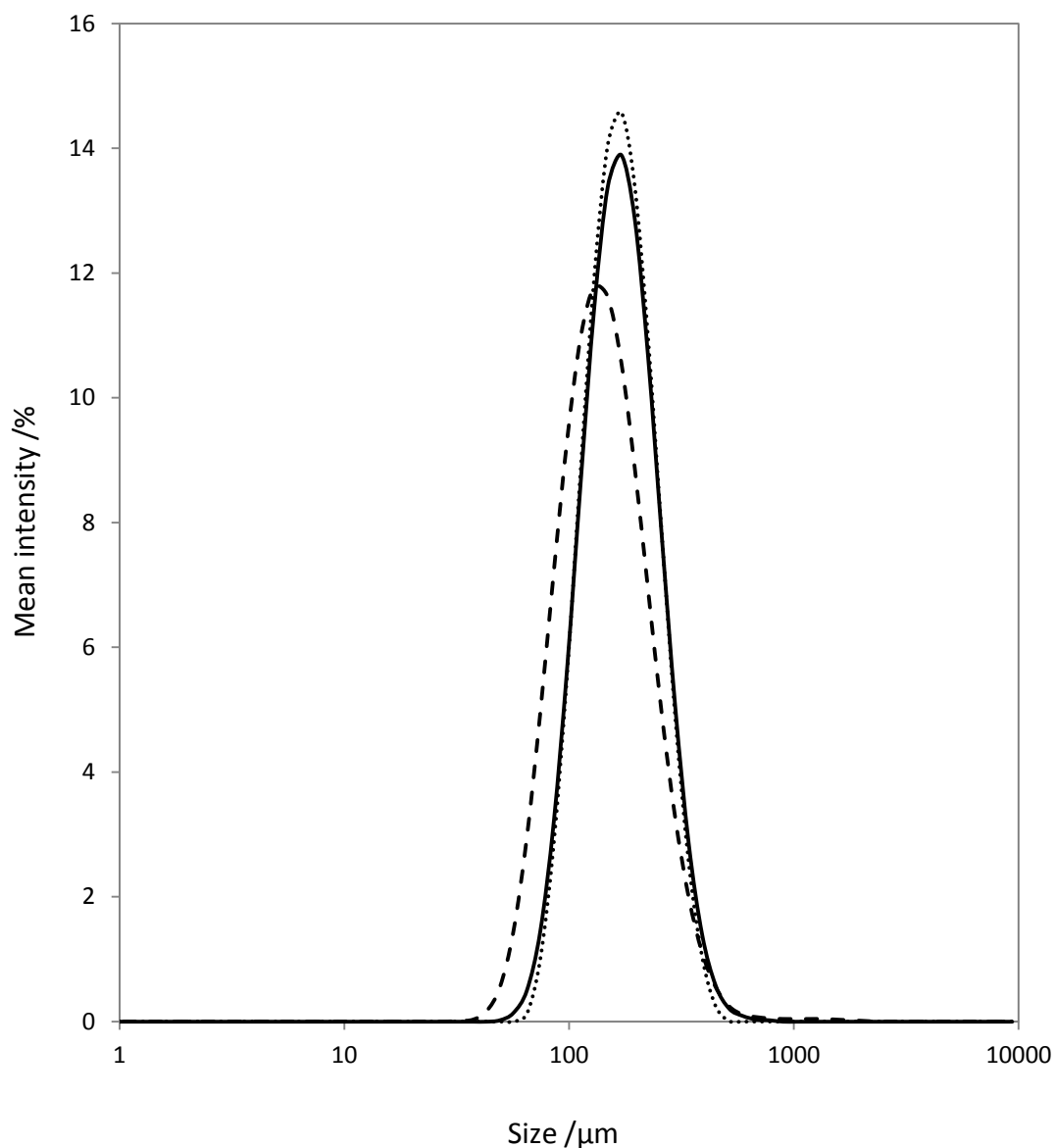


**Figure 5.7.** Drop size profile of Pickering emulsion drops made with three different monomer oils. The dotted line depicts emulsion drops of EHMA, dashed line is BMA and the continuous line shows the IBMA profile. Each emulsion was made via Ultra-Turrax homogenisation over 5 minutes using 1  $\mu\text{m}$  silica particles (3 wt.%) pre-treated with  $5 \times 10^{-4}$  M DCDMS, in water and 30 vol.% oil phase.

A difference in diameter arises between the emulsion droplets and the polymerised beads, shown in Fig. 5.8, where the polymer beads are seen to be approximately ten times bigger than the emulsion droplets when using the EHMA monomer. Comparing the size of beads made (Fig. 5.9) it is seen that there is a greater range of diameters measured between the different monomers in this case than for the emulsion droplets (Fig. 5.7). The monomer BMA was found to polymerise swiftly and the polydispersity of the polymer beads tends to be greater, with a greater proportion of smaller beads compared to those of the other monomers. This suggests that coalescence and Ostwald ripening can occur during polymerisation and occurs to a greater extent for monomers slower to polymerise. There is a well defined upper diameter measured for the polymer beads (Fig. 5.9), which may be partially due to limitations of the equipment, while the lower limit of sizes measured relates to that of the emulsion drops (Fig. 5.10).

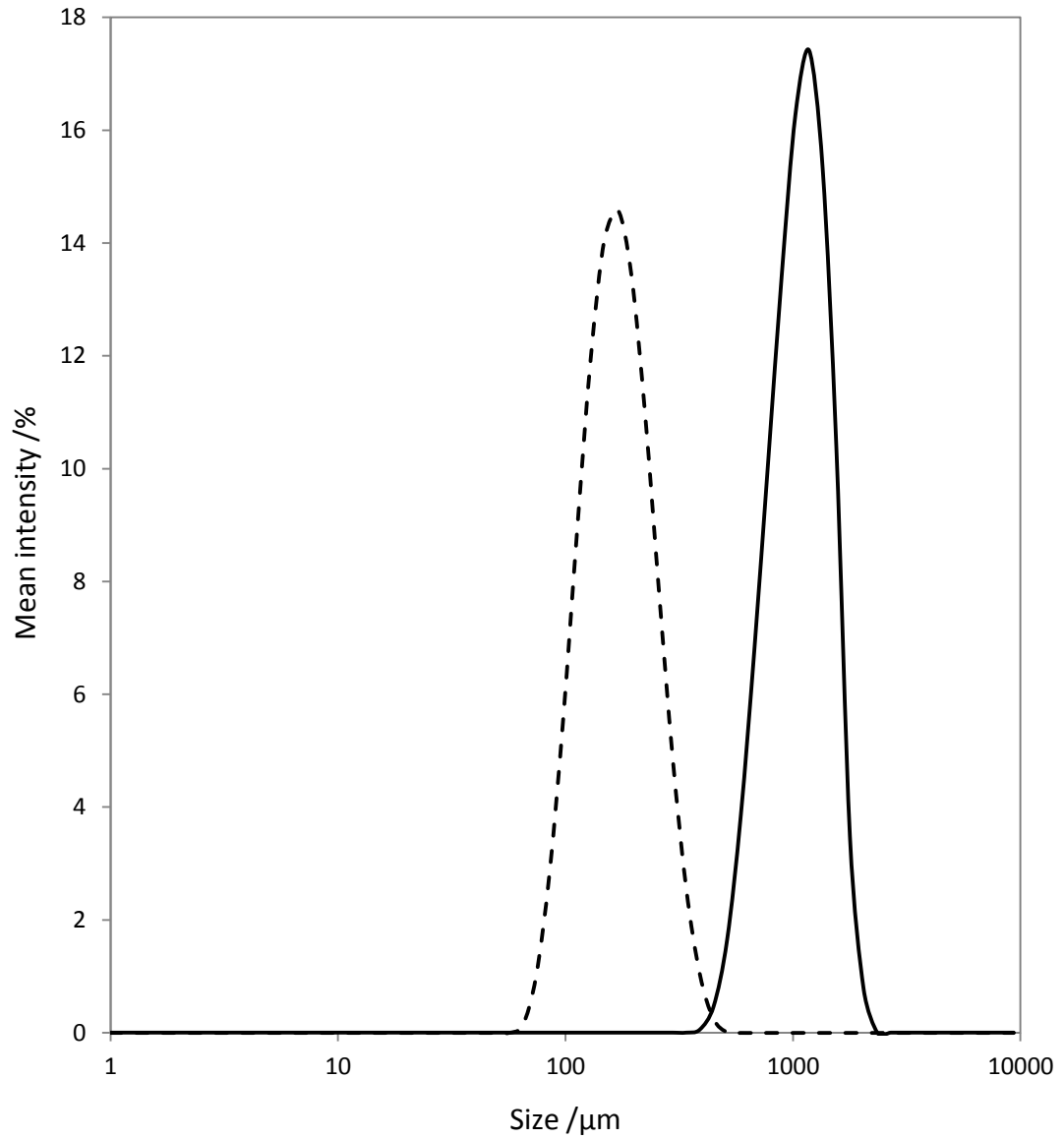


**Figure 5.8.** Size profiles measured for emulsion droplets and polymer beads made with the EHMA monomer. The sizes of emulsion droplets are displayed by the dashed line while the continuous line shows the size profile of polymer beads.

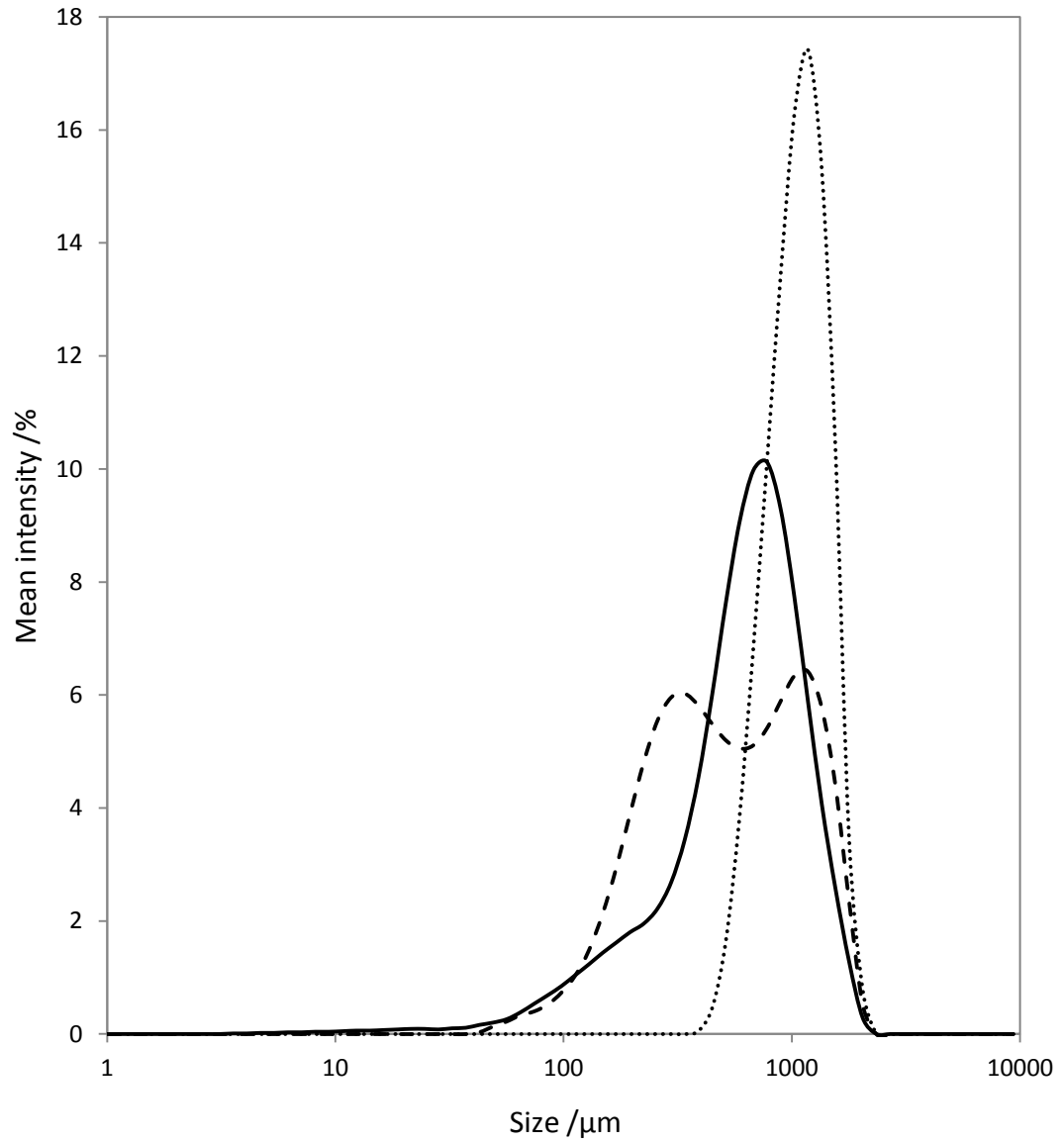


**Figure 5.9.** Size profiles of polymer beads made with three different monomers. The dotted line relates to beads made from EHMA monomer, the dashed line shows beads made from BMA monomer and the continuous line those from IBMA.

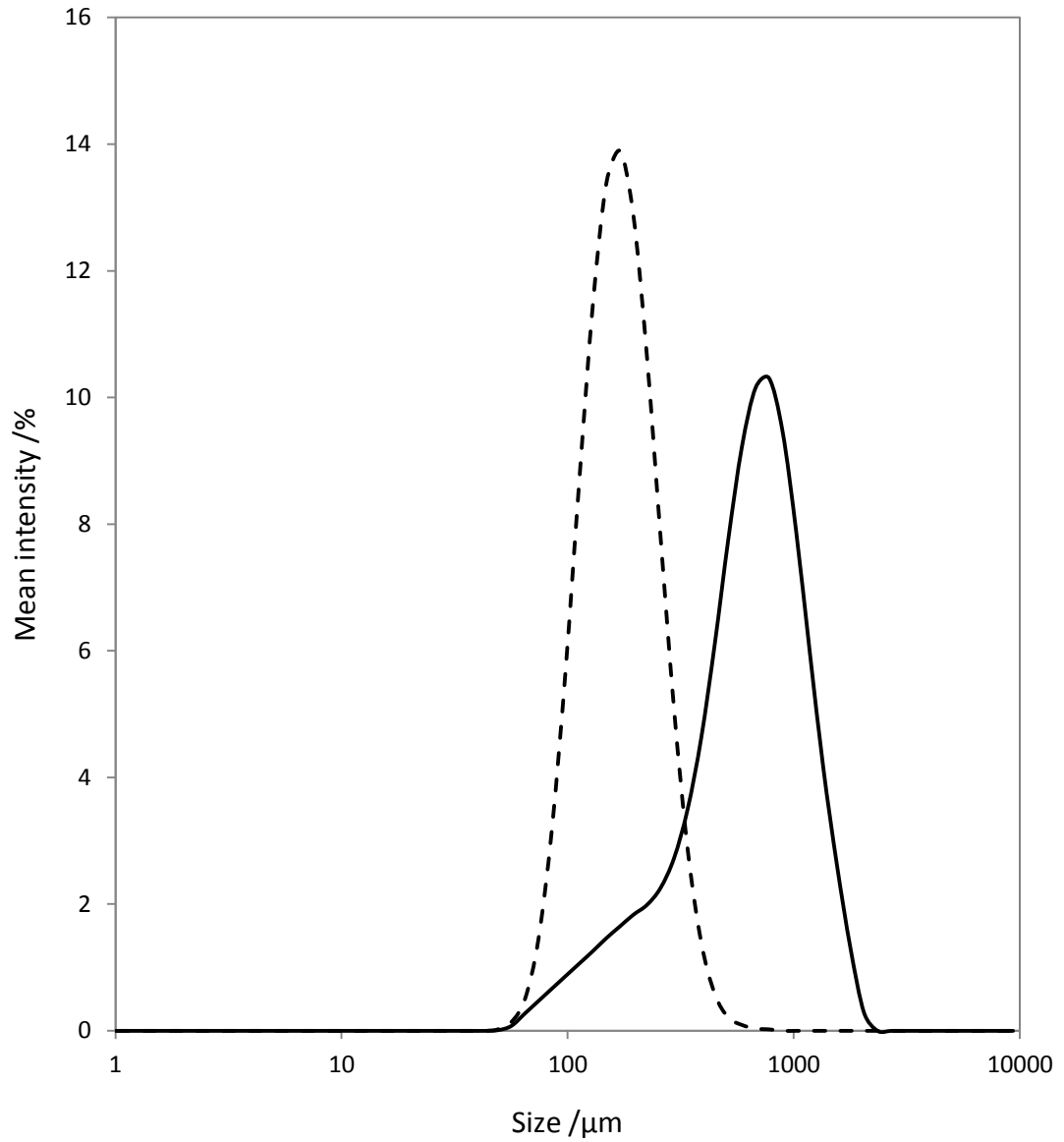


**Figure 5.10.** Size profiles measured for emulsion droplets and polymer beads made with the IBMA monomer. The sizes of emulsion droplets are displayed by the dashed line while the continuous line shows the size profile of polymer beads.

The polymerisation was stopped swiftly after the allocated time period by stirring in a cold water bath to cool the sample. This was to stop additional polymerisation of remaining monomer dissolved in the water phase, reducing detrimental effects such as polymer globules forming on the exposed particle surfaces.

Prior to treatment of the exposed particle surfaces, excess silica particles on the polymer bead surface were removed. The first part of this was the vigorous stirring during the cooling period, followed with two lots of filtration and washing with milli-Q water in a Buchner funnel. Sonication was not used to loosen excess particles as it can detach a lot of the particle monolayer.

The optimum system chosen for our technique of making Janus particles used silica particles initially hydrophobised with DCDMS solutions ( $10^{-5}$  - 0.1 M in toluene) as a base. Oil-in-water emulsions of milli-Q water and 30 vol.% IBMA monomer, containing 1 mol.% AIBN, were stabilised with these particles at a concentration of 3 wt.% with respect to the aqueous phase. The emulsions were prepared with an Ultra-Turrax homogeniser at 8000 rpm over 5 minutes with a total mixing time of 2 minutes. They were then diluted with heated deionised water equal to half of the total emulsion volume and polymerised in a test tube (24/3) over 2 hours at 75 °C while stirring with a magnetic stirrer. The polymerisation was stopped swiftly by stirring in a cold water bath.

### *5.3.3 Preparation of different Janus particle types by varying the chemical treatment of polymerised Pickering drops*

To turn the masked particles into Janus particles 4 treatments were performed on the exposed silica surfaces (see Fig. 5.11): metal deposition, amination, decreasing the surface hydrophobicity with oxidation, and further hydrophobising the exposed surface with DCDMS vapours.

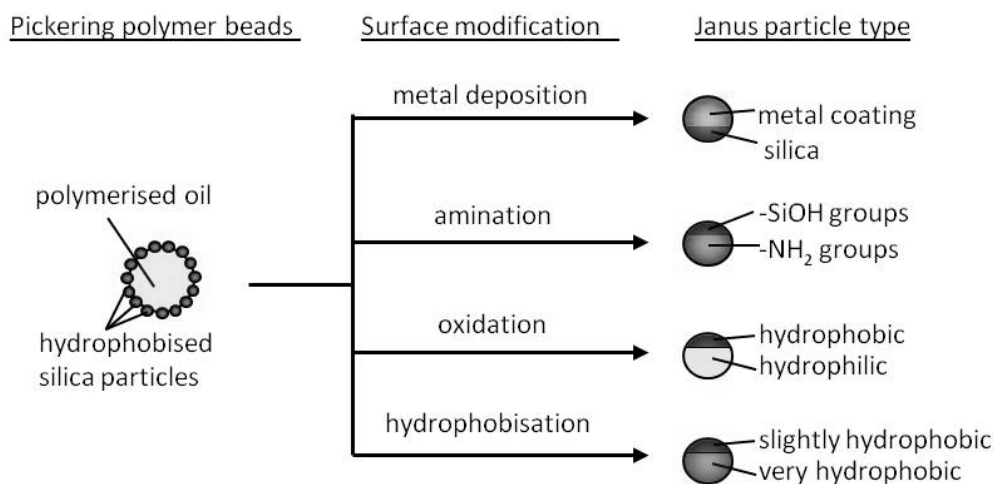


**Figure 5.11.** Exposed surfaces of silica particles trapped at the surface of polymer beads were modified by various techniques to produce 4 types of Janus particle (right).

#### 5.3.3.1 Metal/ dielectric Janus particles

To test the applicability of our approach for making metal/dielectric Janus particles we used the silver mirror reaction to coat the exposed surface of the particles on the polymer beads with a layer of silver. The Tollen's reagent procedure (see section 2.2.11) was used to produce the silver layer. Initial tests were carried out on microscope slides in plastic reaction vessels and showed that the silver layer attached very well to glass but not to plastics. SEM images obtained after dissolving the polymer core show that silver/silica Janus particles have been produced (Fig. 5.12). The unmasked silica particle surface is covered with a layer of silver with grainy structure. It is possible that a slower method of depositing the silver on the particles could produce a thinner, more even layer of silver on the silica.

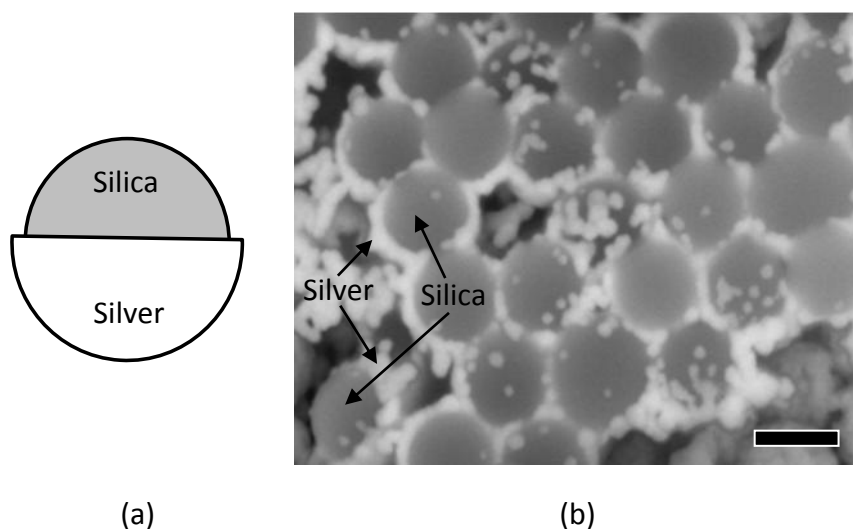


**Figure 5.12.** (a) Schematic of a silver/silica Janus particle. (b) SEM image of silver/silica Janus particles obtained after dissolving the polymer core. The particle diameter and scale bar are 1  $\mu\text{m}$ .

### 5.3.3.2 Bifunctional Janus particles

Silica particles are negatively charged in water due to ionisation of surface silanol groups. Attaching different functional groups (e.g. amine) to the unmasked part of the particles exposed outside of the polymer beads would generate Janus particles with dual functionality. For example, applying an amination reaction to the exposed silica particle surface would form hydroxyl/amine bifunctional Janus particles (Fig. 5.11). Amine groups are neutral at high pH but become protonated and positively charged at low pH. Therefore, such bifunctional Janus particles could have interesting properties because the two surface regions could become oppositely charged, thus forming a macro dipole. Amination of the silica particles could be achieved by treating them with 3-aminopropyltriethoxysilane (APTES) solutions at 10 vol.% in water over 2 hours. This was tested on unmasked bare silica particles first. Zeta potentials of the original and aminated silica particles measured at different pH are shown in Fig. 5.13.

At low pH the untreated silica particles display a positive charge which can be explained by the presence of hydronium species<sup>24</sup> ( $\text{SiOH} + \text{H}^+_{(\text{aq})} \rightarrow \text{SiOH}_2^+$ ). The zeta potential of the aminated particles is shifted positively compared to that of untreated silica at pH lower than 8. The isoelectric point also changes significantly from a pH of approximately 2.5 to a pH of about 7. This occurs as the surface hydroxyl groups are replaced with amine groups.

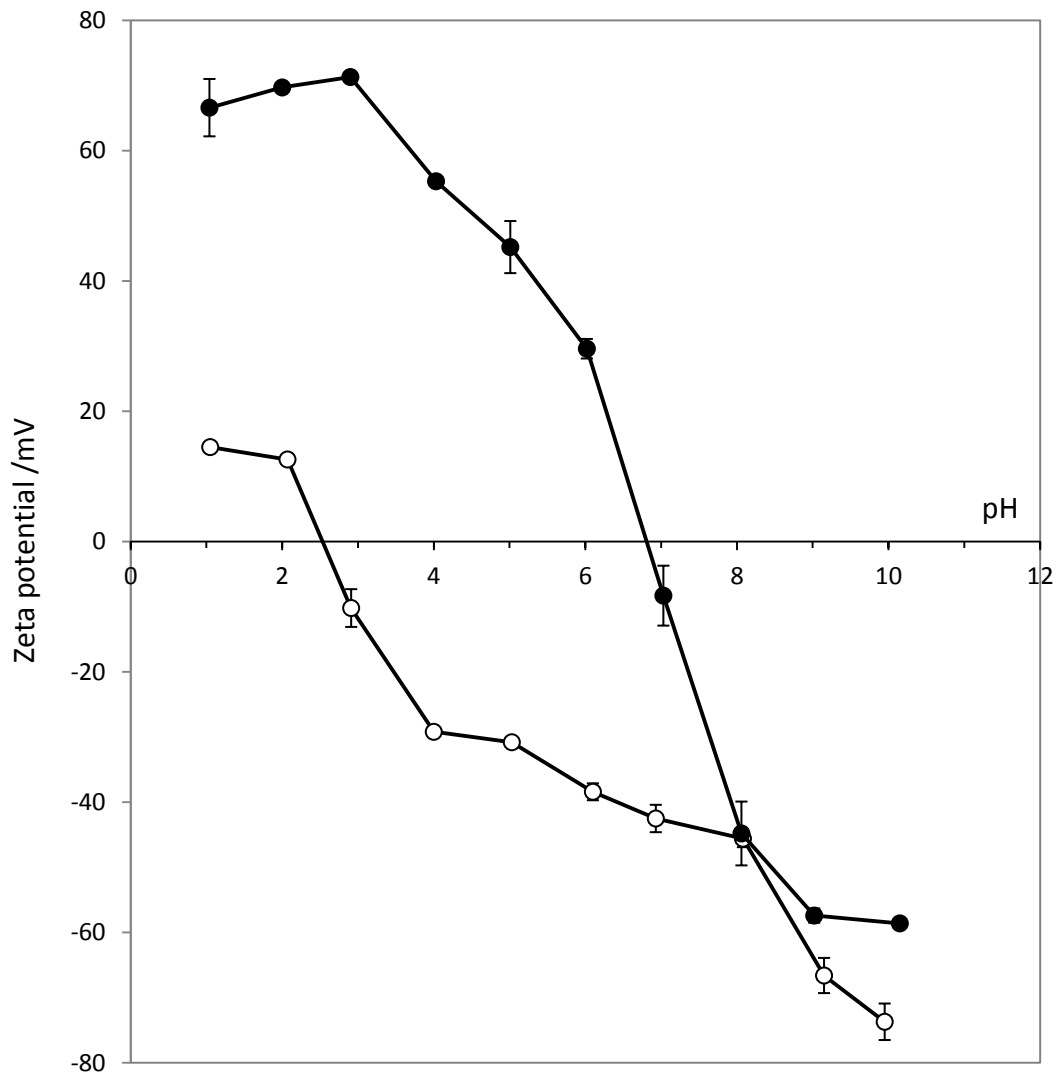


**Figure 5.13.** Zeta potentials of 1  $\mu\text{m}$  silica particles treated with APTES solution (filled circles) or clean i.e. untreated (open circles). The APTES treatment used a 10 vol.% solution in water over 2.5 hours. For each measurement a fresh volume of stock suspension was taken, to which sodium hydroxide or hydrochloric acid were added drop-wise to alter the pH.

APTES was used to aminate the surface of partially masked silica particles hydrophobised at  $5 \times 10^{-4}$  M DCDMS thus making bifunctional Janus particles. The zeta potentials of these particles with varying pH are shown in Fig. 5.14 with those measured on the base particles, and base particles which had been fully treated with APTES. The surfaces of the two types of homogeneous particle therefore match with each region on the bifunctional Janus particles. It was expected that the Janus particles would have a zeta potential and isoelectric point that lay between those of the homogeneous particles.

Zeta potentials of the base particles (Fig. 5.14) hydrophobised with  $5 \times 10^{-4}$  M DCDMS are shifted positively from those of bare silica (Fig. 5.13) in the pH range 3 – 5, increasing the pH of the isoelectric point from  $\sim 2.5$  for bare silica to  $\sim 5$ . The zeta potential of particles treated with both DCDMS and APTES (Fig. 5.14) had a much greater positive shift than that of the base particles and therefore an increase in the pH of the isoelectric point occurred to  $\sim 7.5$ . The zeta potential of the Janus particles is also shifted positively from that of the base particles, with an isoelectric point of  $\sim 6.5$ . Both the zeta potential and isoelectric point of the Janus particles are observed to lie between those of the homogeneous particles, relating to each region on the Janus particle surface. At the isoelectric point of the Janus particles it is expected that the charge of the two different regions cancel each other out, negative for the masked DCDMS treated region and positive for the DCDMS and APTES treated region.

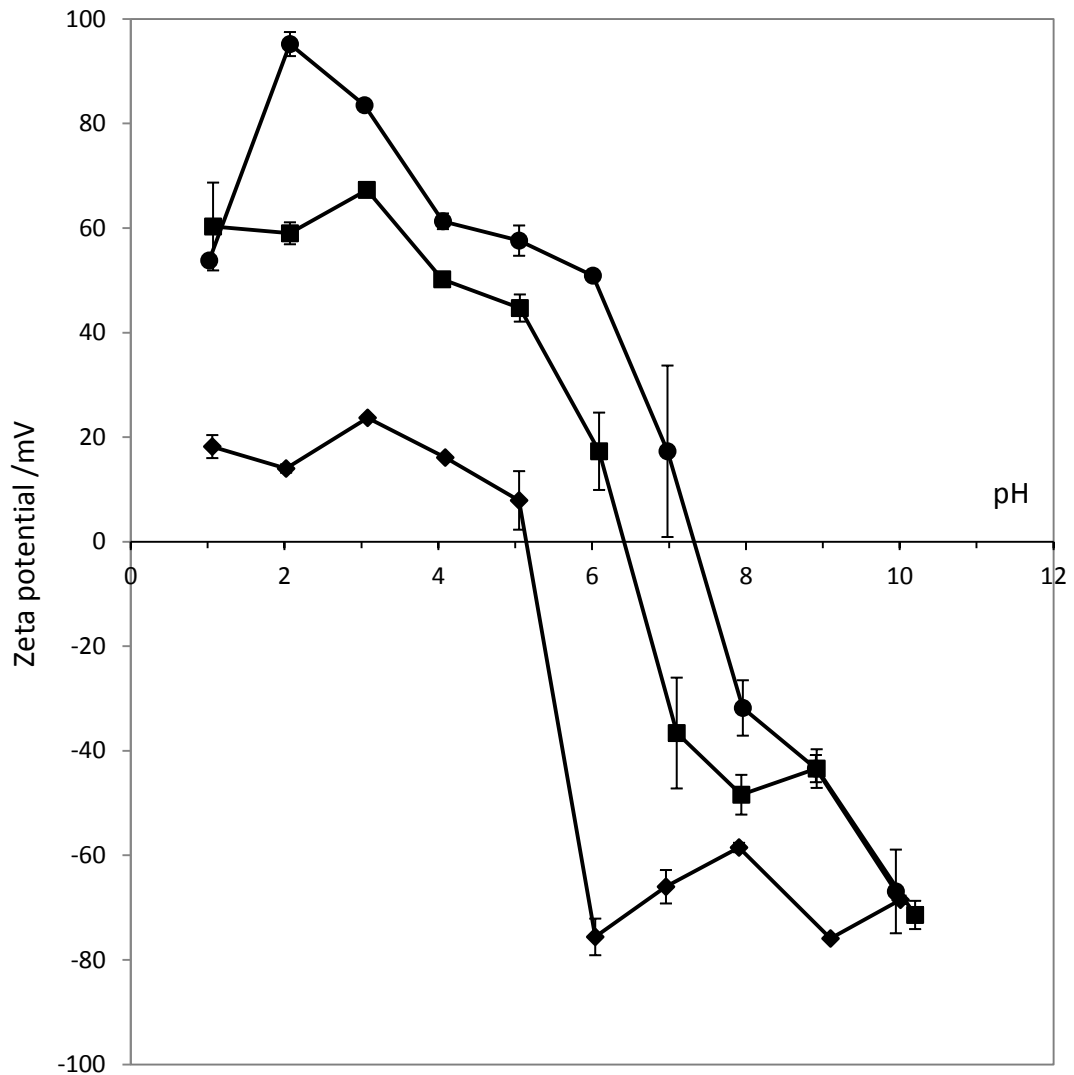


**Figure 5.14.** Plot showing zeta potentials of three 1  $\mu\text{m}$  silica particle samples, all initially treated with  $5 \times 10^{-4}$  M DCDMS. The three plots are for the homogeneous base particles (diamonds), homogeneous particles treated further with APTES solution (circles) and Janus particles made through APTES treatment of masked particles (squares). The APTES treatment used a 10 vol.% solution in water over 2.5 hours. For each measurement Sodium hydroxide or hydrochloric acid was added drop-wise to a fresh volume of the stock suspension to alter the pH.

The results from the zeta potential measurements are convincing, but indirect evidence for the Janus structure of the hydroxyl/amine bifunctional particles obtained. To prove the Janus structure we decided to attach fluorescent markers to the exposed aminated surface of the particles, and use fluorescent microscopy. Rhodamine B isothiocyanate (RBITC) was covalently bonded onto the aminated exposed silica surface. RBITC is traditionally used in alcohol or hydrocarbon solutions. To avoid the damaging effect of these solvents to the polymer mask the RBITC treatment was done using aqueous solutions in milli-Q water which is possibly slower to react but has been used in this way previously<sup>25</sup>. Samples were therefore stirred in  $10^{-3}$  M aqueous RBITC solutions overnight.

Images are presented (Fig. 5.15) showing particles on the surface of a polymer bead which have been treated with a fluorescent dye. In the overlay image it was seen that the polymer surface itself did not become fluorescent but the particles did. When un-dyed particles were viewed with just the fluorescent excitation source switched on nothing was seen except a black image, even when the exposure time was increased significantly.

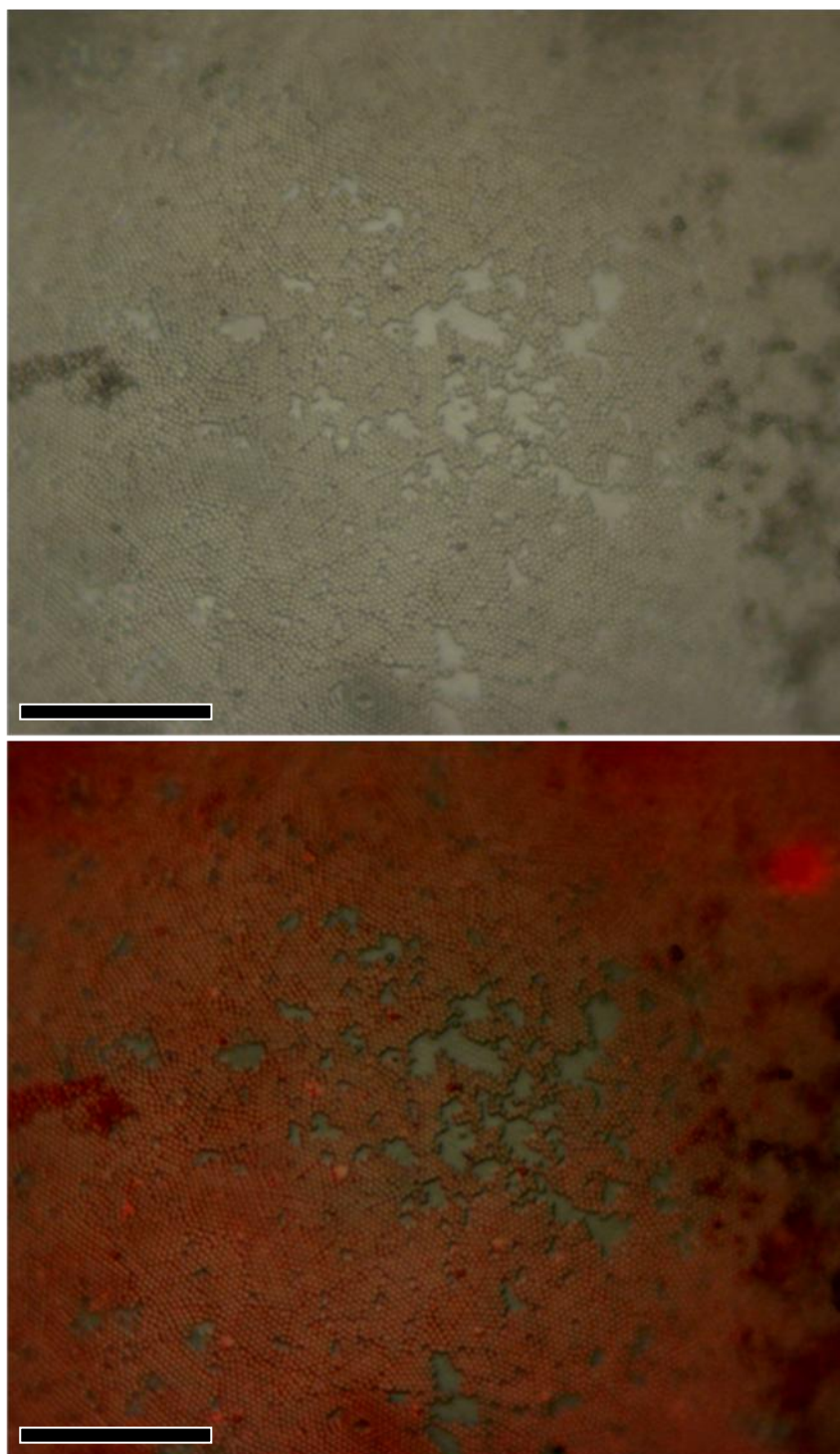


**Figure 5.15.** Images of fluorescently dyed particles on a polymer surface. The top image is taken with bright field microscopy, no fluorescent excitation. The bottom image shows an overlay of the fluorescence image over the bright field image in which it can be seen that the particles fluoresce with a red colour while the exposed polymer does not fluoresce. The dye used was RBITC and the excitation wavelength range was 520 - 550 nm. The scale bars for these images are 30  $\mu\text{m}$ .

To prove that the treatments being performed were producing Janus particles, particles were made with a fluorescent dye (RBITC) on one Janus region. To make the direct observation of the Janus particle fluorescence possible we used larger silica particles with diameters of 2.76, 5.84 and 7.75  $\mu\text{m}$ . Images of Janus particles made with each of these particles are displayed in Fig. 5.16.

|                            | Concentration of DCDMS used to initially hydrophobise the base particles and angle $\alpha_n$ measured for the non-fluorescent region of the Janus particles |            |   |            |  |            |
|----------------------------|--|------------|---|------------|--|------------|
| Diameter ( $\mu\text{m}$ ) | $5 \times 10^{-5} \text{M}$  | $\alpha_n$ | $5 \times 10^{-4} \text{M}$   | $\alpha_n$ | $5 \times 10^{-3} \text{M}$  | $\alpha_n$ |
| 2.76                       |   | 43°        |   | 67°        |   | 120°       |
| 5.84                       |  |            |   | 73°        |  |            |
| 7.75                       |    | 43°        |  | 70°        |  | 123°       |

**Figure 5.16.** Images of Janus particles produced by amination of exposed particle surfaces with 10 vol.% aqueous APTES solutions over 3 h, followed by treatment with aqueous RBITC solutions overnight. The Janus particles were made from base particles of a variety of sizes and a variety of initial hydrophobicities (shown). Also shown is the angle  $\alpha_n$  that was measured for the non-fluorescent region of the particles.

It is clearly seen that the fluorescent portion of the particles changes significantly across particles pre-treated with different concentrations of DCDMS. With changing particle diameter the fluorescent portion of the particles is similar for particles with the same pre-treatment of DCDMS. As the initial particle hydrophobicity increases (increasing DCDMS concentration), the particles are expected to sit further into the oil of the emulsion, which means that a larger proportion of the particle was subsequently masked by the polymer. The treated area of these particles would then be smaller than that of more hydrophilic particles, which sit more in the aqueous phase and would be masked less by the polymer. This is observed in Fig. 5.16 where the portion of fluorescent particle decreased significantly with increasing DCDMS concentration as would be expected. In addition to this it was found that the contact angles measured for these particles were approximately the same for particles made with the same initial hydrophobicity, independent of size, with a variation of  $\sim 3^\circ$ .

These images show that Janus particles can be produced with the emulsion polymerisation method used, and in using this method the area fractions of the two regions on the particle surface can be controlled by varying the initial hydrophobicity. Further to this, the method is transferrable to particles of varying size.

#### *5.3.3.3 Amphiphilic Janus particles and Pickering emulsions stabilised by them*

'Hydrophobic' Janus particles were made by treating the masked particles with DCDMS vapour to increase the hydrophobicity of the exposed silica surface. This procedure was attempted with the DCDMS in several different solvents however the DCDMS as a liquid phase was found to dissolve the polymer masking the particles. The vapour treatment was performed overnight to ensure maximum hydrophobicity was achieved.

'Hydrophilic' Janus particles were made by treating the exposed silica surfaces with nitric acid to lower the hydrophobicity. To determine the agent to use in this treatment previous experiments had been carried out. In these trials microscope slides which had been silanised with DCDMS were washed in either nitric acid or sodium hydroxide to lower the contact angle. Several slides were treated simultaneously for different periods of time and washed thoroughly with milli-Q water to end the treatment. Sodium hydroxide at room temperature reduces the contact angle down to the minimum that can be measured using the sessile drop method within minutes. Nitric acid on the other hand takes a couple of hours at room temperature to reach the minimum contact angle as shown in Fig. 5.17. Using the nitric acid at 40 °C was seen to speed up the treatment if necessary. The nitric acid was chosen over sodium hydroxide as it is less damaging to the silica surface and fast treatment times (as with sodium hydroxide) were not necessary. By using nitric acid there was also the possibility of controlling the reduction in hydrophobicity by varying the treatment times.

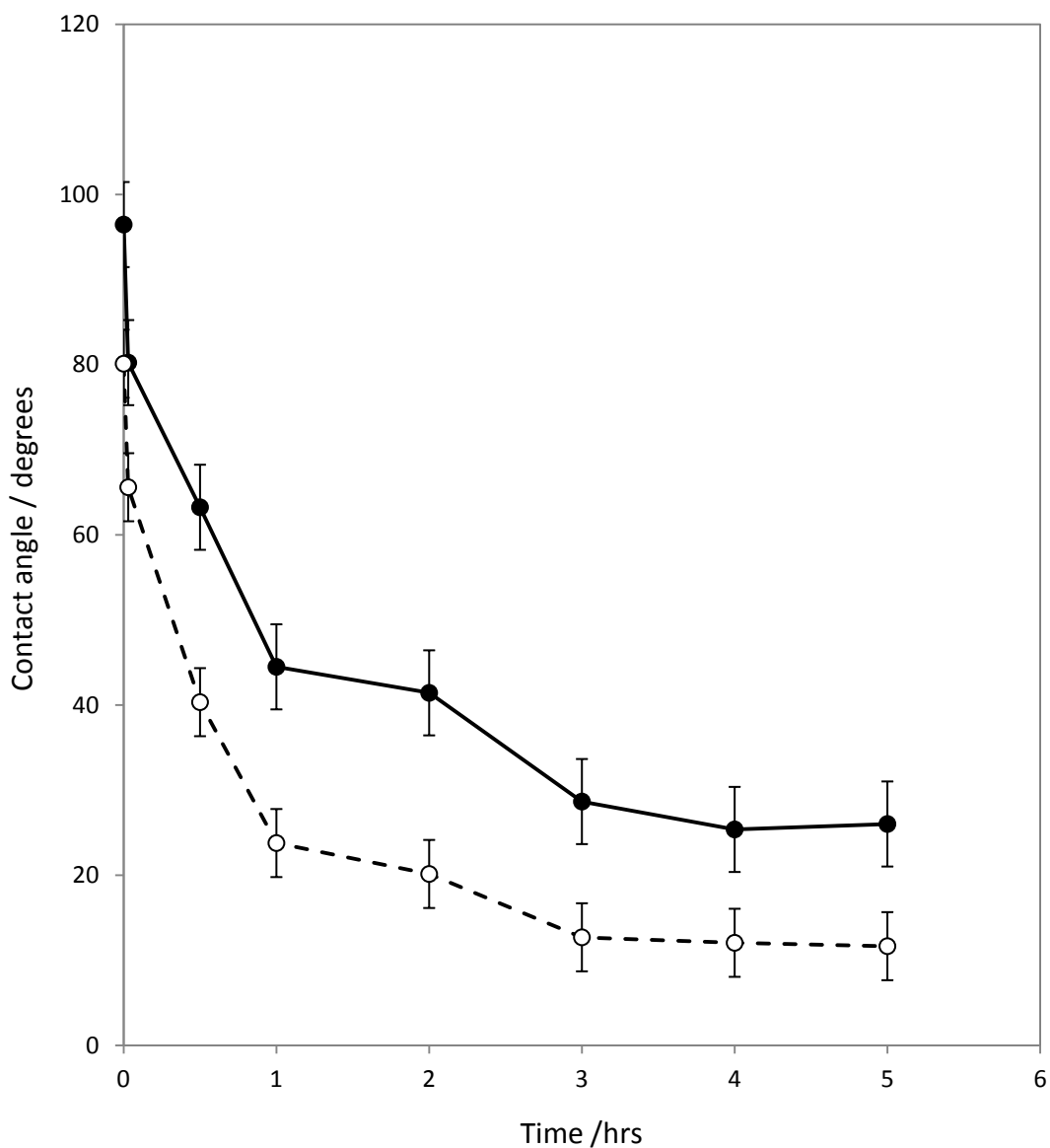


**Figure 5.17.** Plot showing the decrease in the advancing (filled circles) and receding (open circles) contact angles measured on hydrophobised glass slides which was caused by treatment with nitric acid. The slides were submerged in 20 vol.% nitric acid solution for several hours at room temperature, then washed with deionised water and dried before contact angle measurements were made.

A range of amphiphilic Janus particles were made in order to observe their suitability as emulsifiers. Two sizes of silica particles were used, pre-treated to 6 initial hydrophobicities with DCDMS. Two series of amphiphilic particles were made for each size: the masked particles were treated with nitric acid to make the exposed surfaces more hydrophilic, or treated with DCDMS to make them more hydrophobic (Figs. 5.18 and 5.19). Unmasked particles were also fully treated with nitric acid and DCDMS under the same conditions to produce homogeneous particles with the same surface make-up as the treated regions on the Janus particles. Emulsions stabilised by the Janus particles could then be compared with emulsions stabilised with homogeneous particles matching each of the surface regions.

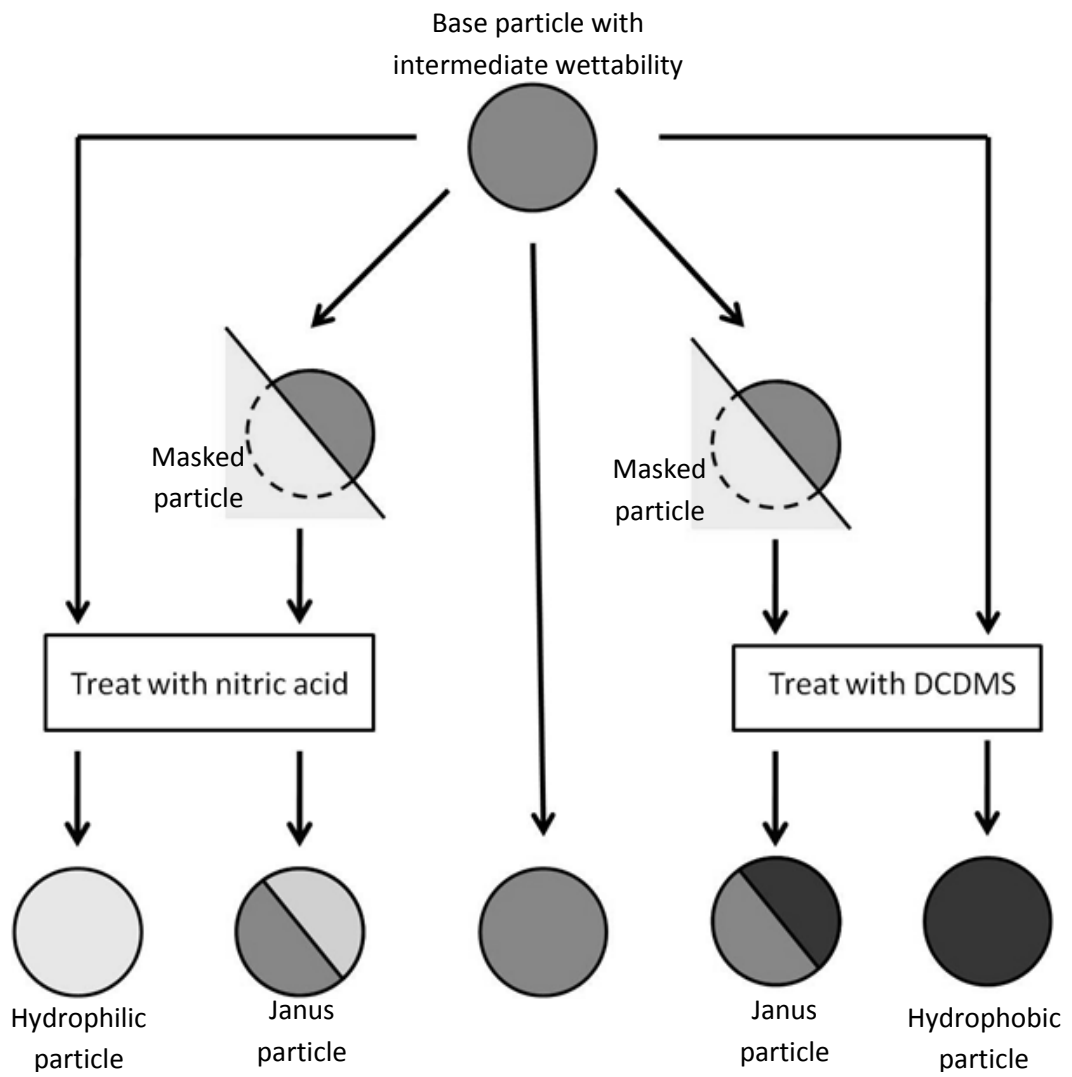


**Figure 5.18.** Schematic of the series of particle types produced from treatments on masked or unmasked base particles of medium hydrophobicity.

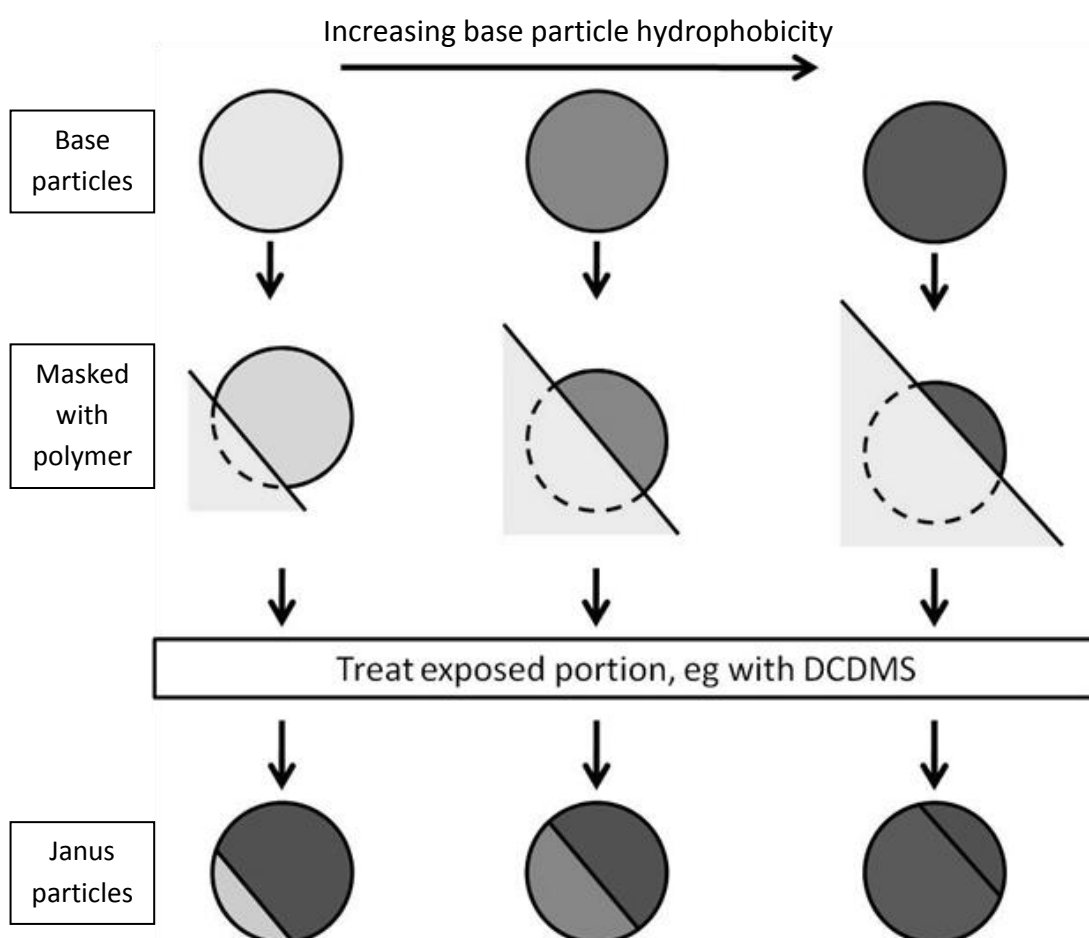


**Figure 5.19.** Schematic of the series of particle types produced from treatments on masked base particles where the initial hydrophobicity of the particles is varied. It is shown that initially hydrophilic particles will have a larger portion of the surface unmasked and therefore treated, so they will be mostly hydrophobic when treated with DCDMS (as shown) or hydrophilic when treated with nitric acid. Particles that were initially hydrophobic will be mostly masked (as shown) and only a small portion of the surface will be treated so whether treated with DCDMS or nitric acid they will remain mostly hydrophobic.

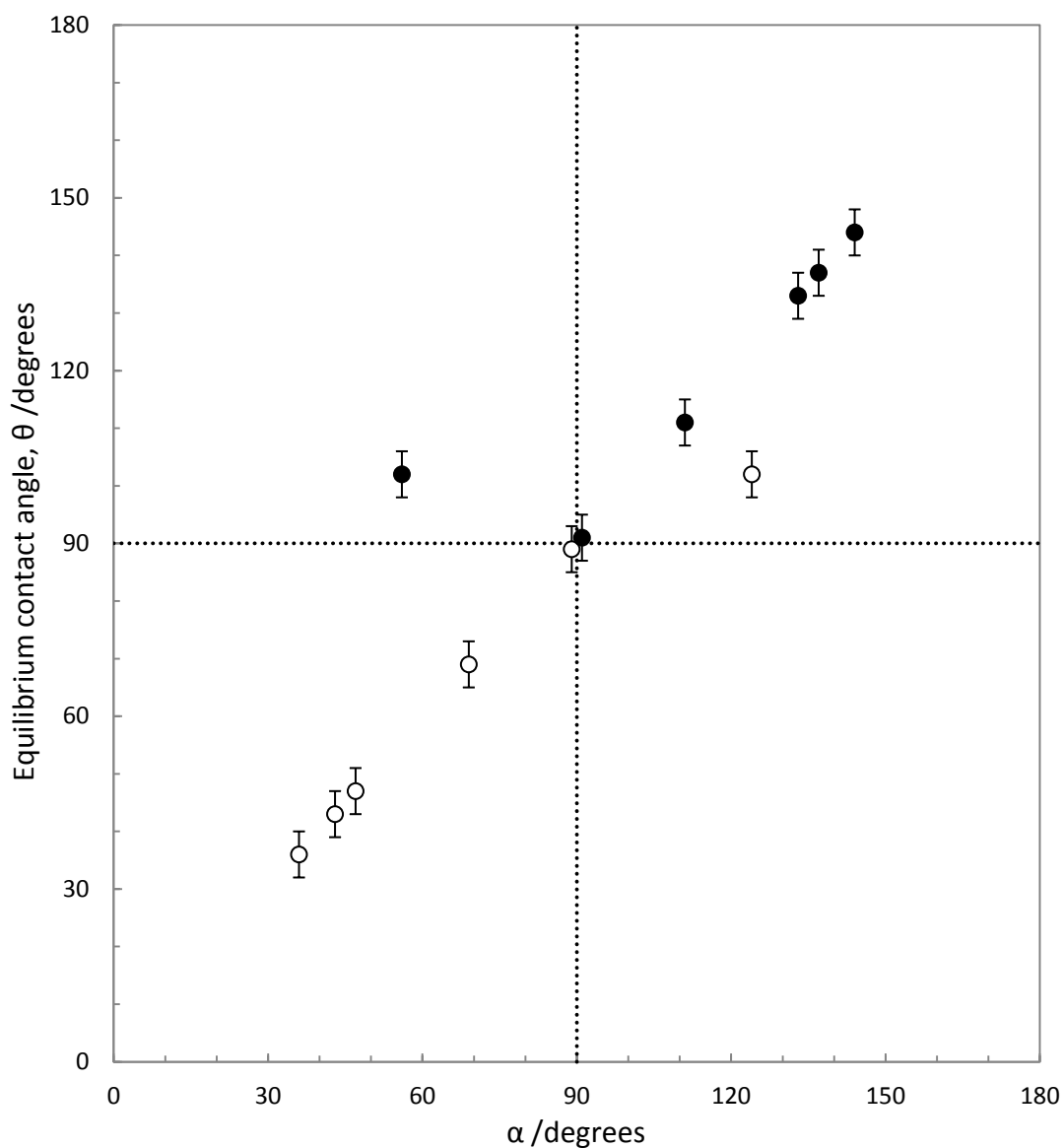


**Figure 5.20.** Expected equilibrium contact angles of Janus particles at the decalin-water interface versus the central angle  $\alpha$  of the more hydrophobic region. The data shown are for Janus particles prepared by oxidation of the unmasked hydrophobised silica particle surface with nitric acid (open circles) or hydrophobisation to the maximum extent with DCDMS vapours (filled circles). Data values are presented in Tables 5.2 and 5.3.

For particles of low initial hydrophobicity, treatment with nitric acid will leave a low equilibrium contact angle whereas treatment with DCDMS will leave a high equilibrium contact angle (Fig. 5.20). On the other hand if the initial hydrophobicity is high the average contact angles are high for both nitric acid and DCDMS treated Janus particles. The reason for this lies in the initial hydrophobicity which determines the amount of each particle masked and therefore treated, and is displayed schematically in Fig. 5.19. When the initial hydrophobicity is low the particle does not protrude far into the monomer prior to polymerisation and is masked only slightly, whereby most of the particle is treated and the small masked portion has low contact angle. When the initial hydrophobicity is high the particle will sit mostly in the monomer oil and will then be largely masked by polymer, whereby only a small proportion of the particle is treated and the larger portion retains its high contact angle.

Janus particles were made using both 1  $\mu\text{m}$  and 500 nm diameter silica particles as a base. Batches of particles of each size were treated with DCDMS to create base particles of a range of initial hydrophobicities. Two series of Janus particles were made for each particle size where the base particles were treated with either nitric acid or DCDMS. The characteristics of these Janus particles are summarised in Tables 5.2 and 5.3. Base particles in suspension (not masked) were treated simultaneously in separate vessels to produce homogenous particles which matched the treated portion of the Janus particles. Emulsions of equal volume water and decalin were prepared from all of the various particles available and observed over a month. Images from the 500 nm particle stabilised emulsions are shown below (Figs. 5.21 & 5.22) with 1  $\mu\text{m}$  particles observed to act similarly. All emulsions were unstable to creaming but were stable to coalescence after the initial 5 minutes with no changes perceived over the period of observation.

**Table 5.2.** Janus particles were obtained by oxidation of silica particles (initially hydrophobised at various DCDMS concentrations) using nitric acid. Given are the contact angles ( $\pm 4^\circ$ ) of the polar ( $\theta_p$ ) and apolar ( $\theta_a$ ) regions at the decalin - water interface (measured with the FCM for similarly treated homogeneous particles), expected mode of attachment, equilibrium contact angle ( $\theta$ ) and observed emulsion type produced from equal phase volumes (1:1) of decalin and water.

| [DCDMS]<br>/M        | $\alpha$ /deg. | $\theta_p$ /deg. | $\theta_a$ /deg. | Mode of attachment | Equilibrium $\theta$ /deg | Emulsion type |
|----------------------|----------------|------------------|------------------|--------------------|---------------------------|---------------|
| $1.0 \times 10^{-5}$ | 36             | 30               | 53               | J                  | 36                        | o/w           |
| $5.0 \times 10^{-5}$ | 43             | 30               | 66               | J                  | 43                        | o/w           |
| $1.0 \times 10^{-4}$ | 47             | 30               | 67               | J                  | 47                        | o/w           |
| $5.0 \times 10^{-4}$ | 69             | 30               | 81               | J                  | 69                        | o/w           |
| $1.0 \times 10^{-3}$ | 89             | 30               | 98               | J                  | 89                        | o/w           |
| $5.0 \times 10^{-3}$ | 124            | 30               | 102              | H2                 | 102                       | o/w           |

**Table 5.3.** Janus particles were obtained by further hydrophobisation of base silica particles (initially hydrophobised at various DCDMS concentrations) using DCDMS vapours. Given are the contact angles ( $\pm 4^\circ$ ) of the polar ( $\theta_p$ ) and apolar ( $\theta_a$ ) regions at the decalin - water interface (measured with the FCM for similarly treated homogeneous particles), expected mode of attachment, equilibrium contact angle ( $\theta$ ) and observed emulsion type produced from equal phase volumes (1:1) of decalin and water.

| [DCDMS]<br>/M        | $\alpha$ /deg | $\theta_p$ /deg. | $\theta_a$ /deg. | Mode of attachment | Equilibrium $\theta$ /deg | Emulsion type |
|----------------------|---------------|------------------|------------------|--------------------|---------------------------|---------------|
| $1.0 \times 10^{-5}$ | 144           | 53               | 130              | H2                 | 144                       | w/o           |
| $5.0 \times 10^{-5}$ | 137           | 66               | 130              | H2                 | 137                       | w/o           |
| $1.0 \times 10^{-4}$ | 133           | 67               | 130              | H2                 | 133                       | w/o           |
| $5.0 \times 10^{-4}$ | 111           | 81               | 130              | J                  | 111                       | w/o           |
| $1.0 \times 10^{-3}$ | 91            | 98               | 130              | J                  | 98                        | w/o           |
| $5.0 \times 10^{-3}$ | 56            | 102              | 130              | H1                 | 102                       | w/o           |

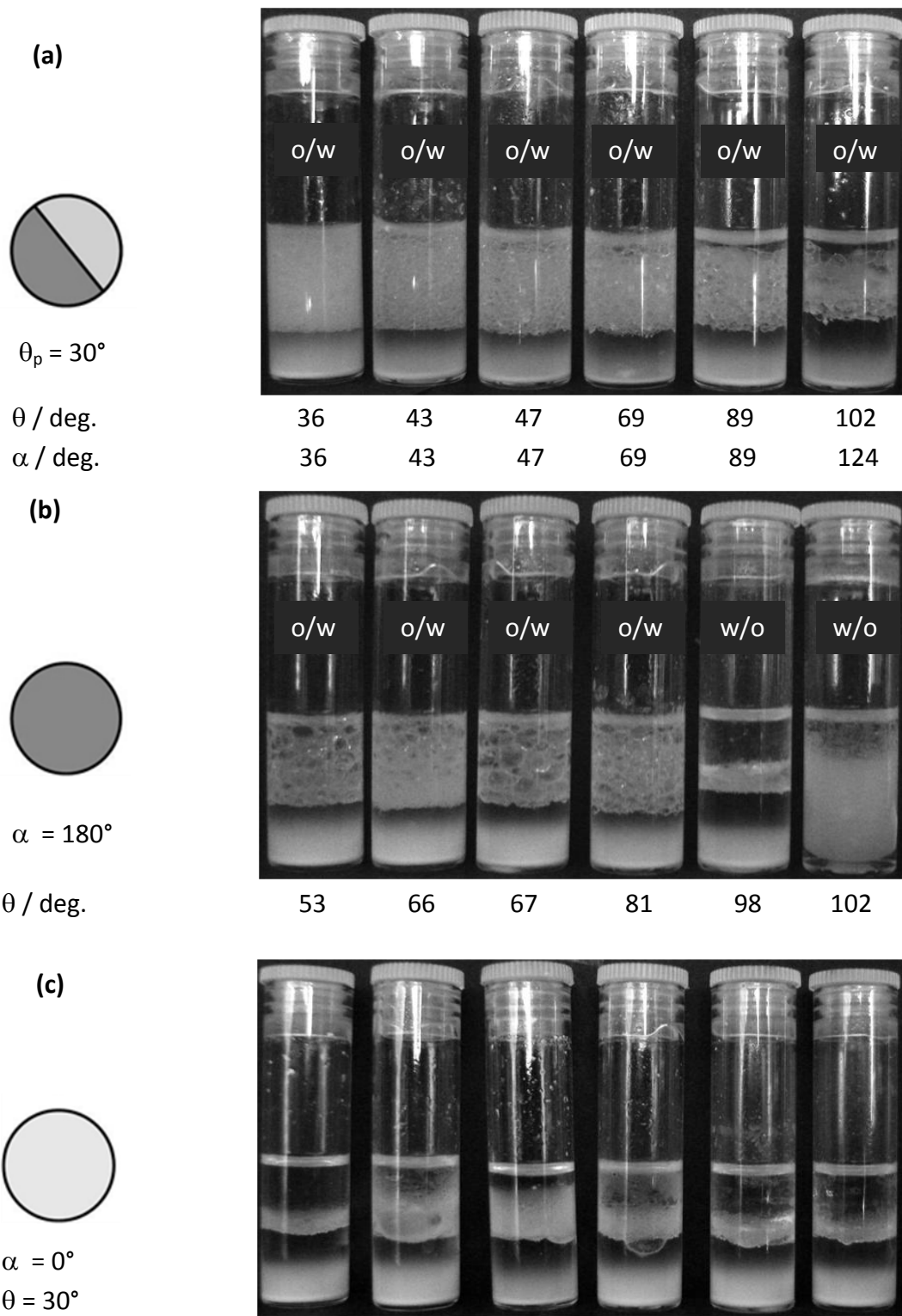


**Figure 5.21.** Images of water and decalin emulsions after 24 hours stabilised by: (a) Janus particles obtained by oxidation of the base hydrophobised silica particles with nitric acid, (b) homogeneous base particles and (c) homogeneous base particles oxidised fully with nitric acid.

As expected with the homogeneous base particles, emulsion inversion is observed from oil-in-water emulsions at lower particle contact angles to water-in-oil emulsions stabilised by hydrophobic particles (Fig. 5.21b). Little emulsion was stabilised by the base particles with contact angle of  $98^\circ$ .

When the particles are fully treated with nitric acid ( $\theta = 30^\circ$ ) they are seen to be poor emulsion stabilisers (c) suggesting that they are in this instance too hydrophilic to be good stabilisers, even compared to the most hydrophilic base particles. In contrast to these it can be seen that the Janus particles are generally good emulsion stabilisers (a). The most stable emulsions are those where the equilibrium contact angle of the Janus particles is expected to be the lowest. As the equilibrium contact angle increases the volume of separated oil also increases. In general the emulsions stabilised by Janus particles appear to be composed of smaller droplets than those stabilised by the base particles.

An inversion from o/w into w/o emulsion is expected to occur when the equilibrium contact angle of homogeneous or Janus particles becomes bigger than  $90^\circ$ . Such an inversion of the emulsion type is observed with the homogeneous particles but not with the Janus particles. This interesting difference in the behaviour of Janus and homogeneous particles needs further investigation.

Based on approximate contact angle measurements we can compare the emulsions stabilised by the base particles ( $\theta = 53^\circ$  and  $67^\circ$ ) with the Janus particles ( $\theta = 47^\circ$  and  $69^\circ$ ) and can see that the emulsion types are the same (o/w) but Janus particles are better stabilisers with smaller emulsion drops. The emulsion types stabilised by particles with a  $102^\circ$  equilibrium contact angle are stable w/o for homogeneous particles and unstable o/w for Janus particles. This unexpected result needs further investigation as mentioned above. Of most significant difference is when comparing the homogeneous nitric acid treated particles ( $\theta = 30^\circ$ ) with the most hydrophilic Janus particles ( $\theta = 36^\circ$ ) where it is seen that the Janus particles are far superior emulsion stabilisers to the homogeneous particles which cannot stabilise emulsion.

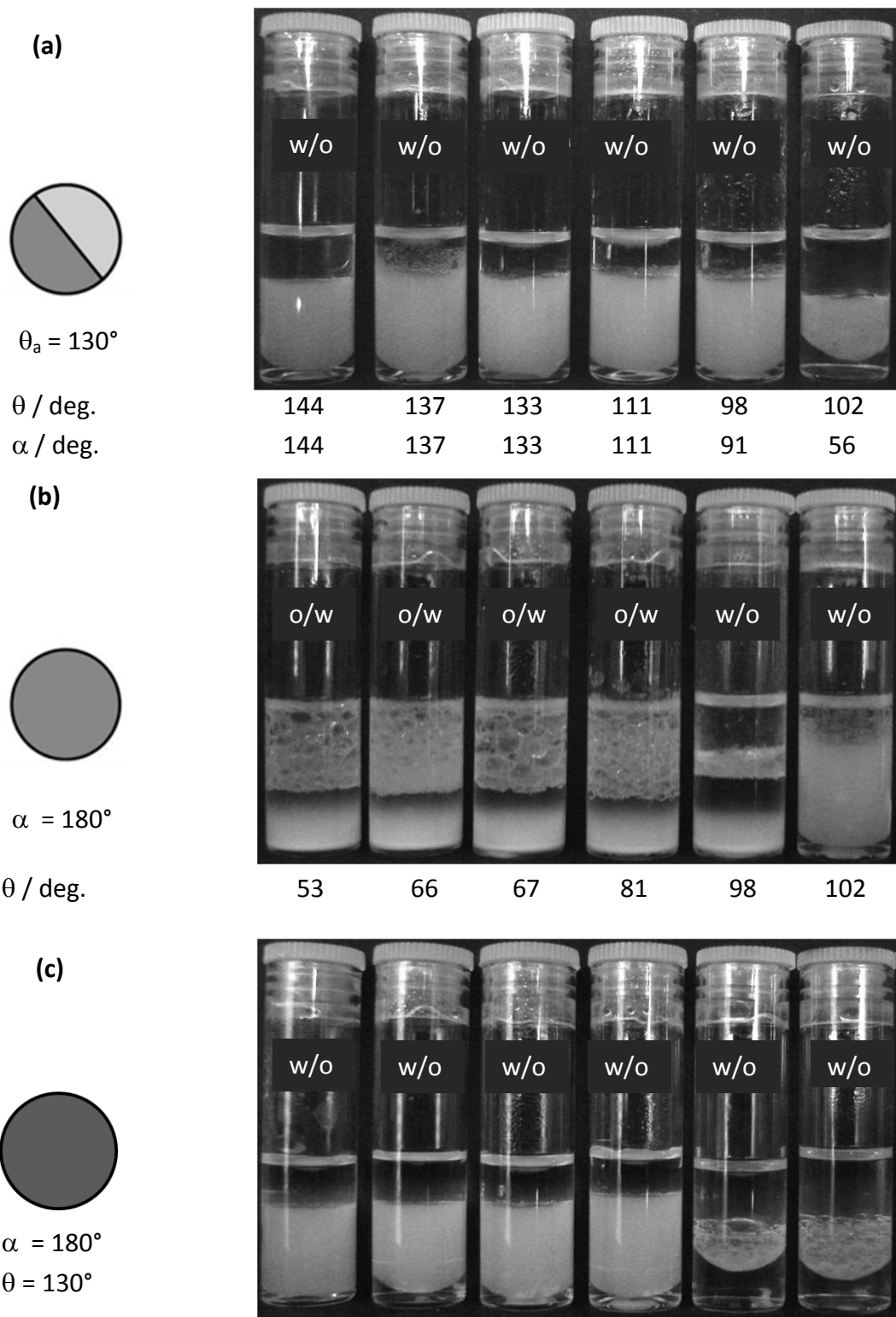


**Figure 5.22.** Images of water and decalin emulsions after 24 hours stabilised by: (a) Janus particles obtained by further hydrophobisation of the base silica particles with DCDMS, (b) homogeneous base particles and (c) homogeneous base particles hydrophobised fully with DCDMS.

The two series of samples stabilised by particles hydrophobised further with DCDMS (Fig. 5.22a,c) are very different to those with nitric acid treated particles. Homogeneous particles treated with DCDMS (c) to an equilibrium contact angle of  $130^\circ$  all stabilise water-in-oil emulsions. It can be seen in this series that those which were initially hydrophilic base particles stabilise emulsions better than the hydrophobic base particles, suggesting that the maximum contact angle was not achieved, although they are still much more hydrophobic than to begin with. One possibility for this is that the hydrophilic particles retained a small amount of water on the surface after drying, which then hindered the silanising procedure. The particles treated with DCDMS which were initially more hydrophobic are assumed to have contact angles that are too high for suitably stabilising emulsions.

The Janus particles also all stabilise water-in-oil emulsions as predicted with the equilibrium contact angle calculations. Almost all the Janus particles are excellent emulsifiers with the sole exception being the particles with equilibrium contact angle  $102^\circ$  which poorly stabilised w/o emulsion. The difference in emulsions stabilised by Janus particles with  $102^\circ$  equilibrium contact angles between Fig. 5.21 and 5.22 could be due to variations in the contact angle of each region or some factor relating to the specific treatment used to make them amphiphilic, i.e. oxidation (Fig 5.21) and hydrophobisation (Fig. 5.22).

It was observed that the emulsions stabilised by the homogeneously treated particles and the Janus particles generally match each other and that stabilised by the most hydrophobic base particles. The emulsions are very similar with neither particle type apparently better emulsion stabilisers, except for the most hydrophobic Janus particles which are good emulsion stabilisers in comparison to those homogeneously treated particles in (c) which are thought to be slightly more hydrophobic than the rest. Based on the results hydrophilic Janus particles are apparently more beneficial as emulsion stabilisers in comparison to homogeneous particles than hydrophobic Janus particles but in all cases the Janus particles are observed to be good stabilisers against coalescence for at least a month. Longer

term studies could show exceptional emulsion stability over extended periods of time, perhaps for longer than homogeneous particles.

#### 5.4 Conclusions

A procedure for producing Janus particles has been developed utilising polymerised Pickering emulsions as a means to mask template silica particles. The procedure is relatively quick and allows for control of the relative proportion of each Janus region (angle  $\alpha$ ) by changing the initial template particle hydrophobicity. The procedure benefits from simplicity while being scalable. In addition to this, the contact angle of both Janus regions can be permanently controlled, as opposed to Janus particles from systems using surfactant which, once removed from the polymer, will lose the hydrophobicity of the region that had been masked.

Using different modifications we produced 4 different types of particles. Particles consisting of a silica core with one hemisphere coated with silver were produced using Tollen's reagent and bifunctional particles were created by aminating the exposed silica surface. Amphiphilic particles were made by reducing the template particle hydrophobicity with oxidation using nitric acid or by increasing the hydrophobicity with DCDMS vapours.

The Janus nature of particles made with this procedure has been proven with zeta potential measurements and fluorescence microscopy. With varying pH the zeta potential of the bifunctional Janus particles was seen to lie between those of homogeneous particles with surface make-up identical to the two Janus regions. The isoelectric point of the Janus particles also occurred at a pH inbetween those of the homogeneous particles. The treated portion of some bifunctional particles were tagged during production with a fluorescent dye and then fluorescent microscopy images were used to show that Janus particles had been produced. It was shown that the Janus balance could be controlled with the hydrophobicity of the base particles and that variations between particles of different sizes were small.

Amphiphilic Janus particles were shown as emulsion stabilisers and compared with emulsions stabilised by homogeneous particles that were treated in a likewise fashion to the individual Janus regions. Emulsions were stable against coalescence over the course of a month for both homogeneous and Janus particles. The emulsions stabilised by hydrophobic Janus particles were similar to those of homogeneous particles with similar equilibrium contact angles, but the Janus particles also stabilised emulsions at very high equilibrium contact angles. Hydrophilic Janus particles were better stabilisers than homogeneous particles with similar equilibrium contact angles. Homogeneous particles oxidised with nitric acid ( $30^\circ$ ) were not able to stabilise emulsions whereas Janus particles with similar equilibrium contact angle ( $36^\circ$ ) made very stable o/w emulsions.

## 5.5 References

1. L. Hong, A. Cacciuto, E. Luijten and S. Granick, *Langmuir*, 2008, **24**, 621.
2. Z. Nie, W. Li, M. Seo, S. Xu and E. Kumacheva, *J. Am. Chem. Soc.*, 2006, **128**, 9408.
3. S. Gangwal, O. J. Cayre and O. D. Velev, *Langmuir*, 2008, **24**, 13312.
4. C. J. Behrend, J. N. Anker, B. H. McNaughton, M. Brasuel, M. A. Philbert and R. Kopelman, *J. Phys. Chem. B*, 2004, **108**, 10408.
5. S. M. Anthony, L. Hong, M. Kim and S. Granick, *Langmuir*, 2006, **22**, 9812.
6. T. Nisisako, T. Torii, T. Takahashi and Y. Takizawa, *Adv. Mater.*, 2006, **18**, 1152.
7. S.-H Kim, S.-J. Jeon, W. C. Jeong, H. S. Park and S.-M. Yang, *Adv. Mater.*, 2008, **20**, 4129.
8. S. Jiang, M. J. Schultz, Q. Chen, J. S. Moore and S. Granick, *Langmuir*, 2008, **24**, 10073.
9. L. Hong, S. Jiang and S. Granick, *Langmuir*, 2008, **22**, 9495.
10. C. Casagrande, P. Fabre, E. Raphaël and M. Veyssié, *Europhys. Lett.*, 1989, **9 (3)**, 251.
11. T. Ondarçuhu, P. Fabre, E. Raphaël and M. Veyssié, *J. Phys. Paris*, 1990, **51**, 1527.
12. Y. K. Takahara, S. Ikeda, S. Ishino, K. Tachi, K. Ikeue, T. Sakata, T. Hasegawa, H. Mori, M. Matsumura and B. Ohtani, *J. Am. Chem. Soc.*, 2005, **127**, 6271.
13. J.-W. Kim, D. Lee, H. C. Shum and D. A. Weitz, *Adv. Mater.*, 2008, **20**, 3239.
14. B. M. Teo, S. K. Suh, T. A. Hatton, M. Ashokkumar and F. Grieser, *Langmuir*, 2011, **27 (1)**, 30.
15. T. Tanaka, M. Okayama, H. Minami and M. Okubo, *Langmuir*, 2010, **26 (14)**, 11732.
16. A. Walther, M. Hoffmann and A. H. E. Müller, *Angew. Chem. Int. Edit.*, 2008, **47**, 711.
17. S. Jiang, Q. Chen, M. Tripathy, E. Luijten, K. S. Schweizer and S. Granick, *Adv. Mater.*, 2010, **22**, 1060.
18. C. Casagrande and M. Veyssié, *Cr. Acad. Sci. II B*, 1988, **306**, 1423.
19. S. Jiang and S. Granick, *J. Chem. Phys.*, 2007, **127**, 161102.
20. B. P. Binks and P. D. I. Fletcher, *Langmuir*, 2001, **17**, 4708.

21. B. P. Binks, *Curr. Opin. Colloid In.*, 2002, **7**, 21.
22. S. Jiang and S. Granick, *Langmuir*, 2008, **24**, 2438.
23. Sigma-Aldrich Co. LLC. (2011) 'Thermal transitions of homopolymers', Available online: <http://www.sigmaaldrich.com/materials-science/polymer-science.html>, (Accessed 23/09/2011).
24. G. B. Raju, S. Prabhakar and S. S. Rao in, *Proc. International Conference on Mineral Processing Technology*, G. V. Rao and V. N. Misra, eds., Allied Publishers Pvt. Ltd. (New Delhi), 2004, p. 322 – 330.
25. R. L. DeRosa, J. A. Cardinale, and A. Cooper, *Thin Solid Films*, 2007, **515**, 4024.

## Chapter 6

### Summary of main findings, conclusions and future work

The main focus of this thesis is to investigate the relationship between the wetting of solid particles and their ability to stabilise foams and emulsions. The investigation of homogeneous colloidal particles of various types described in Chapters 3 and 4 is extended to particles with dual wettability (Janus particles) in Chapter 5. The overall aim of the work with homogeneous particles is to achieve deeper understanding of the role of solid particles in foam and emulsion stability in the absence and presence of surfactants. This is done by developing a method for direct measurements of the particle contact angle at air - water and oil - water interfaces (Chapter 3) and using it to study the effect of solid particles on foam and emulsions from particle-surfactant mixtures (Chapter 4). The main objectives of Janus particle investigation in Chapter 5 are to develop a method for producing large amounts of amphiphilic Janus particles with controlled structure and investigate their ability to stabilise emulsions in comparison to homogeneous particles. The main findings and conclusions from our study are summarised below.

#### 6.1 Main findings and conclusions

In chapter 3 the Film Calliper Method (FCM) was developed further for directly measuring the contact angles of micron and submicron particles at oil - water interfaces. This is demonstrated for different systems such as charge stabilised latex particles at decalin - water interfaces, sterically stabilised latex particles at dodecane - water interfaces and silica particles hydrophobised with DCDMS at decalin - water interfaces. It is shown that the contact angles of charge-stabilised latex particles depend strongly on the density of surface groups and that the wettability of similar latex particles could be very different due to variations in the surface composition introduced at their synthesis. It is also demonstrated for

the first time that the FCM can be used for the direct measurement of contact angles of micron and submicron particles in the presence of surfactants where other methods (e.g. GTT) cannot be used.

The first direct evidence for the relationship between the particle contact angle and the emulsion type using particles of different chemical nature and also particle - surfactant mixtures was given. Particles measured to be hydrophilic ( $\theta < 90^\circ$ ) with the FCM were shown to stabilise oil-in-water emulsions while particles measured to be hydrophobic ( $\theta > 90^\circ$ ) stabilised water-in-oil emulsions. For the first time a double inversion (o/w to w/o to o/w) of emulsion type was observed for emulsions stabilised with a mixture of silica particles and single chain cationic surfactant. It is shown that the particle concentration is an important factor for the emulsion type and phase inversion because it may change the mechanism of stabilisation.

In chapter 4 the contact angles of silica particles in the presence of cationic surfactants (CPC and TTAB) are directly measured and linked to the surfactant adsorption and zeta potential. The results are consistent with changes in the contact angle expected from the reverse orientation adsorption model. The maximum contact angle when zeta potential is ~zero is in agreement with the sedimentation behaviour of particle suspensions.

The foam stability of particle - surfactant mixtures cannot be explained by the variation of the energy of particle detachment from the air - aqueous solution interface with changing contact angle. Observations of spontaneous particle bridging suggest that the stability of the wetting film between particles and bubble surfaces increases with surfactant concentration. Close to or above cmc the wetting films can become sufficiently stable to prevent particles from attaching to the bubble surfaces. Kinetic factors (i.e. wetting film stability) of foam stabilisation are therefore very important. Particles are shown to improve the emulsion stability in a certain range of surfactant concentrations where the particle contact angle is large. Similarly to foams, at concentrations close to or above cmc the particles have an

insignificant effect on emulsion stability because they cannot attach to droplets due to stable wetting films.

In chapter 5 a procedure for producing Janus particles was presented utilising polymerised Pickering emulsions as a means for partially masking template silica particles before subsequent treatment of the exposed particle surfaces. The procedure allows for variable proportions of each surface region by altering the initial template particle hydrophobicity. The technique benefits from simplicity while being scalable. In addition, the contact angle of both Janus regions can be controlled permanently, as opposed to Janus particles from systems using surfactant which will lose the original hydrophobicity with washing or dispersion in a fresh medium

The Janus nature of the particles made with this procedure has been proven with zeta potential measurements and fluorescence microscopy. The particles investigated had different charge on each hemisphere with the zeta potential and isoelectric point measured to lie between that of the two regions. Fluorescence microscopy of fluorescently tagged Janus particles showed that the geometry of the particles could be controlled by adjusting the base particle hydrophobicity and that the technique is applicable to particles of varying size.

Particles with dual wettability were produced and used to stabilise emulsions. The emulsions were unstable to creaming but stable to coalescence over the course of a month for both homogeneous and Janus particles. Emulsions from the Janus particles were compared with emulsions stabilised with homogeneous particles that were treated in a likewise fashion to the individual Janus hemispheres. It was seen that emulsions stabilised with hydrophobic Janus particles were similar to hydrophobic homogeneous particles with similar equilibrium contact angle but the Janus particles were also good stabilisers at high equilibrium contact angles. Hydrophilic Janus particles were shown to be better stabilisers than homogeneous particles with intermediate contact angle and far superior stabilisers at low

equilibrium contact angles ( $36^\circ$ ), where homogeneous particles did not stabilise emulsions.

## **6.2 Future work**

The Film Calliper Method has been shown to be suitable for measuring the contact angles of hydrophilic particles at air - water and oil - water interfaces for a variety of systems and particle types. It would be of major benefit if the method could be developed further still for measuring the contact angles of hydrophobic particles too. For these measurements a stable film of air or oil within the aqueous phase would be required and particles bridging across the film. Achieving both of these conditions could prove difficult and would likely require changes to the experimental setup.

The investigation into mixtures of silica particles and cationic surfactants could be expanded upon by using a series of surfactants of varying tail length. It would be interesting to observe changes in surfactant adsorption and particle contact angle as a result of the changing tail lengths and determine if they can be directly related to the changing surfactant properties. It would also be of interest to investigate how changes in the surfactant tail length or head group would affect the stability of the wetting films at the air-water and oil-water interface and determine whether the stabilisation of foams and emulsions is also affected.

The work with Janus particles presents many opportunities for further work. Comparing particles with dual wettability and homogeneous particles in the role of foam stabilisers would prove interesting. It would also be of great interest to study the orientation of Janus particles at interfaces because it is still unknown if they orientate on adsorption at the interface with the polar region in the more polar phase. The best way to achieve this would be to use fluorescence microscopy with a horizontally mounted microscope.